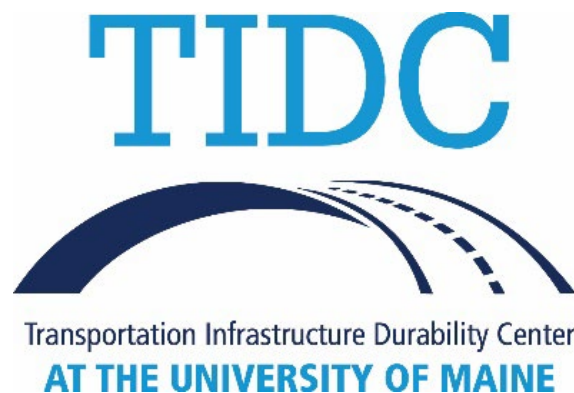# Field Live-Load Testing and Advanced Analysis of Concrete T-Beam Bridges to Extend Service Life

Final Project Report

1/31/2020

Andrew Schanck EI, MS
Graduate Research Assistant, University of Maine Civil Engineering

William Davids PhD, PE
John C. Bridge Professor of Civil and Environmental Engineering, University of Maine (PI)

ACKNOWLEDGEMENTS

DISCLAIMER

Table of Contents

Index of Figures

Index of Tables

1 Project Impetus and Overview

Many older bridges were designed for much lighter loads than are required today, and engineering calculations based on current codes show that these bridges are at risk for posting, closure or replacement. However, many of these structures show few or no signs of distress and provide adequate service. This raises the obvious question: even if a bridge was not designed to carry modern truck traffic, should it be closed – or millions spent – to strengthen or replace it given its good performance history and condition?

Concrete T-beam bridges are an important class of structures that has seen limited investigation. These structures are often perceived as quite robust and are in good condition, but possess very low rating factors based on conventional analysis per the AASHTO *Manual for Bridge Evaluation* (2011). Testing of five T-beam bridges conducted in summer 2017 indicated that conventionally calculated rating factors are generally low for T-beam bridges. However, all of the tested bridges were un-skewed, and the effect of skew angle has not been quantified. Further, the reliance on non-destructive live-load testing (NDLLT) to modify rating factors can be costly. Finally, the use of NDLLT to modify rating factors requires the extrapolation of service-load strain data to predict bridge capacity, and at capacity, the bridges will generally experience significant nonlinearity.

These research questions were addressed with a three-phase approach. In the first phase, UMaine engineers instrumented and field load-tested five, cast-in-place, simple span, skewed concrete T-beam bridges. The specific structures to be tested were determined jointly by MaineDOT and UMaine engineers prior to the start of this project. These bridges, tested in the summer of 2018, were instrumented with the Bridge Diagnostics Incorporated (BDI, 2010) semi-wireless system using multiple strain gages located to assess both load distribution and flexural capacity. Girders were instrumented both at mid-span where moments were at their maximum as well as near the supports to assess any unintended partial fixity. Measured strains were then used to modify the conventional, code-based flexural rating factors of these structures.

In the second phase of this project, the NDLLT results from the five skewed bridges were used in conjunction with prior NDLLT of non-skewed T-beam bridges to assess differences in behavior caused by a skewed alignment. In addition, detailed, linearly elastic, 3D finite-element models of all 10 bridges were developed. These models incorporated all field-verified components such as wearing surface, curbs and railings as well as all reinforcing specified in the original plans. These models were subjected to the loads used during NDLLT, their predictions compared with field-measured response, and their results used to help assess differences in behavior between skewed and un-skewed bridges.

In the final phase of the project, a novel, nonlinear finite-element modeling strategy was developed that permits the accurate inclusion of inherent ductility and a realistic assessment of capacity under the application of factored loads. This method, termed Proxy Finite Element Analysis (PFEA), enhances our ability to rationally assess bridge capacity without relying on NDLLT. PFEA was validated through comparison with experimental data both from the testing conducted in this study

and from strength tests of beams and bridges performed by others. Ultimately, PFEA was used to re-compute flexural rating factors for all ten T-beam bridges considered in this study, and generally indicated less-conservative predictions of bridge capacity than NDLLT. This is consistent with PFEA's explicit consideration of nonlinear structural response and the fact that NDLLT relies on linear extrapolation. PFEA was also used to examine the shear rating factors of the 10 bridges subjected to NDLLT, and indicated generally higher shear rating factors.

2 Phase 1: Bridge NDLLT

The five reinforced concrete (RC) T-beam bridges were tested during the summer of 2018 as part of this program are listed below.

1. Bridge No. 5489 in Levant, carrying Route 222 over Black Stream,
2. Bridge No. 5109 in Hampden, carrying Route 9 over Souadabscook Stream,
3. Bridge No. 2390 in Unity, carrying Town Farm Road over Sandy,
4. Bridge No. 2879 in Atkinson, carrying Stagecoach Road over Piscataquis River,
5. Bridge No. 3848 in Columbia, carrying Saco Road over Western Little River.

All bridges were instrumented with a strain measuring system, loaded with heavy trucks, and then analyzed to determine whether it was reasonable to change the bridge rating factors based on the test results. These bridges were all constructed between 1931 and 1952 and were originally designed as simply supported with a nominal concrete compressive strength of 2.5 ksi. Each bridge utilized a moderately skewed alignment, with angles of skew ranging between 15° and 35°.The primary objective of this study was to determine more appropriate live-load rating factors for these bridges and to determine more realistic live-load distribution factors than those predicted by AASHTO (2012) based on their actual response. Recommendations for rating factor modifications are made based on the observed and computed response of these structures. Characteristics of the bridges tested and analyzed in this study are summarized in Table 1. When two numbers are listed, the first gives the value for interior girders and the second for exterior girders. When one value is listed, the interior and exterior girders are the same.

Table 1: Bridge Characteristics

Bridge	Levant	Hampden	Unity	Atkinson	Columbia
Number	5489	5109	2390	2879	3848
Year Built	1952	1951	1950	1931	1951*
Span - Center to Center of Bearings (feet)	47.0	47.0	37.0	50.0	34.0
Skew (Degrees)	15.0	35.0	30.0	30.0	30.0
Number of Girders	5	5	5	4	5
Girder Spacing (in)	82.0, 54.0	85.8, 57.3	73.5, 42.8	90.0,54.0	70.4, 45.2
Total depth (in)	36.0	39.8	31.3	50.0	29.8
Girder web thickness (in)	19.0	22.8	24.0, 15.0	22.0, 17.0	19.5, 16.0
Slab Thickness (in)	5.50	6.25	5.75	8.00	5.75

*Substructure built in 1943, superstructure built in 1951

2.1 Instrumentation

The strain measurement system used in this research was the Wireless Structural Testing System (STS-Wi-Fi) produced by Bridge Diagnostics Inc. (BDI, 2010). The system used a mobile base station to communicate with up to 6 nodes, with up to 4 strain transducers connected to each node. This system communicates with a dedicated laptop running BDI-specific WinSTS data acquisition software. A sample setup in the field is shown in Figure 1, with strain sensors mounted under a bridge at mid-span and connected to battery-operated wireless nodes. The sensors used in these tests were equipped with aluminum extensions, which are also visible in Figure 1. These extensions increased the gauge length of the transducers so as to minimize the effect of local stress concentrations and concrete cracks. A schematic of the entire network is shown in Figure 2 including strain and displacement sensors, wireless nodes, the wireless base station, autoclicker, and the data recording laptop.

Figure 1: Typical Strain Sensor Mounted under Bridge, Equipped with Extension
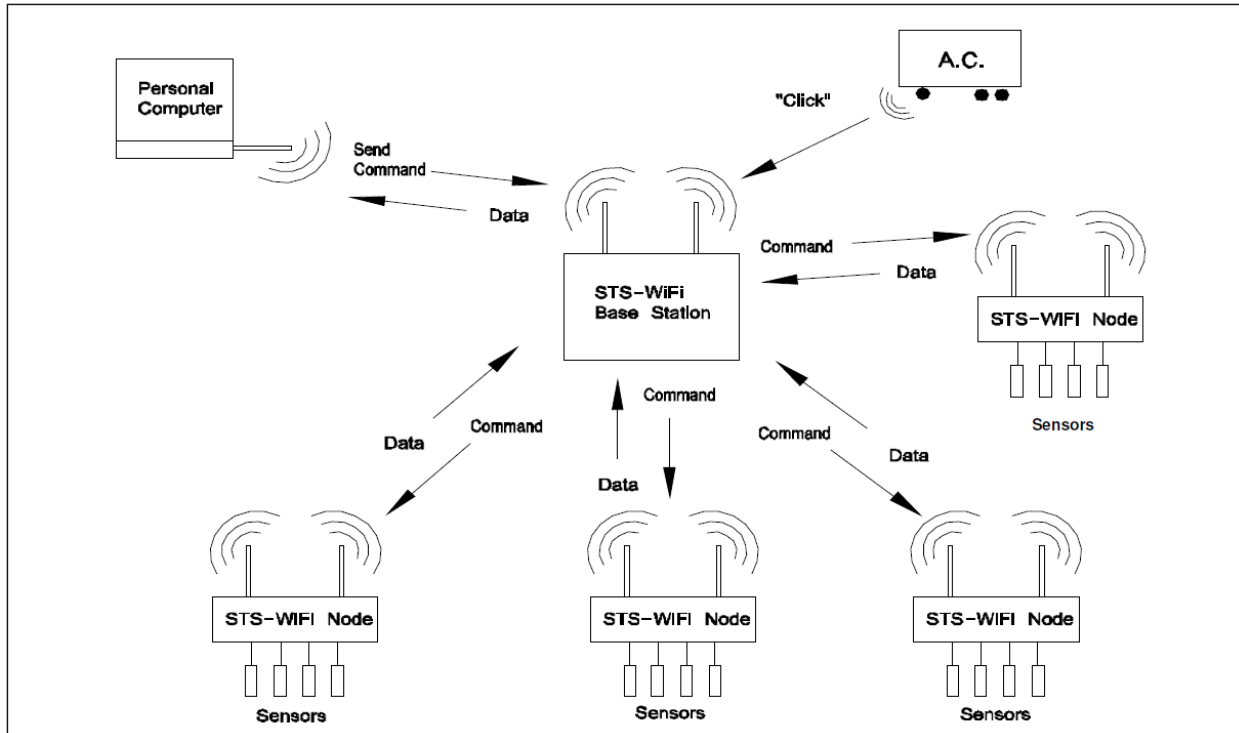
Figure 2: BDI STS-Wi-Fi Network Setup for Bridge Sensor Setup

Strain transducers were mounted under the bridges using a MaineDOT Under-Bridge Inspection Truck (UBIT) as shown in Figure 3. The sensors were mounted to the girders by first grinding the concrete in the instrumented location to be as flat as possible, then using LOCTITE 410 rubberized instant adhesive with LOCTITE SF7453 accelerant to attach the strain transducer mounting tabs. All structures had three strain gages mounted to each girder at midspan - one to the bottom of the slab, one at mid-depth of the web, and one at the web bottom face at mid-span - to measure load distribution and peak flexural strains in each girder. Strain transducers were also installed near the ends of selected girders (generally exterior and central girders as the number of remaining transducers allowed) to determine the extent of any rotational restraint at the supports. Strain sensor layout varied slightly for some bridges, with individual sensor layouts shown in the appendices A.2.2 for Bridge 5489, A.3.2 for Bridge 5109, A.4.2 for Bridge 2390, A.5.2 for Bridge 2879, and A.6.2 for Bridge 3748.

Figure 3: MaineDOT UBIT used to Install Sensors

2.2   Loading

The vehicles used for this testing were MaineDOT standard three-axle dump trucks as shown in Figure 4. Each truck wheel or pair of wheels was weighed using state patrol certified portable scales as shown in Figure 5. Various load cases were applied to each bridge, with each test given a specific identification code with the format: "Test Configuration_Centerline_Test Position_Test Number". Test configurations included two trucks, one in each lane ("SBS"), four trucks, two in each lane arranged to produce maximum moment ("MAX"), and four trucks, two in each lane arranged to produce less than maximum moment ("ALT"). "Centerline" refers to the longitudinal centerline by which truck positions were measured. It was not immediately obvious as to whether positioning trucks relative to the skewed centerline (Figure 6) or perpendicular centerline (Figure 7) would produce larger moments, so both centerline configurations were tested for all configurations. Centerline code "S" refers to tests relative to the skew centerline, and "U" refers to tests with trucks measured relative to the perpendicular centerline. Test positions included load close to the first curb ("1"), load close to the bridge centerline ("2"), and load close to the opposite curb ("3"). Test number refers to the test index if a certain load case was repeated. Not all bridges were subjected to all load cases.

Figure 4: MaineDOT Three Axle Trucks used for Loading

Figure 5: State Highway Patrol Certified Portable Truck Scales used to Verify Vehicle Weight for each Test
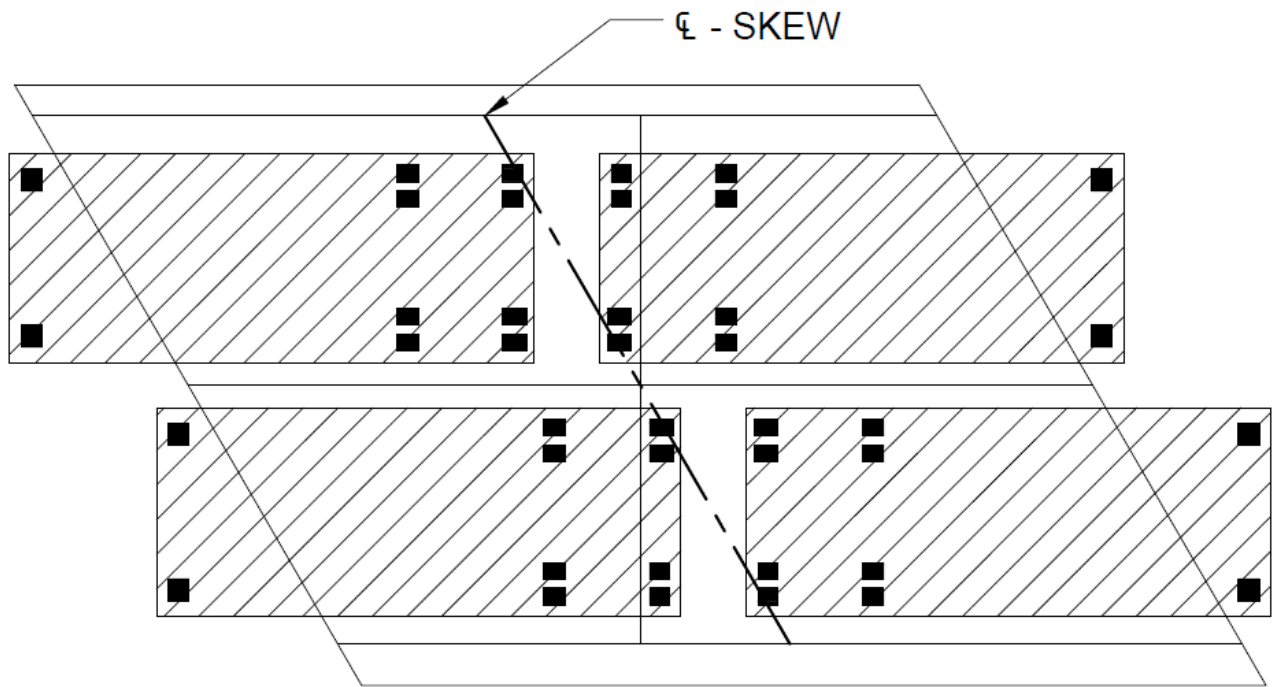
Figure 6: Truck Positioning Relative to Skew Centerline
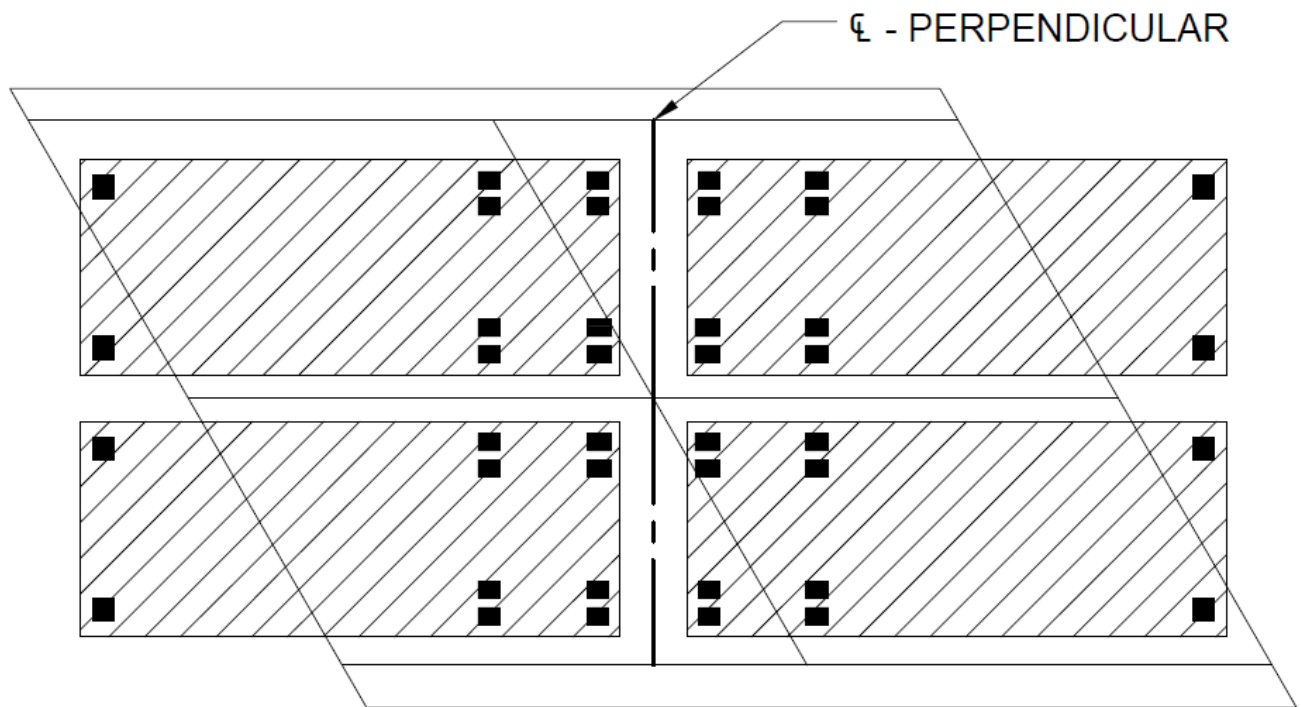
Figure 7: Truck Positioning Relative to Perpendicular Centerline

2.3 Typical Results

Results from a representative test of one of the five bridges are presented in this section to overview the general trends. Bridge No. 3848 had typical geometry and results for all test configurations. Figure 8 shows a time history of the strains measured at midspan of the center girder during the MAX_S_2_1 test, and Figure 9 shows a time history of the strains recorded at the ends of the same girder during the same test. In this test, trucks were backed onto the bridge sequentially and were positioned such that two trucks were arranged back to back in each lane with their rear tandem wheels spaced approximately symmetrically about the skew longitudinal centerline. All four trucks were nominally equidistant from the striped centerline. After all position measurements had been taken, the trucks were then removed from the bridge in reverse order. This sequential loading is seen in the strain plateaus in Figure 8, which demark a truck backing onto or pulling off the bridge.

In addition to showing the girder's response to sequential loading, Figure 8 also demonstrates the typical linear response to flexure seen across all bridges. The sensor at the section bottom recorded modestly high positive (tensile) strain at the maximum strain plateau, while the sensor at the top of the section recorded very small compressive strains and the sensor at the mid-depth of the section roughly split the difference. This strain distribution across the section indicates that the section's neutral axis lies within the web, close to the bottom of the slab. The location of the neutral axis within the section, as well as the relatively low strains recorded, indicate that many of the sections behaved as uncracked under test loading and had not experienced significant flexural cracking due to prior loading. Figure 9 shows the typical behavior of girder ends. At both ends of the girder, the bottom of the section experienced small compressive strains throughout the section depth at one end, indicating that some unintended end restraint was present. This was common of many of the bridges.
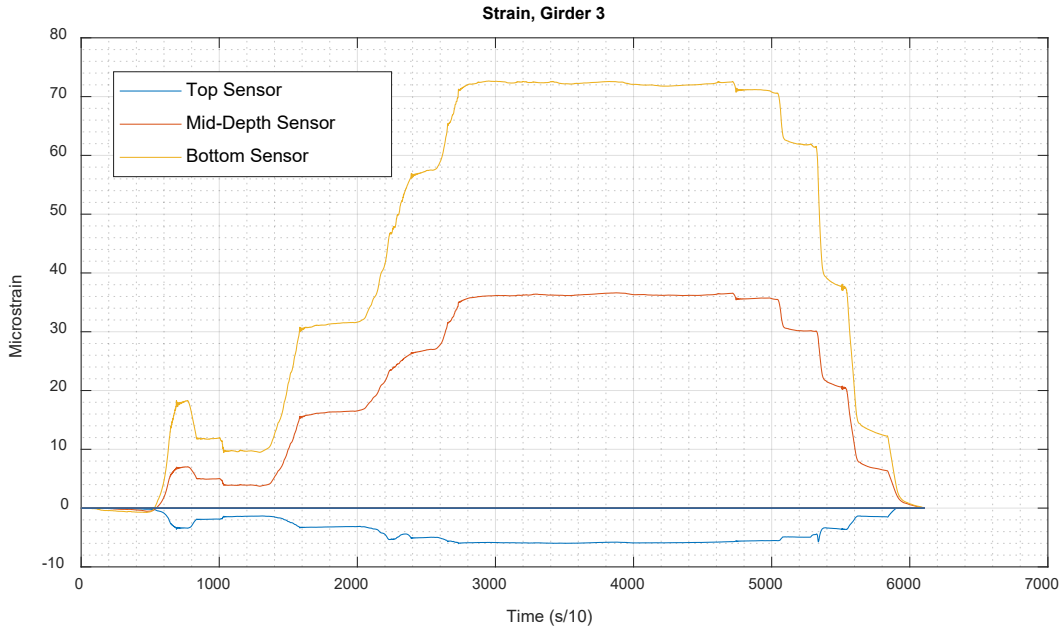
Figure 8: Bridge 3848 – MAX_S_2_1, Center Girder Strains at Midspan
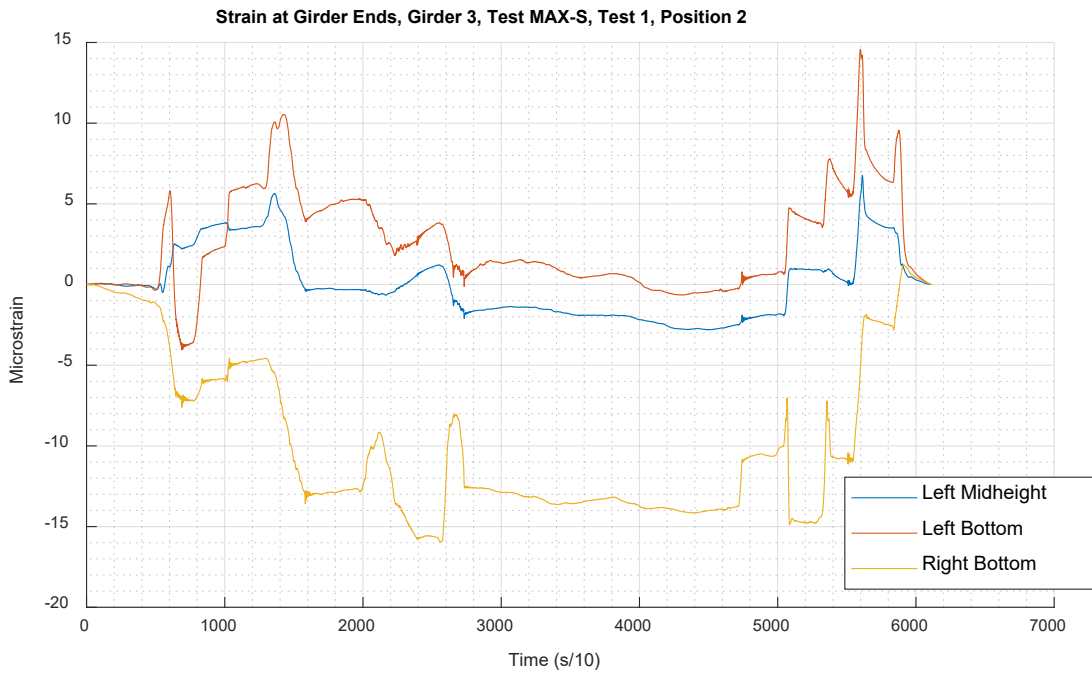
Figure 9: Bridge 3848 – MAX_S_2_1, Center Girder Strains at Ends

2.4 Analysis Methodology

2.4.1 Analysis Overview

Material properties, load and resistance factors, and design live-loads were taken from or calculated as specified in the AASHTO *Manual for Bridge Evaluation* (2011) and used with field-measured geometry to calculate original, nominal rating factors for each of the bridges. Bridges were then tested using heavily loaded trucks and strains were measured and correlated with these applied loads. Resulting strains from live-load testing were then used to verify cracked or uncracked behavior and compute realistic distribution factors. Finally, the results were used to modify rating factors. These calculation sheets are included in the appendices of this report. Appendix A.2.5 contains calculations for Bridge 5489, A.3.5 contains calculations for Bridge 5109, A.4.5 contains calculations for Bridge 2390, A.5.5 contains calculations for Bridge 2879. 2130, and A.6.5 contains calculations for Bridge 3848.

2.4.2 Bridge Characteristics

Material properties and general bridge geometry (i.e. span length, girder section properties, and reinforcement layout and geometry) were required for calculations. Geometric parameters were taken from each bridge's most recent available rating report and were verified in the field when accessible. Material properties were assumed based on the bridges' ages as specified by AASHTO (2011). Dead-load moments were determined from the bridge geometry and typical unit weights as specified in AASHTO.

2.4.3 AASHTO Distribution Factors

Distribution factors for moment for interior and exterior girders were calculated based on in-situ measured bridge characteristics along with nominal values for dimensions that were not possible to verify in the field in accordance with AASHTO *LRFD Bridge Design Specifications* (2012). All live-load distribution factors for moment are taken assuming cross-section "e" from Table 4.6.2.2.1-1 and "Cast-in-Place Concrete Tee Beam, Monolithic concrete." For moment on interior beams this is per Table 4.6.2.2.2b-1, with all ranges of applicability met. For the exterior girder moment distribution factors are per Table 4.6.2.2.2d-1, with all ranges of applicability met.

2.4.4 AASHTO Live-Loads with Impact

AASHTO live-loads with impact (LL + IM) per lane were determined as the maximum load effect with HL-93 per (6A.2.3) and AASHTO LRFD Design 3.6.1.2 and 3.6.2. This includes the worst case of truck or tandem loading with impact as applicable and including lane load. Girder moment was calculated based on this load and the AASHTO Distribution Factors calculated as described in section 1.4.3 of this report.

2.4.5 AASHTO Rating Factor

Flexural rating factors were independently computed per AASHTO (2011) (6A.4.2.1-1) with terms as defined in that section. These were calculated using Equation 1, in which C is the factored resistance of the member under investigation (with resistance factor taken equal to 0.9), $\gamma_{DC}DC$ is the factored structural dead-load (with load factor taken equal to 1.25), $\gamma_{DW}DW$ is the factored non-structural dead-load (with load factor taken equal to 1.25), $\gamma_{DC}(LL + IM)$ is the factored live-load with impact (with load factor taken equal to 1.33),. The live-load per lane computed according to section 1.4.4 of this report with impact was multiplied by the AASHTO distribution factors as described in section 1.4.3 of this report. Where present, integral concrete wearing surfaces and integral curbs were assumed to contribute to interior and exterior girders' moment capacities respectively. It should be noted that only flexural rating factors were computed as bridges were not instrumented to determine effects of shear. This implies that shear rating factors could not be improved based on measured strains.

$$RF = \frac{C - \gamma_{DC}DC - \gamma_{DW}DW}{\gamma_{LL}(LL + IM)}$$

Equation 1

2.4.6 Live-Loads Applied during Testing

Applied moment loadings were determined based on measured truck axle weights for all load configurations. The average of axle loads for side-by-side trucks was used to allow live-load distribution factors to be calculated and applied. The trucks were positioned to produce significant moment effects on the bridge. Continuous data recording was initiated, and then trucks were moved onto the bridge in a series. For each load configuration and position, trucks were moved onto the bridge one after another and the strains were allowed to plateau at the pre-determined configurations with data recording continuing during truck movement.

Applied moments were calculated assuming the bridges to behave as simply supported. The percentage of AASHTO HL-93 loading achieved is the ratio of the moment produced by the live-loads applied during testing and the moment produced by the AASHTO HL-93 loading as described in section 1.4.4 of this report. Total moment applied during testing was determined based on the measured magnitude of truck wheel loads and the positions of wheels measured during testing.

2.4.7 Verification of Uncracked Behavior

For each bridge, the theoretical strains under test loading were computed and compared with the measured strains to verify whether concrete sections behaved as though they had remained uncracked. Theoretical strains were calculated as shown in Equation 2, in which DF is the girder's distribution factor calculated based on AASHTO (2012), M_{max} is the maximum moment applied

to the girder, E_c is the elastic modulus of concrete, and S is the girder's section modulus, cracked or uncracked based on behavior..

$$\varepsilon_C = \frac{DF * M_{max}}{E_c S}$$

Equation 2

In all cases, E_c was calculated using the compressive strength of 2.5 ksi specified by AASHTO (2011). In addition, strains were computed assuming a compressive strength of 5 ksi, which is more conservative and may more accurately reflect the in-service concrete compressive strength of these older structures. Several studies of cast-in-place concrete structures of similar age have shown that concrete strengths can approach 8 ksi in older structures (Buckle et al. 1984, Saraf 1998, Alkhrdaji et al. 2001). The maximum strains recorded were compared with these calculated values. Maximum strains equal to or less than the estimated uncracked strain indicated that the bridge remained uncracked with the assumed compressive strength, while strains greater than the theoretical uncracked strain indicated possible cracking. For all bridges, the strains measured in all girders under maximum loading were smaller than those predicted with uncracked sections and 5 ksi compressive strength. For this reason, the strains computed assuming 5 ksi concrete were used in calculating rating factor improvements. The assumption of a higher-than-nominal strength of 5 ksi is conservative, since it leads to a higher-than-nominal elastic modulus and therefore lower predicted strains.

As an additional comparison to help verify uncracked behavior, the measured neutral axis depth for all girders was determined under maximum loading using the recorded strains. These depths were taken relative to the top of the deck in the case of interior girders and the top of the integral curbs for exterior girders. Where present, integral concrete wearing surfaces were considered part of the sections. These neutral axis locations inferred from measured strains were compared to the sections' theoretical neutral axis locations based on conventional strength of materials assumptions. Neutral axis locations inferred from measured strains were determined using the strains recorded at girder bottoms and at mid-height when the recorded strains were reliable. The strains measured at the bottom of the slab were generally not used per BDI's recommendation against relying on very small measured strains, but were used when recorded strains in another sensor were deemed unreliable. In general, measured neutral axis locations tended to be consistent with either uncracked section behavior or fell between cracked and uncracked behavior ("partially cracked"). In only one case (an exterior girder from Bridge 2390) did a neutral axis depth inferred through recorded strains seem to indicate cracked section behavior. However, the strains recorded at the section's bottom were still significantly less than the strains predicted for an uncracked section and so the girder was conservatively assumed to behave as uncracked.

2.4.8 Distribution Factors Determined from Live-Load Testing

The moment carried by the ith girder was then calculated as per Equation 3 assuming an uncracked section, with variables defined above.

$$M_i = E_c S_i \varepsilon_i \qquad \text{Equation 3}$$

The distribution factor for the ith girder was then calculated by Equation 4, where n is the total number of girders.

$$DF_i = \frac{M_i}{\sum_{i=1}^{n} M_i} \qquad \text{Equation 4}$$

2.4.9 Modified Rating Factor

In accordance with AASHTO (2011), the ratio of computed strain ε_C to measured strain ε_T was then used to compute a rating factor modifier as detailed below in Equation 5 to Equation 7. This analysis is based on the interior girder and exterior girder that experienced the largest measured strains.

$$RF_T = RF_c K \qquad \text{Equation 5}$$

In Equation 5, RF_T is the modified rating factor taking into account test results, RF_c is the rating factor based on standard calculations, and K is an adjustment factor specified by AASHTO (2011 that incorporates the test results. K is computed per Equation 6 below.

$$K = 1 + K_a K_b \qquad \text{Equation 6}$$

The factor K_a accounts for the difference between measured response based on load testing and expected response as shown below in Equation 7. The factor K_b accounts for the magnitude of the applied test load and confidence in extrapolating results; and is defined in Table 8.8.2.3.1-1 by AASHTO (2011). For all structures, K_b was taken as 0.5, which reflects both the magnitude of the applied load and the assumption that results cannot be reliably extrapolated to higher loads. In all cases, the strains used corresponded to the test causing the greatest applied moment. Although the "MAX_2" tests were designed ideally apply the greatest moment of all of the test series, in some cases, other tests caused greater moments to be applied and so those moments and strains were used.

$$K_a = \frac{\varepsilon_c}{\varepsilon_T} - 1 \hspace{4cm} \text{Equation 7}$$

2.5 NDLLT Test Results

2.5.1 Levant No. 5489

The bridge in Levant, No. 3356 over Black Stream, is shown in Figure 10. Testing was conducted on July 31, 2018 with a maximum applied moment producing 79.5% of HL-93 moment loading with impact. The moment rating factors based on AASHTO (2011, 2012) are 0.784 and 1.88 for the interior and exterior girders respectively. Table 2 shows the maximum measured strains for this bridge under typical two-truck and four-truck load-cases. The strains recorded with trucks positioned relative to the skew centerline resulted in consistently higher values of recorded strain than for load-cases positioned relative to the perpendicular centerline. For this reason, these values were reported for Bridge 5489 along with all other bridges. Where two values of strain are reported, the first value is the recorded strain, which was determined to be unreliable and inaccurate due to its magnitude being grossly inconsistent with that of other similarly loaded girders and other strains measured over the section depth. The second value of strain was calculated using the other strains recorded in the same section and assuming linear strain distribution.

Assuming the conservative concrete compressive strength of 5 ksi, the strains recorded indicate the sections remained uncracked. This is supported by the observed neutral axis depths, which are consistently lower in the section than would be predicted for an uncracked section, as can be seen in Table 3. The high level of applied load and low recorded strains allowed interior and exterior girder rating factors to be increased to 1.10 and 2.36 respectively.

The live-load distribution factors determined from the measured strains and those calculated per AASHTO (2012) are shown in in Table 4, and indicate that the AASHTO distribution factors are quite conservative. The distribution factor inferred for each girder was reduced by a minimum of 27% with respect to AASHTO for both two-truck and four-truck load-cases. As shown in Table 2, strain measured at the ends of the girders indicate that the central girder and one of the exterior girders experienced a small amount of unintended fixity as evidenced by the negative strains recorded near the abutments. Original design drawings indicate the presence of dowel bars attaching one abutment to the superstructure. These, along with friction between the superstructure and opposing abutment may contribute to this small, apparent fixity, among other effects.

Figure 10: Bridge 5489 General Condition

Table 2: Bridge 5489 Strains Recorded from Tests SBS_S_2_1 and MAX_S_2_1 with Corrections Noted

Girder	Location	SBS_S_2_1			MAX_S_2_1		
		Midspan	*Abutment 1*	*Abutment 2*	*Midspan*	*Abutment 1*	*Abutment 2*
		$\mu\varepsilon$	$\mu\varepsilon$	$\mu\varepsilon$	$\mu\varepsilon$	$\mu\varepsilon$	$\mu\varepsilon$
1	**Top**	-3.61	-	-	-5.50	-	-
	Center	9.85	-	-	16.8	-	-
	Bottom	11.5 / 23.3	-1.75	2.69	17.2 / 39.0	-3.64	5.10
2	**Top**	-6.90	-	-	-10.3	-	-
	Center	6.05 / 21.3	-	-	8.38 / 30.2	-	-
	Bottom	45.6	-	-	70.7	-	-
3	**Top**	-7.22	-	-	-16.9	-	-
	Center	20.1	-3.66	-	32.5	-7.22	-
	Bottom	21.9 / 47.4	0.537	-14.0	34.5 / 81.8	-5.92	-17.3
4	**Top**	-1.48	-	-	-12.3	-	-
	Center	21.1	-	-	34.2	-	-
	Bottom	14.7 / 43.6	-	-	24.5 / 80.6	-	-
5	**Top**	-5.30	-	-	-8.64	-	-
	Center	10.9	0.167	-	18.8	-0.892	-
	Bottom	-0.00 / 27.0	0.428	-2.68	-0.00 / 46.2	-17.3	-1.13

Table 3: Bridge 5489 Neutral Axis Depths

Girder	Uncracked NA Depth (in)	Cracked NA Depth (in)	Measured NA Depth (in)
1	23.8	17.2	26.7
2	15.7	13.0	35.7
3	15.7	13.0	25.3
4	15.7	13.0	26.5
5	23.8	17.2	25.7

Table 4: Bridge 5489 Distribution Factors

Girder	AASHTO DF	SBS_S_2_1		MAX_S_2_1	
		Measured DF	% Difference	Measured DF	% Difference
1	0.483	0.271	-55.1%	0.272	-43.7%
2	0.685	0.498	-27.3%	0.426	-37.8%
3	0.685	0.477	-30.4%	0.493	-28.0%
4	0.685	0.438	-36.1%	0.486	-29.1%
5	0.483	0.314	-35.0%	0.322	-33.3%

2.5.2 Hampden No. 5109

The bridge in Hampden, No. 5109 over Souadabscook Stream, is shown in Figure 11. Testing was conducted on August 2, 2018 with maximum applied load producing 91.8% of HL-93 flexural moment with impact. Strains recorded during testing are presented in Table 5. Where two values of strain are reported, the first value is the recorded strain, which was determined to be unreliable and inaccurate due to its magnitude being grossly inconsistent with that of other similarly loaded girders and other strains measured over the section depth. The second value of strain was calculated using the other strains recorded in the same section and assuming linear strain distribution. By comparing the recorded strains at the bottom of the girders it was determined that none of the girders had experienced significant flexural cracking throughout their service life and also did not crack during testing. Further evidence for uncracked behavior is provided by the measured neutral axis depths presented in Table 6, which shows that for each of the girders the inferred neutral axis depths were well below those expected for an uncracked section.

The rating factors computed based on the AASHTO (2011, 2012) are 0.686 and 1.59 for the interior and exterior girders respectively. Through testing, the interior and exterior rating factors were able to be increased to 0.942 and 3.78. It should be noted that in the initial calculation of girder capacity, the wearing surface and curbs were included and assumed to act compositely with the superstructure despite having been added to the structure years after its original construction. Design drawings for the replacement indicated that the new curbs would be anchored to the

exterior girders with grouted rebar and that the new concrete wearing surface would be bonded to the deck. These specifications justified the assumption of composite action.

The live-load distribution factors determined per AASHTO as well as those experimentally determined from measured strains are given in Table 7. As is apparent, the AASHTO predicted distribution factors are conservative. This conservatism is greatest for the exterior girders with decreasing conservatism as toward the center girder. From the strains reported in Table 5 near the girder ends, it can be seen that some unintended fixity was experienced in the central girder. This is evidenced by the negative strains recorded at the girder's bottom. Original design drawings indicate that dowel bars were specified to connect interior girders with the Western abutment. These dowel bars are likely the source of some of this apparent fixity.

Figure 11: Bridge 5109 General Condition

Table 5: Bridge 5109 Strains from Tests SBS_S_2_1 and MAX_S_2_1 with Corrections Noted

Girder	Location	SBS_S_2_1			MAX_S_2_1		
		Midspan	*Abutment 1*	*Abutment 2*	*Midspan*	*Abutment 1*	*Abutment 2*
		με	*με*	*με*	*με*	*με*	*με*
1	**Top**	-0.083	-	-	-0.638	-	-
	Center	8.04	-	-	14.3	-	-
	Bottom	20.7	-4.10	-0.01	34.5	-3.92	1.57
2	**Top**	7.09	-	-	-1.59	-	-
	Center	7.80 / 27.7	-	-	11.2 / 33.7	-	-
	Bottom	48.2	-	-	68.9	-	-
3	**Top**	-6.78	-	-	-3.75	-	-
	Center	21.9	-4.79	-	30.9	-12.6	-
	Bottom	57.1	-10.7	-14.4	90.5	-22.8	-19.3
4	**Top**	-1.57	-	-	0.270	-	-
	Center	0 / 20.8	-	-	0 / 35.8	-	-
	Bottom	43.2	-	-	71.3	-	-
5	**Top**	-0.588	-	-	-0.361	-	-
	Center	2.52	0.603	-	4.10	-3.57	-
	Bottom	7.10	0.207	-	11.2	-5.40	-

Table 6: Bridge 5109 Neutral Axis Depths

Girder	Uncracked NA Depth (in)	Cracked NA Depth (in)	Measured NA Depth (in)
1	24.1	15.5	28.7
2	19.5	11.8	34.3
3	19.5	11.8	25.4
4	19.5	11.8	33.4
5	24.1	15.5	26.4

Table 7: Bridge 5109 Distribution Factors

Girder	AASHTO DF	Two Trucks		Four Trucks	
		Measured DF	% Difference	Measured DF	% Difference
1	0.506	0.283	-44.1%	0.300	-40.7%
2	0.686	0.526	-23.3%	0.479	-30.2%
3	0.686	0.623	-9.18%	0.629	-8.31%
4	0.686	0.471	-31.3%	0.495	-27.8%
5	0.506	0.093	-81.6%	0.097	-80.8%

2.5.3 Unity No. 2390

The bridge in Unity, No. 2390 over the Sandy Stream, is shown in Figure 12. Testing was conducted on August 7, 2018 with maximum applied load producing 93.2% of HL-93 moment with impact. This was the largest percentage of HL-93 moment with impact applied to any of the bridges tested. This led to relatively large recorded strains, as shown in Table 8. Where two values of strain are reported, the first value is the recorded strain, which was determined to be unreliable and inaccurate due to its magnitude being grossly inconsistent with that of other similarly loaded girders and other strains measured over the section depth. The second value of strain was calculated using the other strains recorded in the same section and assuming linear strain distribution. Rating factors determined per AASHTO (2011, 2012) equaled 0.757 and 1.05 for interior and exterior girders respectively.

In contrast to other bridges investigated, some of the neutral axis depths inferred from recorded strains indicate either partially or fully cracked behavior, as seen in Table 9. However, the strains recorded at midspan at the sections' bottoms were still below those expected for an uncracked section, suggesting that the sections indeed behaved as though they remained uncracked. Because of this behavior, the interior and exterior rating factors could be increased to 0.838 and 1.15 respectively. A contributing factor to this bridge's lower rating factors is the very thick (~5 in.) asphalt overlay. The thickness of this overlay is seen in Figure 13 which shows a drainage opening. This layer could not be assumed to add to the section's capacity and so only added additional non-structural dead-load.

The live-load distribution factors determined per AASHTO as well as those experimentally determined from measured strains are given in Table 10. These results suggest that AASHTO's distribution factors are conservative for exterior girders and non-central interior girders, but are relatively accurate for the central girder. This is true for both two-truck and four-truck load-cases. The strains recorded in Table 8 indicate that significant fixity was experienced in the central girder. This is evidenced by the relatively large negative strains recorded at the bottom of this girder near the abutments. This unintended fixity is likely due in part to dowel bars specified in the original design drawings which attach the interior girders to the West abutment.

Figure 12: Bridge 2390 General Condition

Figure 13: Thick Asphalt Overlay

Table 8: Bridge 2390 Strains from Tests SBS_S_2_1 and MAX_S_2_1 with Corrections Noted

Girder	Location	SBS_S_2_1			MAX_2_S_1		
		Midspan	*Abutment 1*	*Abutment 2*	*Midspan*	*Abutment 1*	*Abutment 2*
		με	*με*	*με*	*με*	*με*	*με*
1	**Top**	0.920	-	-	-1.98	-	-
	Center	8.89	-	-	15.4	-	-
	Bottom	29.9	0.355	-4.11	50.4	-10.9	-19.6
2	**Top**	-5.77	-	-	-12.0	-	-
	Center	19.3	-	-	24.7	-	-
	Bottom	66.1	-	-	83.1	-	-
3	**Top**	-3.76	-	-	-4.65	-	-
	Center	34.5	-4.68	-	41.3	-5.96	-
	Bottom	97.5	-20.9	-29.2	117	-26.7	-36.8
4	**Top**	-9.21	-	-	-8.96	-	-
	Center	32.5	-	-	40.8	-	-
	Bottom	22.9 / 74.2	-	-	30.3 / 90.6	-	-
5	**Top**	-0.067	-	-	-0.923	-	-
	Center	14.4	-	-	25.6	-	-
	Bottom	9.31 / 28.9	-0.009	-	13.4 / 52.2	4.54	-

Table 9: Bridge 2390 Neutral Axis Depths

Girder	Uncracked NA Depth (in)	Cracked NA Depth (in)	Measured NA Depth (in)
1	22.1	13.9	16.9
2	14.5	8.60	17.1
3	14.5	8.60	15.5
4	14.5	8.60	12.0
5	22.1	13.9	10.2

Table 10: Bridge 2390 Distribution Factors

Girder	AASHTO DF	SBS_S_2_1		MAX_S_2_1	
		Measured DF	**% Difference**	**Measured DF**	**% Difference**
1	0.428	0.196	-54.2%	0.250	-41.9%
2	0.635	0.449	-29.3%	0.427	-32.8%
3	0.635	0.662	4.25%	0.599	-5.67%
4	0.635	0.504	-20.6%	0.465	-26.8%
5	0.428	0.190	-55.6%	0.259	-39.5%

2.5.4 *Atkinson No. 2879*

The bridge in Atkinson, No. 2879 over the Piscataquis River, is shown in Figure 14. Testing occurred on August 9, 2018 with maximum applied load producing 92.4% of HL-93 live-load

moment with impact. This bridge was unique in that it consisted of four simple spans, each with supported by four girders. Only the Eastern, interior span was tested and so results may or may not be applicable to other spans. Rating factors determined per AASHTO (2011, 2012) were 1.09 and 2.57 for interior and exterior girders respectively, making it the only bridge investigated with an operating rating factor above 1.0. The strains recorded during testing are presented in Table 11 for two-truck and four-truck loadings. Intuitively, it would appear that the strains presented at midspan at the bottom of girders 3 and 4 have been switched, with the reading of one being valid for the other and vice-versa. However, no definitive evidence was found to support this and so it was assumed that the recorded strains were correct. Regardless, recorded strains were consistently lower than predicted for an uncracked section, suggesting that the section behaved as uncracked. This is further evidenced by the inferred neutral axis depths shown in Table 12, which show that inferred neutral axis depths were close to or below predicted neutral axis locations for uncracked sections. These conditions allowed interior and exterior rating factors to be increased to 1.35 and 2.76 respectively.

The live-load distribution factors determined per AASHTO as well as those experimentally determined from measured strains are given in Table 13. These distribution factors were lower than those predicted by AASHTO, but to a smaller degree than was seen on other bridges. This suggests that AASHTO may be less conservative for bridges with four girders rather than five. From the consistently positive girder end strains reported in Table 11, no unintended fixity was measured during testing for this particular span.

Figure 14: Bridge 2879 General Condition

Table 11: Bridge 2879 Strains from Tests SBS_S_2_1 and MAX_S_2_1

		SBS_S_2_1			MAX_S_2_1		
		Midspan	*Abutment 1*	*Abutment 2*	*Midspan*	*Abutment 1*	*Abutment 2*
Girder	*Location*	*με*	*με*	*με*	*με*	*με*	*με*
1	**Top**	-6.40	-	-	-8.76	-	-
	Center	7.38	-	-	14.4	-	-
	Bottom	34.6	6.28	3.46	56.4	8.77	7.67
2	**Top**	-8.84	-	-	-11.6	-	-
	Center	16.2	0.136	-	24.5	-0.858	-
	Bottom	45.5	9.19	1.49	65.5	8.16	8.37
3	**Top**	-5.32	-	-	-9.65	-	-
	Center	17.9	4.73	-	27.6	2.70	-
	Bottom	35.8	6.89	-0.103	54.9	5.69	7.73
4	**Top**	-4.04	-	-	-7.29	-	-
	Center	8.20	-	-	15.0	-	-
	Bottom	39.9	7.96	-	65.5	11.0	-

Table 12: Bridge 2879 Neutral Axis Depths

Girder	Uncracked NA Depth (in)	Cracked NA Depth (in)	Measured NA Depth (in)
1	28.5	18.3	28.2
2	21.4	13.2	33.5
3	21.4	13.2	42.2
4	28.5	18.3	27.2

Table 13: Bridge 2879 Distribution Factors

Girder	AASHTO DF	SBS_S_S_2_1		MAX_S_S_2_1	
		Measured DF	% Difference	Measured DF	% Difference
1	0.498	0.377	-24.3%	0.397	-20.3%
2	0.701	0.662	-5.56%	0.621	-11.4%
3	0.701	0.526	-25.0%	0.521	-25.7%
4	0.498	0.435	-12.7%	0.461	-7.43%

2.5.5 Columbia No. 3848

The bridge in Columbia, No. 3848 over Western Little Stream, is shown in Figure 15. Testing occurred on August 28, 2018 with maximum applied load producing 80.9% of HL-93 moment with impact. Rating factors determined per AASHTO (2011, 2012) equaled 0.887 and 1.41 for interior and exterior girders respectively. Strains measured during two-truck and four-truck load-cases are given in Table 14. Where two values of strain are reported, the first value is the recorded strain, which was determined to be unreliable and inaccurate due to its magnitude being grossly inconsistent with that of other similarly loaded girders and other strains measured over the section

depth. The second value of strain was calculated using the other strains recorded in the same section and assuming linear strain distribution. Strains measured at girder bottoms were consistently smaller than would be predicted with an uncracked section, suggesting the girders behaved as uncracked. This behavior is supported by the inferred neutral axis depths, which indicate uncracked behavior for all girders as seen in Table 15. Based on these conditions, the interior and exterior flexural rating factors could be increased to 1.15 and 2.20 respectively.

The live-load distribution factors determined per AASHTO as well as those experimentally determined from measured strains are given in Table 16. Unexpectedly, significantly more load was distributed to one of the non-central interior girders (girder 4) than to other interior girders, specifically the heavily loaded center girder. The reason for this anomaly is not immediately apparent, however the strain recorded was still smaller than was expected for an uncracked section and so the outlyer status should not be cause for concern. A small amount of fixity was experienced in the central girder, as is shown by the negative strains reported in Table 14. This may be partially due to dowel bars, which were designed to connect the interior girders with one of the abutments.

Figure 15: Bridge 3848 General Condition

Table 14: Bridge 3848 Strains from Tests SBS_S_2_1 and MAX_S_2_1 with Corrections Noted

Girder	Location	SBS_S_2_1			MAX_S_2_1		
		Midspan	*Abutment 1*	*Abutment 2*	*Midspan*	*Abutment 1*	*Abutment 2*
		$\mu\varepsilon$	$\mu\varepsilon$	$\mu\varepsilon$	$\mu\varepsilon$	$\mu\varepsilon$	$\mu\varepsilon$
1	**Top**	0.503	-	-	-2.54	-	-
	Center	9.94	-	-	22.1	-	-
	Bottom	28.4	1.22	5.96	53.6	6.16	8.78
2	**Top**	-7.58	-	-	-7.66	-	-
	Center	21.5	-	-	31.2	-	-
	Bottom	55.9	-	-	74.2	-	-
3	**Top**	-5.67	-	-	-5.98	-	-
	Center	27.5	-3.19	-	36.2	-1.83	-
	Bottom	53.0	-8.60	-14.7	72.2	0.600	-13.6
4	**Top**	-5.51	-	-	-4.76	-	-
	Center	-0.00 / 32.5	-	-	-0.00 / 36.5	-	-
	Bottom	70.6	-	-	77.8	-	-
5	**Top**	-0.132	-	-	-0.262	-	-
	Center	12.5	-	-	16.0	-	-
	Bottom	30.3	12.9	-	39.0	19.5	-

Table 15: Bridge 3848 Neutral Axis Depths

Girder	Uncracked NA Depth (in)	Cracked NA Depth (in)	Measured NA Depth (in)
1	19.8	12.7	20.9
2	12.9	7.6	20.4
3	12.9	7.6	25.9
4	12.9	7.6	25.4
5	19.8	12.7	20.8

Table 16: Franklin No. 3307 Distribution Factors

Girder	AASHTO DF	SBS_S_2_1		MAX_S_2_1	
		Measured DF	% Difference	Measured DF	% Difference
1	0.431	0.239	-44.5%	0.339	-21.3%
2	0.611	0.469	-23.2%	0.468	-23.4%
3	0.611	0.444	-27.3%	0.455	-25.5%
4	0.611	0.593	-2.95%	0.491	-19.6%
5	0.431	0.255	-40.8%	0.247	-42.7%

2.6 Conclusions from NDLLT of Skewed T-Beam Bridges

Analyses of the tested bridges are described in detail in Section 2. In general, calculations were based on mechanics of materials principles and AASHTO (2011, 2012) code requirements.

Overall, a high percentage of HL-93 loading with impact was applied to the structures. In all cases, the maximum applied moment was at above 70% of HL-93 service moment with impact, which is required to justify rating factor increases per AASHTO. Numerically, this translates to a test-understanding factor, K_b equal to 0.5 for all bridges, which effectively reduces the measured benefit by 50%. Because measured strains were invariably smaller than those predicted, all test benefit factors, K_a were greater than zero, and all rating factors could be increased based on measure strains.

Live-load distribution factors inferred from the test data showed reasonable agreement with AASHTO-recommended values, although the AASHTO values are nearly always conservative. The maximum differences between values inferred from the tests and values computed per AASHTO were generally seen for exterior for each of the bridges. Assuming a concrete compressive strength of 5 ksi (which conservatively reduces the predicted strains under loading relative to those resulting from the AASHTO specified 2.5 ksi), all bridges exhibited uncracked behavior under maximum applied moment. This was generally supported by the calculated neutral axis depths which were often much lower in the section than would be computed for a theoretical uncracked section.

The test results and analyses presented here justify significant increases in the rating factors for four of the five bridges according to AASHTO *(2011)*. The average increase in HL-93 flexural operating rating factors for the critical interior girders of all bridges was 28.3%, with minimum and maximum increases of 10.7% and 40.2% respectively. All rating factor increases have been calculated based on the assumption that the observed results cannot be confidently extrapolated to loads of 30% beyond that produced by HL-93 load with impact, largely due to uncertainty of uncracked section behavior at higher loads. The controlling operating flexural rating factor could be increased to 1.0 or greater for HL-93 loading with impact for Bridges 5489, 2879, and 3848, indicating that they are sufficient for such loading. The controlling rating factors for Bridges 5109 and 2390 were unable to be raised above 1.0, using the noted conservative assumptions.

3   Comparison of Skewed and Un-skewed Bridge Response

3.1   *Description of Un-skewed Bridges*

Characteristics of the five un-skewed bridges tested previously in the summer of 2017 are given below in Table 17. These bridges were subjected to similar loads to those applied to the skewed bridges in this project, and were instrumented in the same manner. Prior to live-load testing, these bridges' operating flexural *RFs* ranged between 0.24 and 1.12, but based on the results of testing were increased to between 0.30 and 1.95, bringing the controlling *RF* of four of the five bridges above 1.0.

Table 17: Un-Skewed Bridge Characteristics (tested in 2017)

Bridge	Canton	Peru	Jackson	Alna	Franklin
Number	3356	5432	3776	2130	3307
Year Built	1936	1950	1941	1939	1941
Span - Center to Center of Bearings (feet)	27.50	40.50	31.00	27.00	43.08
Number of Girders	6	5	5	4	5
Girder Spacing (in)	67.5, 59.5	76	68.63	72,70	68.75
Total depth (in)	28.00	35.75	30.50	33.00	31.00
Girder web thickness (in)	18.5, 14	20.0	19.5	16,12	19
Slab Thickness (in)	6.50	5.75	5.50	8.00	5.75

Initially, linearly elastic, solid FE models were developed for each structure to aid in response comparisons. Following this, the strains recorded during NDLLT of all bridges were examined to determine any possible differences in the behavior of skewed RC T-beam bridges relative to similar un-skewed bridges. This required comparing the strains recorded within individual girders for similar tests of bridges, as well as comparing bridges' responses under different load-cases. These comparisons led to the identification of two specific differences in behavior between the types of bridges which will be explained in detail. The results of the linear FE models were then examined to better understand these behaviors and how skewness could contribute to them.

3.2   Linear Finite Element Model Development

To enhance the understanding of bridge behavior observed from live-load testing, linear, 3-D FE models were generated of each bridge which simulated the conditions of each test. These models were highly detailed, incorporating many of the features present in the real bridges that may affect live-load response, including discrete reinforcing steel, composite curbs and wearing surfaces, and railings. These models were first built with their respective bridge's nominal geometric and material parameters, and then were systematically calibrated such that they adequately predicted the real bridges' responses to loading.

Modeling and analysis were performed using the commercial FE software ABAQUS (n.d.) due to the authors' familiarity with its use and its availability. The components of bridges made from concrete were modeled as isotropic, elastic continua using C3D20R 20-node, quadratic, brick elements with three degrees of freedom per node and reduced integration. These elements are able to yield accurate results with a coarser mesh than similar, linear continuum elements. In general, all concrete components that could reasonably be assumed to contribute to a bridge's stiffness were modeled, including girders, deck, diaphragms, curbs, railings, and integral wearing surfaces. Reinforcing steel was explicitly modeled as isotropic, elastic beams using B32 quadratic, three-node beam elements with six degrees of freedom per node. All significant reinforcing bars, including girder longitudinal reinforcement, shear stirrups, and deck longitudinal and transverse reinforcement were modeled and kinematically tied to the concrete elements with embedment constraints. Typically, a model consisted of between 100,000 and 300,000 elements with 500,000

to 1,000,000 nodes and 1,000,000 to 3,000,000 degrees of freedom. For illustration, a model of Bridge No. 2390 is given in Figure 16.
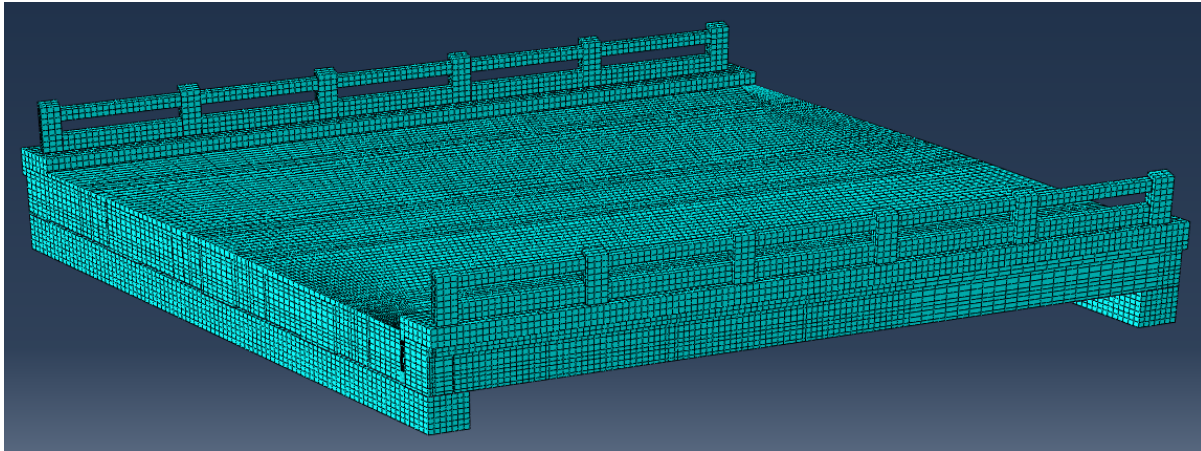
Figure 16: Meshed 3D Liner Model of Bridge 2390

Load was applied to mimic the loading from trucks during testing while also accounting for the bridge's initial dead-load conditions. To simulate the effects of dead-loading and test live-loading independently, load was applied in two separate load-steps with the effects of subsequent steps adding to the effects of previous steps. In the first load-step, gravitational dead-load was applied by assigning concrete elements a unit weight of 150 lb/ft^3 and subjecting the entire model to a unit, downward gravitational field. The dead-load contributions from nonstructural components (for instance bituminous concrete wearing surfaces) were applied as pressure loads across the area of the superstructure over which they acted. In the live-load step, the test trucks' wheel weights were assumed to act uniformly over their tire contact areas and so were applied to the models as pressure loads. These pressure loads were distributed over areas corresponding to tire contact area, which were in turn located on the model in the locations measured during testing.

Boundary conditions were enforced to reasonably approximate the conditions of the real bridges. None of the bridges used true pin or roller type bearings. Instead, most were designed such that one end rested on the abutment with a layer of roofing felt between the girder and support, and the other rested on flat, bronze or steel expansion bearings. Additionally, the "pinned" side (the side without the expansion bearing) was often connected to the abutment with steel dowels embedded into both the foot of the girders and the top of the abutment. To emulate these conditions, rigid abutments were modeled upon which the bridge sat, with a frictionless contact condition enforced between them. This reasonably approximated the conditions of the actual bridge much better than would ideal displacement boundary conditions. Where present, the dowel rods were explicitly modeled and embedded within both the superstructure and rigid abutment. This prevented instability due to transverse rigid body motion and rotation of the superstructure. Where dowel rods were not present, minimally restrictive displacement restraints were added to prevent rigid body displacements and rotations.

After all the models were constructed, they were calibrated such that their predicted strains agreed reasonably well with measured strains. Being that the models were perfectly linearly elastic, the models' responses could be reasonably controlled by altering their stiffnesses. This allowed calibration to be controlled by changing the elastic modulus of the concrete components of the models. In nearly all cases, the uncalibrated models predicted much larger strains than were measured in the field. This indicated that the models were not stiff enough and that increases to the concrete's elastic modulus in some or all of the concrete components would likely bring predictions better into line with measurements. This is justifiable given that concrete's elastic modulus was assumed proportional to the square root of compressive strength (per AASHTO, 2012) and that previous studies of older bridges have shown the in-situ concrete compressive strengths of older bridges to be up to 220% greater than the design compressive strength (for instance Saraf (1998), Buckle et al. (1985)). Models' concrete elastic moduli were systematically updated and simulations rerun until the moduli giving the best predictions were obtained for each bridge. These models could then be further examined to investigate observed behavioral differences between un-skewed and skewed bridges.

3.3 Assessment of Load Distribution

A major point of interest when analyzing bridge structures is the way in which live-loads applied to the deck are distributed to individual girders. This has a significant impact on a bridge's *RF* – the primary measure of its live-load capacity and ability to carry modern loads – as live-load distribution directly scales the demand placed on a particular girder from a given load. Therefore, gaining a better understanding of a bridge's live-load distribution characteristics is instrumental to understanding its overall behavior and live-load capacity. It should be noted that the load distribution properties discussed here are related to, but not the same as, distribution factors (*DFs*) as defined by AASHTO (2012) for design and analysis. *DFs* represent the maximum fraction of HL-93 live-load that can be carried by any individual girder from all possible live-loading scenarios. The fractions of live-load discussed here, termed girder lane fractions (*GLFs*), describe the portion of live-load carried by a particular girder under one specific loading condition. However, due to the narrow, two-lane geometry of these simple-span bridges, and the fact that multiple load-cases were applied in the field where trucks were shifted both longitudinally and transversely, the maximum *GLFs* derived from testing are expected to be very good approximations of the true girder *DFs*. Therefore, comparison between the *GLFs* and AASHTO *DFs* as presented later is appropriate.

GLFs, whether from live-load testing or FE analysis, are calculated by Equation 8, where $S_{i,j}$ is the uncracked section modulus of the ith or j^{th} girder, $\varepsilon_{i,j}$ is the measured or calculated strain in the ith or j^{th} girder, n is the total number of girders, and the 2 in the numerator indicates that two lanes of loading were applied in the load-cases considered.

$$GLF_i = \frac{2S_i\varepsilon_i}{\sum_{j=1}^{n} S_j\varepsilon_j}$$

GLFs were calculated from a set of three tests in which the applied loading was the same but the loads were placed in separate transverse positions (for instance, three tests in which four trucks were located longitudinally to produce maximum midspan moment but transversely close to the left curb, centerline, and right curb respectively). These were then examined to observe the particular bridges' sensitivity to transverse load position. To illustrate this, an example from an un-skewed bridge (Bridge 3307) and skewed bridge (Bridge 5489) are presented in Figures 17 and 18 respectively, with similar plots of seven of the remaining bridges presented in Figures 123-129 in Appendix A. (Note that because a set of three similar longitudinal but differing transverse loading tests were not performed for Bridge 3356, no plot was included.)
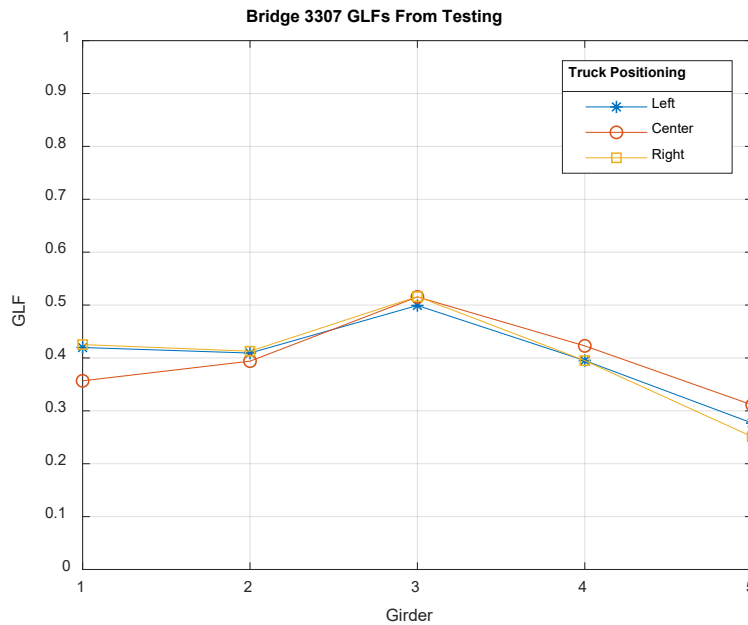
Figure 17: *GLFs* Calculated from Live-Load Testing – Bridge 3307 (Un-Skewed)
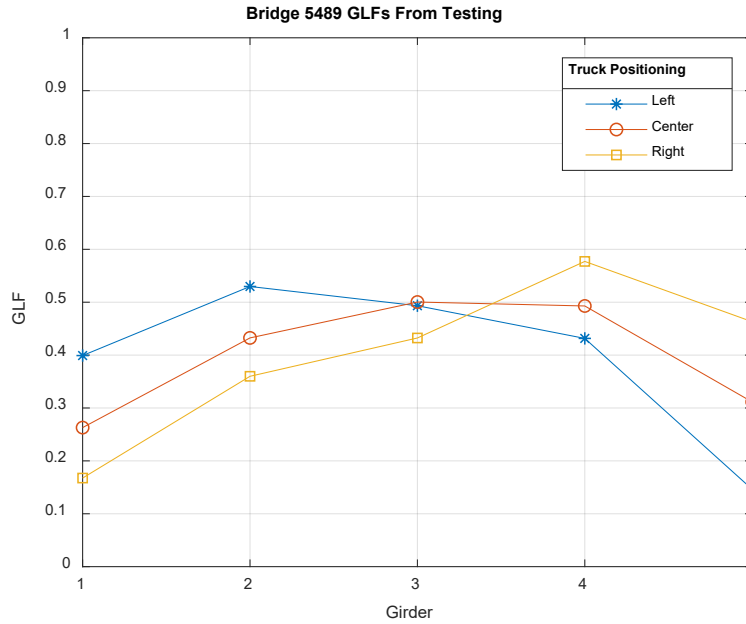
Figure 18: *GLFs* Calculated from Live-Load Testing – Bridge 5489 (Skewed)

GLFs calculated for these sets of tests appear to indicate a correlation between skewness and a bridge's sensitivity to load position. As seen from Figure 17, movement of trucks transversely from the left side of Bridge 3307 to the center and then to the right side had very small effects on individual girders' *GLF*. The opposite is true for Bridge 5489 as seen in Figure 18, where transverse movement of loads resulted in large changes of *GLF*, especially for exterior girders. Table 18 presents the difference between maximum and minimum calculated *GLF* for each girder of each bridge from the three, 4-truck load-cases.

Table 18: Maximum Change in *GLF* from Live-Load Testing

Bridge	Skew Angle (deg)	Change in *GLF*				
		Girder 1	Girder 2	Girder 3	Girder 4	Girder5
2130	0	0.018	0.054	0.039	0.102	-
3307	0	0.069	0.019	0.017	0.028	0.060
3776	0	0.118	0.098	0.009	0.071	0.142
5432	0	0.090	0.074	0.029	0.046	0.088
2390	30	0.110	0.088	0.039	0.070	0.162
2879	30	0.143	0.084	0.052	0.175	-
3848	30	0.157	0.098	0.051	0.084	0.119
5109	35	0.282	0.195	0.063	0.291	0.130
5489	15	0.232	0.170	0.068	0.146	0.317

As can immediately be seen, the skewed bridges tended to display much larger changes in GLF than un-skewed bridges under similar load configurations. Additionally, the largest changes in *GLF* tended to occur in exterior girders, while smaller changes tended to occur in the central

girders. The large changes in load distribution of skewed bridges as compared with un-skewed bridges is likely due in part to differences in available load-path. In un-skewed bridges, a load applied at the center (longitudinally and transversely) of the deck is equidistant to each of the four corners of the bridge and so, all else being equal, load will be attracted evenly by both ends longitudinally, and at each end, load would be attracted to supports symmetrically about the transverse centerline. Conversely, in a skewed bridge, the same load is closer to the obtuse corners than to the acute corners, and so the load-path will tend to favor the obtuse side much more heavily.

To investigate whether differences in load-path could contribute to the differences in load distribution between un-skewed and skewed bridges, the results of the linear FE models were examined, paying attention to the live-load reactions at each end of each girder under load from the three tests with differing transverse truck placement. This revealed the percentage of load attracted to each end of the bridge as well as the amount of load attracted by each girder for the same levels of loading placed in three transverse positions across the deck. Figures 19 and 20 show the reaction forces calculated for each support of Bridge 5432 (an un-skewed bridge) as fractions of the total load attracted by each end, and Figures 21 and 22 show the reaction forces calculated for each support of Bridge 3848 (a skewed bridge), also as fractions of the load attracted by each end. Similar plots for the other bridges (again with the exception of Bridge 3356) are presented in Figures 130-143 in Appendix A.
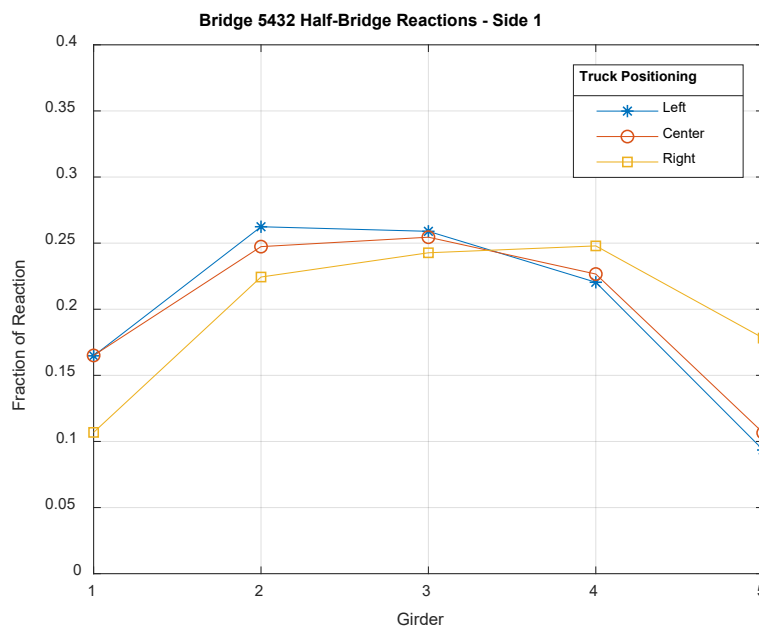
Figure 19: Fractions of Reaction Force Attracted to Each Support at Side 1 – Bridge 5432 (Un-Skewed)
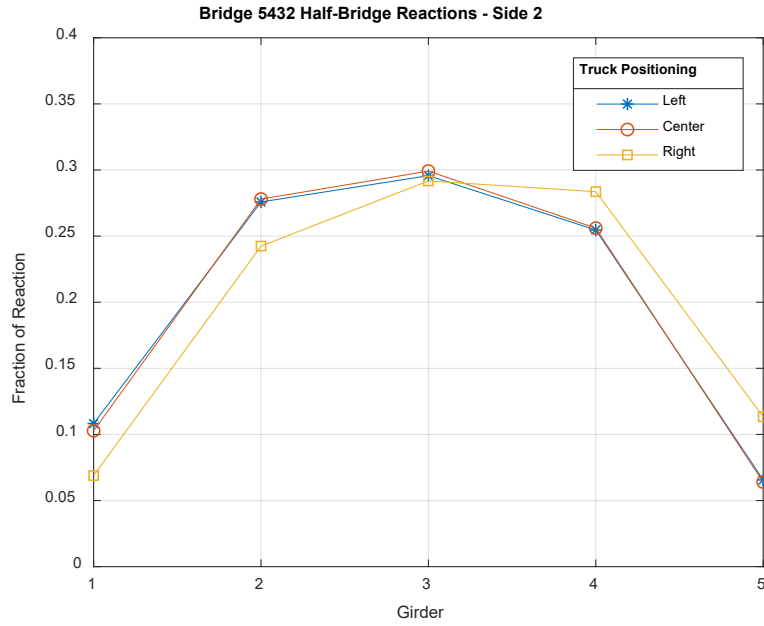
Figure 20: Fractions of Reaction Force Attracted to Each Support at Side 2 – Bridge 5432 (Un-Skewed)
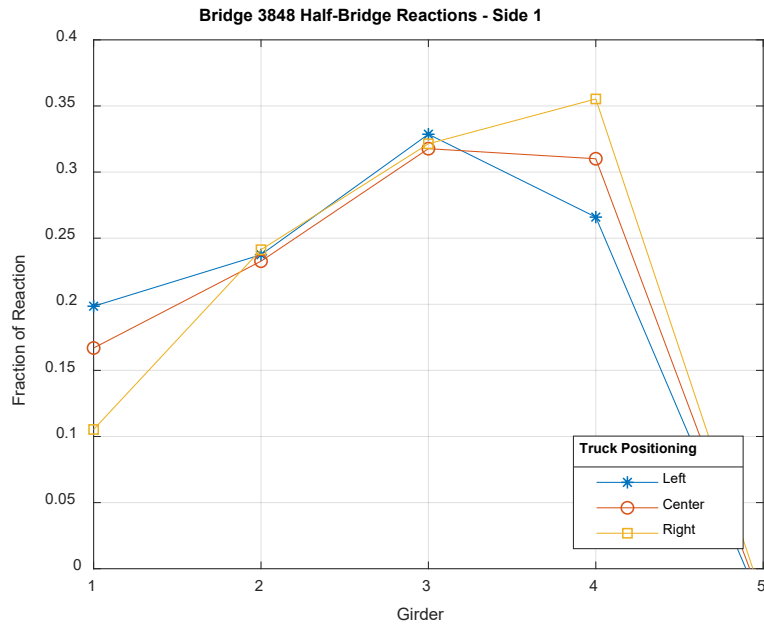
Figure 21: Fractions of Reaction Force Attracted to Each Support at Side 1 – Bridge 3848 (Skewed)
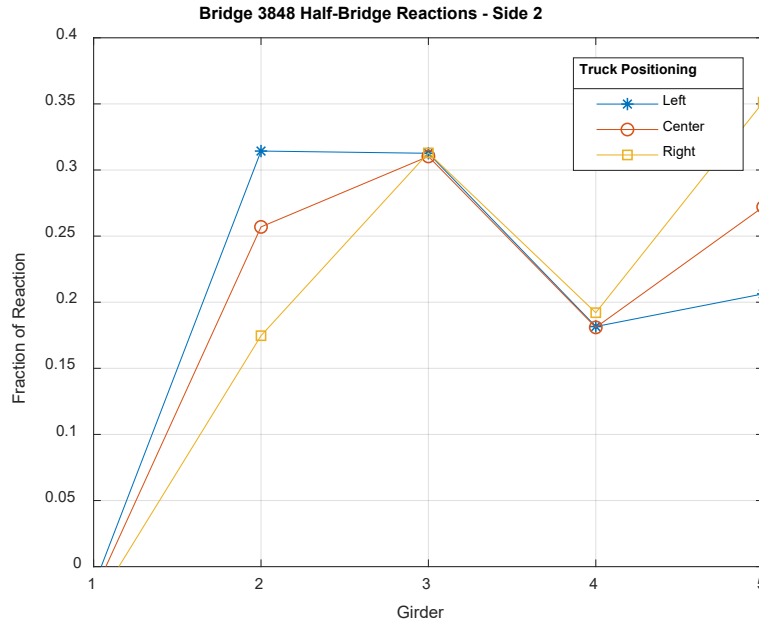
Figure 22: Fractions of Reaction Force Attracted to Each Support at Side 2 – Bridge 3848
(Skewed)

Figures 19 and 20 show that the support reactions are roughly consistent with those expected for the un-skewed bridge: reactions are reasonably symmetric about the transverse centerline with a small amount of offset due to the different weights of the trucks used and their transverse positions. On the other hand, Figures 21 and 22 show very different behavior. For each end of Bridge 3848, one transverse side attracts significantly more load than the other does. The preferred side corresponds with the lateral side with the obtuse corner for each longitudinal end. It should also be noted that the reactions at the acute corners are negative for live-loading, meaning that the loading caused a lessening of the reaction due to dead-load. This behavior is consistent with the assumption that the bridge's load-path is significantly affected by the load's proximity to the obtuse corner. This could partially explain why the skewed bridges' load distributions appear to be more sensitive to transverse load placement as loads closer to one side of the bridge will be much more heavily attracted to the obtuse corner.

3.4   Comparison with AASHTO Live-Load Distribution Factors

As noted before, the *GLF*s inferred from the results of live-load testing and calculated based on results of FE analyses are related to AASHTO (2012) *DF*s in that they describe the distribution of loads to individual girders, but are valid only for the loading configuration from which they were inferred or calculated. However, the tested bridges were relatively narrow, allowing the three transverse loading positions considered to capture the effects of most possible transverse loading conditions. This allows flexural *DF*s to be reasonably approximated as the maximum *GLF*s from any interior and exterior girder inferred or calculated for each bridge. Table 19 presents the

AASHTO calculated *DF*s and *DF*s approximated from testing and FEA for each bridge (with the exception of Bridge 3356).

Table 19: Comparison of AASHTO *DF*s and Approximate *DF*s

Bridge	Skew (°)	AASHTO *DF*		Max *GLF* from Testing		Max *GLF* from FEA	
		Interior	*Exterior*	*Interior*	*Exterior*	*Interior*	*Exterior*
2130	0	0.707	0.485	0.870	0.351	0.808	0.315
3307	0	0.600	0.432	0.516	0.425	0.506	0.358
3776	0	0.635	0.396	0.579	0.439	0.471	0.484
5432	0	0.680	0.473	0.522	0.382	0.474	0.387
2390	30	0.635	0.428	0.629	0.325	0.560	0.411
2879	30	0.701	0.498	0.660	0.543	0.642	0.499
3848	30	0.611	0.431	0.528	0.440	0.526	0.460
3848	35	0.686	0.506	0.646	0.440	0.531	0.567
5489	15	0.685	0.483	0.577	0.463	0.491	0.495

As Table 19 shows, nearly all of the AASHTO interior girder *DF*s were conservative, whereas more than half the AASHTO exterior *DF*s were unconservative relative to the approximate *DF*s from testing and/or FEA. For the skewed bridges, two exterior AASHTO *DF*s were unconservative relative to the *GLFs* from field-testing, as compared to one unconservative *DF* for the un-skewed bridges. To examine whether a trend exists, the percent error in approximate *DF*s relative to AASHTO *DF*s were calculated and are plotted in Figure 23. In these plots, a negative percent error represents a conservative estimation of *DF* by AASHTO and a positive percent error represents an unconservative estimation. These plots do not show a clear trend in *DF* prediction accuracy with increasing angle of skew, suggesting that such a correlation may not exist.
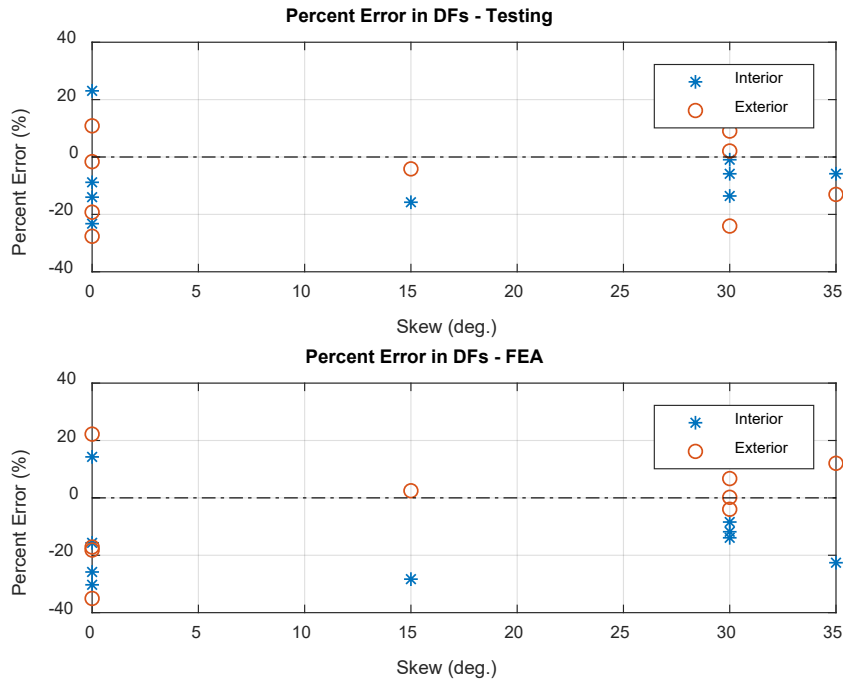
Figure 23: Percent Error in Approximate *DF*s Relative to AASHTO *DF*s

3.5 *Assessment of Support Fixity*

Support conditions play a vital role in a bridge's behavior – especially as pertains to the level of strain to which a girder is subjected (and thus the resulting midspan moment). Although many bridges (including all of the bridges investigated as part of this study) are designed to behave as simply-supported, actual conditions can result in a certain amount of bearing fixity that affects their behavior. This fixity can be caused by numerous factors, and can often be detected through live-load testing as negative strains recorded close to the girder supports.

Along with the transducers used to detect strains at midspan, some girders of each bridge were instrumented at their ends to monitor unintended fixity. At a minimum, for the instrumented girders, one transducer was applied to the girder's bottom at around one web-depth from the abutment face, although some also received a second transducer at the girder's mid-height with the same longitudinal position. The bottom-mounted transducers recorded the maximum negative or positive strain response at the girder's end depending on whether or not the girder experienced fixity, with large negative strains indicating a significant degree of unintended fixity. Table 20 presents the average, maximum, and minimum strains measured at the bottom of the ends of each girder for each bridge under 4-truck loading.

Table 20: Recorded Strains at Girder Ends from Live-Load Testing

Bridge	Skew Angle (deg.)	Average Strain (με)	Maximum Strain (με)	Minimum Strain (με)
2130	0	2.27	8.12	-2.88
3307	0	-0.43	7.62	-7.17
3356	0	6.21	13.73	-3.13
3776	0	6.39	13.14	1.55
5432	0	4.51	14.88	-5.13
2390	30	-15.50	1.24	-36.77
2879	30	7.89	11.04	5.69
3848	30	3.43	4.61	-22.82
5109	35	-10.33	4.61	-22.82
5489	15	-5.83	8.01	-24.19

The strains measured at the bottoms of girders near bearings were small relative to the maximum strains recorded at midspan. However, relative to each other the data recorded for skewed and un-skewed bridges show very different behavior. For all of the un-skewed bridges, the recorded strains were generally positive or at most only slightly negative indicating little to no fixity. The direct opposite is true for four of the skewed bridges. Relatively large negative strains were recorded from four of the five skewed bridges, indicating a high degree of support fixity, which likely reduced the strains recorded at midspan. Determining the sources of this fixity was important to determining its future reliability.

It was initially attempted to identify the sources of the skewed bridges' apparent fixity as part of the model calibration process. However, this strategy proved ineffective. The method used to reach better predictions of actual behavior – changing the elastic moduli of all or individual girders – improved the prediction of midspan strains, but could not produce negative girder end strains since it did not affect loading or support conditions. Adding fixity at the supports – either by enforcing additional boundary conditions or by applying resistance in the form of linear spring elements to the girder ends – tended to moderately improve the prediction of strains at girder ends, but was severely detrimental to the prediction of midspan strains. Because of this, it was decided to ignore girder end strains in the calibration process in order to better predict midspan strains, as these were deemed more important to accurately predict.

With end fixity ignored, calibration of the skew bridge models commenced as described previously with the models analyzed under the load conditions from live-load testing. However, in reviewing the analysis results, a response was observed that had not been seen for the un-skewed bridges. Figure 24 presents images taken from the results of the analysis of the model of Bridge 3776 loaded by four trucks in the centered position from a top and bottom perspective (the model's deflected shape has been highly exaggerated for clarity). The colors on the model represent longitudinal displacement. This is contrasted with similar images from the results of Bridge 2390 under the same type of loading. As can be seen, Bridge 3776's longitudinal extension is reasonably

symmetric, with the difference between the extension of the center girder and the exterior girders being around 0.004 in. This is in contrast with the results from similar loading of the model of Bridge 2390 in Figure 25, which shows asymmetrical displacement and a difference in extension between the exterior girders of around 0.013 in. This difference arises from torsional effects that are not present in the un-skewed bridges but are present in the results of the models of each of the skewed bridges.
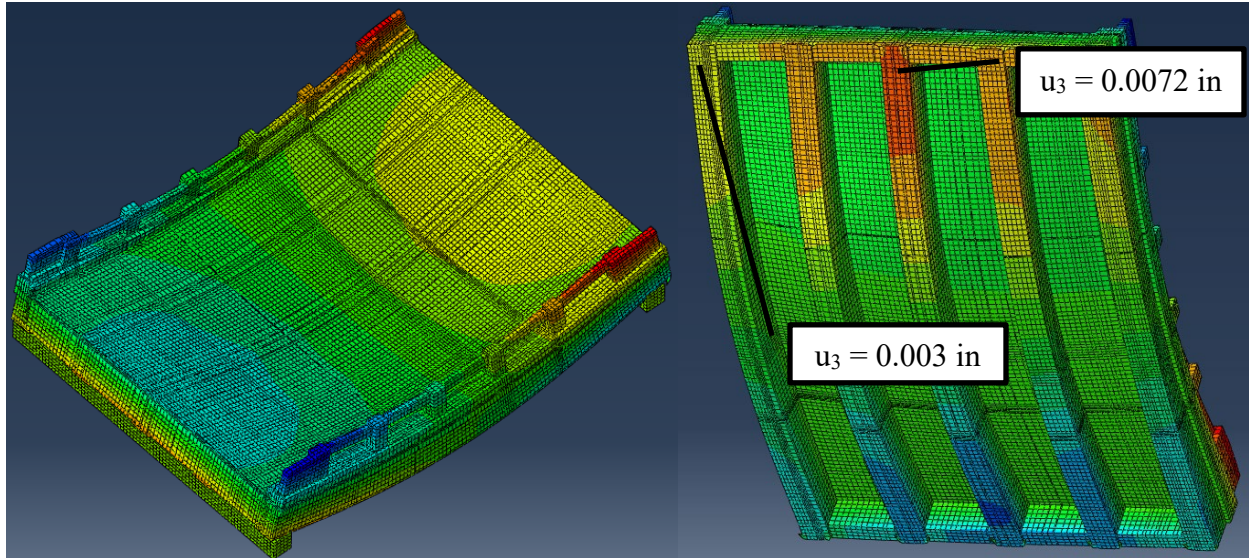
Figure 24: Calculated Longitudinal Displacement of Bridge 3776 (Left: Top View, Right: Bottom View)
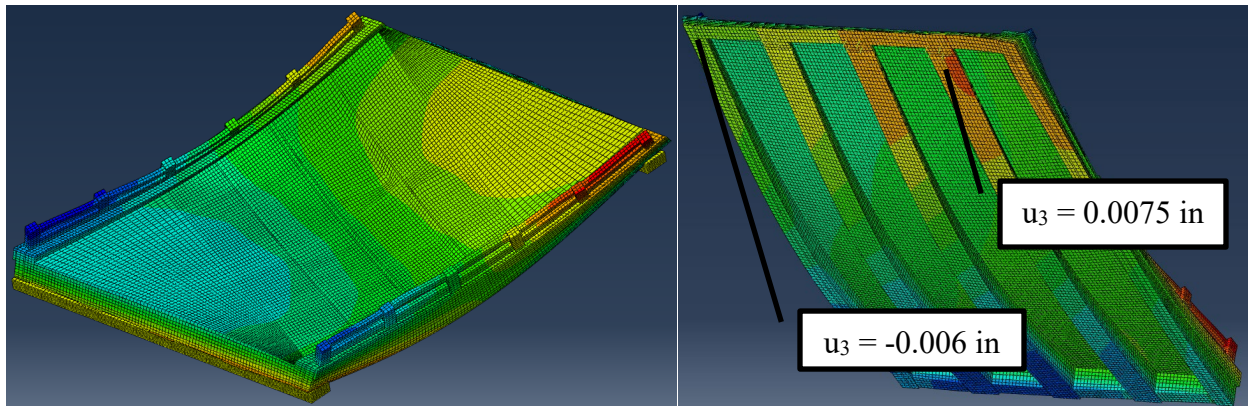
Figure 25: Calculated Longitudinal Displacement of Bridge 2390 (Left: Top View, Right: Bottom View)

The identification of asymmetrical extension and twisting effects in skewed bridges does not lead directly to the cause of apparent girder end fixity. Rather, it points to the bridges' behaviors absent the cause of the observed fixity. However, consideration of the actual conditions of the bridges (as opposed to the models) allows for some speculation into a reasonable cause for the observed fixity.

Each of these bridges include end diaphragms forming their backwalls. These backwalls are battered by a few degrees at the rear with granular fill behind. It is possible that due to their twisting motion, the skewed bridges have allowed more granular backfill to migrate underneath their backwalls, fouling their motion more than on the un-skewed bridges. This restriction of motion by debris, though difficult to identify and model, could lead to some of the apparent end fixity observed during testing.

As additional evidence of the hypothesis that skewed bridges' motion may be restricted by increased amounts of debris, photographs of the individual bridges taken during test set-up were examined, focusing on images that revealed the conditions of the girder ends and bearing areas. Figure 26 presents an image taken of one of the abutment and backwalls from Bridge 5432, an un-skewed bridge. As the image shows, the gap between the back-wall and the top of the abutment is fairly clean, with only a small amount of visible debris. This is contrasted with Figure 27, which presents a similar image taken from Bridge 5109. A significant amount of debris is visible in the gap between abutment and backwall, which could partially restrict the bridge's end rotation causing negative strains to develop.
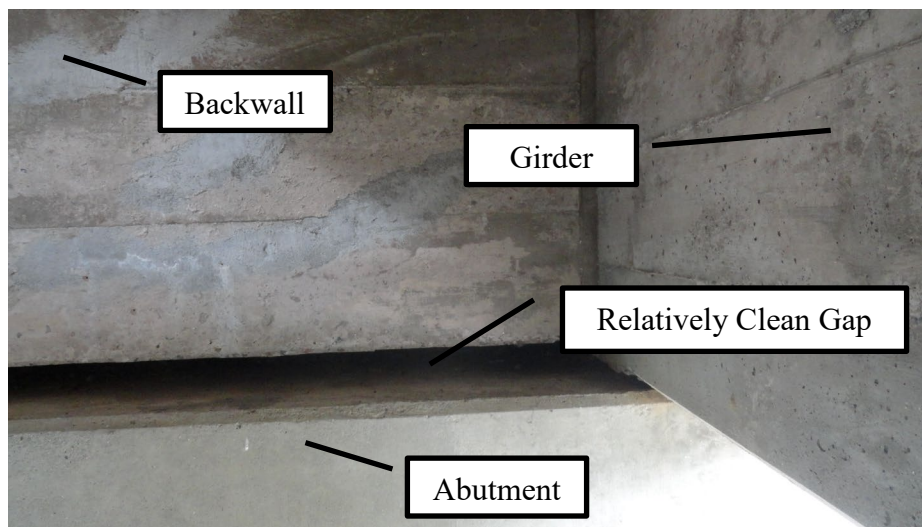
Figure 26: Condition of Gap between Abutment and Backwall – Bridge 5432
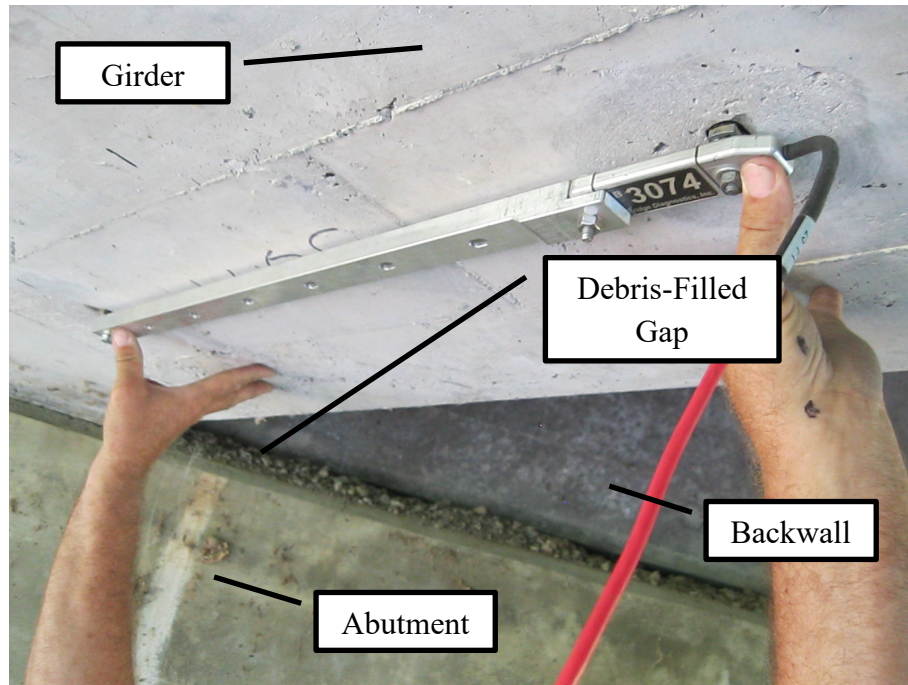
Figure 27: Condition of Gap between Abutment and Backwall – Bridge 5109

Finally, this hypothesis of skewed bridges' tendency to collect bearing-fouling debris also explains why one of the five skewed bridges, Bridge 2879, did not appear to exhibit any significant girder end fixity. Bridge 2879 consists of four nominally identical, simple spans, with interior spans resting on piers and exterior spans resting on piers and abutments. The span that was live-load tested was an interior span, without any fill behind its backwalls. Without any fill available to restrict its motion, the tested span was able to deform much more freely, exhibiting end conditions that were much closer to simply supported than were observed for the other four skewed bridges. This may not have been the case had an exterior span been tested, as one of the ends would have had the potential to collect debris, restricting its motion.

4   Proxy Finite-Element Analysis

The current method by which bridge live-load capacity is most often evaluated, using AASHTO (2011, 2012) code-based calculations to determine *RFs*, is analogous to the design of new bridges, using most of the same assumptions and empirical relations, and is thus subject to similar capacity requirements. However, for bridges designed under previous specifications, this method often predicts inadequate flexural capacity, leading to the perceived need for remedial actions, such as load posting, repair, or replacement. However, many of these bridges, such as most of the bridges live-load tested as part of this study, carry modern loads regularly with no apparent signs of distress despite their low *RFs*. This suggests that these bridges have higher capacities than are able to be identified under the assumptions from normal load rating, and that a method of load rating is

required that overcomes the assumptions and limitations leading to this under-prediction of capacity.

To address the need for a new, more accurate method of load rating older RC T-beam bridges, a novel, nonlinear FE analysis technique, dubbed proxy finite element analysis (PFEA), has been developed and is presently being further enhanced. This method overcomes the shortcomings of standard bridge flexural rating by accounting for the full, nonlinear constitutive properties of concrete and reinforcing steel and by treating a bridge as a system of interrelated, interdependent components rather than a collection of individual, disparate members. Even still, it endeavors to remain consistent with AASHTO's specifications and recommendations (2011, 2012), and retains a number of AASHTO's conservative assumptions. Further, PFEA is much simpler to implement and more computationally tractable than a 3D nonlinear finite-element continuum analysis that accounts for concrete cracking and crushing. Using this method, the live-load tested bridges from this study were load rated with promising, yet conservative results.

4.1 Proxy Finite Element Analysis Concept

The basic premise of PFEA is to capture a bridge girder's full longitudinal flexural behavior up to failure, including contributions from its geometry and possibly complicated material nonlinearity, and condense it into a single nonlinear relationship. This relationship is then imparted onto an equivalent section (a proxy section) whose geometry and constitutive behavior are straightforward to implement into commercial FE software. Proxy section girder models are then assembled into a 3D model of a full bridge which is loaded by both dead-load and increasing multiples of HL-93 live-load to complete bridge failure. The multiple of HL-93 live-load required to cause model failure directly corresponds with the bridge's live-load capacity, from which its flexural *RF* may then be calculated.

4.2 Proxy Finite Element Analysis Process

The process of rating a bridge by PFEA includes four major steps, which are briefly outlined below. These are discussed in greater detail by Schanck and Davids (2020). Although they were developed with the analysis of RC T-beam bridges as a main focus, as mentioned later, the concept is applicable to other types of slab-on-girder structures provided the appropriate constitutive models are used. Figure 28 shows a schematic overview of the PFEA analysis process, which will be explained in greater detail below.
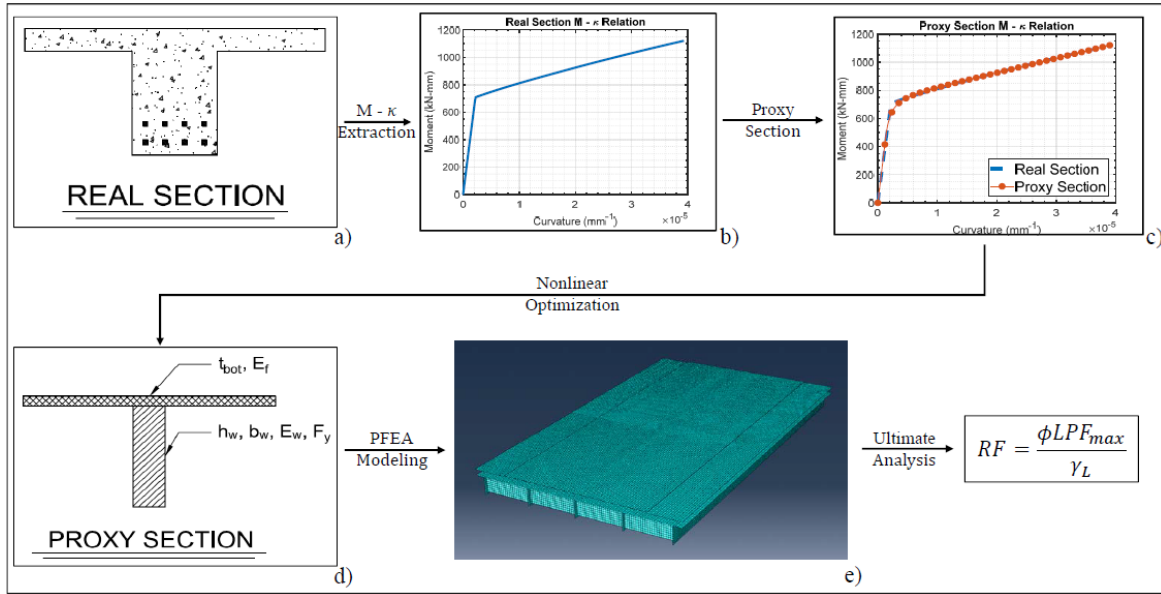
Figure 28: PFEA Procedural Overview: a) Real Section; b) Extracted Moment-Curvature Relationship; c) Proxy Section Moment-Curvature Match; d) Proxy Section with Optimized Geometry and Material Constants; d) Full-Bridge, Meshed PFEA Model

4.2.1 Moment-Curvature Relationship Extraction

The first step in PFEA is the extraction of the nonlinear moment-curvature relationships defining each girder's bending resistance when subjected to flexural loading up to and including failure. Starting from zero, a girder section is subjected to a particular level of curvature and is discretized vertically into n layers of equal thickness Compatibility is enforced by assuming strain in a layer to be proportional to curvature and height, and from these strains corresponding stresses are calculated. For the case of RC bridges, concrete is assumed to behave in compression as described by Hognestad (1951) with no strength in tension, and reinforcing steel is assumed to exhibit tension stiffening behavior, as suggested by Belarbi and Hsu (1994).

For a given level of curvature, Equation 9 is solved iteratively to determine the neutral axis location required for horizontal force equilibrium in the section under the current level of curvature, and Equation 10 is then used to compute the internal bending moment corresponding to the given curvature. In Equations 9 and 10, b_j is the width of the jth layer (either the width of the web or the flange, depending on the height of the layer from the bottom of the section, y_j and the presence of the feature), t is the layer thickness, f_{c_j} is the concrete stress in the jth layer, f_s and y_s are the stress in the reinforcing steel and the height of its centroid from the section bottom, and A_s is the cross-sectional area of the reinforcing steel. The process of iteratively solving Equation 9 and using Equation 10 to determine moment is repeated for increasing values of curvature until failure – defined by the concrete reaching its ultimate compressive strain of 0.003 at the extreme

compression fiber (AASHTO 2012) – is reached. Figure 29 includes the extracted moment-curvature relationship for an interior girder from Bridge 5489 which is plotted as the blue curve.

$$\int \sigma dA \approx \left(\sum_{j=1}^{n} f_{cj} b_j t \right) + f_s A_s = 0 \qquad \text{Equation 9}$$

$$\int \sigma y dA - M \approx \left(\sum_{j=1}^{n} f_{cj} b_j y_j t \right) + f_s A_s y_s - M = 0 \qquad \text{Equation 10}$$
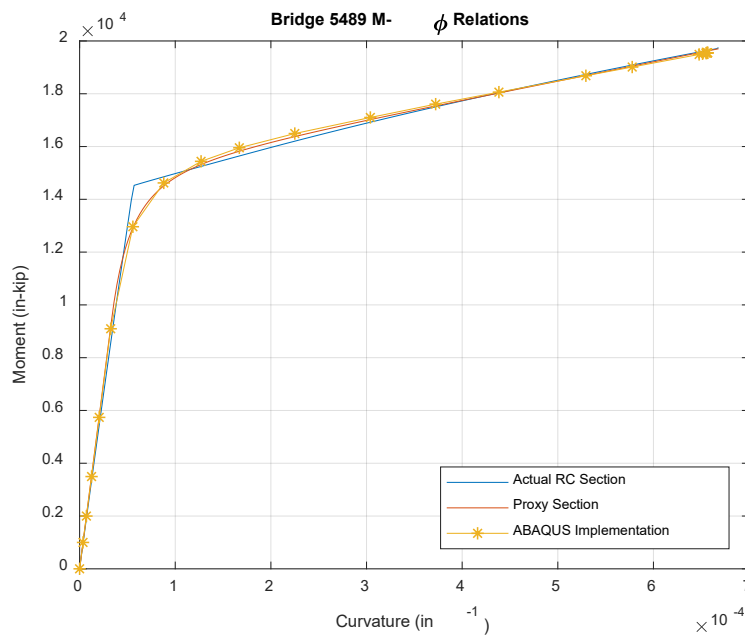
Figure 29: Moment Curvature Relationships for Bridge 5489 – Actual Section, Proxy Section, and ABAQUS Implementation

4.2.2 Proxy Section Creation

Once a section's moment-curvature relationship has been extracted, a proxy section is developed that possesses an identical moment-curvature relationship to the actual section. In general, the overall geometry of the proxy section can be (but need not be) nearly the same as the actual section, but can also be altered in order to facilitate modeling. However, the constitutive behavior of the proxy section is very much simplified in comparison to the actual section, significantly easing the difficulty of implementing complex constitutive models in a 3D finite-element model. For the bridges from this study, the proxy sections consisted of T-shaped sections with webs and flanges whose geometries were similar to the actual gross sections they represented.

To emulate the nonlinear moment-curvature relationship of the actual section, the proxy section's web was assigned elastic-perfectly plastic constitutive behavior, and the flange was assigned elastic behavior. The required material constants were determined by nonlinear optimization with a least-squares objective function defined by Equation 11 where f is a function of the decision variables x_i. The function f defines the proxy section's moment response when subjected to the curvatures used to find the real section's moment-curvature relationship, M are the bending moments from the actual RC section's moment-curvature relationship, and the double bars indicate the Euclidian norm. The function f applies a similar layered discretization technique as that used to determine the actual section's moment-curvature relationship while accounting for the proxy section's geometric and constitutive properties. For these bridges, a total of three decision variables (web elastic modulus, web yield stress, and flange elastic modulus) were optimized to fully define the proxy section because the geometry of the proxy section could be assumed. However, more variables can be included to change geometric properties or add additional material properties if needed. Figure 29 shows the moment-curvature relation for a proxy section corresponding to an interior girder from Bridge 5489 as the red curve. As can be seen, the proxy section, with significantly simpler constitutive behavior, possesses a very similar moment-curvature relation to that of the actual section.

$$\lambda = \left\| f(x_1, x_2, \cdots x_j) - M \right\|_2 \qquad \text{Equation 11}$$

It should be noted that the assumptions made in formulating proxy sections lead to one limitation of PFEA's broad use across a large range of bridge types. To this point, the bridges used in developing and verifying PFEA have had relatively thick decks and relatively close girder spacings. This has enabled the assumption of a linearly-elastic material model for the deck, both when optimizing proxy parameters, and in implementation into a FE model. This assumption may be less valid for bridges with thin decks or large girder spacing, which may experience a significant amount of material nonlinearity within their decks. Live-load data taken from such bridges would be needed to verify this limitation, and the limitation could then be addressed.

4.2.3 Finite Element Implementation

A FE analysis of a single girder with proxy section properties is conducted before it is synthesized into a full bridge model. This is done to verify that the implementation of the proxy section behaves appropriately, and allows fine-tuning of a failure strain parameter. This failure strain, when reached by any girder, causes the entire bridge to be considered failed and corresponds with concrete crushing at the girder's extreme compression fiber. The individual girder models (as well as the full bridge models) are implemented in ABAQUS using S8R quadratic, reduced integration shell elements with 8 nodes and six degrees of freedom per node, to which appropriate geometric and material parameters are assigned. A convergence study revealed that a characteristic element length of around 3 in. consistently led to accurate results and so was used to form the mesh of individual girder models and full bridge models alike. The girder models used for verification are simply supported with a known moment applied. At each load increment in which convergence is

achieved, resulting girder curvatures are directly extracted from the results and compared with the theoretical moment-curvature relationships for both the actual and proxy sections. Figure 29 shows the ABAQUS implementation of a proxy girder from Bridge 5489 as the yellow curve. As can be seen, the ABAQUS implementation agrees very well with both the theoretical proxy section and the actual section, showing that the implementation emulates the behavior of the actual section quite well.

Full bridge PFEA models are constructed by placing the appropriate proxy girders side-by-side and tying adjacent flange degrees of freedom. Additionally, girder end-diaphragms are added between the webs of the proxy girders, which are modeled using S8R elements and whose geometry and material parameters were selected to ensure that their flexural rigidity was equal to those present in the actual bridges. Initially, intermediate diaphragms were also modeled. However, these tended to cause unrealistic stress concentrations leading to unreaslistic premature failure, and so were omitted thereafter, regardless of their presence on actual bridges. This omission aids in modeling, but also is conservative as it reduces bridges' ability to transversely distribute load. A meshed model of Bridge 3307 is presented in Figure 30. The models are simply supported and are configured with two loading steps: a dead-load step in which a uniform dead-load pressure is applied to the entire deck, and a live-load step in which the appropriate HL-93 live-load model is applied. This allows live-load effects to be isolated from dead-load effects while the entire loading history of the bridge, up to and including failure, is applied.
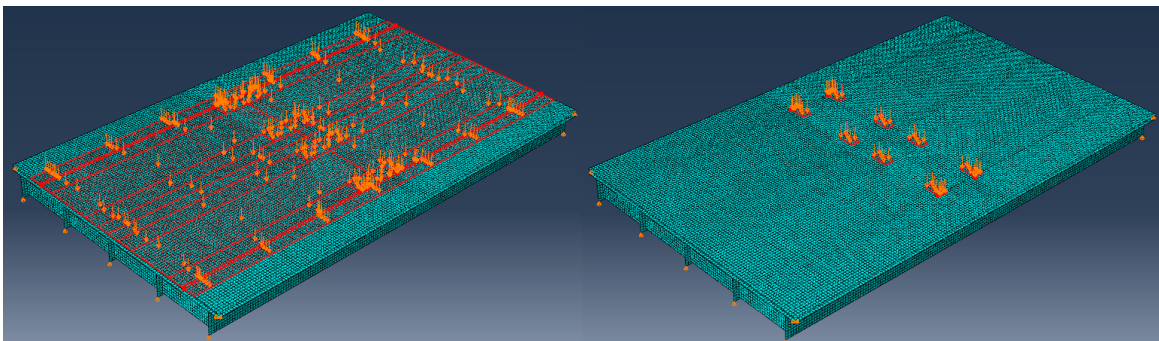
Figure 30: Bridge 3307 Full Proxy Bridge Model (Left: Showing Lane Load, Right: Showing Tandem Wheel Loads)

4.2.4 Analysis and Rating Factor Calculation

Live-loading is applied to match HL-93 notional loading with impact. Lane loads are applied to 10 ft wide strips in each lane as uniform pressures and HL-93 truck or tandem wheel loads are applied in both lanes. The wheel loads are positioned to produce maximum moment effects and are applied as pressure loads distributed over the tire contact pattern specified by AASHTO (2012) (over a 20 in. by 10 in. patch). Figure 30 includes the positions of both the lane and tandem wheel loads for illustration.

The initial, dead-loading step is solved with a standard Newton-Raphson iterative solver with the effects of geometric nonlinearity considered and results held constant in the subsequent step. However, rather than using a standard Newton-Raphson iterative solver to analyze the PFEA models in the live-load step, a Riks arc-length solver is employed (Riks, 1979). This allows *RF*s to be determined directly from the results of the model without prior knowledge of the load causing failure. At each iteration, the Riks solver used by ABAQUS scales the applied load by a load proportionality factor (*LPF*) and solves for the associated displacements. It then increases the *LPF* and continues to iterate until a stopping criterion is met, or until the model becomes unstable. When a very large maximum *LPF* is used as the solver's termination criterion, the solver will increase *LPF* and solve for additional increments of displacement until one or more girders reaches their previously defined failure strains, at which point the model becomes unstable and the solver issues an analysis abort. This instability itself does not hold physical significance, as it is purely numerical. The material damage model that initializes failure expects elements to gradually soften rather than immediately lose all stiffness, and as such, the immediate loss of stiffness causes numerical ill-conditioning. However, as mentioned previously, the strain at which proxy section instability occurs directly corresponds with the strain causing top fiber crushing in the actual section, using their common moment-curvature relationship and the assumption of linear strain distribution over the section depth. Therefore, the instability of the PFEA model is a direct mapping of the flexural failure of the actual bridge as defined by AASHTO, with the *LPF* causing that instability equal to the multiples of HL-93 loading causing the real bridge's flexural failure.

Using this basis, PFEA models can be used for load rating older bridges with while adhering to the AASHTO specifications. Equations 12 describe how a PFEA model can be used for bridge rating, where *RF* is the bridge's rating factor, ϕ is the AASHTO strength reduction factor (taken as 0.9 for under-reinforced concrete members in flexure), M_n is the bridge's moment capacity, γ_{DL} and γ_{LL} are the AASHTO dead-load and live-load factors (taken as 1.25 and 1.35 respectively for operating conditions), M_{DL} and M_{LL} are the applied dead and live-load moments, respectively, and LPF_{max} is the maximum model-predicted *LPF*. The conventional capacity rating equation for individual members (taken from AASHTO (2011)) is given in Equation 12a, but used to describe the rating of the entire bridge acting as a system of interrelated members (as is seen in the behavior of actual structures and the PFEA model). Equation 12a is subsequently re-arranged in Equations 12b and 12c to solve for a term represented by the maximum *LPF* predicted by the model, which can then be used to determine the *RF* with Equation 12d. This development shows that when dead-loading is applied to the model and is amplified by both the AASHTO dead-load factor and the inverse of the strength reduction factor, *RFs* can be computed that explicitly follow AASHTO guidelines for rating (2011) and analysis (2012). It should be noted that this rigorous consideration of load and resistance factor rating was not implemented in Schanck and Davids (2020).

$$RF = \frac{\phi M_n - \gamma_{DL} M_{DL}}{\gamma_{LL} M_{LL}} \qquad \text{Equation 12a}$$

$$\frac{\gamma_{LL}}{\phi} RF * M_{LL} + \frac{\gamma_{DL}}{\phi} M_{DL} = M_n \qquad \text{b}$$

$$\frac{\gamma_{LL}}{\phi} RF = \frac{M_n - \frac{\gamma_{DL}}{\phi} M_{DL}}{M_{LL}} = LPF_{max} \qquad \text{c}$$

$$RF = \phi \frac{LPF_{max}}{\gamma_{LL}} \qquad \text{d}$$

4.3 Results for Tested Bridges

The previously described PFEA rating process was applied to each of the 10 RC T-beam bridges that had been live-load tested in this study. The resulting flexural *RFs* are presented in Table 21, along with their original AASHTO determined *RFs*, and *RFs* updated by field live-load testing. As can be seen, PFEA resulted in significant increases in flexural *RF* for all bridges with respect to the original, AASHTO-determined *RFs*, and all but one saw additional increases relative to the *RFs* updated based on live-load testing. While some of these predictions seem optimistic, they are based solely on the mechanics of the problem at hand and assume nominal concrete compressive strength and steel yield strength, neglect any concrete tensile strength, and neglect of the effects of integral curbs, wearing surfaces, and railings. Additionally, they incorporate the load factors and strength reduction factors required by AASHTO for rating and design. Additionally, the truck or tandem loads applied to each land were offset longitudinally based on the bridges' angles of skew, further limiting the possible increases in *RF*.

Table 21: Flexural Rating Factors

Bridge	Skew (deg)	AASHTO Flexural RF	Field-Test Updated Flexural RF	PFEA Updated Flexural RF
2130	0	0.920	1.28	1.87
3307	0	0.920	1.61	1.30
3356	0	0.280	0.300	1.83
3776	0	0.690	1.20	1.43
5432	0	0.750	1.10	1.96
2390	30	0.757	0.838	1.56
2879	30	1.09	1.35	2.23
3848	30	0.887	1.15	1.72
5109	35	0.686	0.942	2.35
5489	15	0.784	1.10	1.91

As seen in Table 21, some of the increases in flexural *RF* are quite dramatic. However, the most dramatic is that of Bridge 3356, whose *RF* was increased by over 550% relative to its AASHTO *RF*. This seems overly optimistic, until the actual conditions of the bridge and the PFEA results are considered. The controlling *RF* for Bridge 3356 came from an extended, exterior girder that

had been designed to carry a sidewalk but had been put into traffic service when the roadway was widened. Even after live-load testing, the bridge's *RF* could not be significantly increased because the capacity of the bridge as a whole was assumed dependent on the capacity of its individual, isolated members. On the other hand, analysis with PFEA revealed a much less conservative prediction of the ultimate behavior of the bridge as it considered the bridge whole rather than as a collection of individual members. When loaded, the extended girder soon became nonlinear. However, because of its considerable ductility (captured accurately by the proxy section's moment-curvature relationship), this girder was able to deform inelastically with additional load being redistributed to the other girders. This continued until one of the interior girders reached its failure strain. In fact, the reported *RF* comes from an analysis in which the loads were moved as close to the exterior girder as was allowable, yet the girder was still able to avoid premature failure due to its ductility and the bridge's ability to redistribute load. This displays PFEA's ability to account for a bridge as a whole, allowing for realistic redistribution of load when nonlinearity is incurred and the ability to account for the ductility of lightly reinforced members.

4.4 Shear Effects

PFEA is intended to take advantage of the ductile, nonlinear behavior of slab-on-girder bridge girders (especially those of RC T-beam bridges) and the system behavior they exhibit at higher loads, up to and including ultimate flexural capacity. The beneficial nonlinear behavior of these bridges' girders do not readily extend to their response in shear, as their shear resisting mechanisms tend to be non-ductile. However, bridges' system responses do affect how shear load is distributed to individual girders, which can significantly affect the shear demand placed upon them. Since PFEA predicts the way in which a bridge works as a system to distribute loads, there is a potential to achieve a better understanding of shear demand through more realistic shear load distribution predicted by PFEA. The 10 bridges that had been live-load tested were therefore analyzed for shear with PFEA, with the aim of gaining additional understanding of the bridges' system response to shear loading.

The bridges' shear load distribution was investigated by analyzing two separate load-cases: a case with loads applied to maximize shear, and one with loads arranged to maximize moment. To maximize shear, live-loads that had been applied at the bridges' midspans were moved so that the rearmost load patches were applied one girder depth away from the bearing line. The bridges' dead-loads and the lane load were kept in their original positions. These models were then analyzed with the resulting reaction forces at the loaded bearings assumed equal to the corresponding girders' maximum shear forces. To determine the shear resulting from loads positioned to maximize moment, the reaction forces from the original, moment-rating models were recovered and were again assumed equal to the maximum shear force in the respective girder.

In contrast to for the models used for flexural rating, the shear distribution models' *RF*s could not be automatically determined by the maximum achieved *LPF* from the Riks solver. Instead, the bridges' shear capacities were calculated based on AASHTO (2012) as implemented in a separate

MATLAB function (provided in chapter A.2) which takes as input a model's dead-load and total dead and live-load reaction forces and reports each girder's resulting rating factor. AASHTO load and resistance factors were explicitly considered. These rating factors are presented in Table 22, along with the number of girders making up each bridge and the controlling girder (with girders numbered consecutively from one side to the other). It must be noted that these *RF*s are not necessarily representative of the capacities of the entire bridges. Because they assume maximum shear forces to be equal to reaction forces, they reflect capacity at girder ends only. In reality, the critical location for shear may be at a location away from the girders' ends, due to the girders' variable shear reinforcement spacing. For comparison, Table 22 also presents shear *RFs* calculated using the same MATLAB code, but using loads determined with AASHTO (2012) shear distribution factors.

Table 22: Shear Rating Factors

Bridge	Skew (deg)	Number of Girders	AASHTO Shear *RF*	PFEA Shear *RF* – Moment Loading		PFEA Shear *RF* – Shear Loading	
				RF	Controlling Girder	*RF*	Controlling Girder
2130	0	4	1.71	2.87*	2/3	2.20	2/3
3307	0	5	1.32	2.11*	3	1.64	3
3356	0	6	1.14	2.84	4	1.55	3
3776	0	5	1.22	2.27*	3	1.19	3
5432	0	5	0.886	2.63	3	1.43	3
2390	30	5	0.650	1.80	5	1.21	3
2879	30	4	0.710	1.74	2	1.06	2
3848	30	5	0.560	2.00	5	1.22	3
5109	35	5	0.570	1.96	2	1.14	3
5489	15	5	0.726	2.18	3	1.11	3

*Bridge fails in flexure, larger loads cannot be applied

From the results presented in Table 22, difference in behavior between skewed and un-skewed bridges can be observed. For four of the five un-skewed bridges, the girder controlling the shear ratings was the center girder (or girders), which did not change with the positioning of the load. In the case of Bridge 3356, the controlling girder switched between two of the central girders as load was moved, and so can be thought to experience similar behavior, taking into account its unique geometry. Similar behavior can also be observed for Bridge 5489, which had the smallest angle of skew of the skewed bridges. For the remaining skewed bridges, a different behavior can be observed. When the loads were placed at midspan, the controlling girder for each of these bridges was an exterior girder or one of the non-central interior girders. These controlling girders correspond to the respective bridges' obtuse corners. However, when the loads are moved closer to the bearing line, each of these bridges' controlling girders shifted to their center girder (or one of the central girders in the case of Bridge 2390).

The tendency for the obtuse corner bearing of a skewed bridge to attract additional load has been observed and documented in previous studies. For instance, Ebeido & Kennedy (1996) observed from scale models of slab-on-girder bridges that the bearing at the obtuse corner tended to attract much greater amounts of load for concentric load-cases than the acute corner, which they were able to simulate using FE analysis. Barr & Amin (2006), and Théoret et al. (2012) analyzed FE models of skewed slab-on-girder and flat-slab bridges (respectively), both noting that the obtuse corners tended to attract significant additional shear load as compared with the acute corners. The results of this behavior were also observed during live-load testing of the skewed bridges, as discussed in detail above. This behavior arises as a result of the skewed bridges' geometries and the fact that the truck or tandem wheel loads used are not parallel to the angle of skew. When the loads on the more highly skewed bridges are distant from the bearing line, a significant amount of load is attracted to the bearing at the bridges' obtuse corners due to the shorter distance relative to the distance to interior bearings. However, when the loads are moved closer to the bearing line, much less load is attracted to that bearing due to the shorter distance to the center girder bearings. The prediction of this behavior by the PFEA models suggests that they are accurately predicting the system-behavior of the bridges, thus distributing shear load realistically.

As a final note, comparison of the PFEA and AASHTO shear *RFs* reveals additional insight into the differing accuracy between PFEA and AASHTO code-based predictions of shear load distribution for skewed bridges. For the un-skewed bridges, the AASHTO *RFs* are generally conservative relative to the PFEA *RFs*, but the disparity between them is not unreasonably large (with the exception of Bridge 3776, for which PFEA predicted a shear *RF* slightly lower than AASHTO). For each of these bridges, PFEA predicted a *RF* between 97.5% and 161% of AASHTO. Since the shear capacities for both *RF*s are calculated identically, this suggests that the AASHTO *DFs* for shear are reasonably accurate, yet conservative in describing shear load transfer. However, this is not the case for the skewed bridges. The AASHTO *RF*s for shear on the skewed bridges are very conservative relative to those calculated based on the results of PFEA, with PFEA predicting between 150% and 200% of AASHTO *RFs*. Again, given that shear capacities were calculated identically for AASHTO and PFEA ratings, these differences can be largely attributed to shear load distribution. These differences suggest over-conservatism in AASHTO shear *DF*s or their skew correction factors which is not present in PFEA. This is consistent with findings reported by Barr and Amin (2006) who noted that AASHTO shear *DFs* to be conservative compared with the shear load distribution inferred by linearly elastic finite element analysis. Because PFEA treats bridge models as systems rather than individual members, it can more accurately simulate distribution of shear force in skewed bridges, leading to better predictions of shear rating. However, these predictions should also remain reasonably conservative as they use girder capacities calculated with AASHTO specifications (2012).

4.5   Consideration of AASHTO Specifications

As shown above, analysis of bridges by PFEA can provide a more accurate assessment of bridge behavior than conventional beam-line analysis, tracking both ductility and load redistribution up

to and including failure. However, for the technique to be acceptable in practice, it must reflect the standards and specifications governing bridge design and assessment, namely the AASHTO *LRFD Bridge Design Specifications* (2012) and *Manual for Bridge Evaluation* (2011). This section explicitly addresses PFEA's adherence to the practices allowed by the standards, and addresses the few discrepancies that exist. The three general steps of load rating by PFEA – moment-curvature relation extraction; development of proxy sections; and analysis with the finite element method – will be addressed, and it is shown that the techniques used in PFEA are generally allowable under the current code and/or abide by the letter and spirit of the current code.

Extraction of moment-curvature relationships as a method of member analysis is a well-accepted method and is fully allowed in the current AASHTO specifications (2012). The code specifies that, "[a]ny method of analysis that satisfies the requirements of equilibrium and compatibility and utilizes stress-strain relationships for the proposed materials may be used" (AASHTO 2012, 4.4). As described above, PFEA moment-curvature extraction ensures equilibrium of internal forces and moments, and uses conventional beam theory assumptions to ensure strain compatibility through the section. Additionally, stress-strain relations are used for both concrete and reinforcing steel. The relation used for concrete, that proposed by Hognestad (1951), is fully acceptable by the code which allows stress distributions which are, "assumed to be rectangular, parabolic, or any other shape that results in a prediction of strength in substantial agreement with the test results" (AASHTO 2012, 5.7.2.1). The use of a concrete crushing strain of 0.003 is generally conservative and in line with AASHTO for bridges in good condition, like those tested here. For bridges in poorer condition whose ductility is in doubt, reduction of the concrete crushing strain (to 0.002 for instance) will effectively reduce predicted girder ductility, thus reducing the PFEA model's ability to redistribute load and increase the conservatism in the analysis.

The constitutive relation for steel proposed by Belarbi and Hsu (1994) and utilized by PFEA is not explicitly allowed by AASHTO, but is widely accepted in the literature. Although the relation represents a "stress-strain curve representative of the steel" (AASHTO 2012, 5.7.2.1), it leads to ultimate moment capacities in excess of those determined assuming an elastic-perfectly plastic model, which may cause some concern. To ease this concern, moment-curvature analysis (using both the Hognestad (1951) concrete and Belarbi and Hsu (1994) reinforcing steel constitutive models) was used to reproduce test data of actual RC beam failure tests, providing evidence of the model's applicability. Moment-curvature relationships for the control beams described by Loring and Davids (2015) and beams by Xing et al. (2010) were extracted and used to predict load-deflection behavior. Deflection was predicted numerically using a 5th order boundary-value problem solver in MATLAB to solve the nonlinear beam differential equation. Figures 31 and 32 show the behavior predicted from the moment-curvature relationships compared with the measured load-deflection data. As is clear, the load deflection behavior predicted matches the measured behavior quite well. In addition, if required, the maximum predicted moment of a girder can be reduced in moment-curvature extraction by reducing the assumed yield stress of the steel. This would have the effect of reducing the maximum moment supported by a girder, without

greatly affecting its ductility. The yield stress used could be tuned such that the maximum predicted moment equaled the maximum moment determined by conventional analysis.
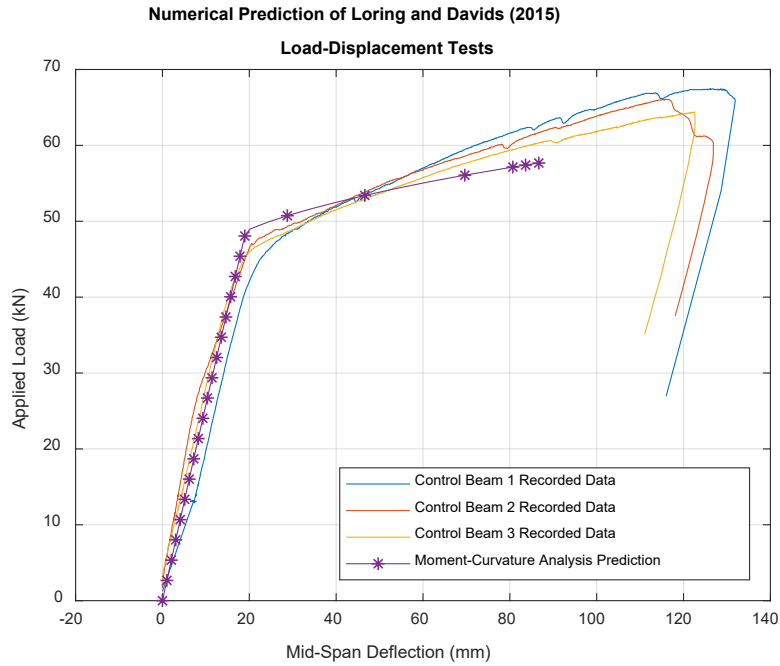

Figure 31: Comparison of Predicted and Measured Load-Deflection Behavior from Loring and Davids (2015)
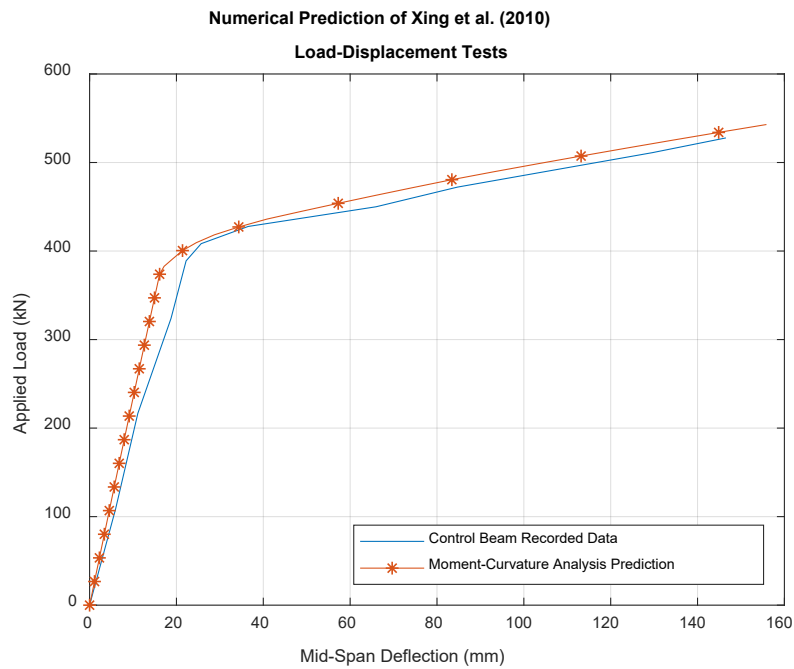

Figure 32: Comparison of Predicted and Measured Load-Deflection Behavior Xing et al. (2010)

The creation of proxy sections to represent a bridge's actual girders is not specifically addressed by AASHTO (2012), does falls under the analysis category of "Equivalent Members" defined in section 4.5.5 given below.

> Components or groups of components of bridges with or without variable cross-sections may be modeled as a single equivalent component provided that it represents all the stiffness properties of the components or group of components. The equivalent stiffness properties may be obtained by closed-form solutions, numerical integration, submodel analysis, and series and parallel analogies.

Modeling real girders with proxy sections is consistent with this provision. The stiffness characteristics of the real girders are determined by numerical integration, which are then given to the proxy sections based on the results of nonlinear optimization. Proxy sections mimic all of the relevant stiffness and strength characteristics required for flexural analysis of the actual section and thus are a valid option.

Finally, the use of 3D, nonlinear FE models for analysis is accepted by AASHTO, and the model formulation explicitly considers the requirements for bridge rating factor evaluation. As mentioned above, AASHTO specifies that "[a]ny method of analysis that satisfies the requirements of equilibrium and compatibility and utilizes stress-strain relationships for the proposed materials may be used" (AASHTO 2012, 4.4), and specifically lists FE analysis as an example of an approved analysis technique. In addition, the use of inelastic material behavior (4.5.2.3) and geometric nonlinearity (4.5.3.2) are explicitly allowed, solidifying the models' formulations. Finally, as discussed and presented in Equations 12, the application of dead-loads and live-loads are formulated such that *RF*s governed by AASHTO (2011) can easily be computed while incorporating the requisite strength reduction factors, load factors, and impact factors.

4.6 Current and Future Development

In its current state, PFEA has been shown to produce what appear to be realistic estimates of simple-span RC T-beam bridge *RFs*. It has shown utility for both un-skewed and skewed bridges as seen in the results displayed in Tables 21 and 22. PFEA is currently being extended to account for prestressing such that it may be used to analyze prestressed concrete bridges, and is being verified against data from a full-scale destructive test of a prestressed concrete girder bridges as described by Burdette and Goodpasture (1971). The technique can also be extended to cover steel-girder bridges and continuous bridges, and would benefit from integration into a self-contained program used to increase the accuracy of ratings for older girder bridges.

5 Summary and Conclusions

5.1 Skewed and Un-Skewed Bridge Behavioral Differences

Live-load testing of five un-skewed and five skewed RC T-beam bridges allowed their behaviors to be directly compared under reasonably similar conditions, and two main differences to be identified. Through calibration and simulation using linear FE models, the bridges' behaviors and some possible causes for these behaviors were further explored, with results extending beyond those revealed by testing alone.

The strain data collected during live-load testing showed a tendency for skewed bridges' load distribution to have a much greater dependence on load positioning than did similar un-skewed bridges, as shown by *GLFs* calculated using recorded mid-span strains. Using the calibrated, linear FE models, the reaction forces between the girders and abutments were recovered. This confirmed that the skew bridges' high dependence on transverse load positioning is likely due in part to the shortened distance to obtuse corners, which in-turn attracts a greater amount of load. The same live-load tests also revealed skewed bridges' much greater susceptibility to unintended end fixity, indicated by negative strains recorded at girder ends. The linear FE models revealed the skewed bridges' tendency to undergo warping displacements. These predicted displacements, along with observations of the bridges' actual bearing conditions led to the hypothesis of skewed bridges' tendency to collect debris between the abutment and backwall, restricting their displacement and inducing negative strains.

These observations and associated explanations, while important to furthering the understanding of actual bridges' behaviors, also can be practically useful when considering a bridge for permitting and load rating. They are also useful and when evaluating the results of future live-load testing of similar bridges. For instance, noting the dependence of skewed T-beam bridge response on transverse load positioning for load distribution can inform decisions on permit-load planning, particularly whether overweight loads should be carried in normal travel lanes or whether they should be centered, with other traffic temporarily stopped or diverted. Additionally, live-load test results revealed some unintended end-fixity for skewed T-beam bridges which was not observed for the un-skewed bridges. This appears to be due to debris fouling the bearings, which was more apparent for the skewed bridges.

5.2 Proxy Finite Element Analysis

A novel, nonlinear FE analysis technique, PFEA, has been developed for the purpose of load rating older bridges with a higher level of accuracy than is available through standard engineering analysis. It condenses the complex flexural behavior of a bridge girder into a single, nonlinear relationship describing its curvature response when subjected to an external moment. This relationship is then used to develop a proxy section that maintains the actual section's moment-curvature relationship, but can have a much simpler geometries and can use much simpler constitutive models. Proxy sections are assembled into full bridge models loaded by factored dead-

load and HL-93 live-load. Solutions are achieved using a Riks arc-length algorithm, which continues to increase applied load until the model becomes unstable, signifying capacity of the bridge has been reached.

PFEA was used to update the load ratings of each of the ten RC T-beam bridges tested as a part of this study with promising results. The *RFs* for each bridge were able to be increased relative to the *RFs* calculated using standard AASHTO provisions, and *RFs* for nine of the ten were increased relative to the results from live-load testing. An important observation from these results is that, although they seem optimistic, they rely solely on well-established mechanics principles and incorporate conservative assumptions that limit the technique's possible benefit. Notably, the technique is able to account for both the entire, nonlinear moment-curvature response of individual girders to take advantage of their ductility, and the bridge system's ability to redistribute load to more lightly loaded girders when others become nonlinear. The technique is also able to provide some additional insight into bridges' behavior under shear, as it allows realistic distribution of load effects (both moment and shear) to individual girders based on load position, geometry, and material nonlinearity. With continued development, this technique has the potential to improve the *RFs* of older bridges that are known to carry modern loading without distress despite having low *RFs* based on conventional engineering analysis.

6 References

1. AASHTO (2011). *The Manual for Bridge Evaluation.* American Association of State Highway and Transportation Officials, Washington DC.

2. AASHTO (2012). *AASHTO LRFD Bridge Design Specifications*. American Association of State Highway and Transportation Officials, Washington DC.

3. *ABAQUS 6.13* [Computer software]. Vélizy-Villacoublay, France, Dassault Systèmes.

4. Albraheemi, M.J.A., Davids, W.G., Schanck, A., & Tomlinson, S. (2019). Evaluation and rating of older non-composite steel girder bridges using field live load testing and nonlinear finite element analysis. *Bridge Struct.* 15(1-2). 27-41.

5. Alkhrdaji, T., Barker, M., Chen, G., Mu, H., Nanni, A., & Yang, X. (2001). Destructive and non-destructive testing of bridge J857, Phelps County, Missouri. Center for Infrastructure Engineering Studies, University of Missouri at Rolla. Rolla, MO.

6. Barr, P.J., & Amin, MD., N. (2006). Shear live-load distribution factors for I-girder bridges. *J. of Bridge Eng.* 11(2). 197-204.

7. Buckle, I.G., Dickson, A.R., & Phillips, M.H. (1985). Ultimate strength of three reinforced concrete highway bridges. *Can. J. of Civ. Eng.* 12, 63-72.

8. Burdette, E.G., & Goodpasture, D.W. (1971). Final Report for "Full-Scale Bridge Testing". University of Tennessee, Knoxville, TN.

9. Belarbi, A. & Hsu, T.T.C. (1994). Constitutive laws of concrete in tension and reinforcing bars stiffened by concrete. *ACI Struct. J.,* July-August, 465-74.

10. Bridge Diagnostics Inc. (2010). *Wireless structural testing system STS-WiFi operations manual.* Boulder, CO.: BDI.

11. Ebeido, T. & Kennedy, J.B. (1996). Shear and reaction distributions in continuous skew composite bridges. *J. of Bridge Eng.* 1(4). 155-65.

12. Hognestad, E. (1951). *A study of combined bending and axial load in reinforced concrete members.* Urbana, IL.: University of Illinois, Urbana.

13. Loring, H.B., & Davids, W.G. (2015). Mechanically fastened composite strips for flexural strengthening of concrete beams. *Constr. and Build. Mater.*, 76, 118-29.

14. Riks, E. (1979). An incremental approach to the solution of snapping and buckling problems. *Int. J. of Solids and Struct.*, 15(7), 529-51.

15. Saraf, V. (1998). Evaluation of existing RC slab bridges. *J. of Perform. of Constr. Facil.*, 12(1), 20-4.

16. Schanck, A. & Davids, W. (2018a). *Live Load Testing and Load Rating of Five Reinforced Concrete T-Beam Bridges.* Orono, ME.: University of Maine.

17. Schanck, A. & Davids, W. (2018b). *Live Load Testing and Load Rating of Five Skewed Reinforced Concrete T-Beam Bridges.* Orono, ME,: University of Maine.

18. Schanck, A. & Davids, W. (2020). Capacity assessment of older T-beam bridges by nonlinear proxy finite element analysis. *Struct.* 23(2020), 267-78.

19. Théoret, P., Massicotte, B., & Conciatori, D. (2012). Analysis and design of straight and skewed slab bridges. *J. of Bridge Eng.* 17(2). 289-301.

20. Xing, G., Wu, Tao, Liu, B., Huang, H., & Gu, S. (2010). Experimental investigation of reinforced concrete T-beams strengthened with steel wire mesh embedded in polymer mortar overlay. *Adv. in Struct Eng.* 13(1): 69-79.

A.1 Experimental Configuration and Data Collected

For each of the five bridges tested, a collection of data files is provided which contains input data, experimental configuration data, and data collected during tests. The files pertaining to each bridge are tabulated in the following appendices.

A.1.1 Input Data

A Comma Separated Variable (.csv) file is provided for each bridge which gives a list of the serial numbers of the sensors in the order as well as a MATLAB variable file (.mat) giving the layout of those sensors on each bridge. The sensor list .csv file provides sensors in the order that they are used and tabulated by STS-WiFi, and consequently in resulting test data. The sensor layout gives relative positions of sensors as they appeared for each bridge. Each girder is represented by three rows of data representing its top, middle and bottom respectively. Each collection of rows is placed in its relative position as it appears on the bridge. From left to right, columns represent the end receiving two sensors, mid-span, and the end receiving one sensor respectively. In this way, the relative position of each sensor can be determined. For example, a sensor in the second column of the second row would represent a sensor placed at mid-height of the first girder at midspan.

A.1.2 Collected Data

For each test configuration, a .mat file is provided which contains strain data recorded during the test. This data has been rectified by a linear correction function to correct for the sensors' tendency to drift its zero-point during a test.

A.2 Levant No. 5489

A.2.1 Experimental Configuration and Experimental Data Collected

Table 23: Bridge 5489 Experimental Configuration and Experimental Data Collected

| File Contents	File Name	File Type
Sensors	Br5489_Sensors.csv	CSV Format
Sensor Layout	Br5489_SensorLayout.mat	MATLAB Data File
Sensor Data	Br5489_ALT_S_2_1_Strain.mat	MATLAB Data File
	Br5489_ALT_U_2_1_Strain.mat	MATLAB Data File
	Br5489_MAX_S_1_1_Strain.mat	MATLAB Data File
	Br5489_MAX_S_2_1_Strain.mat	MATLAB Data File
	Br5489_MAX_S_3_1_Strain.mat	MATLAB Data File
	Br5489_MAX_U_2_1_Strain.mat	MATLAB Data File
	Br5489_SBS_S_2_1_Strain.mat	MATLAB Data File
	Br5489_SBS_U_2_2_Strain.mat	MATLAB Data File

A.2.2 Instrumentation
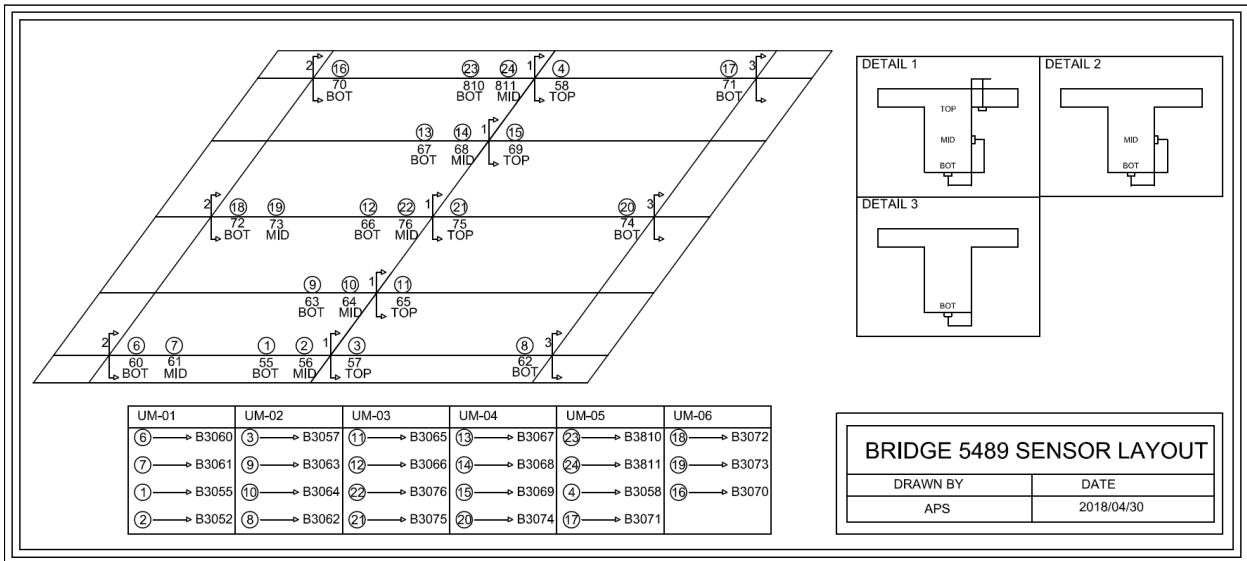
Figure 33: Bridge 5489 Sensor Layout

A.2.3 Loading

Figure 34: Bridge 5489 Truck T01-316 Loading

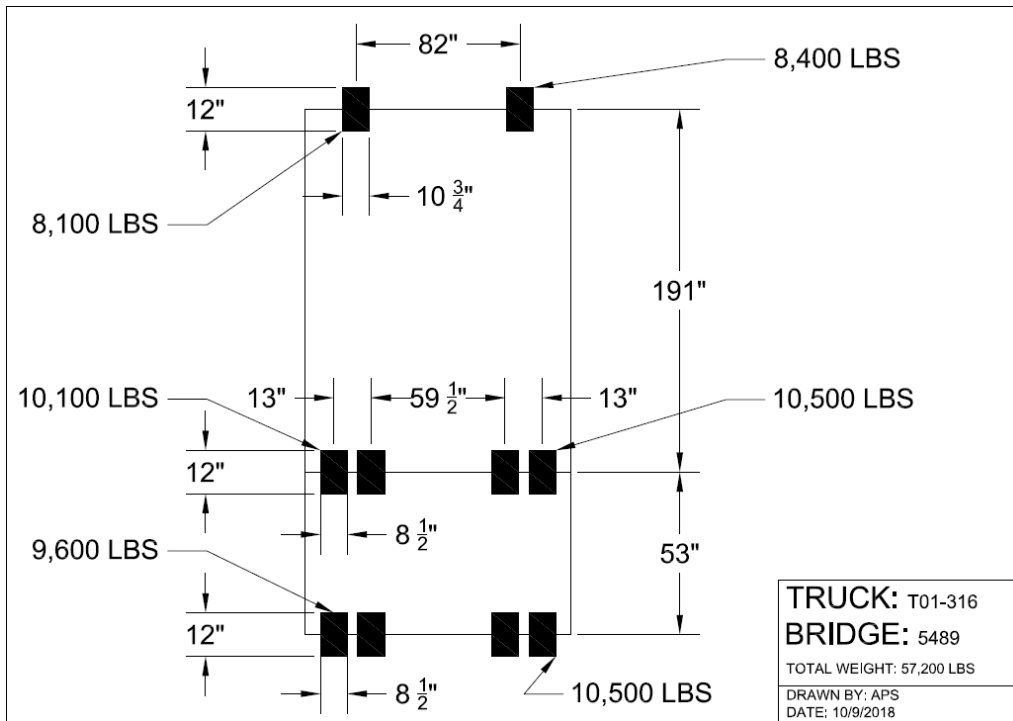Figure 35: Bridge 5489 Truck T01-907 Loading

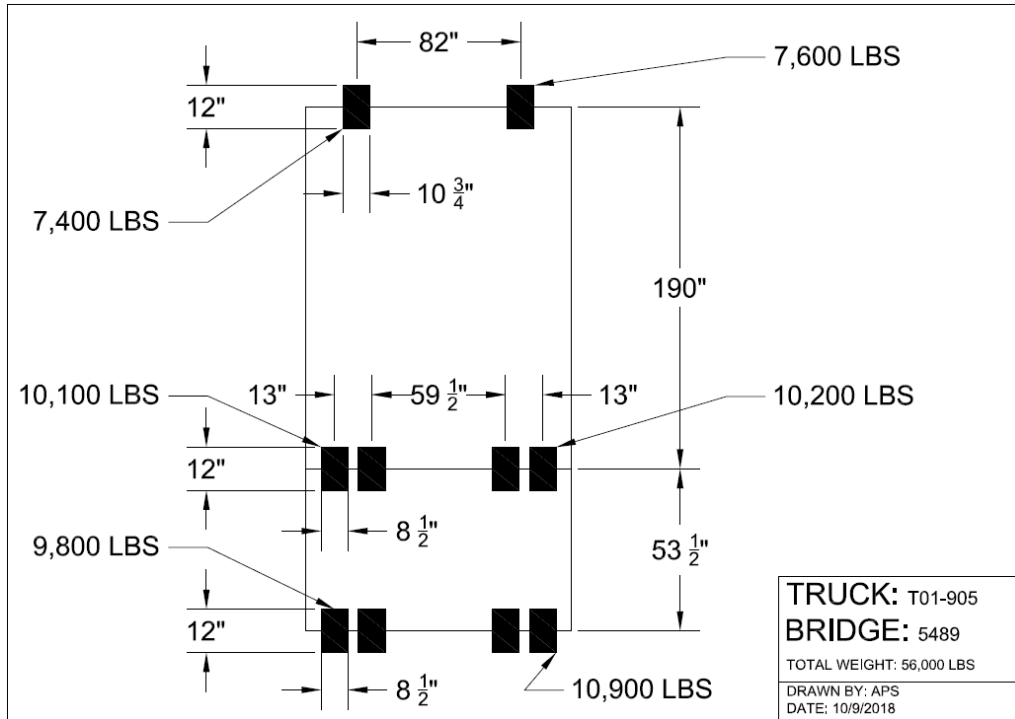Figure 36: Bridge 5489 Truck T01-906 Loading

Figure 37: Bridge 5489 Truck T01-904 Loading
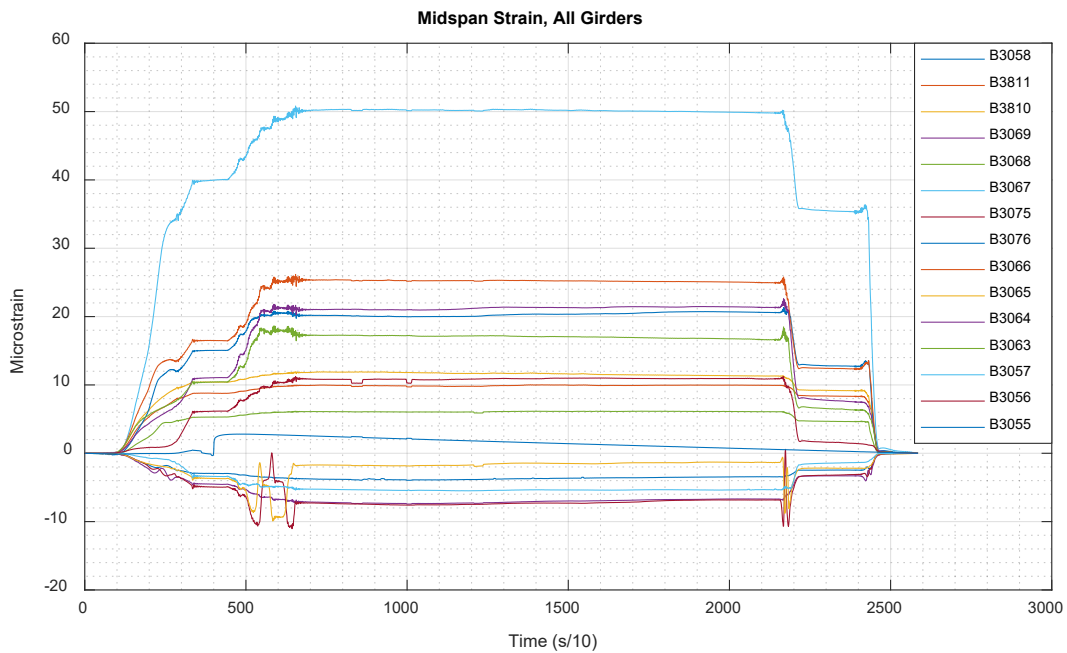
A.2.4 Representative Data Plots

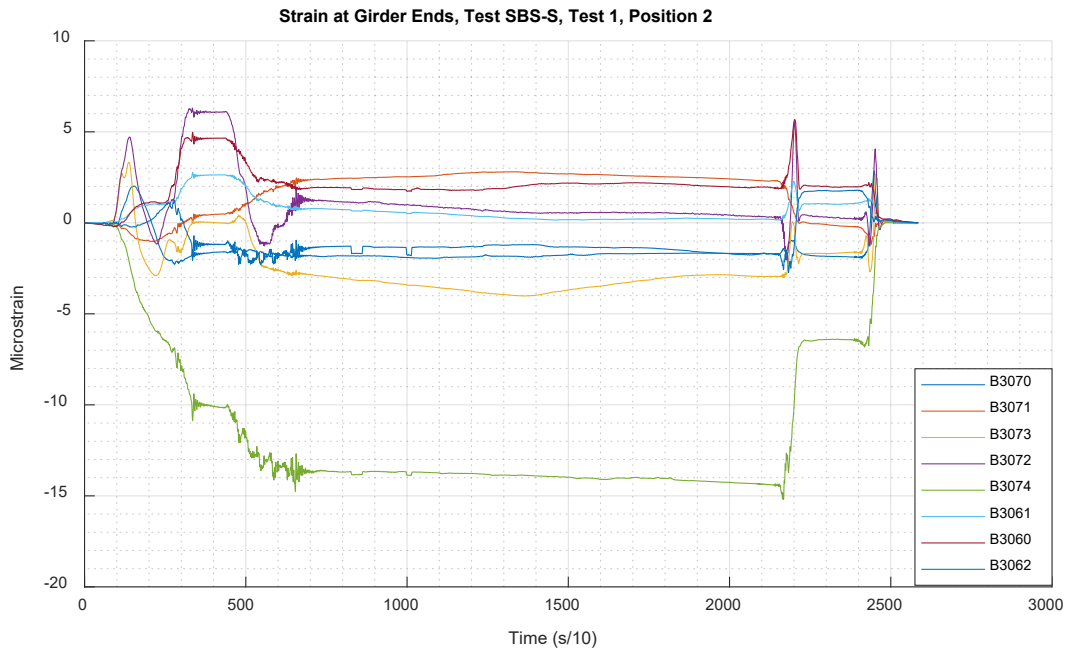Figure 38: Bridge 5489 SBS_S_2_1 Strains - Midspan

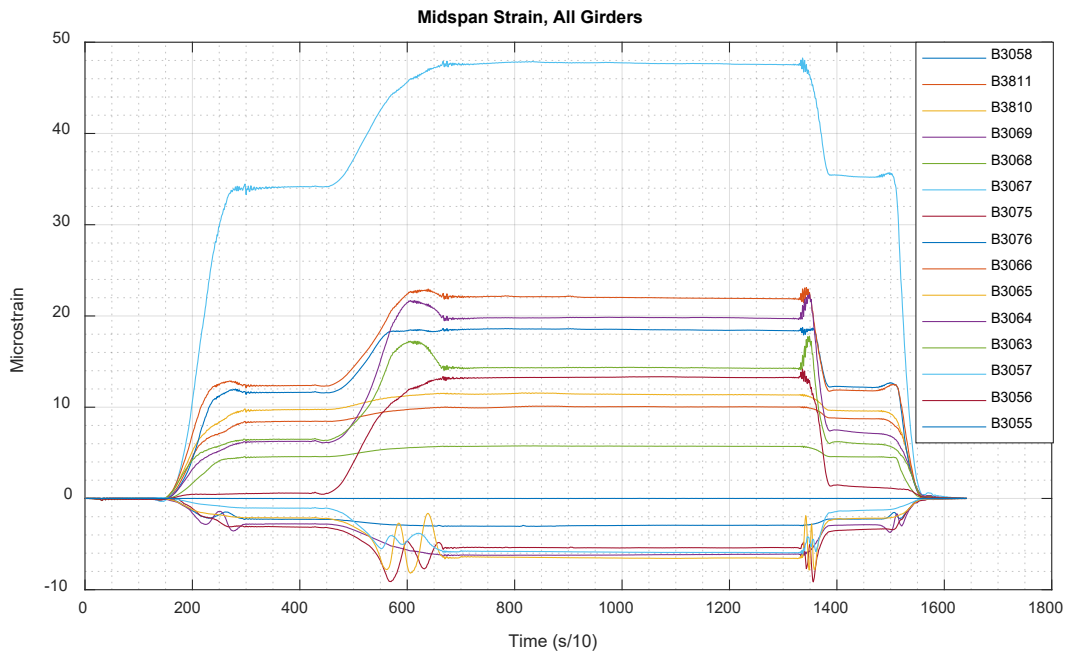Figure 39: Bridge 5489 SBS_S_2_1 Strains - Ends

Figure 40: Bridge 5489 SBS_U_2_2 Strains - Midspan
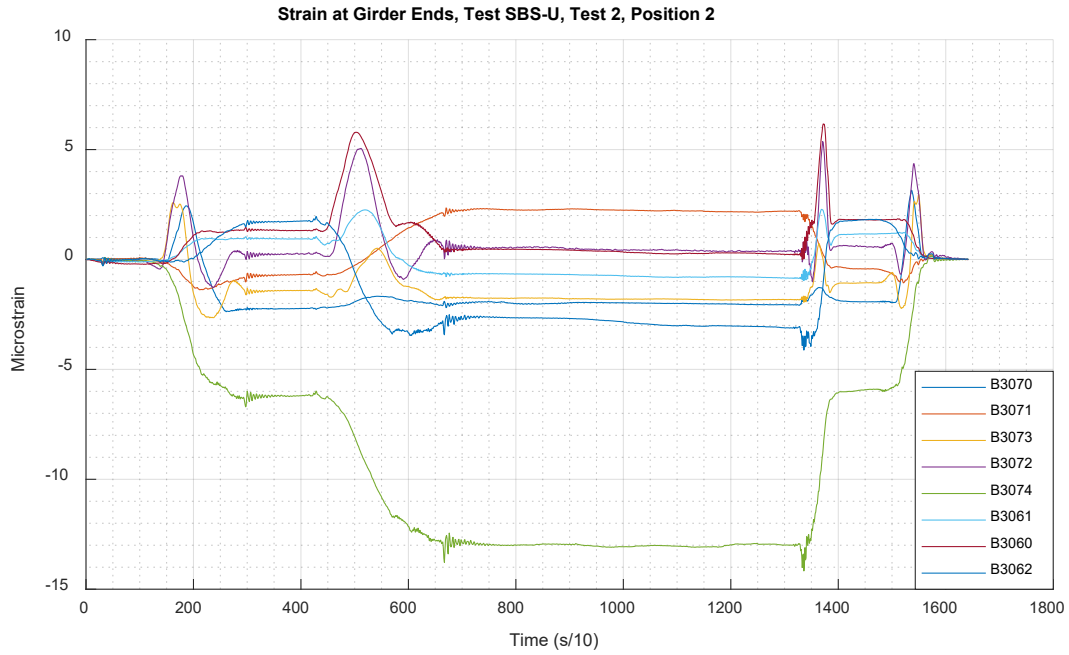
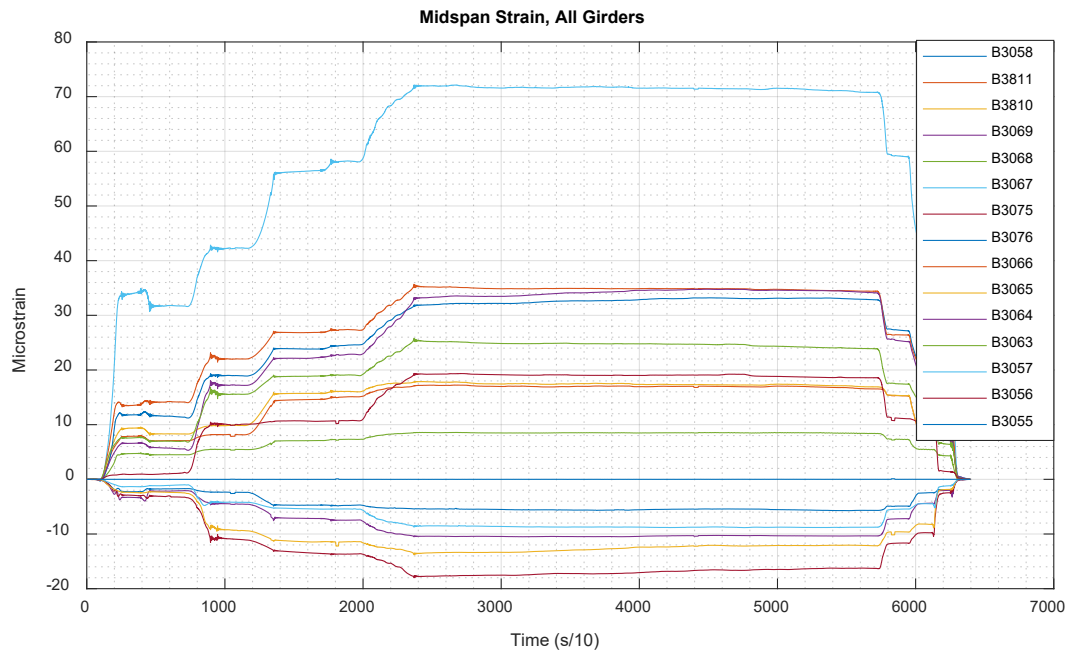Figure 41: Bridge 5489 SBS_U_2_2 Strains - Ends

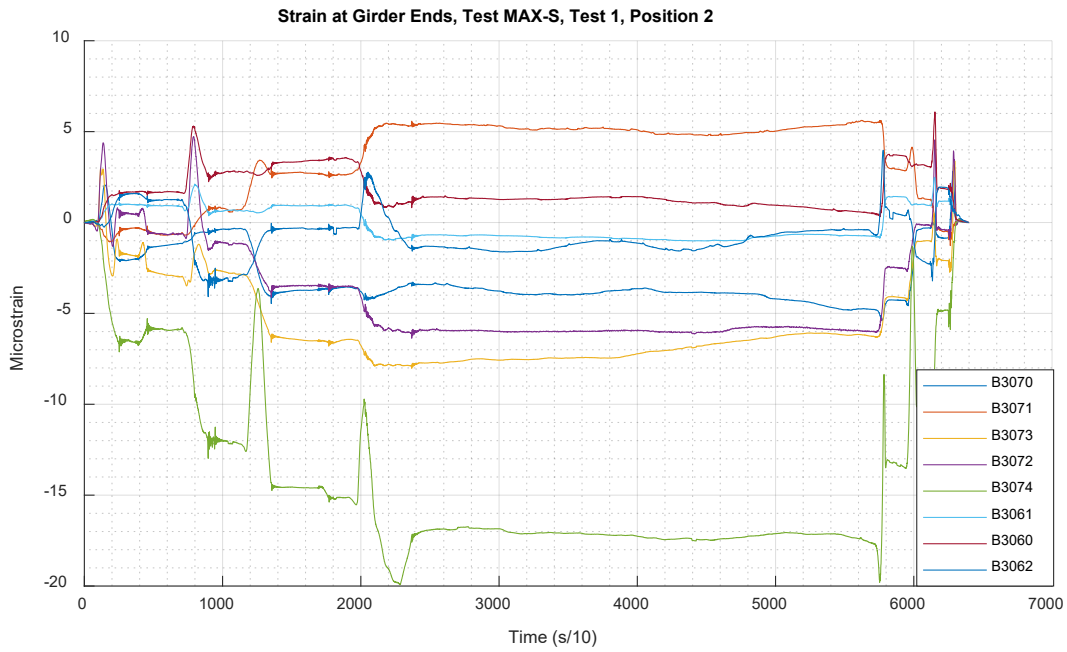Figure 42: Bridge 5489 MAX_S_2_1 Strains - Midspan

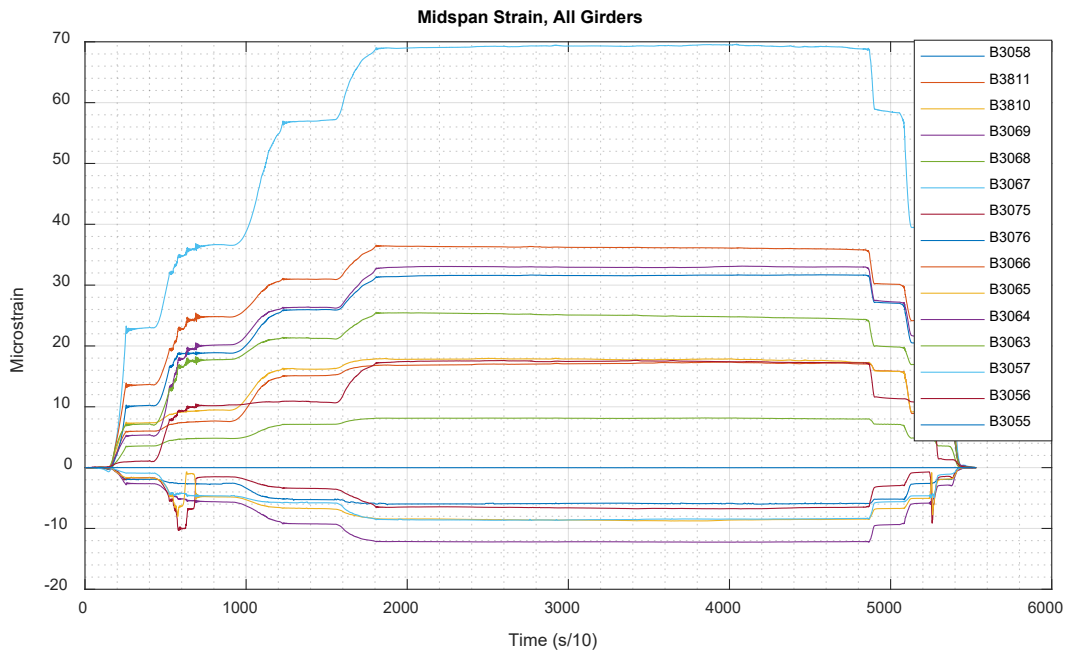Figure 43: Bridge 5489 MAX_2_1 Strains – Ends

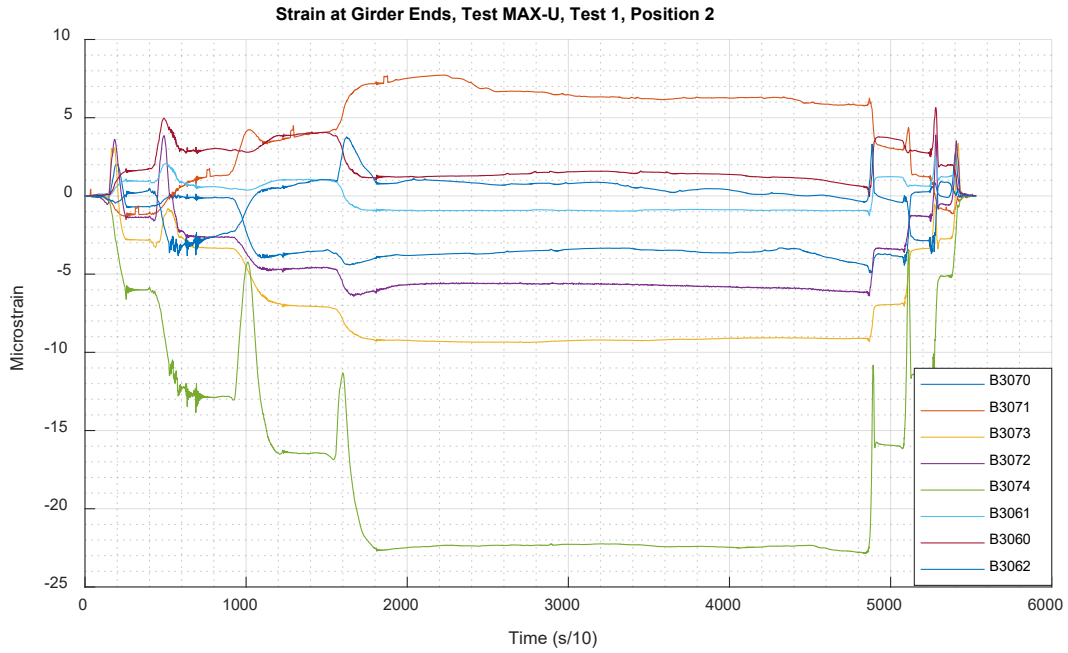
Figure 44: Bridge 5489 MAX_U_2_1 Strains – Midspan

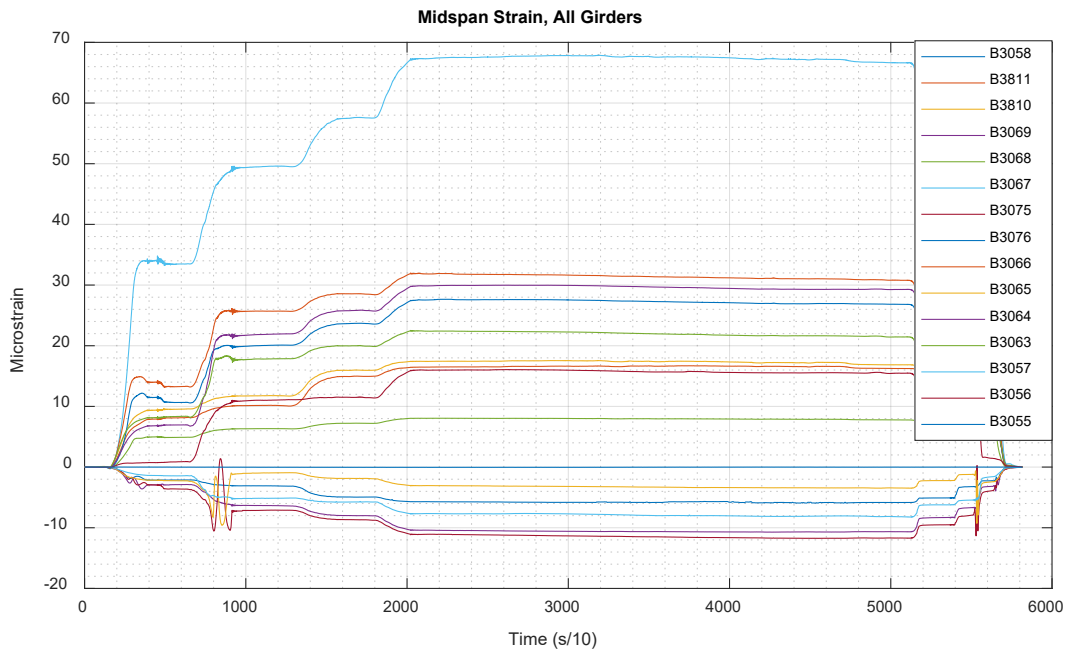Figure 45: Bridge 5489 MAX_U_2_1 Strains – Ends

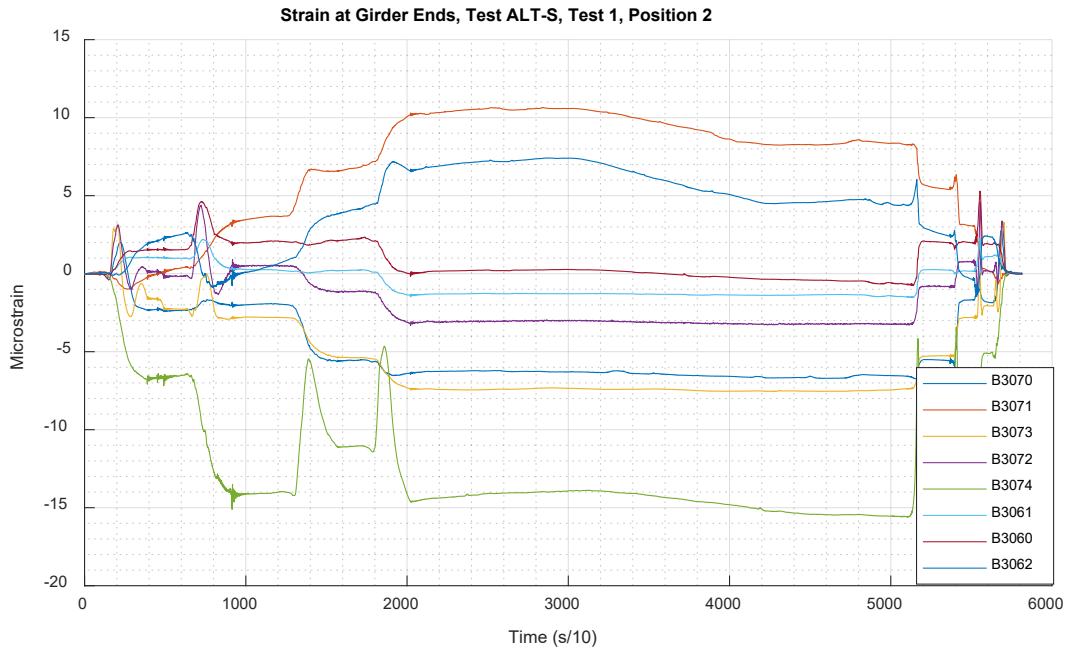Figure 46: Bridge 5489 ALT_S _2_1 Strains – Midspan
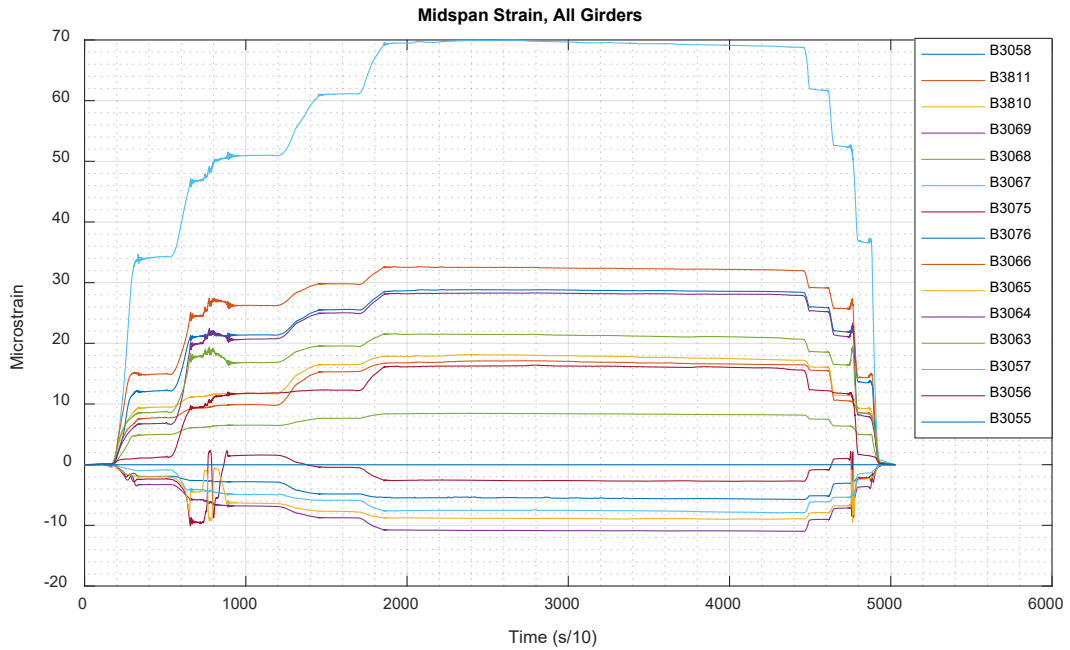
Figure 47: Bridge 5489 ALT_S_2_1 Strains – Ends

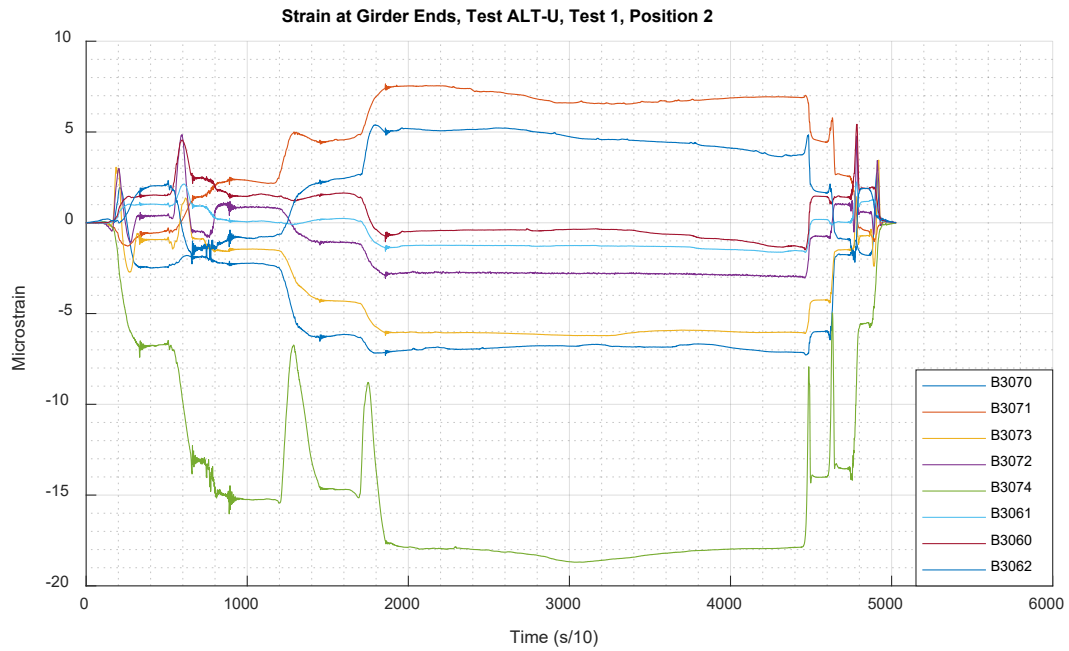Figure 48: Bridge 5489 ALT_U_2_1 Strains – Midspan

Figure 49: Bridge 5489 ALT_U_2_1 Strains – Ends

A.2.5 Rating Factor Calculations

AASHTO Rating Calculations:

Bridge 5489 - Levant, Maine

Material Parameters:

Concrete Compressive Strength	$f'_c := 2.5 \; \boldsymbol{ksi}$
Reinforcement Yield Strength	$F_y := 33 \; \boldsymbol{ksi}$
Unit Weight: Reinforced Concrete	$\gamma_{RC} := 0.150 \; \dfrac{\boldsymbol{kip}}{\boldsymbol{ft}^3}$
Unit Weight: Wearing Surface	$\gamma_{ws} := 0.150 \; \dfrac{\boldsymbol{kip}}{\boldsymbol{ft}^3}$

Geometric Properties:

Span Length	$L := 47 \; \boldsymbol{ft}$
Girder Spacing - Interior	$S := 82 \; \boldsymbol{in}$
Girder Spacing - Exterior	$S_x := 54 \; \boldsymbol{in}$
Number of Girders	$NG := 5$
Skew Angle	$skew := 15 \; °$
Lane Width	$lanewidth := 13 \; \boldsymbol{ft}$
Number of Lanes	$Nlane := 2$
Wearing Surface Thickness	$ws := 3 \; \boldsymbol{in}$
Thickness of Pavement Overlay	$ws_2 := 0 \; \boldsymbol{in}$
Girder Height - Interior	$h := 36 \; \boldsymbol{in}$
Girder Height - Exterior	$h_x := 36 \; \boldsymbol{in}$
Deck Thickness	$d_s := 5.5 \; \boldsymbol{in}$
Web Width - Interior	$b_w := 19 \; \boldsymbol{in}$
Web Width - Exterior	$b_{wx} := 19 \; \boldsymbol{in}$
Curb Depth	$h_{curb} := 12 \; \boldsymbol{in}$
Curb Width	$b_{curb} := 20 \; \boldsymbol{in}$

Height to Centroid of Reinforcement - Interior	$y_{bar} := \begin{bmatrix} 4.893 \\ 6.077 \\ 8.27 \\ 6.077 \\ 4.893 \end{bmatrix} \boldsymbol{in}$
Height to Centroid of Reinforcement - Exterior	$y_{barx} := \begin{bmatrix} 4.893 \\ 6.077 \\ 8.27 \\ 6.077 \\ 4.893 \end{bmatrix} \boldsymbol{in}$
Area of Reinforcement - Interior	$A_s := \begin{bmatrix} 12.016 \\ 15.142 \\ 18.268 \\ 15.142 \\ 12.016 \end{bmatrix} \boldsymbol{in}^2$

Area of Reinforcement - Exterior

$$A_{sx} := \begin{bmatrix} 12.016 \\ 15.142 \\ 18.268 \\ 15.142 \\ 12.016 \end{bmatrix} in^2$$

Distance from Centerline of Girder to Edge of Curb $\qquad d_e := -7 \; in$

Eccentricity of Centerline of Girders w.r.t. Centerline of Roadway $\qquad exc := 0 \; in$

Concentrated Load Due to Diaphragms on One Girder $\qquad P_{dint} := 1.99 \; kip$

Location of Intermediate Diaphragm
(Half, Third, Quarter) $\qquad loc_d := \text{"Half"}$

Distributed Load Due to Rail $\qquad w_{rail} := 0.328 \; \dfrac{kip}{ft}$

Structural Dead Load Factor $\qquad \gamma_{DC} := 1.25$
Wearing Surface Dead Load Factor $\qquad \gamma_{DW} := 1.25$
Live Load Factor $\qquad \gamma_{LL} := 1.35$
Live Load Impact Factor $\qquad IM := 0.33$

Flexural Resistance Factor $\qquad \phi := .9$
System Factor $\qquad \phi_s := 1.0$
Condition Factor $\qquad \phi_c := 1.0$

Web Height - Interior $\qquad d_g := h - d_s$
Web Height - Exterior $\qquad d_{gx} := h_x - d_s$

Include Wearing Surface in Section Height $\qquad h := h + \textbf{if}\left(\gamma_{ws} = 0.15 \; \dfrac{kip}{ft^3}, ws, 0\right) = 39 \; in$

Depth to Centroid of Reinforcement - Interior $\qquad d := h - y_{bar}$
Depth to Centroid of Reinforcement - Exterior $\qquad d_x := h_x - y_{barx} + h_{curb}$
Moment Applied to Interor Girders from Diaphragm $\qquad M_d :=$ if $loc_d = \text{"Half"} \qquad\quad = 23.383 \; ft \cdot kip$

$$\left\| P_{dint} \cdot \frac{L}{4} \right.$$

else if $loc_d = \text{"Third"}$

$$\left\| P_{dint} \cdot \frac{L}{3} \right.$$

else if $loc_d = \text{"Quarter"}$

$$\left\| P_{dint} \cdot \frac{L}{4} + P_{dint} \cdot \frac{L}{4} \right.$$

Moment Applied to Exterior Girders from Diaphragm $\qquad M_{dx} := \dfrac{M_d}{2} = 11.691 \; ft \cdot kip$

Dictance Between Centroids of Deck and Web

$$e_g := \frac{d_g + d_s}{2} = 18 \; \boldsymbol{in}$$

Area of Web

$$A := d_g \cdot b_w = 579.5 \; \boldsymbol{in}^2$$

Moment of Inertia of Web

$$I := \frac{b_w \cdot d_g^3}{12} = \left(4.492 \cdot 10^4\right) \; \boldsymbol{in}^4$$

Modular Ratio - Deck and Web

$$n := 1$$

Longitudinal Stiffness Parameter

$$K_g := n \cdot \left(I + A \cdot e_g^2\right) = \left(2.327 \cdot 10^5\right) \; \boldsymbol{in}^4$$

Interior Moment Distribution Factor - 1 Lane

$$g_{m1} := 0.06 + \left(\frac{S}{14 \; \boldsymbol{ft}}\right)^{0.4} \cdot \left(\frac{S}{L}\right)^{0.3} \cdot \left(\frac{K_g}{L \cdot d_s^3}\right)^{0.1} = 0.521$$

Interior Moment Distribution Factor - 2 Lane

$$g_{m2} := 0.075 + \left(\frac{S}{9.5 \; \boldsymbol{ft}}\right)^{0.6} \cdot \left(\frac{S}{L}\right)^{0.2} \cdot \left(\frac{K_g}{L \cdot d_s^3}\right)^{0.1} = 0.686$$

Controling Interior Moment Distribution Factor

$$g_m := \max \langle g_{m1}, g_{m2} \rangle$$

Roadway Width

$$W_r := lanewidth \cdot Nlane$$

Eccentricity of Design Lane From C.G. of Girders

$$e_1 := \frac{W_r}{2} - 5 \; \boldsymbol{ft} + exc = 8 \; \boldsymbol{ft}$$

Eccentricity of Exterior Girder From C.G. of Girders

$$X_{ext} := (NG - 1) \cdot \frac{S}{2} = 13.667 \; \boldsymbol{ft}$$

Eccentricity of Each Girder

$$x_1 := X_{ext}$$
$$x_2 := X_{ext} - S$$
$$x_3 := X_{ext} - 2 \cdot S$$
$$x_4 := \mathbf{if}\left(NG > 3, X_{ext} - 3 \cdot S, 0 \; \boldsymbol{ft}\right)$$
$$x_5 := \mathbf{if}\left(NG > 4, X_{ext} - 4 \cdot S, 0 \; \boldsymbol{ft}\right)$$

Lever Rule Distribution Factor - One Lane

$$R_1 := \frac{1}{NG} + \frac{X_{ext} \cdot e_1}{x_1^2 + x_2^2 + x_3^2 + x_4^2 + x_5^2} = 0.434$$

$$g_{mR1} := \mathbf{if}\left(P_{dint} > 0, 1.2 \cdot R_1, 0\right) = 0.521$$

Lever Rule Distribution Factor - Two Lanes

$$R_2 := \frac{2}{NG} + \frac{X_{ext} \cdot \left(e_1 - 5 \; \boldsymbol{ft}\right)}{x_1^2 + x_2^2 + x_3^2 + x_4^2 + x_5^2} = 0.488$$

$$g_{mR2} := \mathbf{if}\left(P_{dint} > 0, R_2, 0\right) = 0.488$$

Exterior Moment Distribution Factor

$$g_{mx1} := \frac{1.2 \cdot \left(S + d_e - 2 \; \boldsymbol{ft}\right)}{2 \cdot S} = 0.373$$

$$ee := 0.77 + \frac{d_e}{9.1 \; \boldsymbol{ft}} = 0.706$$

$$g_{mx2} := g_{m2} \cdot ee = 0.484$$

Skew Correction Factor	$g_{mx} := \max\left(g_{mx1}, g_{mx2}\right) = 0.484$
	$c_1 := 0.25 \cdot \left(\dfrac{K_g}{12 \cdot L \cdot d_s^{\,3}}\right)^{0.25} \cdot \left(\dfrac{S}{L}\right)^{.5} = 0.064$
	$\theta := \mathbf{if}\left(skew \geq 30\,^\bullet,\ skew,\ 0\,^\bullet\right)$
	$C_\theta := 1 - c_1 \cdot \left(\tan\left(\theta\right)\right)^{1.5} = 1$
	$g_m := g_m \cdot C_\theta = 0.686$
	$g_{mx} := g_{mx} \cdot C_\theta = 0.484$

Interior DF   Exterior DF

$g_m = 0.686$ $g_{mx} = 0.484$

Interior Girder Dead Load	$w_{girder} := \gamma_{RC} \cdot b_w \cdot d_g = 0.604\ \dfrac{kip}{ft}$
Deck Dead Load	$w_{deck} := \gamma_{RC} \cdot S \cdot d_s = 0.47\ \dfrac{kip}{ft}$
Curb Dead Load	$w_{curb} := 2 \cdot \gamma_{RC} \cdot h_{curb} \cdot b_{curb} = 0.5\ \dfrac{kip}{ft}$
Dead Load from Nonstructural Components	$w_{ns} := \dfrac{w_{curb}}{NG} + w_{rail} = 0.428\ \dfrac{kip}{ft}$
Total Structural Dead Load on Interior Girders	$DC := w_{girder} + w_{deck} + w_{ns} = 1.501\ \dfrac{kip}{ft}$
Exterior Girder Dead Load	$w_{girderx} := \gamma_{RC} \cdot b_{wx} \cdot d_{gx} = 0.604\ \dfrac{kip}{ft}$
Exterior Deck Dead Load	$w_{deckx} := \gamma_{RC} \cdot S_x \cdot d_s = 0.309\ \dfrac{kip}{ft}$
Total Structural Dead Load on Exterior Girders	$DC_x := w_{girderx} + w_{deckx} + w_{ns} = 1.341\ \dfrac{kip}{ft}$
Wearing Surface Dead Load on Interior Girders	$DW := \gamma_{ws} \cdot \left(ws + ws_2\right) \cdot S = 0.256\ \dfrac{kip}{ft}$
Wearing Surface Dead Load on Exterior Girders	$DW_x := \gamma_{ws} \cdot \left(ws + ws_2\right) \cdot S_x = 0.169\ \dfrac{kip}{ft}$
Dead Load Moments	$M_{DC} := \dfrac{DC \cdot L^2}{8} + M_d \qquad M_{DCx} := \dfrac{DC_x \cdot L^2}{8} + M_{dx}$
	$M_{DW} := \dfrac{DW \cdot L^2}{8} \qquad\qquad M_{DWx} := \dfrac{DW_x \cdot L^2}{8}$

$M_{DC} = 437.967 \ \boldsymbol{ft \cdot kip}$ $\qquad$ $M_{DCx} = 381.981 \ \boldsymbol{ft \cdot kip}$

$M_{DW} = 70.757 \ \boldsymbol{ft \cdot kip}$ $\qquad$ $M_{DWx} = 46.596 \ \boldsymbol{ft \cdot kip}$

Live Load Moment - Truck Load $\qquad$ $M_{Truck} := 32 \ \boldsymbol{kip} \cdot \left(\dfrac{L}{4}\right) + \dfrac{40 \ \boldsymbol{kip}}{2} \cdot \left(\dfrac{L}{2} - 14 \ \boldsymbol{ft}\right) = 566 \ \boldsymbol{ft \cdot kip}$

Live Load Moment - Tandem $\qquad$ $M_{Tandem} := 25 \ \boldsymbol{kip} \cdot \dfrac{L}{4} + \dfrac{25 \ \boldsymbol{kip}}{2} \cdot \left(\dfrac{L}{2} - 4 \ \boldsymbol{ft}\right) = 537.5 \ \boldsymbol{ft \cdot kip}$

Live Load Moment - Lane $\qquad$ $M_{Lane} := 0.64 \ \dfrac{\boldsymbol{kip}}{\boldsymbol{ft}} \cdot \dfrac{L^2}{8} = 176.72 \ \boldsymbol{ft \cdot kip}$

Total HL-93 Live Load $\qquad$ $M_{LL} := M_{Lane} + (1 + IM) \cdot \max\left(M_{Truck}, M_{Tandem}\right)$

$M_{LL} = 929.5 \ \boldsymbol{ft \cdot kip}$

Nominal Resistance

Depth Whitney Stress Block - Interior $\qquad$ $a := A_s \cdot \dfrac{F_y}{0.85 \cdot f'_c \cdot S} = \begin{bmatrix} 2.276 \\ 2.868 \\ 3.46 \\ 2.868 \\ 2.276 \end{bmatrix} \ \boldsymbol{in}$

Nominal Moment Resistance - Interior $\qquad$ $\overrightarrow{M_n := F_y \cdot A_s \cdot \left(d - \dfrac{a}{2}\right)} = \begin{bmatrix} 1.089 \cdot 10^3 \\ 1.311 \cdot 10^3 \\ 1.457 \cdot 10^3 \\ 1.311 \cdot 10^3 \\ 1.089 \cdot 10^3 \end{bmatrix} \ \boldsymbol{ft \cdot kip}$

Interior Nominal Moment Capacity

$M_{capacity} := \max \langle M_n \rangle = \left(1.457 \cdot 10^3\right) \ \boldsymbol{ft \cdot kip}$

Depth Whitney Stress Block - Exterior $\qquad$ $a_x := A_{sx} \cdot \dfrac{F_y}{0.85 \cdot f'_c \cdot S_x} = \begin{bmatrix} 3.456 \\ 4.355 \\ 5.254 \\ 4.355 \\ 3.456 \end{bmatrix} \ \boldsymbol{in}$

Nominal Moment Resistance - Exterior $\qquad$ $\overrightarrow{M_{nx} := F_y \cdot A_{sx} \cdot \left(d_x - \dfrac{a_x}{2}\right)} = \begin{bmatrix} 1.367 \cdot 10^3 \\ 1.655 \cdot 10^3 \\ 1.864 \cdot 10^3 \\ 1.655 \cdot 10^3 \\ 1.367 \cdot 10^3 \end{bmatrix} \ (\boldsymbol{ft \cdot kip})$

Exterior Nominal Moment Capacity

$M_{capacityx} := \max \langle M_{nx} \rangle = \left(1.864 \cdot 10^3\right) \ \boldsymbol{ft \cdot kip}$

Interior Moment Rating Factor

$$RF_{Interior} := \frac{\phi \cdot \phi_s \cdot \phi_c \cdot M_{capacity} - \gamma_{DC} \cdot M_{DC} - \gamma_{DW} \cdot M_{DW}}{\gamma_{LL} \cdot M_{LL} \cdot g_m}$$

Exterior Moment Rating Factor

$$RF_{Exterior} := \frac{\phi \cdot \phi_s \cdot \phi_c \cdot M_{capacityx} - \gamma_{DC} \cdot M_{DCx} - \gamma_{DW} \cdot M_{DWx}}{\gamma_{LL} \cdot M_{LL} \cdot g_{mx}}$$

Interior   Exterior

$RF_{Interior} = 0.784$ $RF_{Exterior} = 1.879$

Rating Factor Improvements

Concrete Compressive Strength - Larger is More Conservative

$$f'_c := 5 \; \textbf{ksi}$$

Concrte Elastic Modulus

$$E_c := 1820 \; \textbf{ksi} \cdot \sqrt{\frac{f'_c}{\textbf{ksi}}} = \left(4.07 \cdot 10^3\right) \; \textbf{ksi}$$

Interior Girders

Maximum Recorded Strain

$$\varepsilon_T := 87.2 \cdot 10^{-6}$$

Maximum Applied Moment per Lane

$$M_{Max} := 738.7 \; \textbf{ft} \cdot \textbf{kip}$$

Uncracked Section Modulus

$$S_{unc} := 9507 \; \textbf{in}^3$$

Cracked Section Modulus

$$S_{cr} := 4565 \; \textbf{in}^3$$

Section Behavior

$$Behavior := \text{"Uncracked"}$$

Section Modulus Effective for Behavior

$$S_e := \textbf{if} \left(Behavior = \text{"Uncracked"}, S_{unc}, S_{cr}\right)$$

Calculated Strain

$$\varepsilon_c := \frac{M_{Max} \cdot g_m}{S_e \cdot E_c} = 1.572 \cdot 10^{-4}$$

Test Benefit Factor

$$k_a := \frac{\varepsilon_c}{\varepsilon_T} - 1 = 0.803$$

Ratio of Applied to HL-93 Moment

$$r_M := \frac{M_{Max}}{M_{LL}} = 0.795$$

Test Understanding Factor

$$k_b := \textbf{if} \left(r_M > 0.7, 0.5, 0\right) = 0.5$$

Rating Improvement Factor

$$k := 1 + k_a \cdot k_b = 1.401$$

Improved Rating Factor

$$RF_{Improved} := RF_{Interior} \cdot k = 1.099$$

Exterior Girders

Maximum Recorded Strain

$$\varepsilon_T := 63.5 \cdot 10^{-6}$$

Maximum Applied Moment per Lane

$$M_{Max} := 738.7 \; \textbf{ft} \cdot \textbf{kip}$$

Uncracked Section Modulus

$$S_{unc} := 11008 \; \textbf{in}^3$$

Cracked Section Modulus

$$S_{cr} := 3469 \; \textbf{in}^3$$

Section Behavior

$$Behavior := \text{"Uncracked"}$$

Section Modulus Effective for Behavior

$$S_e := \textbf{if} \left(Behavior = \text{"Uncracked"}, S_{unc}, S_{cr}\right)$$

Calculated Strain

$$\varepsilon_c := \frac{M_{Max} \cdot g_{mx}}{S_e \cdot E_c} = 9.583 \cdot 10^{-5}$$

Test Benefit Factor

$$k_a := \frac{\varepsilon_c}{\varepsilon_T} - 1 = 0.509$$

Ratio of Applied to HL-93 Moment

$$r_M := \frac{M_{Max}}{M_{LL}} = 0.795$$

Test Understanding Factor

$$k_b := \mathbf{if}\left(r_M > 0.7, 0.5, 0\right) = 0.5$$

Rating Improvement Factor

$$k := 1 + k_a \cdot k_b = 1.255$$

Improved Rating Factor

$$RF_{ImprovedExt} := RF_{Exterior} \cdot k = 2.357$$

Improved Rating Factors

Interior

$$RF_{Improved} = 1.099$$

Exterior

$$RF_{ImprovedExt} = 2.357$$

Figure 50: Bridge 5489 Calculations

A.3   Hampden No. 5109

A.3.1 Experimental Configuration and Experimental Data Collected

Table 24: Bridge 5109 Experimental Configuration and Experimental Data Collected

File Contents	File Name	File Type
Sensors	Br5109_Sensors.csv	CSV Format
Sensor Layout	Br5109_SensorLayout.mat	MATLAB Data File
Sensor Data	Br5109_ALT_S_2_1_Strain.mat	MATLAB Data File
	Br5109_ALT_U_2_1_Strain.mat	MATLAB Data File
	Br5109_MAX_S_1_1_Strain.mat	MATLAB Data File
	Br5109_MAX_S_2_1_Strain.mat	MATLAB Data File
	Br5109_MAX_S_3_1_Strain.mat	MATLAB Data File
	Br5109_MAX_U_2_1_Strain.mat	MATLAB Data File
	Br5109_SBS_U_2_1_Strain.mat	MATLAB Data File
	Br_5432_MAX_1_2_Strain.mat	MATLAB Data File

A.3.2 Instrumentation
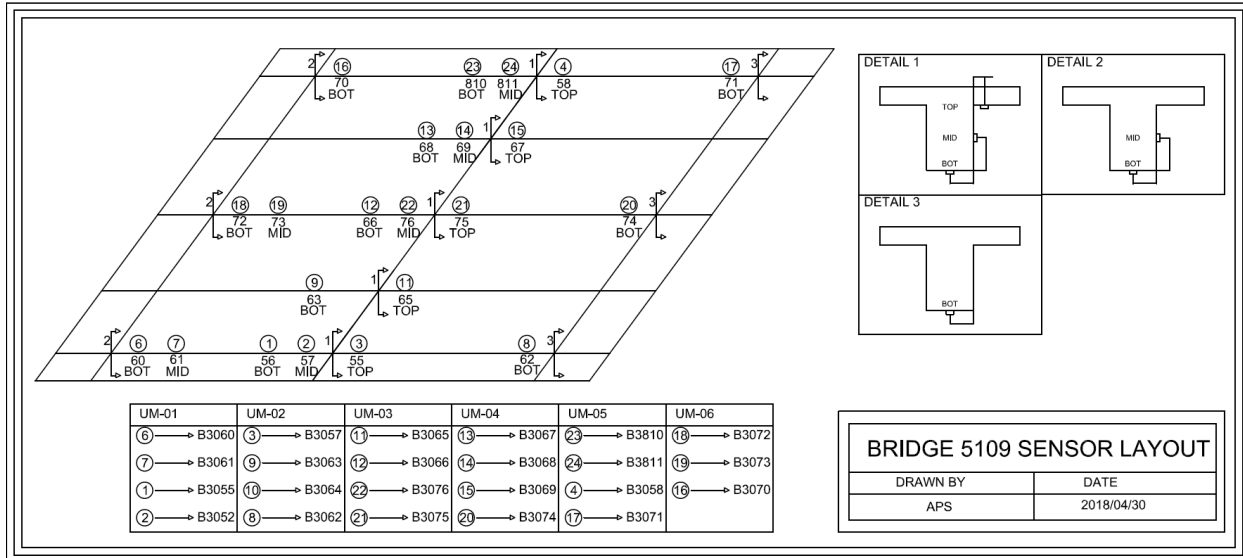
Figure 51: Bridge 5109 Sensor Layout

A.3.3 Loading
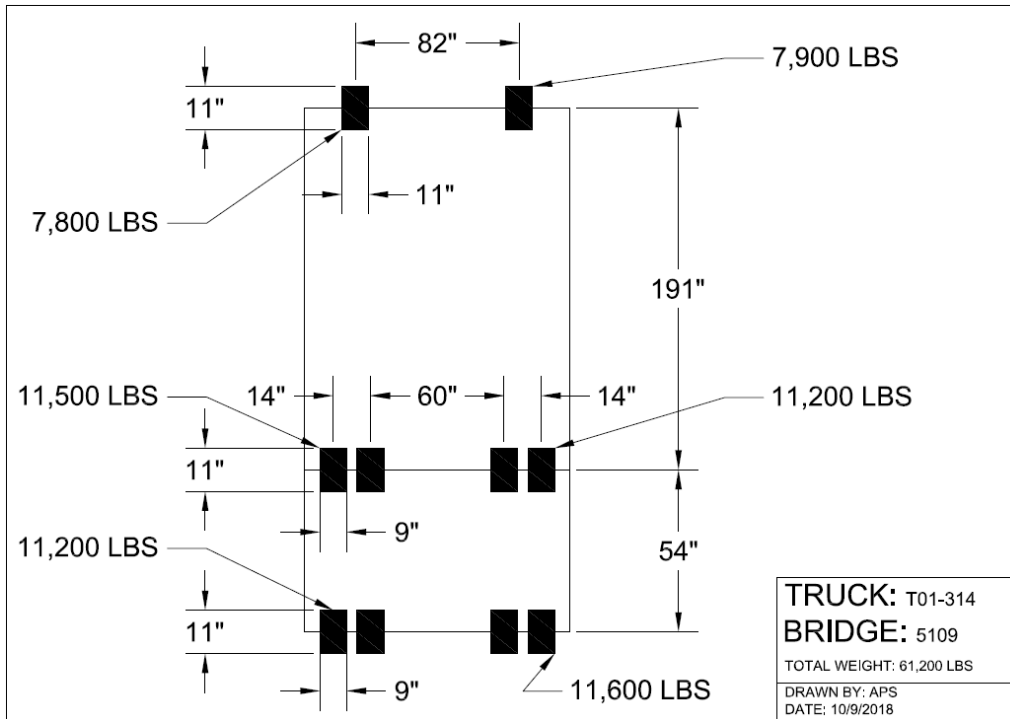
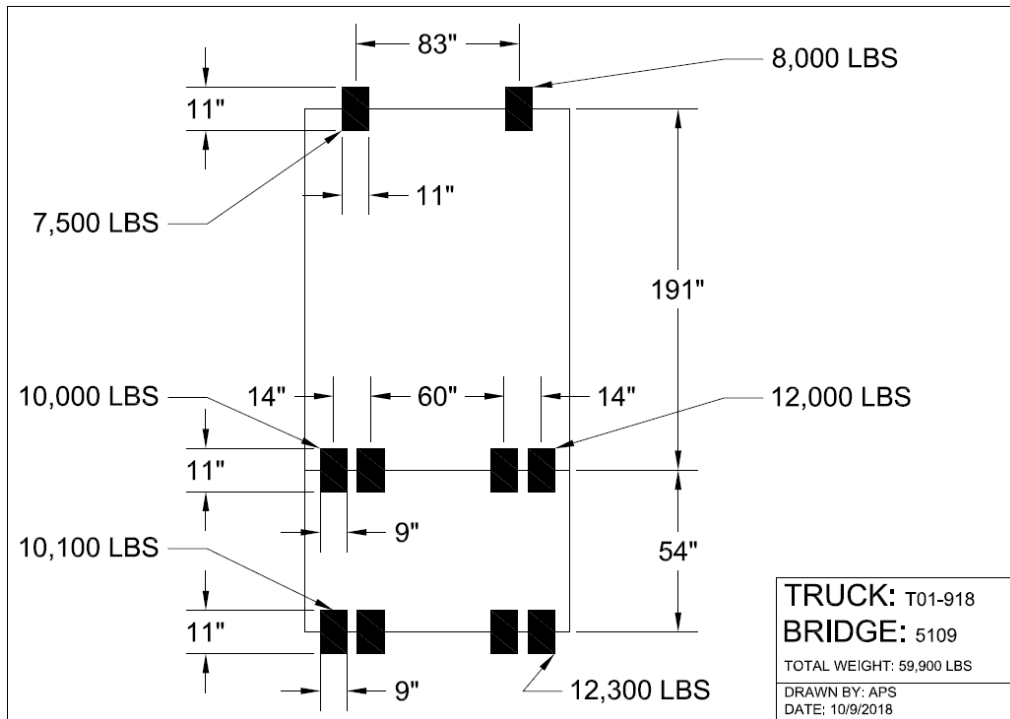Figure 52: Bridge 5109 Truck T01-314 Loading

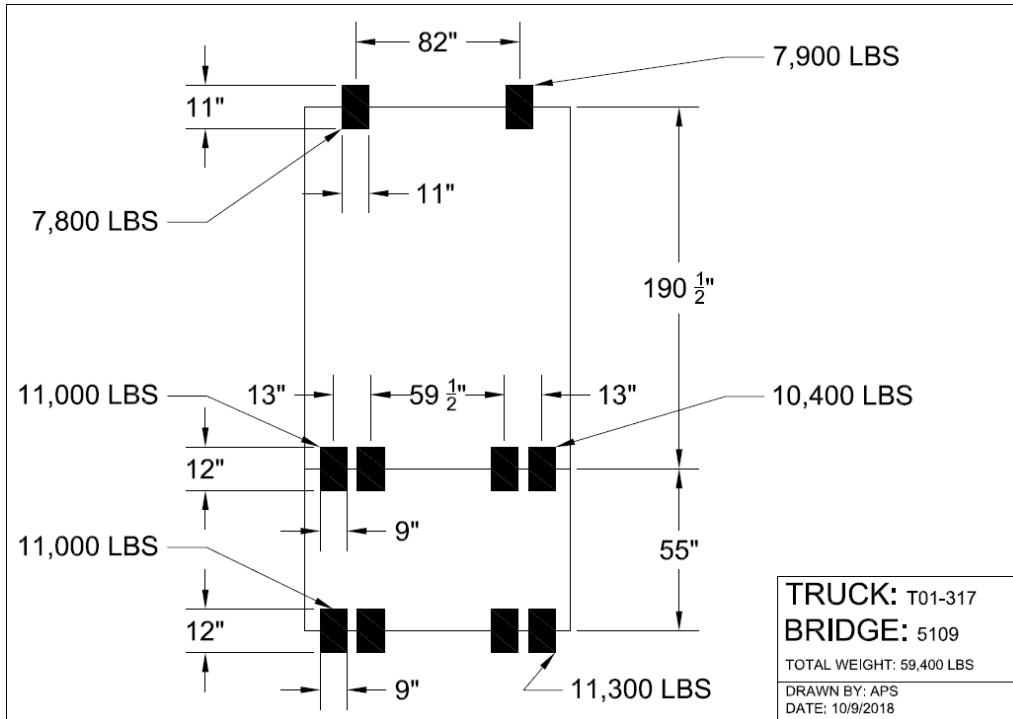Figure 53: Bridge 5109 Truck T01-918 Loading

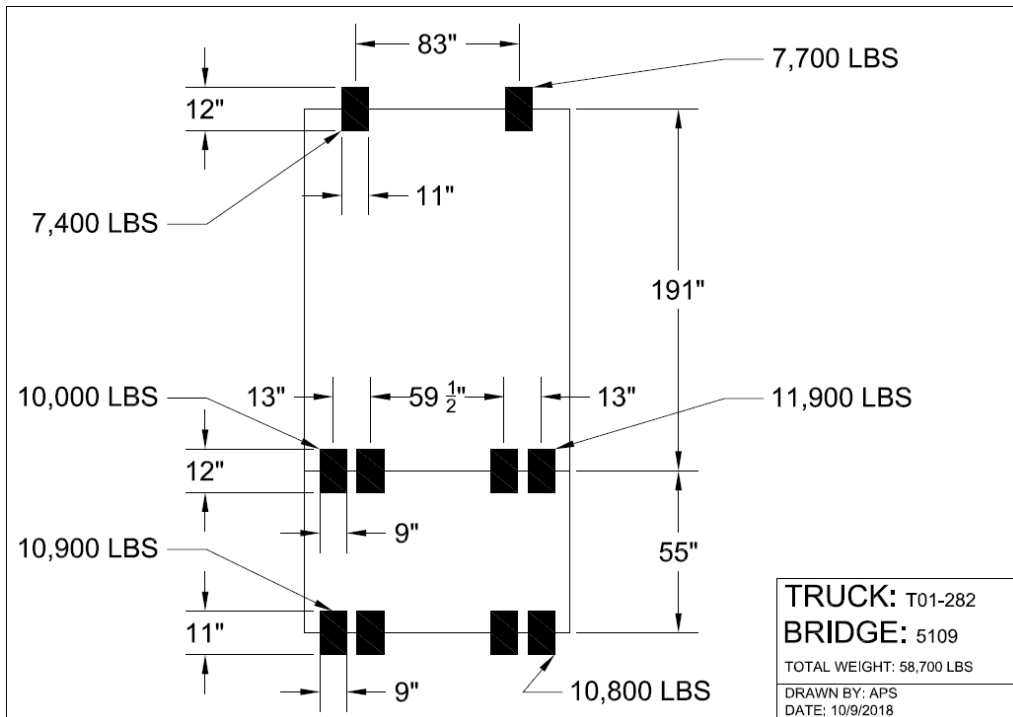Figure 54: Bridge 5109 Truck T01-317 Loading

Figure 55: Bridge 5109 Truck T01-282 Loading

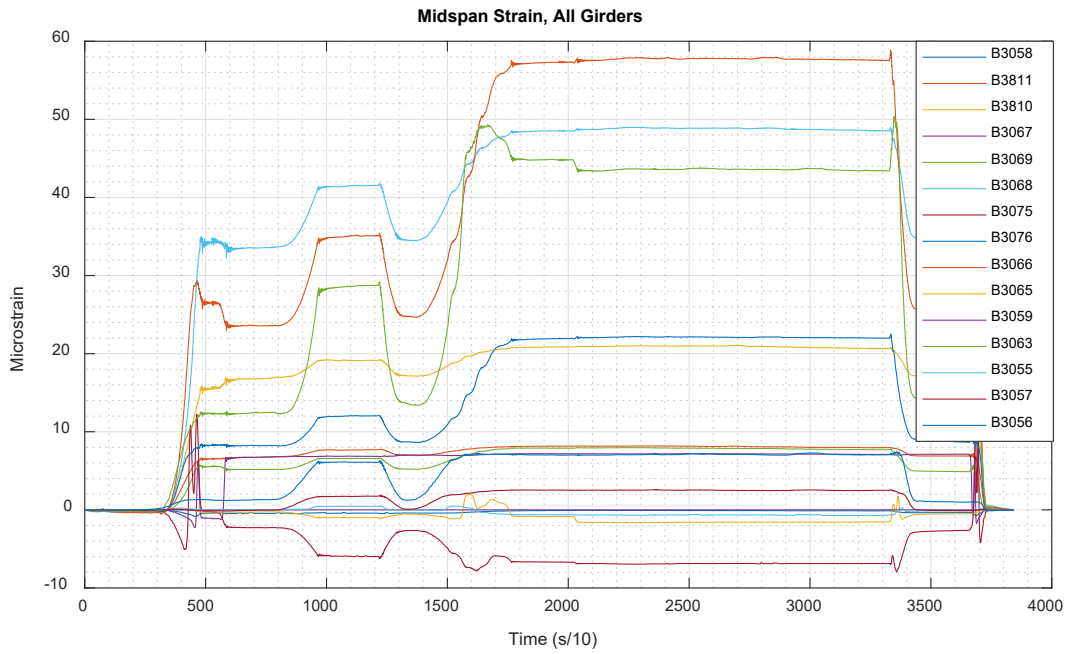## A.3.4 Representative Data Plots

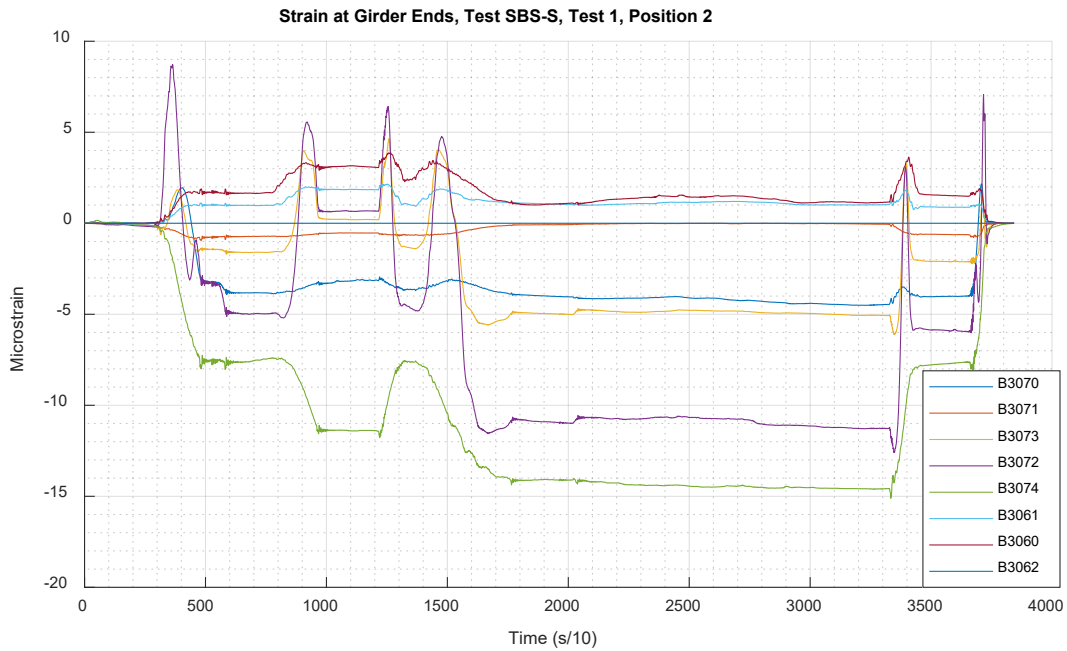Figure 56: Bridge 5109 SBS_S_2_1 Strains - Midspan

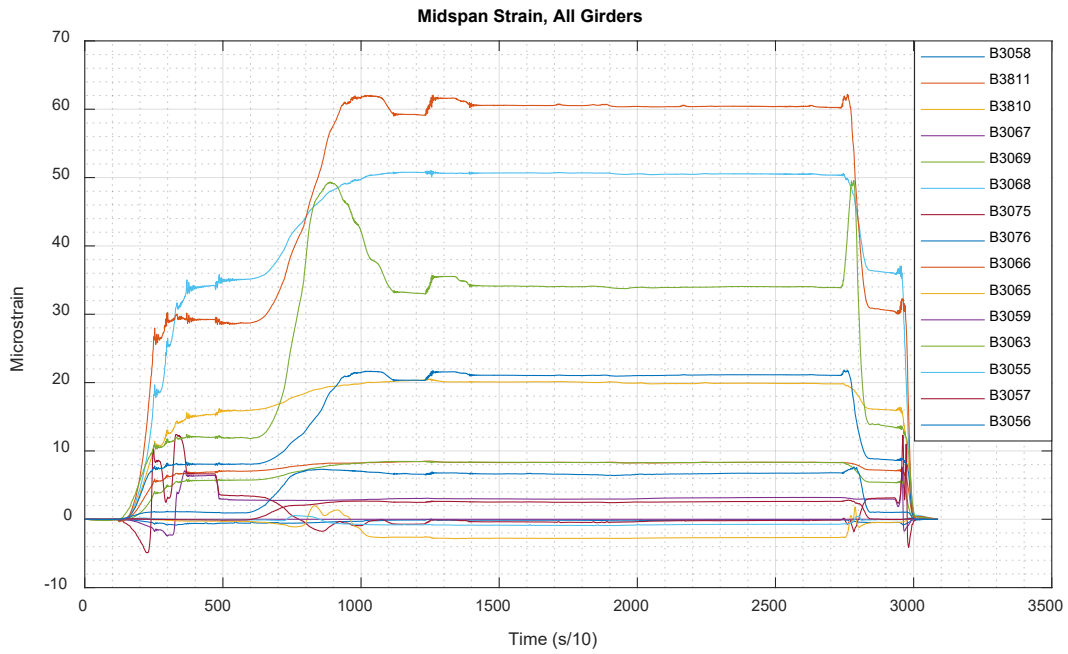Figure 57: Bridge 5109 SBS_S_2_1 Strains - Ends

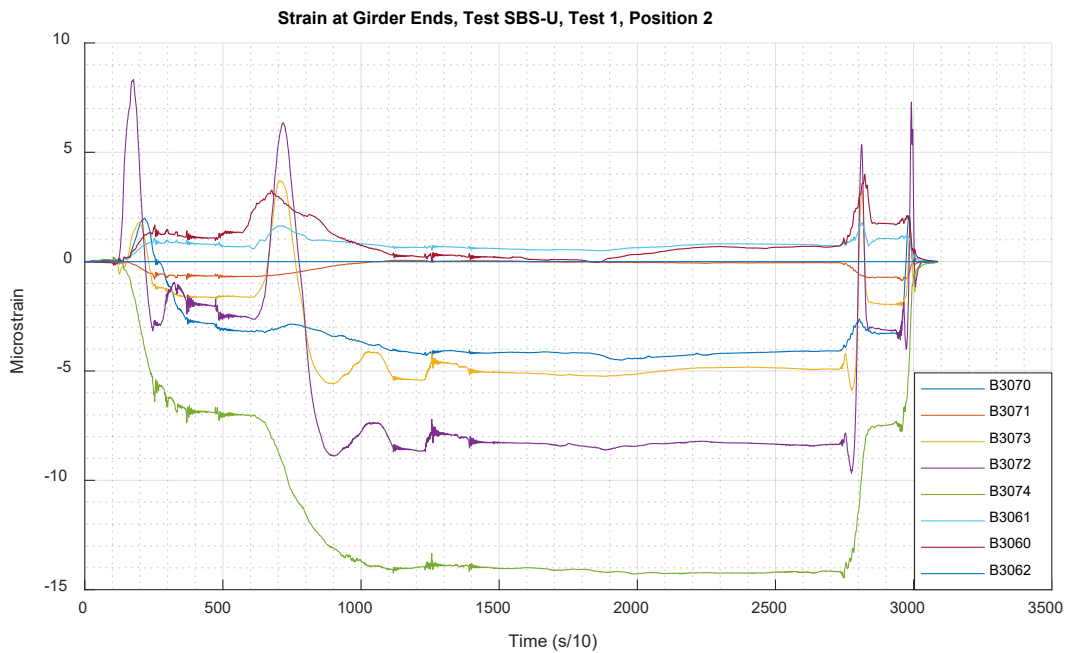Figure 58: Bridge 5109 SBS_U_2_1 Strains - Midspan

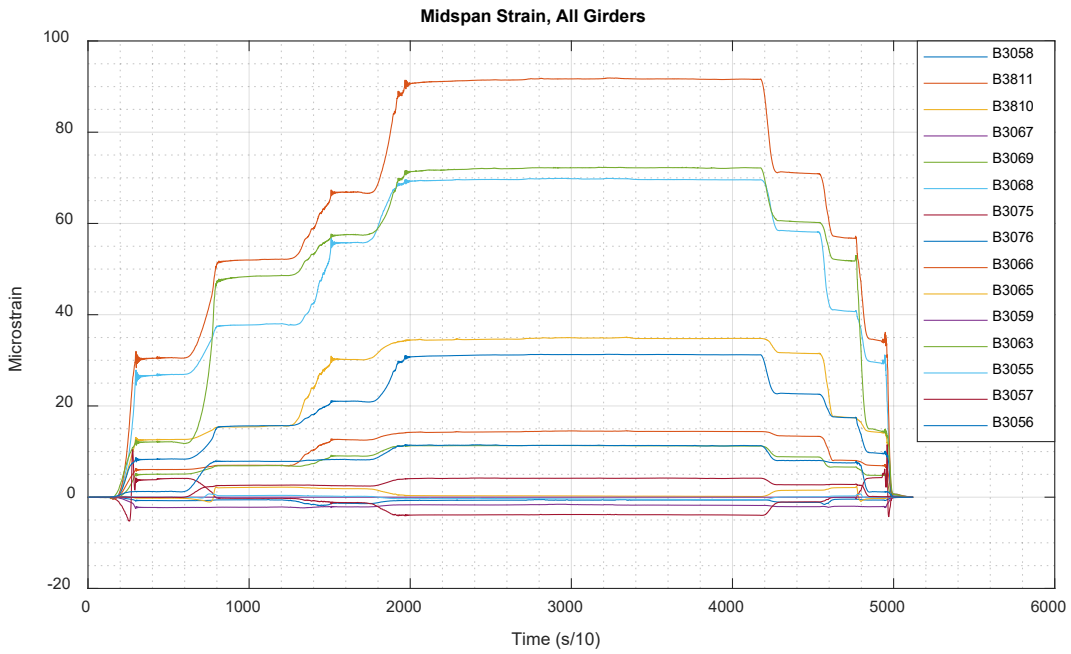Figure 59: Bridge 5109 SBS_U_2_1 Strains – Ends

Figure 60: Bridge 5109 MAX_2_1 Strains - Midspan
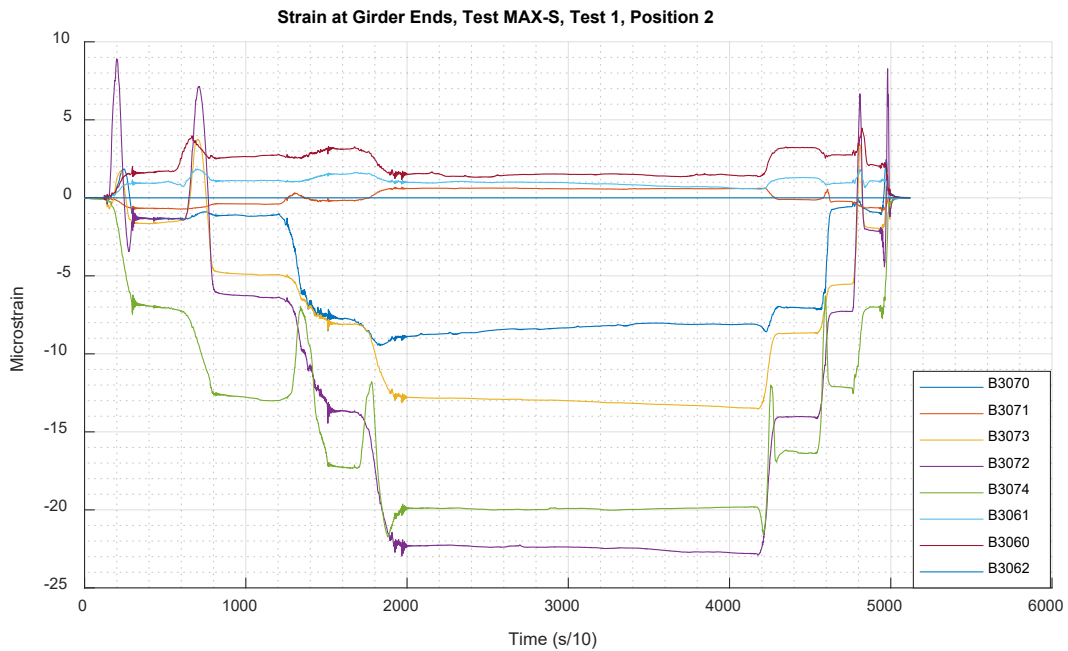

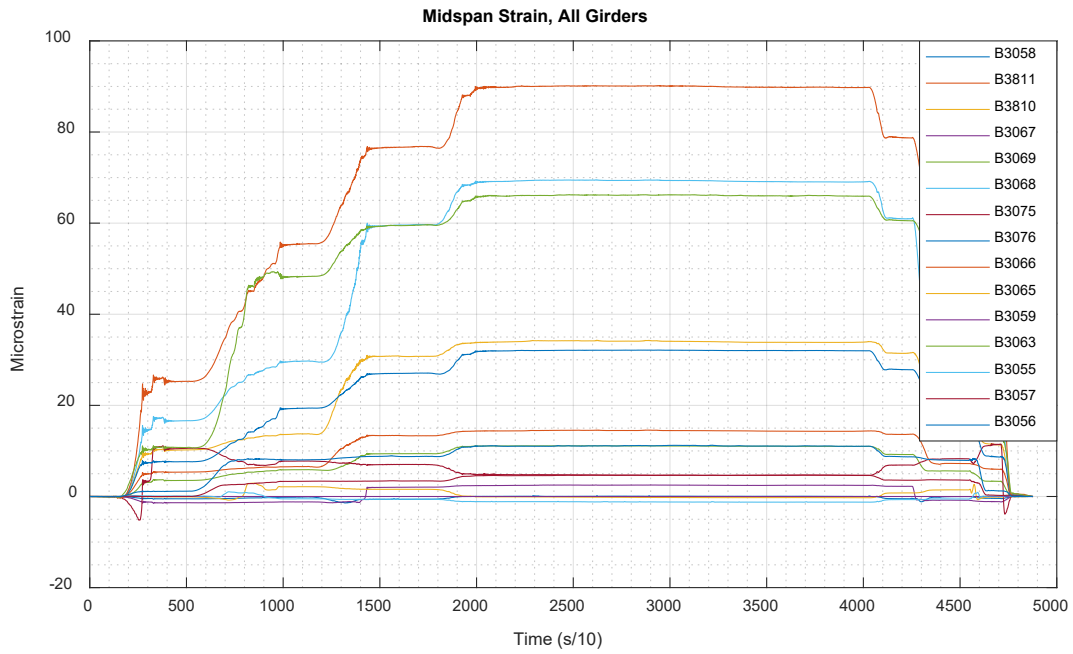Figure 61: Bridge 5109 MAX_2_1 Strains- Ends

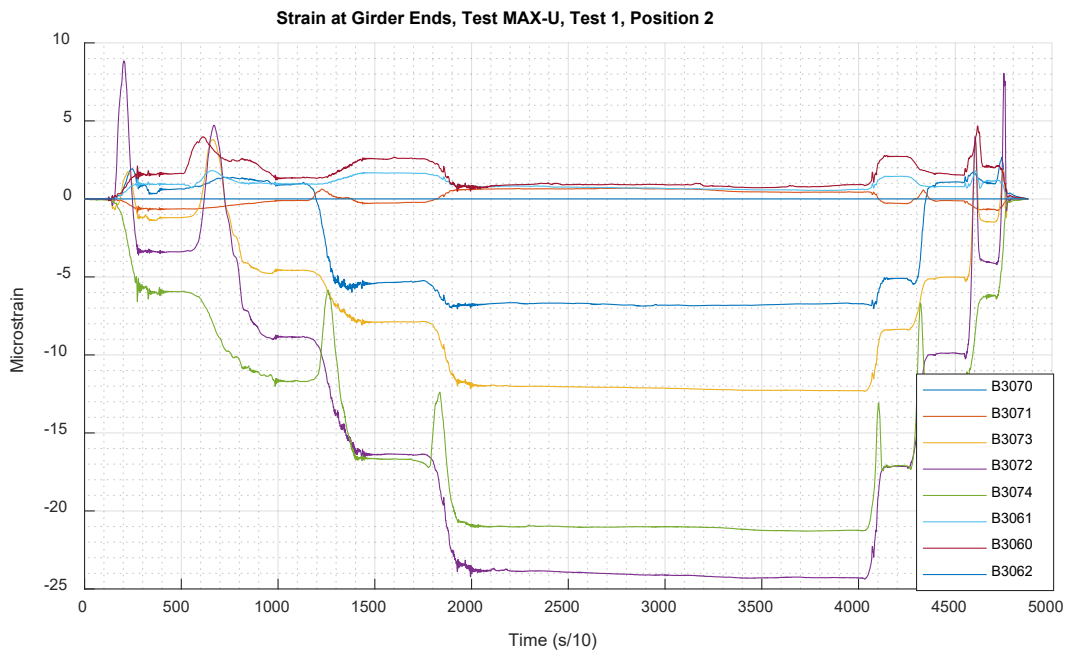Figure 62: Bridge 5109 MAX_U_2_1 Strains - Midspan

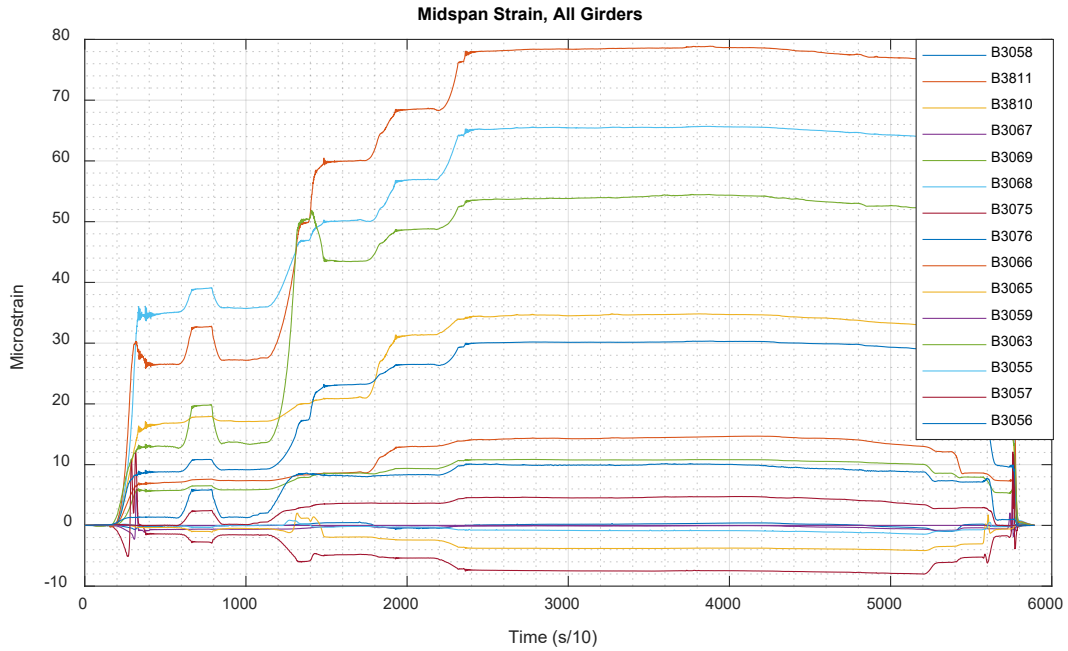Figure 63: Bridge 5109 MAX_U_2_1 Strains – Ends

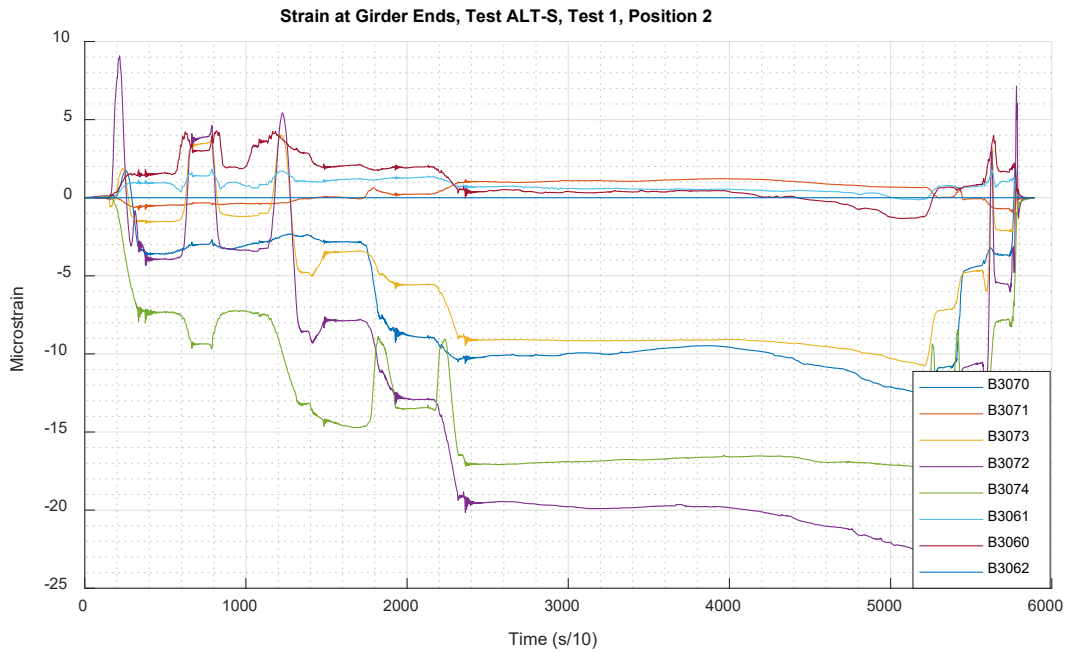Figure 64: Bridge 5109 ALT_S_2_1 Strains - Midspan
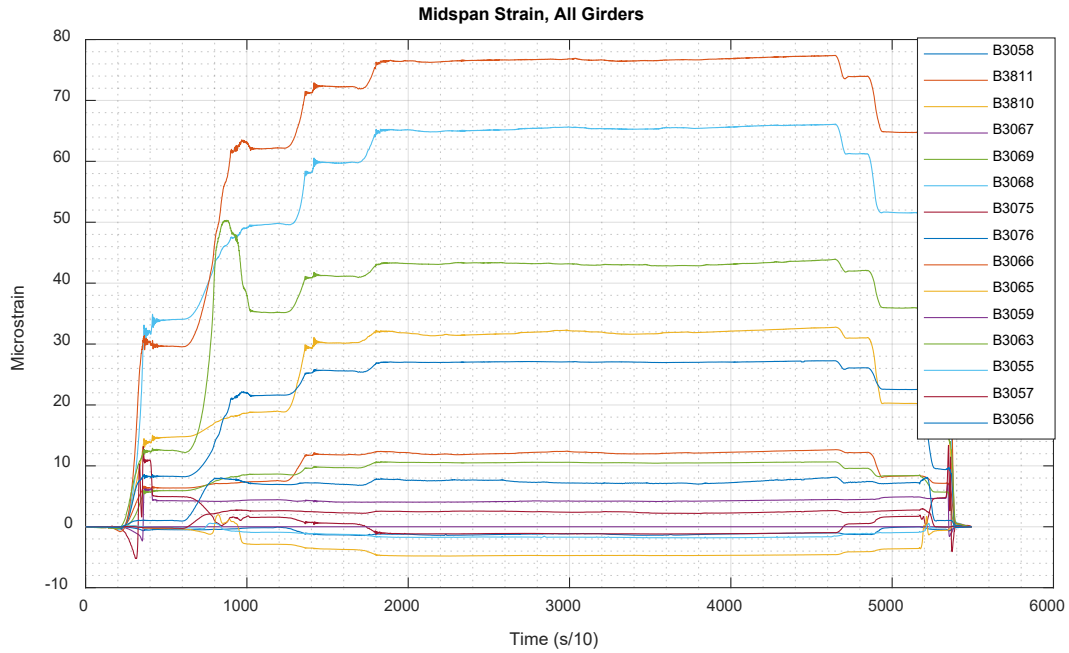

Figure 65: Bridge 5109 ALT_S_2_1 Strains - Ends

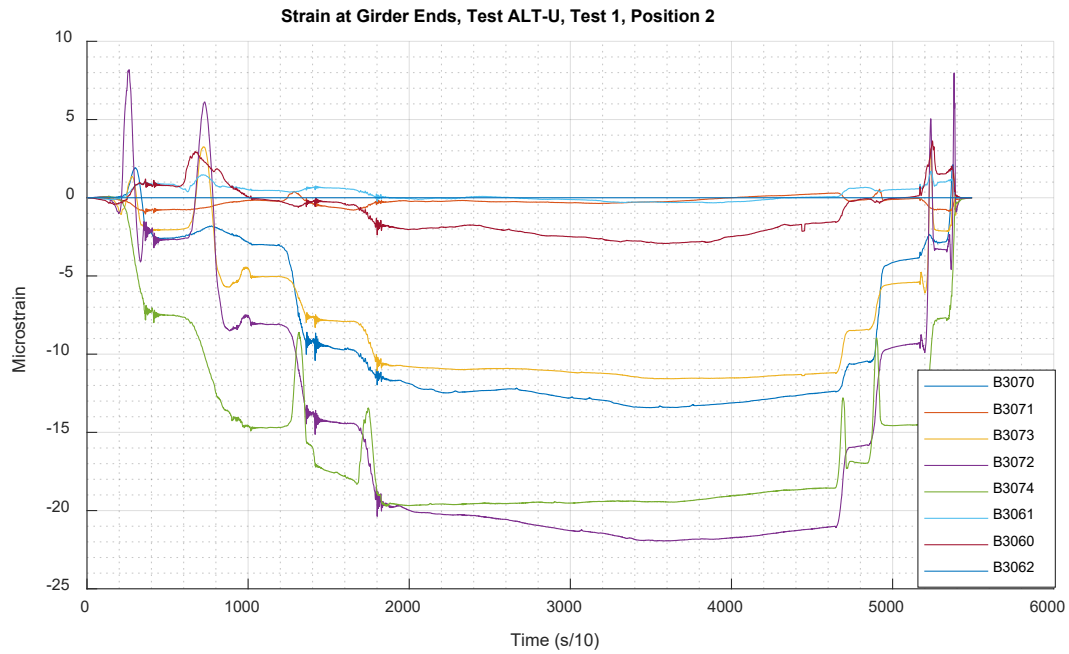Figure 66: Bridge 5109 ALT_U_2_1 Strains - Midspan

Figure 67: Bridge 5109 ALT_U_2_1 Strains – Ends

A.3.5 Rating Factor Calculations

Bridge 5109 - Hampden, Maine

Material Parameters:

Concrete Compressive Strength	$f'_c := 2.5 \; \textbf{ksi}$
Reinforcement Yield Strength	$F_y := 33 \; \textbf{ksi}$
Unit Weight: Reinforced Concrete	$\gamma_{RC} := 0.150 \; \dfrac{\textbf{kip}}{\textbf{ft}^3}$
Unit Weight: Wearing Surface	$\gamma_{ws} := 0.150 \; \dfrac{\textbf{kip}}{\textbf{ft}^3}$

Geometric Properties:

Span Length	$L := 47 \; \textbf{ft}$
Girder Spacing - Interior	$S := 85.813 \; \textbf{in}$
Girder Spacing - Exterior	$S_x := 57.31 \; \textbf{in}$
Number of Girders	$NG := 5$
Skew Angle	$skew := 35°$
Lane Width	$lanewidth := 13 \; \textbf{ft}$
Number of Lanes	$Nlane := 2$
Wearing Surface Thickness	$ws := 2.25 \; \textbf{in}$
Thickness of Pavement Overlay	$ws_2 := 0 \; \textbf{in}$
Girder Height - Interior	$h := 39.75 \; \textbf{in}$
Girder Height - Exterior	$h_x := 39.75 \; \textbf{in}$
Deck Thickness	$d_s := 6.25 \; \textbf{in}$
Web Width - Interior	$b_w := 22.75 \; \textbf{in}$
Web Width - Exterior	$b_{wx} := 22.75 \; \textbf{in}$
Curb Depth	$h_{curb} := 11.25 \; \textbf{in}$
Curb Width	$b_{curb} := 18 \; \textbf{in}$
Height to Centroid of Reinforcement - Interior	$y_{bar} := \begin{bmatrix} 4.844 \\ 5.375 \\ 6.44 \\ 5.375 \\ 4.844 \end{bmatrix} \textbf{in}$
Height to Centroid of Reinforcement - Exterior	$y_{barx} := \begin{bmatrix} 4.844 \\ 5.375 \\ 6.44 \\ 5.375 \\ 4.844 \end{bmatrix} \textbf{in}$
Area of Reinforcement - Interior	$A_s := \begin{bmatrix} 10.125 \\ 12.656 \\ 15.188 \\ 12.656 \\ 10.125 \end{bmatrix} \textbf{in}^2$

Area of Reinforcement - Exterior

$$A_{sx} := \begin{bmatrix} 10.125 \\ 12.656 \\ 15.188 \\ 12.656 \\ 10.125 \end{bmatrix} in^2$$

Distance from Centerline of Girder to Edge of Curb $\quad d_e := -3.625\ in$

Eccentricity of Centerline of Girders w.r.t. Centerline of Roadway $\quad exc := 0\ in$

Load and Analysis Parameters

Concentrated Load Due to Diaphragms on One Girder $\quad P_{dint} := 2.07\ kip$

Location of Intermediate Diaphragm
(Half, Third, Quarter) $\quad loc_d := \text{"Half"}$

Distributed Load Due to Rail $\quad w_{rail} := 0.287\ \dfrac{kip}{ft}$

Structural Dead Load Factor $\quad \gamma_{DC} := 1.25$

Wearing Surface Dead Load Factor $\quad \gamma_{DW} := 1.25$

Live Load Factor $\quad \gamma_{LL} := 1.35$

Live Load Impact Factor $\quad IM := 0.33$

Flexural Resistance Factor $\quad \phi := .9$

System Factor $\quad \phi_s := 1.0$

Condition Factor $\quad \phi_c := 1.0$

Initial Calculations

Web Height - Interior $\quad d_g := h - d_s$

Web Height - Exterior $\quad d_{gx} := h_x - d_s$

Include Wearing Surface in Section Height $\quad h := h + \mathbf{if}\left(\gamma_{ws} = 0.15\ \dfrac{kip}{ft^3}, ws, 0\right) = 42\ in$

Depth to Centroid of Reinforcement - Interior $\quad d := h - y_{bar}$

Depth to Centroid of Reinforcement - Exterior $\quad d_x := h_x - y_{barx} + h_{curb}$

Moment Applied to Interor Girders from Diaphragm

$$M_d := \mathbf{if}\ loc_d = \text{"Half"} \qquad\qquad = 24.323\ ft \cdot kip$$

$$\left\| \ P_{dint} \cdot \dfrac{L}{4} \right.$$

$$\mathbf{else\ if}\ loc_d = \text{"Third"}$$

$$\left\| \ P_{dint} \cdot \dfrac{L}{3} \right.$$

$$\mathbf{else\ if}\ loc_d = \text{"Quarter"}$$

$$\left\| \ P_{dint} \cdot \dfrac{L}{4} + P_{dint} \cdot \dfrac{L}{4} \right.$$

Moment Applied to Exterior Girders from Diaphragm $\quad M_{dx} := \dfrac{M_d}{2} = 12.161\ ft \cdot kip$

Dictance Between Centroids of Deck and Web

$$e_g := \frac{d_g + d_s}{2} = 19.875 \ \boldsymbol{in}$$

Area of Web

$$A := d_g \cdot b_w = 762.125 \ \boldsymbol{in}^2$$

Moment of Inertia of Web

$$I := \frac{b_w \cdot d_g^3}{12} = \left(7.127 \cdot 10^4\right) \ \boldsymbol{in}^4$$

Modular Ratio - Deck and Web

$$n := 1$$

Longitudinal Stiffness Parameter

$$K_g := n \cdot \left(I + A \cdot e_g^2\right) = \left(3.723 \cdot 10^5\right) \ \boldsymbol{in}^4$$

Interior Moment Distribution Factor - 1 Lane

$$g_{m1} := 0.06 + \left(\frac{S}{14 \ \boldsymbol{ft}}\right)^{0.4} \cdot \left(\frac{S}{L}\right)^{0.3} \cdot \left(\frac{K_g}{L \cdot d_s^3}\right)^{0.1} = 0.54$$

Interior Moment Distribution Factor - 2 Lane

$$g_{m2} := 0.075 + \left(\frac{S}{9.5 \ \boldsymbol{ft}}\right)^{0.6} \cdot \left(\frac{S}{L}\right)^{0.2} \cdot \left(\frac{K_g}{L \cdot d_s^3}\right)^{0.1} = 0.714$$

Controling Interior Moment Distribution Factor

$$g_m := \max \left(g_{m1}, g_{m2}\right)$$

Roadway Width

$$W_r := lanewidth \cdot Nlane$$

Eccentricity of Design Lane From C.G. of Girders

$$e_1 := \frac{W_r}{2} - 5 \ \boldsymbol{ft} + exc = 8 \ \boldsymbol{ft}$$

Eccentricity of Exterior Girder From C.G. of Girders

$$X_{ext} := (NG - 1) \cdot \frac{S}{2} = 14.302 \ \boldsymbol{ft}$$

Eccentricity of Each Girder

$$x_1 := X_{ext}$$
$$x_2 := X_{ext} - S$$
$$x_3 := X_{ext} - 2 \cdot S$$
$$x_4 := \mathbf{if}\left(NG > 3, X_{ext} - 3 \cdot S, 0 \ \boldsymbol{ft}\right)$$
$$x_5 := \mathbf{if}\left(NG > 4, X_{ext} - 4 \cdot S, 0 \ \boldsymbol{ft}\right)$$

Lever Rule Distribution Factor - One Lane

$$R_1 := \frac{1}{NG} + \frac{X_{ext} \cdot e_1}{x_1^2 + x_2^2 + x_3^2 + x_4^2 + x_5^2} = 0.424$$

$$g_{mR1} := \mathbf{if}\left(P_{dint} > 0, 1.2 \cdot R_1, 0\right) = 0.508$$

Lever Rule Distribution Factor - Two Lanes

$$R_2 := \frac{2}{NG} + \frac{X_{ext} \cdot \left(e_1 - 5 \ \boldsymbol{ft}\right)}{x_1^2 + x_2^2 + x_3^2 + x_4^2 + x_5^2} = 0.484$$

$$g_{mR2} := \mathbf{if}\left(P_{dint} > 0, R_2, 0\right) = 0.484$$

Exterior Moment Distribution Factor

$$g_{mx1} := \frac{1.2 \ \left(S + d_e - 2 \ \boldsymbol{ft}\right)}{2 \cdot S} = 0.407$$

$$ee := 0.77 + \frac{d_e}{9.1 \ \boldsymbol{ft}} = 0.737$$

$$g_{mx2} := g_{m2} \cdot ee = 0.526$$

	$g_{mx} := \max\left(g_{mx1}, g_{mx2}\right) = 0.526$
Skew Correction Factor	$c_1 := 0.25 \cdot \left(\dfrac{K_g}{12 \cdot L \cdot d_s^{\,3}}\right)^{0.25} \cdot \left(\dfrac{S}{L}\right)^{.5} = 0.067$
	$\theta := \mathbf{if}\left(skew \geq 30^{\bullet}, skew, 0^{\bullet}\right)$
	$C_\theta := 1 - c_1 \cdot \left(\tan(\theta)\right)^{1.5} = 0.961$
	$g_m := g_m \cdot C_\theta = 0.686$
	$g_{mx} := g_{mx} \cdot C_\theta = 0.506$

__Interior DF__   __Exterior DF__

$g_m = 0.686$ $g_{mx} = 0.506$

Interior Girder Dead Load	$w_{girder} := \gamma_{RC} \cdot b_w \cdot d_g = 0.794\ \dfrac{kip}{ft}$
Deck Dead Load	$w_{deck} := \gamma_{RC} \cdot S \cdot d_s = 0.559\ \dfrac{kip}{ft}$
Curb Dead Load	$w_{curb} := 2 \cdot \gamma_{RC} \cdot h_{curb} \cdot b_{curb} = 0.422\ \dfrac{kip}{ft}$
Dead Load from Nonstructural Components	$w_{ns} := \dfrac{w_{curb}}{NG} + w_{rail} = 0.371\ \dfrac{kip}{ft}$
Total Structural Dead Load on Interior Girders	$DC := w_{girder} + w_{deck} + w_{ns} = 1.724\ \dfrac{kip}{ft}$
Exterior Girder Dead Load	$w_{girderx} := \gamma_{RC} \cdot b_{wx} \cdot d_{gx} = 0.794\ \dfrac{kip}{ft}$
Exterior Deck Dead Load	$w_{deckx} := \gamma_{RC} \cdot S_x \cdot d_s = 0.373\ \dfrac{kip}{ft}$
Total Structural Dead Load on Exterior Girders	$DC_x := w_{girderx} + w_{deckx} + w_{ns} = 1.538\ \dfrac{kip}{ft}$
Wearing Surface Dead Load on Interior Girders	$DW := \gamma_{ws} \cdot \left(ws + ws_2\right) \cdot S = 0.201\ \dfrac{kip}{ft}$
Wearing Surface Dead Load on Exterior Girders	$DW_x := \gamma_{ws} \cdot \left(ws + ws_2\right) \cdot S_x = 0.134\ \dfrac{kip}{ft}$
Dead Load Moments	$M_{DC} := \dfrac{DC \cdot L^2}{8} + M_d \qquad M_{DCx} := \dfrac{DC_x \cdot L^2}{8} + M_{dx}$
	$M_{DW} := \dfrac{DW \cdot L^2}{8} \qquad\qquad M_{DWx} := \dfrac{DW_x \cdot L^2}{8}$

$M_{DC} = 500.344 \; \textbf{ft} \cdot \textbf{kip}$ $\qquad$ $M_{DCx} = 436.943 \; \textbf{ft} \cdot \textbf{kip}$

$M_{DW} = 55.535 \; \textbf{ft} \cdot \textbf{kip}$ $\qquad$ $M_{DWx} = 37.089 \; \textbf{ft} \cdot \textbf{kip}$

Live Load Moment - Truck Load $\qquad$ $M_{Truck} := 32 \; \textbf{kip} \cdot \left(\dfrac{L}{4}\right) + \dfrac{40 \; \textbf{kip}}{2} \cdot \left(\dfrac{L}{2} - 14 \; \textbf{ft}\right) = 566 \; \textbf{ft} \cdot \textbf{kip}$

Live Load Moment - Tandem $\qquad$ $M_{Tandem} := 25 \; \textbf{kip} \cdot \dfrac{L}{4} + \dfrac{25 \; \textbf{kip}}{2} \cdot \left(\dfrac{L}{2} - 4 \; \textbf{ft}\right) = 537.5 \; \textbf{ft} \cdot \textbf{kip}$

Live Load Moment - Lane $\qquad$ $M_{Lane} := 0.64 \; \dfrac{\textbf{kip}}{\textbf{ft}} \cdot \dfrac{L^2}{8} = 176.72 \; \textbf{ft} \cdot \textbf{kip}$

Total HL-93 Live Load $\qquad$ $M_{LL} := M_{Lane} + (1 + IM) \cdot \max\left(M_{Truck}, M_{Tandem}\right)$

$M_{LL} = 929.5 \; \textbf{ft} \cdot \textbf{kip}$

Nominal Resistance

Depth Whitney Stress Block - Interior $\qquad$ $a := A_s \cdot \dfrac{F_y}{0.85 \cdot f'_c \cdot S} = \begin{bmatrix} 1.832 \\ 2.29 \\ 2.749 \\ 2.29 \\ 1.832 \end{bmatrix} \; \textbf{in}$

Nominal Moment Resistance - Interior

Interior Nominal Moment Capacity $\qquad$ $\overrightarrow{M_n := F_y \cdot A_s \cdot \left(d - \dfrac{a}{2}\right)} = \begin{bmatrix} 1.009 \cdot 10^3 \\ 1.235 \cdot 10^3 \\ 1.428 \cdot 10^3 \\ 1.235 \cdot 10^3 \\ 1.009 \cdot 10^3 \end{bmatrix} \; \textbf{ft} \cdot \textbf{kip}$

$M_{capacity} := \max\langle M_n \rangle = \left(1.428 \cdot 10^3\right) \; \textbf{ft} \cdot \textbf{kip}$

Depth Whitney Stress Block - Exterior $\qquad$ $a_x := A_{sx} \cdot \dfrac{F_y}{0.85 \cdot f'_c \cdot S_x} = \begin{bmatrix} 2.744 \\ 3.429 \\ 4.116 \\ 3.429 \\ 2.744 \end{bmatrix} \; \textbf{in}$

Nominal Moment Resistance - Exterior

Exterior Nominal Moment Capacity $\qquad$ $\overrightarrow{M_{nx} := F_y \cdot A_{sx} \cdot \left(d_x - \dfrac{a_x}{2}\right)} = \begin{bmatrix} 1.247 \cdot 10^3 \\ 1.528 \cdot 10^3 \\ 1.775 \cdot 10^3 \\ 1.528 \cdot 10^3 \\ 1.247 \cdot 10^3 \end{bmatrix} \; (\textbf{ft} \cdot \textbf{kip})$

$M_{capacityx} := \max\langle M_{nx} \rangle = \left(1.775 \cdot 10^3\right) \; \textbf{ft} \cdot \textbf{kip}$

Interior Moment Rating Factor

$$RF_{Interior} := \frac{\phi \cdot \phi_s \cdot \phi_c \cdot M_{capacity} - \gamma_{DC} \cdot M_{DC} - \gamma_{DW} \cdot M_{DW}}{\gamma_{LL} \cdot M_{LL} \cdot g_m}$$

Exterior Moment Rating Factor

$$RF_{Exterior} := \frac{\phi \cdot \phi_s \cdot \phi_c \cdot M_{capacityx} - \gamma_{DC} \cdot M_{DCx} - \gamma_{DW} \cdot M_{DWx}}{\gamma_{LL} \cdot M_{LL} \cdot g_{mx}}$$

Interior   Exterior

$RF_{Interior} = 0.686$ $RF_{Exterior} = 1.585$

Concrete Compressive Strength - Larger is More Conservative

$$f'_c := 5 \text{ ksi}$$

Concrte Elastic Modulus

$$E_c := 1820 \text{ ksi} \cdot \sqrt{\frac{f'_c}{\text{ksi}}} = \langle 4.07 \cdot 10^3 \rangle \text{ ksi}$$

Interior Girders

Maximum Recorded Strain

$$\varepsilon_T := 90.50 \cdot 10^{-6}$$

Maximum Applied Moment per Lane

$$M_{Max} := 830.05 \text{ ft} \cdot \text{kip}$$

Uncracked Section Modulus

$$S_{unc} := 10619 \text{ in}^3$$

Cracked Section Modulus

$$S_{cr} := 3672 \text{ in}^3$$

Section Behavior

$$Behavior := \text{``Uncracked''}$$

Section Modulus Effective for Behavior

$$S_e := \textbf{if} \langle Behavior = \text{``Uncracked''}, S_{unc}, S_{cr} \rangle$$

Calculated Strain

$$\varepsilon_c := \frac{M_{Max} \cdot g_m}{S_e \cdot E_c} = 1.581 \cdot 10^{-4}$$

Test Benefit Factor

$$k_a := \frac{\varepsilon_c}{\varepsilon_T} - 1 = 0.747$$

Ratio of Applied to HL-93 Moment

$$r_M := \frac{M_{Max}}{M_{LL}} = 0.893$$

Test Understanding Factor

$$k_b := \textbf{if} \langle r_M > 0.7, 0.5, 0 \rangle = 0.5$$

Rating Improvement Factor

$$k := 1 + k_a \cdot k_b = 1.374$$

Improved Rating Factor

$$RF_{Improved} := RF_{Interior} \cdot k = 0.942$$

Exterior Girders

Maximum Recorded Strain

$$\varepsilon_T := 34.5 \cdot 10^{-6}$$

Maximum Applied Moment per Lane

$$M_{Max} := 853.3 \text{ ft} \cdot \text{kip}$$

Uncracked Section Modulus

$$S_{unc} := 9767 \text{ in}^3$$

Cracked Section Modulus

$$S_{cr} := 3552 \text{ in}^3$$

Section Behavior

$$Behavior := \text{``Uncracked''}$$

Section Modulus Effective for Behavior

$$S_e := \textbf{if} \langle Behavior = \text{``Uncracked''}, S_{unc}, S_{cr} \rangle$$

Calculated Strain

$$\varepsilon_c := \frac{M_{Max} \cdot g_{mx}}{S_e \cdot E_c} = 1.302 \cdot 10^{-4}$$

Test Benefit Factor

$$k_a := \frac{\varepsilon_c}{\varepsilon_T} - 1 = 2.775$$

Ratio of Applied to HL-93 Moment

$$r_M := \frac{M_{Max}}{M_{LL}} = 0.918$$

Test Understanding Factor

$$k_b := \mathbf{if}\left(r_M > 0.7, 0.5, 0\right) = 0.5$$

Rating Improvement Factor

$$k := 1 + k_a \cdot k_b = 2.387$$

Improved Rating Factor

$$RF_{ImprovedExt} := RF_{Exterior} \cdot k = 3.783$$

Improved Rating Factors

Interior

$$RF_{Improved} = 0.942$$

Exterior

$$RF_{ImprovedExt} = 3.783$$

Figure 68: Bridge 5109 Calculations

A.4 Unity No. 2390

A.4.1 Experimental Configuration and Experimental Data Collected

Table 25: Bridge 2390 Experimental Configuration and Experimental Data Collected

File Contents	File Name	File Type
Sensors	Br2390 _Sensors.csv	CSV Format
Sensor Layout	Br2390 _SensorLayout.mat	MATLAB Data File
Sensor Data	Br2390_ALT_S_2_1_Strain.mat	MATLAB Data File
	Br2390_ALT_U_2_1_Strain.mat	MATLAB Data File
	Br2390_MAX_S_1_2_Strain.mat	MATLAB Data File
	Br2390_MAX_S_2_1_Strain.mat	MATLAB Data File
	Br2390_MAX_S_3_1_Strain.mat	MATLAB Data File
	Br2390_MAX_U_2_1_Strain.mat	MATLAB Data File
	Br2390_SBS_S_2_1_Strain.mat	MATLAB Data File
	Br2390_SBS_U_2_1_Strain.mat	MATLAB Data File

A.4.2 Instrumentation
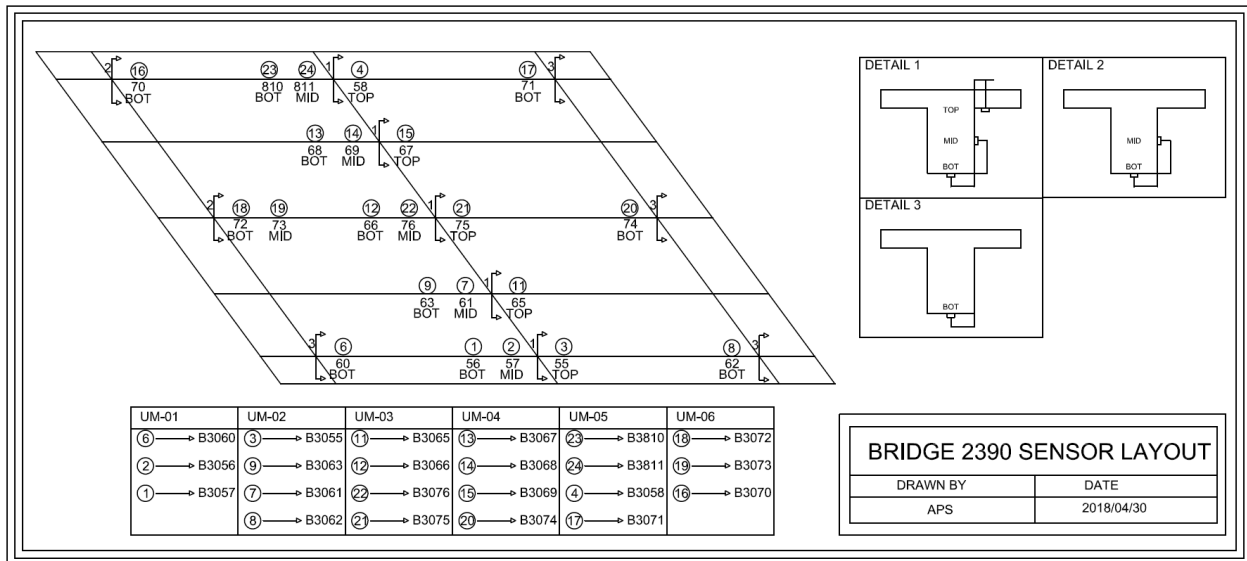
Figure 69: Bridge 2390 Sensor Layout

A.4.3 Loading
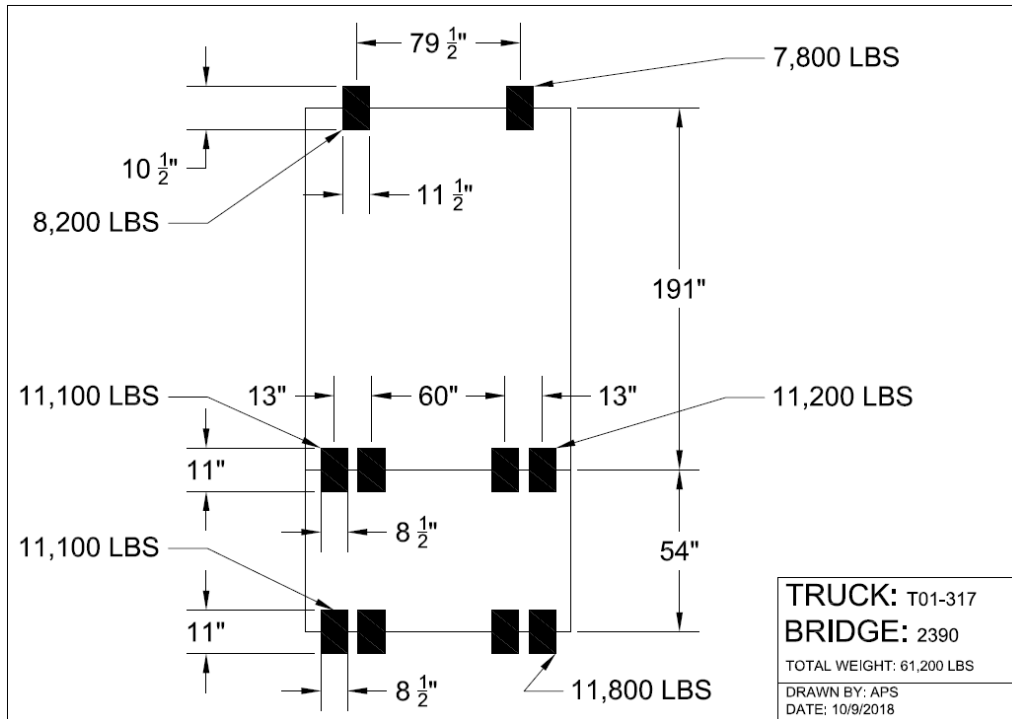
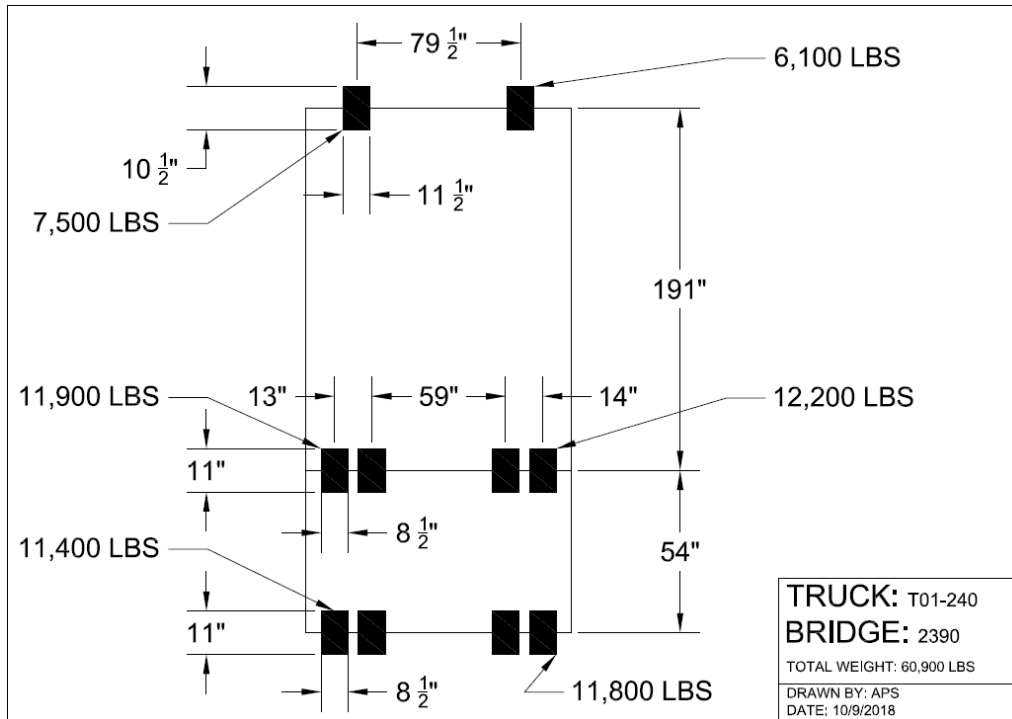Figure 70: Bridge 2390 Truck T01-317 Loading
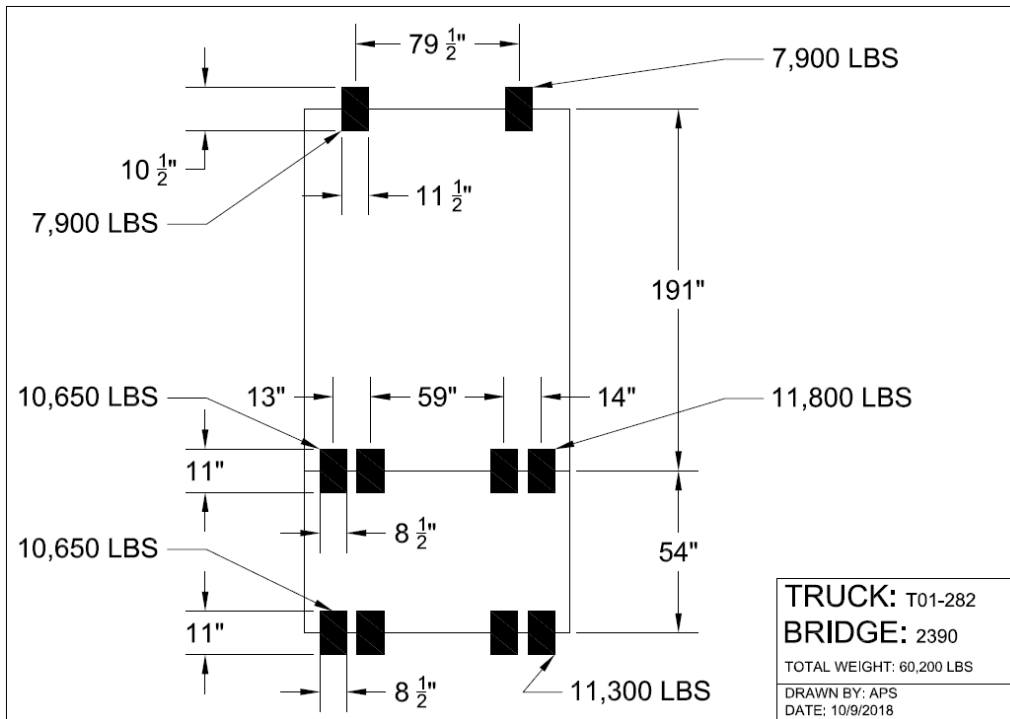

Figure 71: Bridge 2390 Truck T01-240 Loading

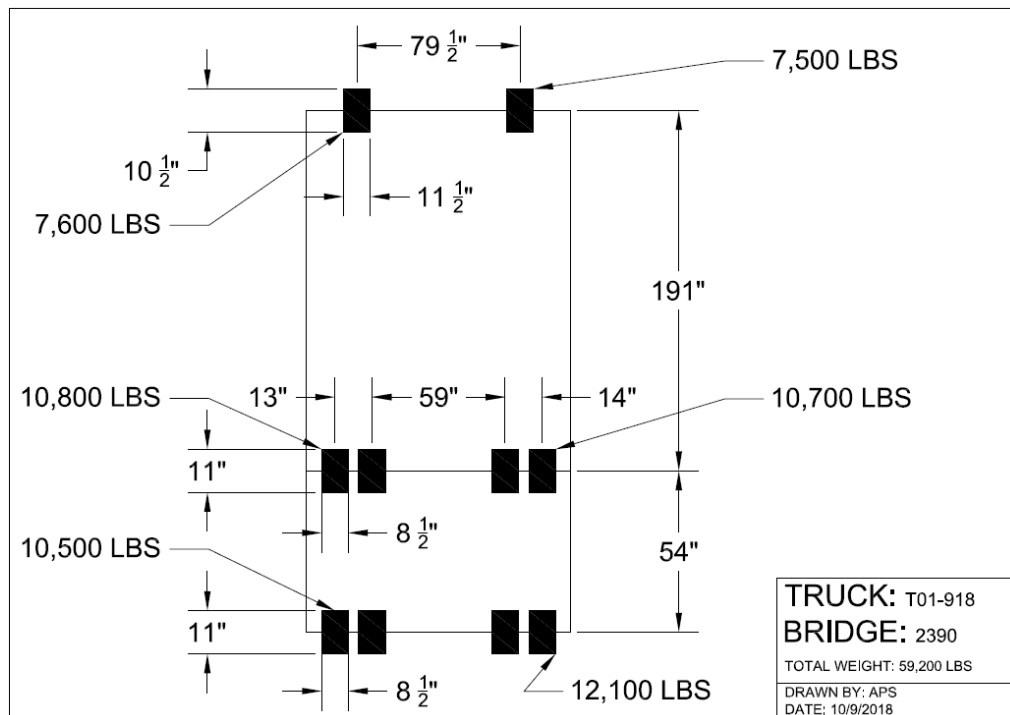Figure 72: Bridge 2390 Truck T01-282 Loading

Figure 73: Bridge 2390 Truck T01-918 Loading

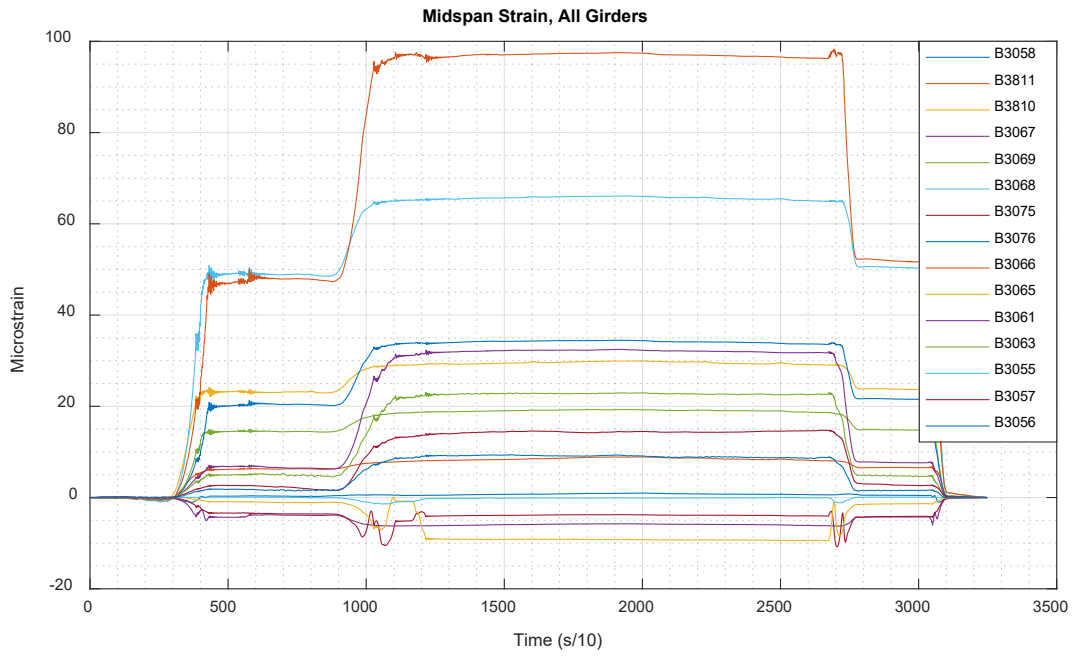## A.4.4 Representative Data Plots

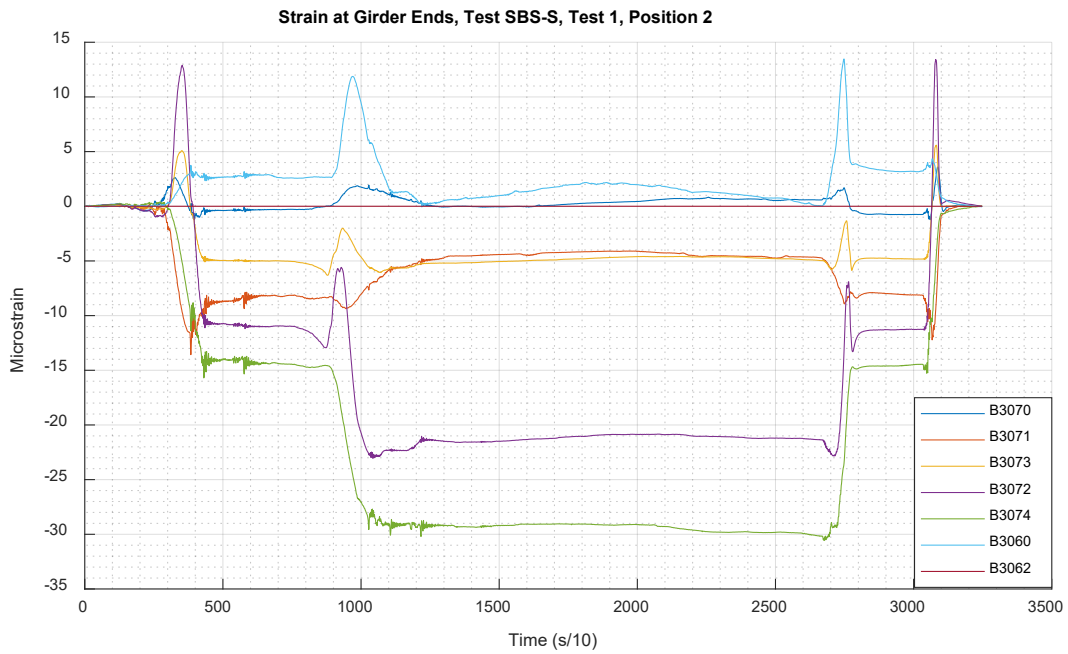Figure 74: Bridge 2390 SBS_S_2_2 Strains - Midspan

Figure 75: Bridge 2390 SBS_S_2_1 Strains - Ends

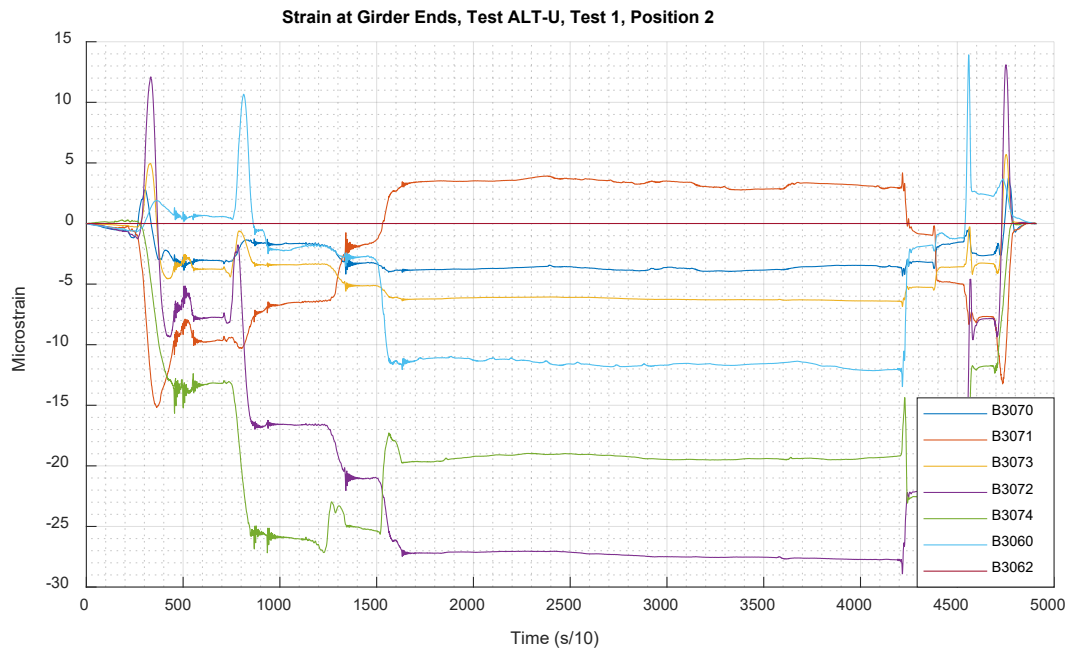Figure 76: Bridge 2390 SBS_U_2_1 Strains - Midspan

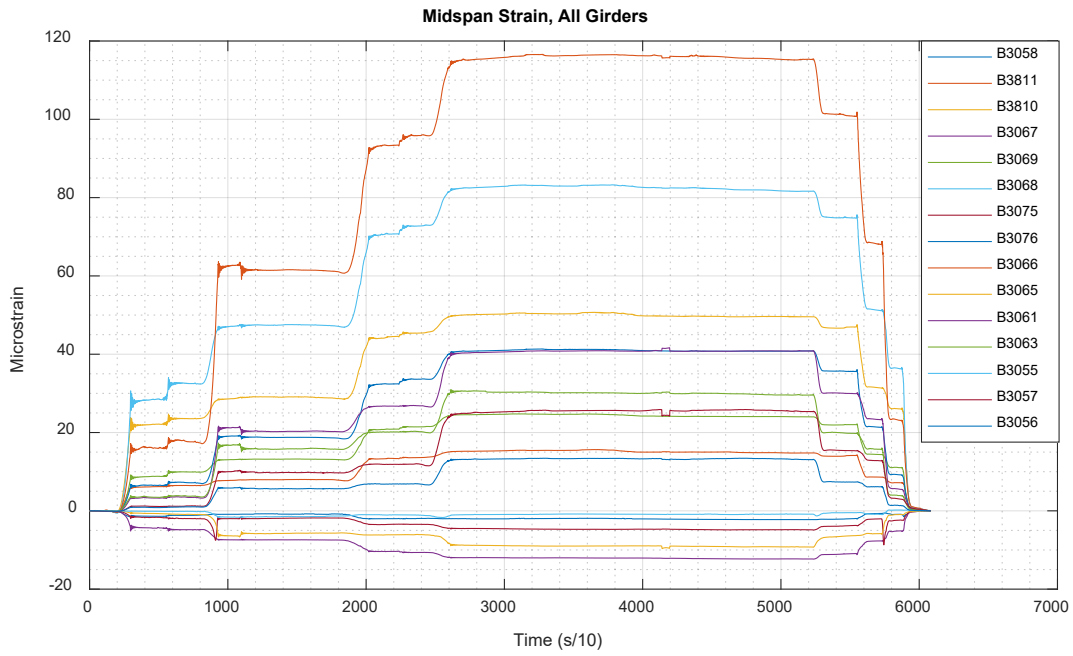Figure 77: Bridge 2390 SBS_U_2_1 Strains – Ends

Figure 78: Bridge 2390 MAX_S_2_1 Strains - Midspan
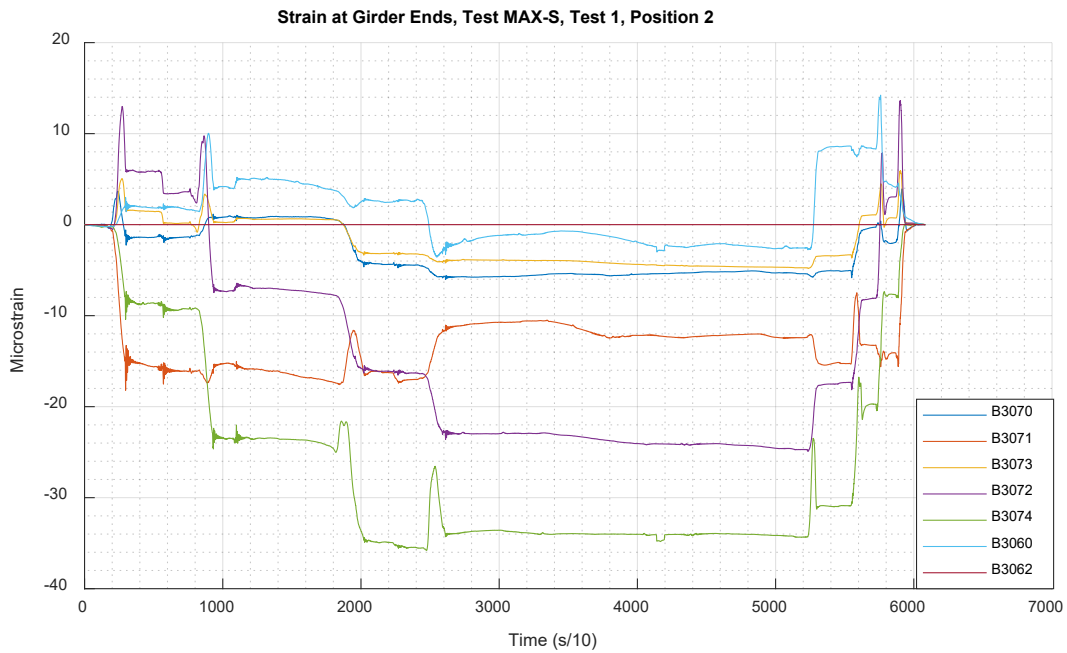

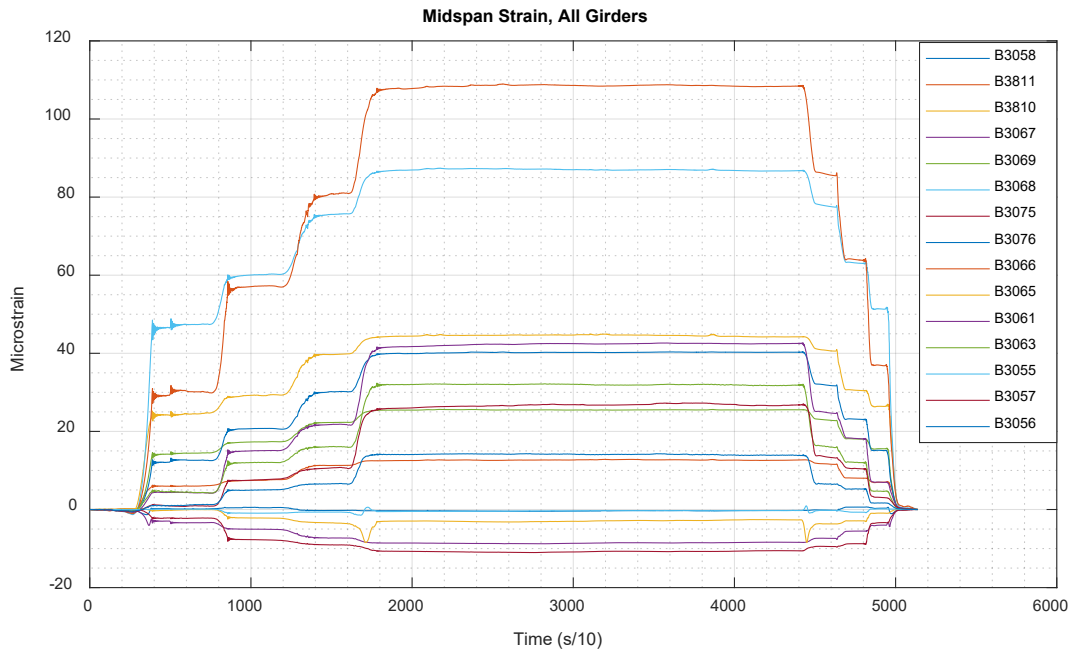Figure 79: Bridge 2390 MAX_S_2_1 Strains - Ends

Figure 80: Bridge 2390 MAX_U_2_1 Strains - Midspan
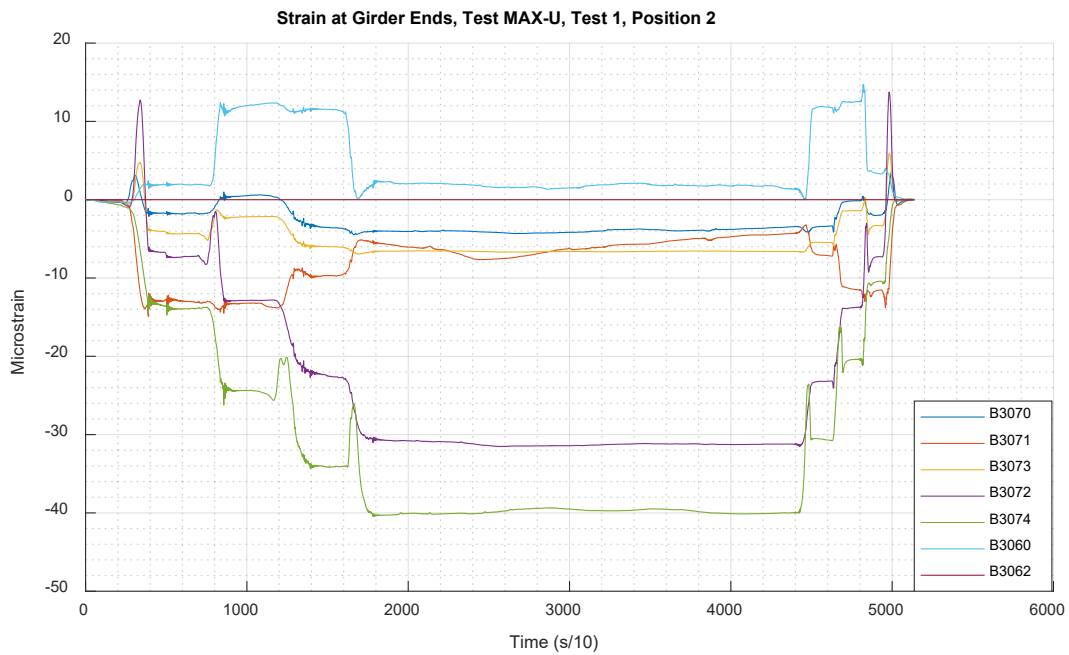

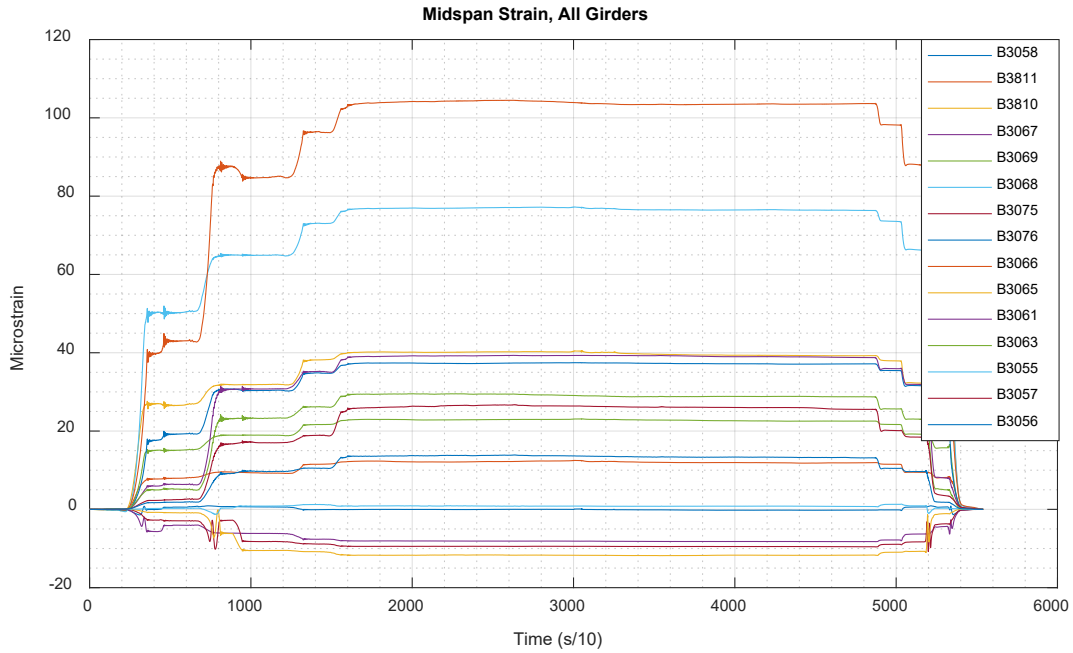Figure 81 Bridge 2390 MAX_U_2_1 Strains – Ends
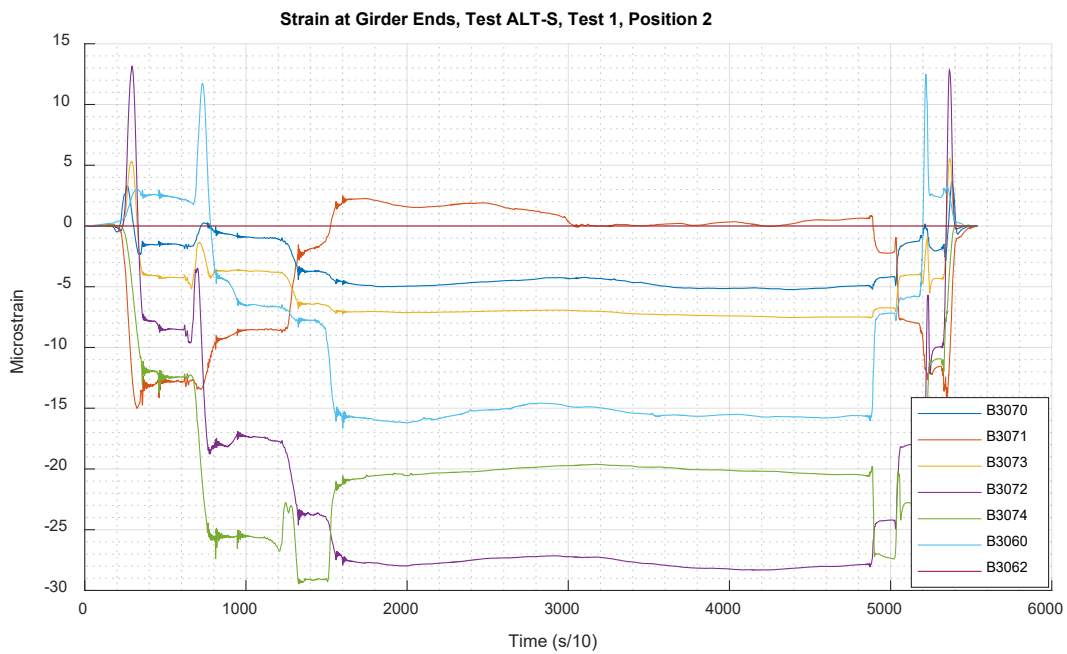
Figure 82: Bridge 2390 ALT_S_2_1 Strains - Midspan
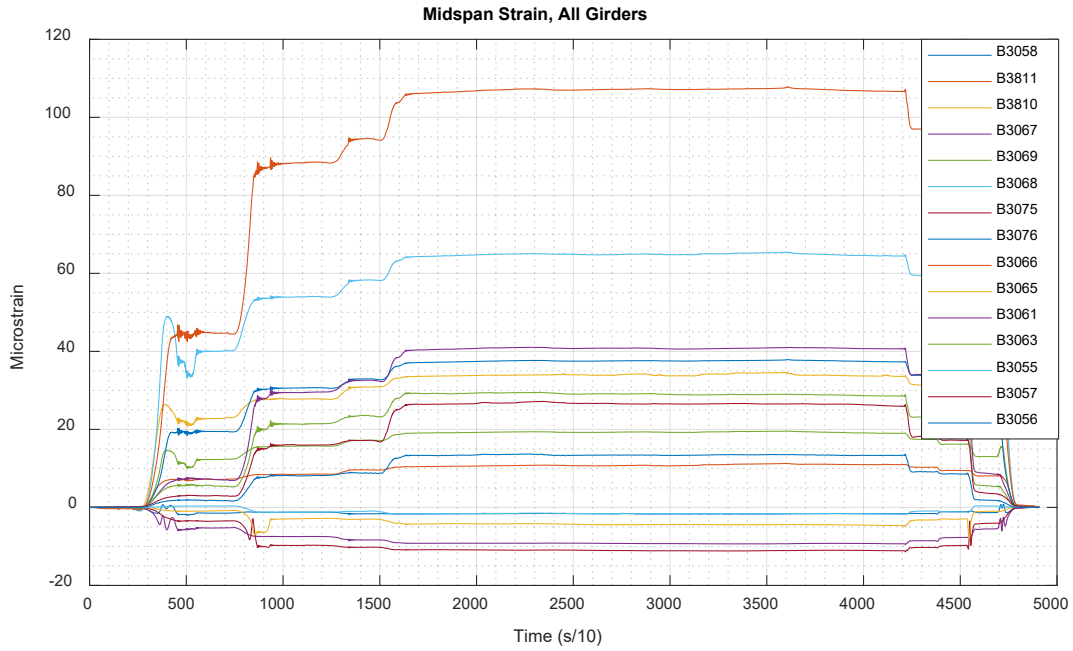

Figure 83 Bridge 2390 ALT_S_2_1 Strains – Ends
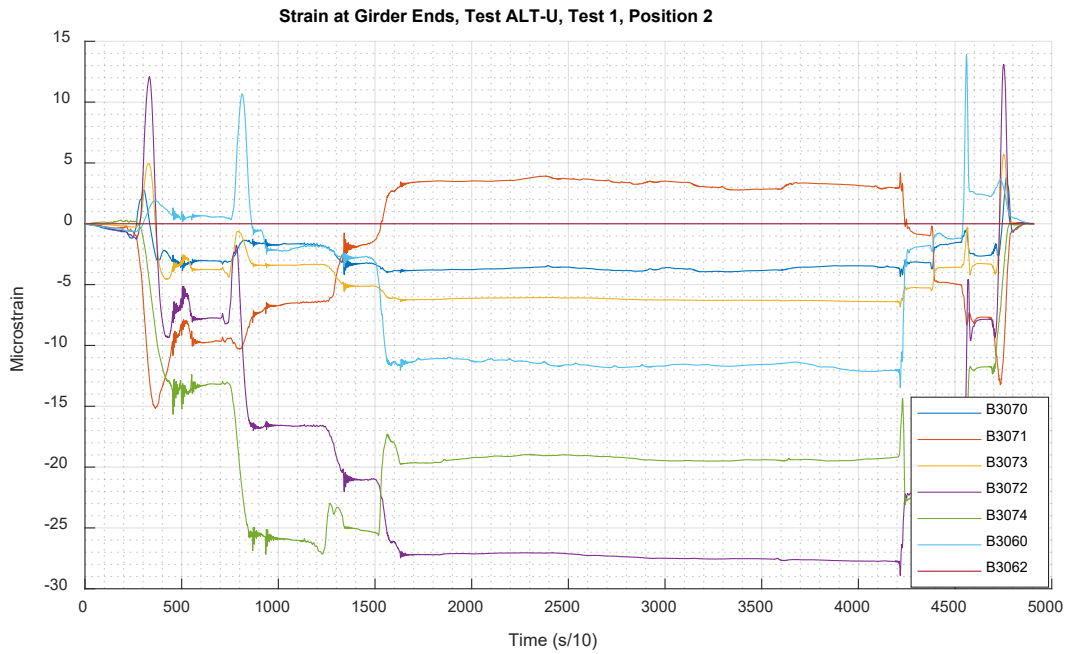
Figure 84: Bridge 2390 ALT_U_2_1 Strains - Midspan

Figure 85 Bridge 2390 ALT_U_2_1 Strains - Ends

A.4.5 Rating Factor Calculations

AASHTO Rating Calculations:

Bridge 2390 - Unity, Maine

Material Parameters:

Concrete Compressive Strength $\qquad\qquad\qquad\qquad\qquad f'_c := 2.5 \; \textbf{ksi}$

Reinforcement Yield Strength $\qquad\qquad\qquad\qquad\qquad F_y := 33 \; \textbf{ksi}$

Unit Weight: Reinforced Concrete $\qquad\qquad\qquad\qquad \gamma_{RC} := 0.150 \; \dfrac{\textbf{kip}}{\textbf{ft}^3}$

Unit Weight: Wearing Surface $\qquad\qquad\qquad\qquad\qquad \gamma_{ws} := 0.150 \; \dfrac{\textbf{kip}}{\textbf{ft}^3}$

Geometric Properties:

Span Length $\qquad\qquad\qquad\qquad\qquad\qquad\qquad\qquad L := 37 \; \textbf{ft}$

Girder Spacing - Interior $\qquad\qquad\qquad\qquad\qquad\quad S := 73.5 \; \textbf{in}$

Girder Spacing - Exterior $\qquad\qquad\qquad\qquad\qquad\quad S_x := 42.75 \; \textbf{in}$

Number of Girders $\qquad\qquad\qquad\qquad\qquad\qquad\quad NG := 5$

Skew Angle $\qquad\qquad\qquad\qquad\qquad\qquad\qquad\qquad skew := 30 \; °$

Lane Width $\qquad\qquad\qquad\qquad\qquad\qquad\qquad\qquad lanewidth := 11 \; \textbf{ft}$

Number of Lanes $\qquad\qquad\qquad\qquad\qquad\qquad\qquad Nlane := 2$

Wearing Surface Thickness $\qquad\qquad\qquad\qquad\qquad ws := 4 \; \textbf{in}$

Thickness of Pavement Overlay $\qquad\qquad\qquad\qquad ws_2 := 5 \; \textbf{in}$

Girder Height - Interior $\qquad\qquad\qquad\qquad\qquad\quad h := 31.25 \; \textbf{in}$

Girder Height - Exterior $\qquad\qquad\qquad\qquad\qquad\quad h_x := 31.25 \; \textbf{in}$

Deck Thickness $\qquad\qquad\qquad\qquad\qquad\qquad\qquad d_s := 5.75 \; \textbf{in}$

Web Width - Interior $\qquad\qquad\qquad\qquad\qquad\qquad b_w := 24 \; \textbf{in}$

Web Width - Exterior $\qquad\qquad\qquad\qquad\qquad\qquad b_{ux} := 15 \; \textbf{in}$

Curb Depth $\qquad\qquad\qquad\qquad\qquad\qquad\qquad\qquad h_{curb} := 12 \; \textbf{in}$

Curb Width $\qquad\qquad\qquad\qquad\qquad\qquad\qquad\qquad b_{curb} := 21 \; \textbf{in}$

Height to Centroid of Reinforcement - Interior $\qquad y_{bar} := \begin{bmatrix} 4.375 \\ 5.069 \\ 5.3125 \\ 5.069 \\ 4.375 \end{bmatrix} \textbf{in}$

Height to Centroid of Reinforcement - Exterior $\qquad y_{barx} := \begin{bmatrix} 4.875 \\ 4.875 \\ 4.875 \\ 4.875 \\ 4.875 \end{bmatrix} \textbf{in}$

Area of Reinforcement - Interior $\qquad\qquad\qquad A_s := \begin{bmatrix} 8.859 \\ 11.391 \\ 12.656 \\ 11.391 \\ 8.859 \end{bmatrix} \textbf{in}^2$

Area of Reinforcement - Exterior

$$A_{sx} := \begin{bmatrix} 7.8125 \\ 7.8125 \\ 7.8125 \\ 7.8125 \\ 7.8125 \end{bmatrix} \boldsymbol{in}^2$$

Distance from Centerline of Girder to Edge of Curb $\qquad$ $d_e := -10.5 \ \boldsymbol{in}$

Eccentricity of Centerline of Girders w.r.t. Centerline of Roadway $\qquad$ $exc := 0 \ \boldsymbol{in}$

Load and Analysis Parameters

Concentrated Load Due to Diaphragms on One Girder $\qquad$ $P_{dint} := 0 \ \boldsymbol{kip}$

Location of Intermediate Diaphragm
(Half, Third, Quarter) $\qquad$ $loc_d := \text{“Half”}$

Distributed Load Due to Rail $\qquad$ $w_{rail} := 0.319 \ \dfrac{\boldsymbol{kip}}{\boldsymbol{ft}}$

Structural Dead Load Factor $\qquad$ $\gamma_{DC} := 1.25$

Wearing Surface Dead Load Factor $\qquad$ $\gamma_{DW} := 1.25$

Live Load Factor $\qquad$ $\gamma_{LL} := 1.35$

Live Load Impact Factor $\qquad$ $IM := 0.33$

Flexural Resistance Factor $\qquad$ $\phi := .9$

System Factor $\qquad$ $\phi_s := 1.0$

Condition Factor $\qquad$ $\phi_c := 1.0$

Initial Calculations

Web Height - Interior $\qquad$ $d_g := h - d_s$

Web Height - Exterior $\qquad$ $d_{gx} := h_x - d_s$

Include Wearing Surface in Section Height $\qquad$ $h := h + \mathbf{if}\left(\gamma_{ws} = 0.15 \ \dfrac{\boldsymbol{kip}}{\boldsymbol{ft}^3}, ws, 0\right) = 35.25 \ \boldsymbol{in}$

Depth to Centroid of Reinforcement - Interior $\qquad$ $d := h - y_{bar}$

Depth to Centroid of Reinforcement - Exterior $\qquad$ $d_x := h_x - y_{barx} + h_{curb}$

Moment Applied to Interor Girders from Diaphragm $\qquad$ $M_d := \mathbf{if} \ loc_d = \text{“Half”} \qquad\qquad = 0 \ \boldsymbol{ft \cdot kip}$

$$\qquad\qquad \left\| \ P_{dint} \cdot \dfrac{L}{4} \right.$$

$$\text{else if } loc_d = \text{“Third”}$$

$$\qquad\qquad \left\| \ P_{dint} \cdot \dfrac{L}{3} \right.$$

$$\text{else if } loc_d = \text{“Quarter”}$$

$$\qquad\qquad \left\| \ P_{dint} \cdot \dfrac{L}{4} + P_{dint} \cdot \dfrac{L}{4} \right.$$

Moment Applied to Exterior Girders from Diaphragm $\qquad$ $M_{dx} := \dfrac{M_d}{2} = 0 \ \boldsymbol{ft \cdot kip}$

==Distribution Factors==

Dictance Between Centroids of Deck and Web

$$e_g := \frac{d_g + d_s}{2} = 15.625 \; \textbf{\textit{in}}$$

Area of Web

$$A := d_g \cdot b_w = 612 \; \textbf{\textit{in}}^2$$

Moment of Inertia of Web

$$I := \frac{b_w \cdot d_g^{\;3}}{12} = \left(3.316 \cdot 10^4\right) \; \textbf{\textit{in}}^4$$

Modular Ratio - Deck and Web

$$n := 1$$

Longitudinal Stiffness Parameter

$$K_g := n \cdot \left(I + A \cdot e_g^{\;2}\right) = \left(1.826 \cdot 10^5\right) \; \textbf{\textit{in}}^4$$

Interior Moment Distribution Factor - 1 Lane

$$g_{m1} := 0.06 + \left(\frac{S}{14 \; \textbf{\textit{ft}}}\right)^{0.4} \cdot \left(\frac{S}{L}\right)^{0.3} \cdot \left(\frac{K_g}{L \cdot d_s^{\;3}}\right)^{0.1} = 0.512$$

Interior Moment Distribution Factor - 2 Lane

$$g_{m2} := 0.075 + \left(\frac{S}{9.5 \; \textbf{\textit{ft}}}\right)^{0.6} \cdot \left(\frac{S}{L}\right)^{0.2} \cdot \left(\frac{K_g}{L \cdot d_s^{\;3}}\right)^{0.1} = 0.654$$

Controling Interior Moment Distribution Factor

$$g_m := \max\left(g_{m1}, g_{m2}\right)$$

Roadway Width

$$W_r := lanewidth \cdot Nlane$$

Eccentricity of Design Lane From C.G. of Girders

$$e_1 := \frac{W_r}{2} - 5 \; \textbf{\textit{ft}} + exc = 6 \; \textbf{\textit{ft}}$$

Eccentricity of Exterior Girder From C.G. of Girders

$$X_{ext} := (NG - 1) \cdot \frac{S}{2} = 12.25 \; \textbf{\textit{ft}}$$

Eccentricity of Each Girder

$$x_1 := X_{ext}$$
$$x_2 := X_{ext} - S$$
$$x_3 := X_{ext} - 2 \cdot S$$
$$x_4 := \textbf{if}\left(NG > 3, X_{ext} - 3 \cdot S, 0 \; \textbf{\textit{ft}}\right)$$
$$x_5 := \textbf{if}\left(NG > 4, X_{ext} - 4 \cdot S, 0 \; \textbf{\textit{ft}}\right)$$

Lever Rule Distribution Factor - One Lane

$$R_1 := \frac{1}{NG} + \frac{X_{ext} \cdot e_1}{x_1^{\;2} + x_2^{\;2} + x_3^{\;2} + x_4^{\;2} + x_5^{\;2}} = 0.396$$

$$g_{mR1} := \textbf{if}\left(P_{dint} > 0, 1.2 \cdot R_1, 0\right) = 0$$

Lever Rule Distribution Factor - Two Lanes

$$R_2 := \frac{2}{NG} + \frac{X_{ext} \cdot \left(e_1 - 5 \; \textbf{\textit{ft}}\right)}{x_1^{\;2} + x_2^{\;2} + x_3^{\;2} + x_4^{\;2} + x_5^{\;2}} = 0.433$$

$$g_{mR2} := \textbf{if}\left(P_{dint} > 0, R_2, 0\right) = 0$$

Exterior Moment Distribution Factor

$$g_{mx1} := \frac{1.2 \cdot \left(S + d_e - 2 \; \textbf{\textit{ft}}\right)}{2 \cdot S} = 0.318$$

$$ee := 0.77 + \frac{d_e}{9.1 \; \textbf{\textit{ft}}} = 0.674$$

$$g_{mx2} := g_{m2} \cdot ee = 0.441$$

	$g_{mx} := \max\left(g_{mx1}, g_{mx2}\right) = 0.441$
Skew Correction Factor	$c_1 := 0.25 \cdot \left(\dfrac{K_g}{12 \cdot L \cdot d_s^{\ 3}}\right)^{0.25} \cdot \left(\dfrac{S}{L}\right)^{.5} = 0.066$
	$\theta := \mathbf{if}\left(skew \geq 30^{\bullet}, skew, 0^{\bullet}\right)$
	$C_\theta := 1 - c_1 \cdot \left(\tan\left(\theta\right)\right)^{1.5} = 0.971$
	$g_m := g_m \cdot C_\theta = 0.635$
	$g_{mx} := g_{mx} \cdot C_\theta = 0.428$

Interior DF   Exterior DF

$g_m = 0.635$ $g_{mx} = 0.428$

Interior Girder Dead Load	$w_{girder} := \gamma_{RC} \cdot b_w \cdot d_g = 0.638 \ \dfrac{kip}{ft}$
Deck Dead Load	$w_{deck} := \gamma_{RC} \cdot S \cdot d_s = 0.44 \ \dfrac{kip}{ft}$
Curb Dead Load	$w_{curb} := 2 \cdot \gamma_{RC} \cdot h_{curb} \cdot b_{curb} = 0.525 \ \dfrac{kip}{ft}$
Dead Load from Nonstructural Components	$w_{ns} := \dfrac{w_{curb}}{NG} + w_{rail} = 0.424 \ \dfrac{kip}{ft}$
Total Structural Dead Load on Interior Girders	$DC := w_{girder} + w_{deck} + w_{ns} = 1.502 \ \dfrac{kip}{ft}$
Exterior Girder Dead Load	$w_{girderx} := \gamma_{RC} \cdot b_{wx} \cdot d_{gx} = 0.398 \ \dfrac{kip}{ft}$
Exterior Deck Dead Load	$w_{deckx} := \gamma_{RC} \cdot S_x \cdot d_s = 0.256 \ \dfrac{kip}{ft}$
Total Structural Dead Load on Exterior Girders	$DC_x := w_{girderx} + w_{deckx} + w_{ns} = 1.078 \ \dfrac{kip}{ft}$
Wearing Surface Dead Load on Interior Girders	$DW := \gamma_{ws} \cdot \left(ws + ws_2\right) \cdot S = 0.689 \ \dfrac{kip}{ft}$
Wearing Surface Dead Load on Exterior Girders	$DW_x := \gamma_{ws} \cdot \left(ws + ws_2\right) \cdot S_x = 0.401 \ \dfrac{kip}{ft}$
Dead Load Moments	$M_{DC} := \dfrac{DC \cdot L^2}{8} + M_d \qquad M_{DCx} := \dfrac{DC_x \cdot L^2}{8} + M_{dx}$
	$M_{DW} := \dfrac{DW \cdot L^2}{8} \qquad M_{DWx} := \dfrac{DW_x \cdot L^2}{8}$

$$M_{DC} = 256.984 \ ft \cdot kip \qquad M_{DCx} = 184.557 \ ft \cdot kip$$

$$M_{DW} = 117.916 \ ft \cdot kip \qquad M_{DWx} = 68.584 \ ft \cdot kip$$

Live Load Moment - Truck Load
$$M_{Truck} := 32 \ kip \cdot \left(\frac{L}{4}\right) + \frac{40 \ kip}{2} \cdot \left(\frac{L}{2} - 14 \ ft\right) = 386 \ ft \cdot kip$$

Live Load Moment - Tandem
$$M_{Tandem} := 25 \ kip \cdot \frac{L}{4} + \frac{25 \ kip}{2} \cdot \left(\frac{L}{2} - 4 \ ft\right) = 412.5 \ ft \cdot kip$$

Live Load Moment - Lane
$$M_{Lane} := 0.64 \ \frac{kip}{ft} \cdot \frac{L^2}{8} = 109.52 \ ft \cdot kip$$

Total HL-93 Live Load
$$M_{LL} := M_{Lane} + (1 + IM) \cdot \max\left(M_{Truck}, M_{Tandem}\right)$$

$$M_{LL} = 658.145 \ ft \cdot kip$$

Nominal Resistance

Depth Whitney Stress Block - Interior
$$a := A_s \cdot \frac{F_y}{0.85 \cdot f'_c \cdot S} = \begin{bmatrix} 1.872 \\ 2.407 \\ 2.674 \\ 2.407 \\ 1.872 \end{bmatrix} in$$

Nominal Moment Resistance - Interior
$$M_n := F_y \cdot \overrightarrow{A_s \cdot \left(d - \frac{a}{2}\right)} = \begin{bmatrix} 729.384 \\ 907.731 \\ 995.412 \\ 907.731 \\ 729.384 \end{bmatrix} ft \cdot kip$$

Interior Nominal Moment Capacity

$$M_{capacity} := \max \langle M_n \rangle = 995.412 \ ft \cdot kip$$

Depth Whitney Stress Block - Exterior
$$a_x := A_{sx} \cdot \frac{F_y}{0.85 \cdot f'_c \cdot S_x} = \begin{bmatrix} 2.838 \\ 2.838 \\ 2.838 \\ 2.838 \\ 2.838 \end{bmatrix} in$$

Nominal Moment Resistance - Exterior
$$M_{nx} := F_y \cdot \overrightarrow{A_{sx} \cdot \left(d_x - \frac{a_x}{2}\right)} = \begin{bmatrix} 793.977 \\ 793.977 \\ 793.977 \\ 793.977 \\ 793.977 \end{bmatrix} (ft \cdot kip)$$

Exterior Nominal Moment Capacity

$$M_{capacityx} := \max \langle M_{nx} \rangle = 793.977 \ ft \cdot kip$$

Interior Moment Rating Factor

$$RF_{Interior} := \frac{\phi \cdot \phi_s \cdot \phi_c \cdot M_{capacity} - \gamma_{DC} \cdot M_{DC} - \gamma_{DW} \cdot M_{DW}}{\gamma_{LL} \cdot M_{LL} \cdot g_m}$$

Exterior Moment Rating Factor

$$RF_{Exterior} := \frac{\phi \cdot \phi_s \cdot \phi_c \cdot M_{capacityx} - \gamma_{DC} \cdot M_{DCx} - \gamma_{DW} \cdot M_{DWx}}{\gamma_{LL} \cdot M_{LL} \cdot g_{mx}}$$

<u>Interior</u>

<u>Exterior</u>

$RF_{Interior} = 0.757$

$RF_{Exterior} = 1.047$

Concrete Compressive Strength - Larger is More Conservative $\qquad f'_c := 5 \; \boldsymbol{ksi}$

Concrte Elastic Modulus $\qquad E_c := 1820 \; \boldsymbol{ksi} \cdot \sqrt{\dfrac{f'_c}{\boldsymbol{ksi}}} = \langle 4.07 \cdot 10^3 \rangle \; \boldsymbol{ksi}$

==Interior Girders==

Maximum Recorded Strain $\qquad \varepsilon_T := 112.56 \cdot 10^{-6}$

Maximum Applied Moment per Lane $\qquad M_{Max} := 613.45 \; \boldsymbol{ft \cdot kip}$

Uncracked Section Modulus $\qquad S_{unc} := 8415 \; \boldsymbol{in}^3$

Cracked Section Modulus $\qquad S_{cr} := 2764 \; \boldsymbol{in}^3$

Section Behavior $\qquad Behavior := \text{"Uncracked"}$

Section Modulus Effective for Behavior $\qquad S_e := \mathbf{if} \langle Behavior = \text{"Uncracked"}, S_{unc}, S_{cr} \rangle$

Calculated Strain $\qquad \varepsilon_c := \dfrac{M_{Max} \cdot g_m}{S_e \cdot E_c} = 1.366 \cdot 10^{-4}$

Test Benefit Factor $\qquad k_a := \dfrac{\varepsilon_c}{\varepsilon_T} - 1 = 0.213$

Ratio of Applied to HL-93 Moment $\qquad r_M := \dfrac{M_{Max}}{M_{LL}} = 0.932$

Test Understanding Factor $\qquad k_b := \mathbf{if} \langle r_M > 0.7, 0.5, 0 \rangle = 0.5$

Rating Improvement Factor $\qquad k := 1 + k_a \cdot k_b = 1.107$

Improved Rating Factor $\qquad RF_{Improved} := RF_{Interior} \cdot k = 0.838$

==Exterior Girders==

Maximum Recorded Strain $\qquad \varepsilon_T := 79.28 \cdot 10^{-6}$

Maximum Applied Moment per Lane $\qquad M_{Max} := 613.45 \; \boldsymbol{ft \cdot kip}$

Uncracked Section Modulus $\qquad S_{unc} := 8132 \; \boldsymbol{in}^3$

Cracked Section Modulus $\qquad S_{cr} := 2071 \; \boldsymbol{in}^3$

Section Behavior $\qquad Behavior := \text{"Uncracked"}$

Section Modulus Effective for Behavior $\qquad S_e := \mathbf{if} \langle Behavior = \text{"Uncracked"}, S_{unc}, S_{cr} \rangle$

Calculated Strain $\qquad \varepsilon_c := \dfrac{M_{Max} \cdot g_{mx}}{S_e \cdot E_c} = 9.522 \cdot 10^{-5}$

Test Benefit Factor

$$k_a := \frac{\varepsilon_c}{\varepsilon_T} - 1 = 0.201$$

Ratio of Applied to HL-93 Moment

$$r_M := \frac{M_{Max}}{M_{LL}} = 0.932$$

Test Understanding Factor

$$k_b := \mathbf{if}\left(r_M > 0.7, 0.5, 0\right) = 0.5$$

Rating Improvement Factor

$$k := 1 + k_a \cdot k_b = 1.101$$

Improved Rating Factor

$$RF_{ImprovedExt} := RF_{Exterior} \cdot k = 1.152$$

Improved Rating Factors

Interior

$$RF_{Improved} = 0.838$$

Exterior

$$RF_{ImprovedExt} = 1.152$$

Figure 86: Bridge 2390 Calculations

A.5 Atkinson No. 2879

A.5.1 Experimental Configuration and Experimental Data Collected

Table 26: Bridge 2879 Experimental Configuration and Experimental Data Collected

File Contents	*File Name*	*File Type*
Sensors	Br2130_Sensors.csv	CSV Format
Sensor Layout	Br2130_SensorLayout.csv	MATLAB Data File
Sensor Data	Br2879_ALT_S_2_1_Strain.mat	MATLAB Data File
	Br2879_ALT_U_2_1_Strain.mat	MATLAB Data File
	Br2879_MAX_S_1_1_Strain.mat	MATLAB Data File
	Br2879_MAX_S_2_1_Strain.mat	MATLAB Data File
	Br2879_MAX_S_3_1_Strain.mat	MATLAB Data File
	Br2879_MAX_U_2_1_Strain.mat	MATLAB Data File
	Br2879_SBS_S_2_1_Strain.mat	MATLAB Data File
	Br2879_SBS_U_2_1_Strain.mat	MATLAB Data File

A.5.2 Instrumentation
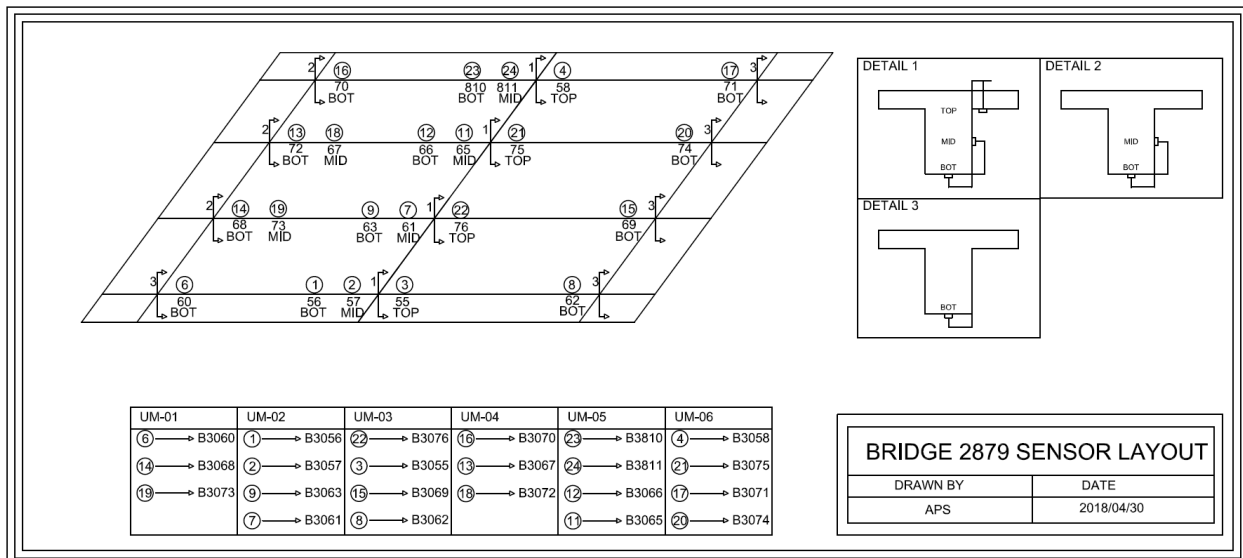
Figure 87: Bridge 2879 Sensor Layout

A.5.3 Loading
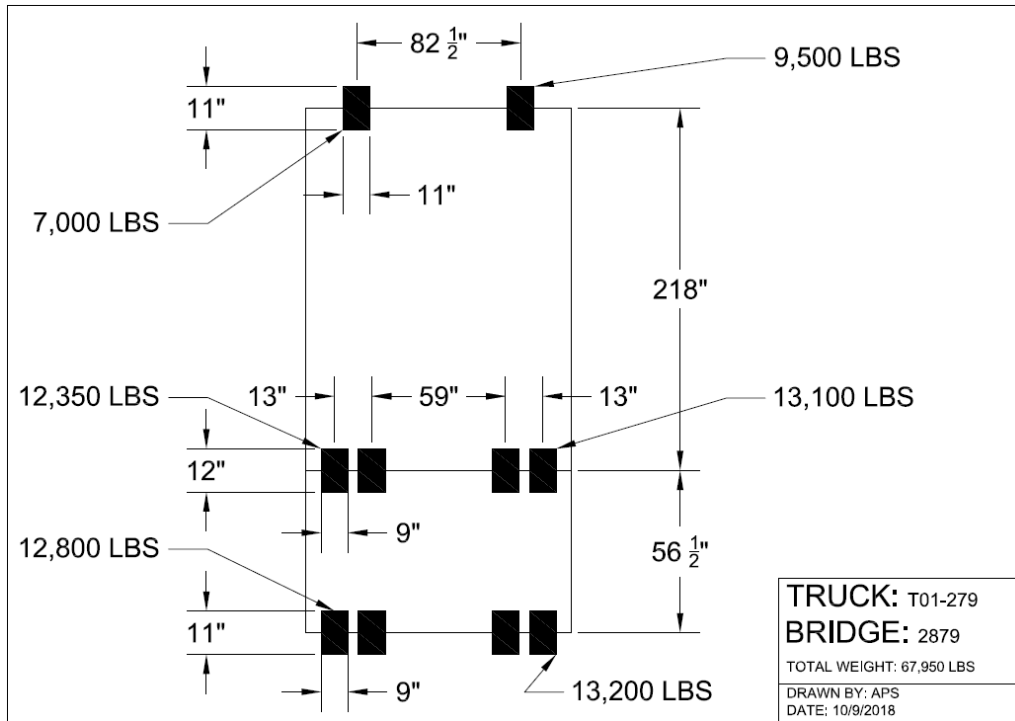
Figure 88: Bridge 2879 Truck T01-279 Loading
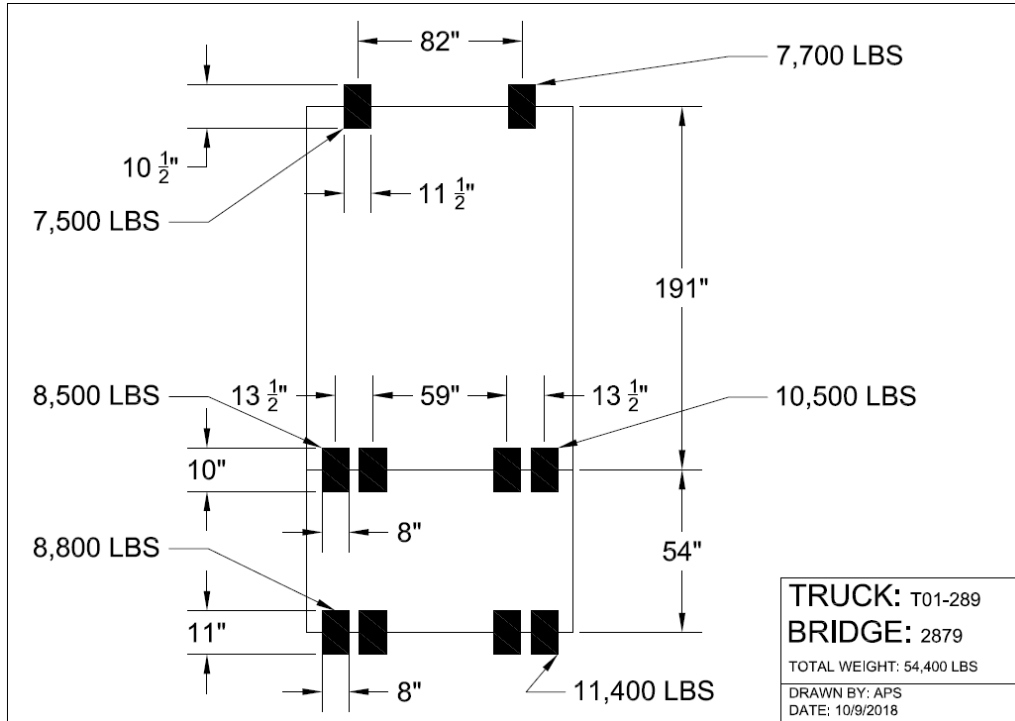
Figure 89: Bridge 2879 Truck T01-289 Loading
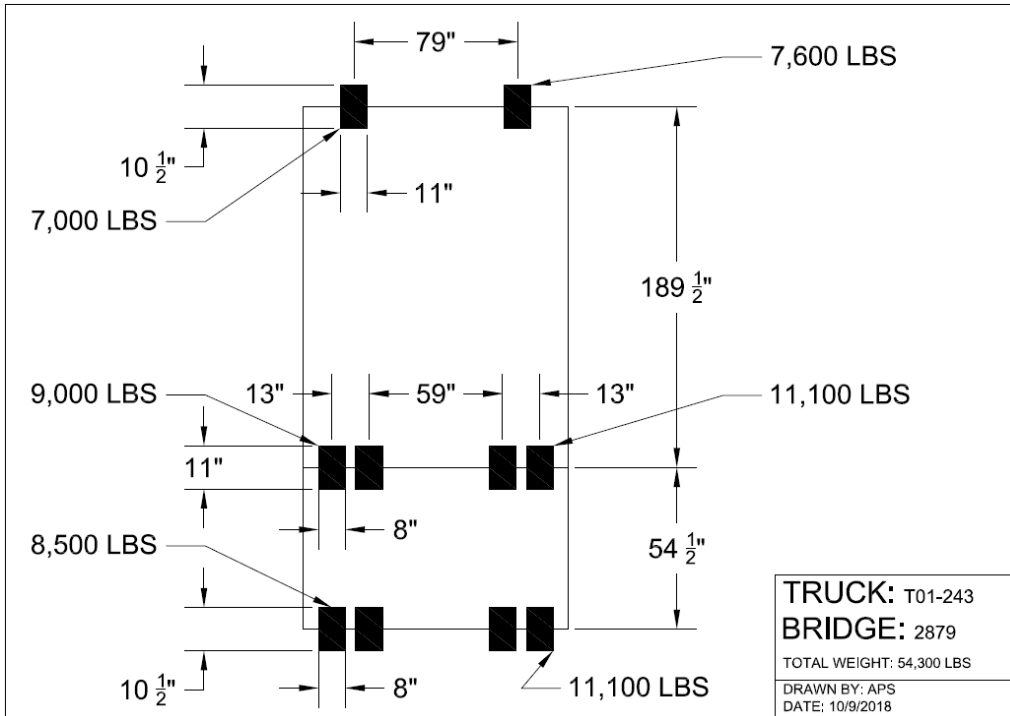
Figure 90: Bridge 2879 Truck T01-243 Loading
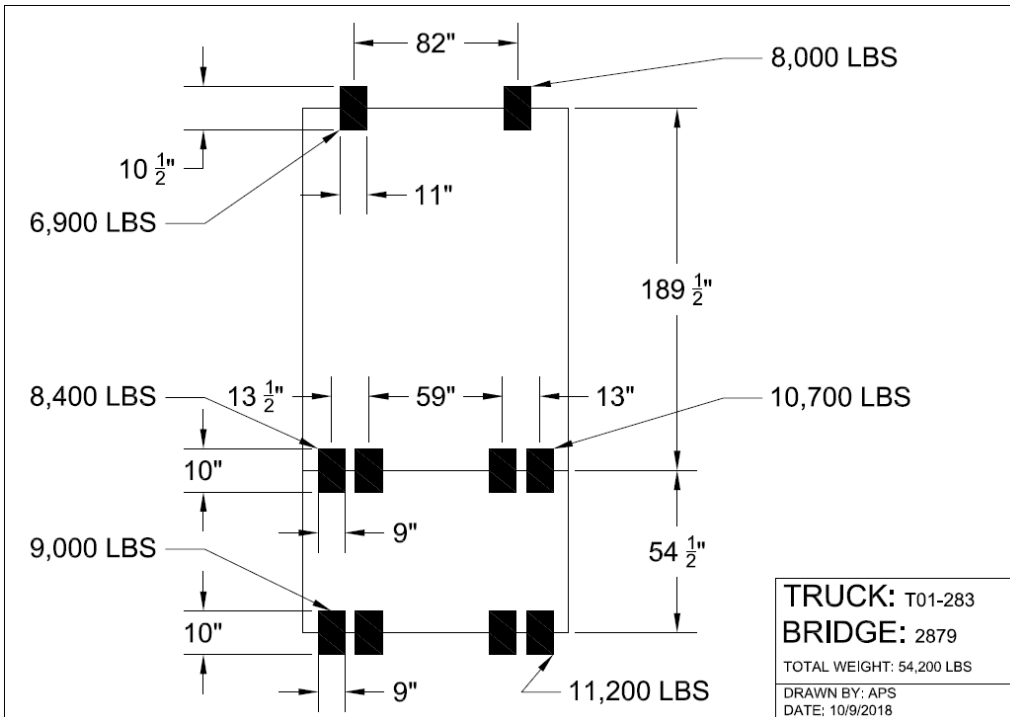
Figure 91: Bridge 2879 Truck T01-283 Loading

A.5.4 Representative Data Plots
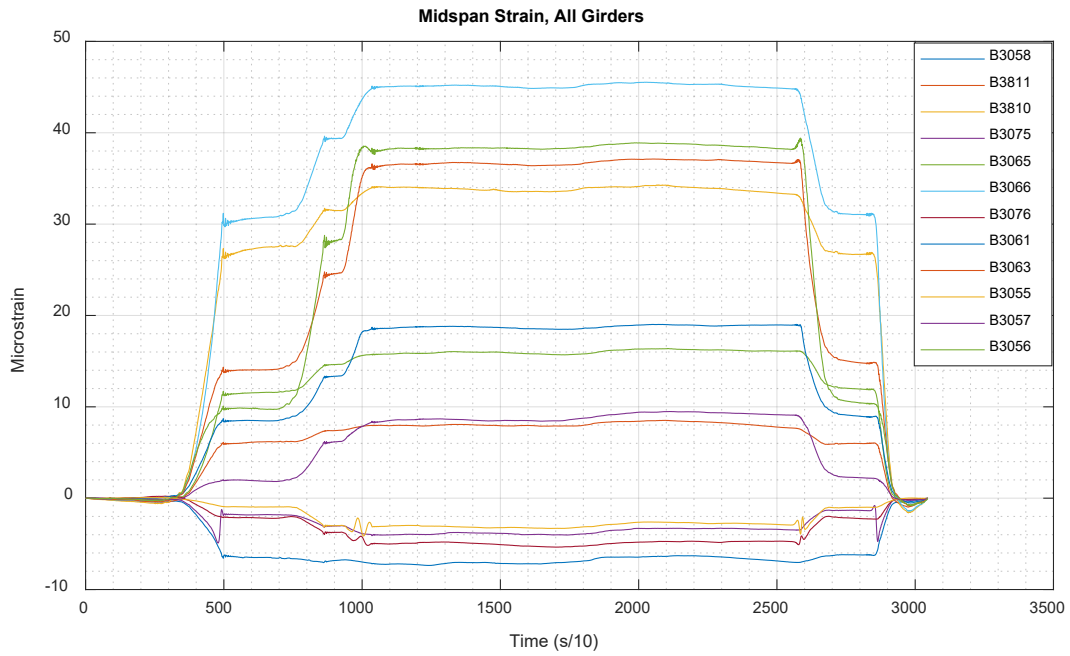
Figure 92: Bridge 2879 SBS_S_2_1 Strains - Midspan
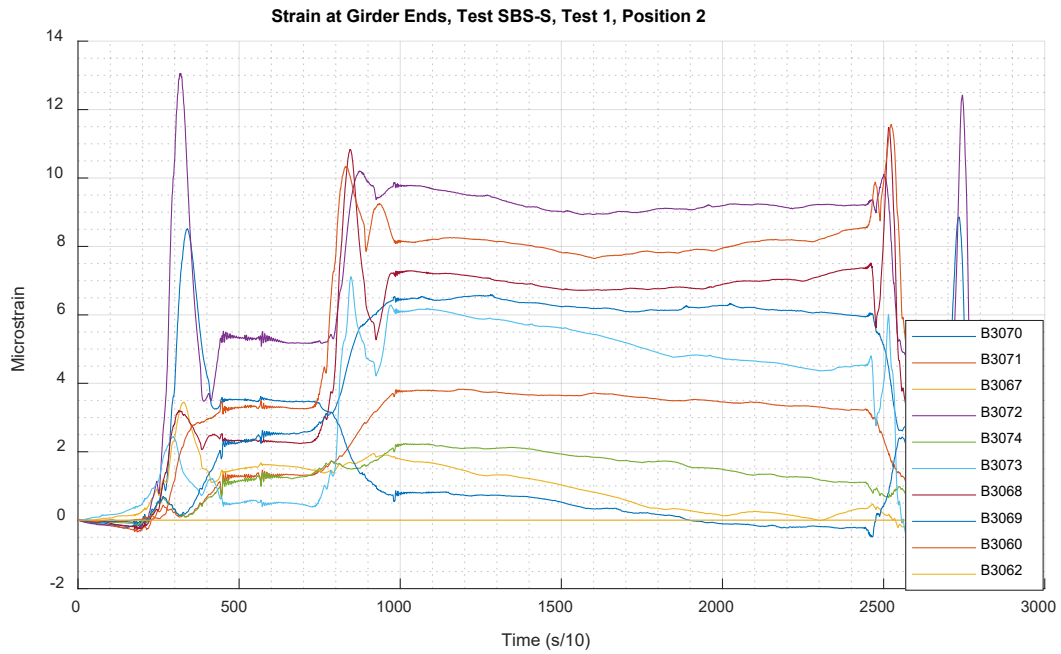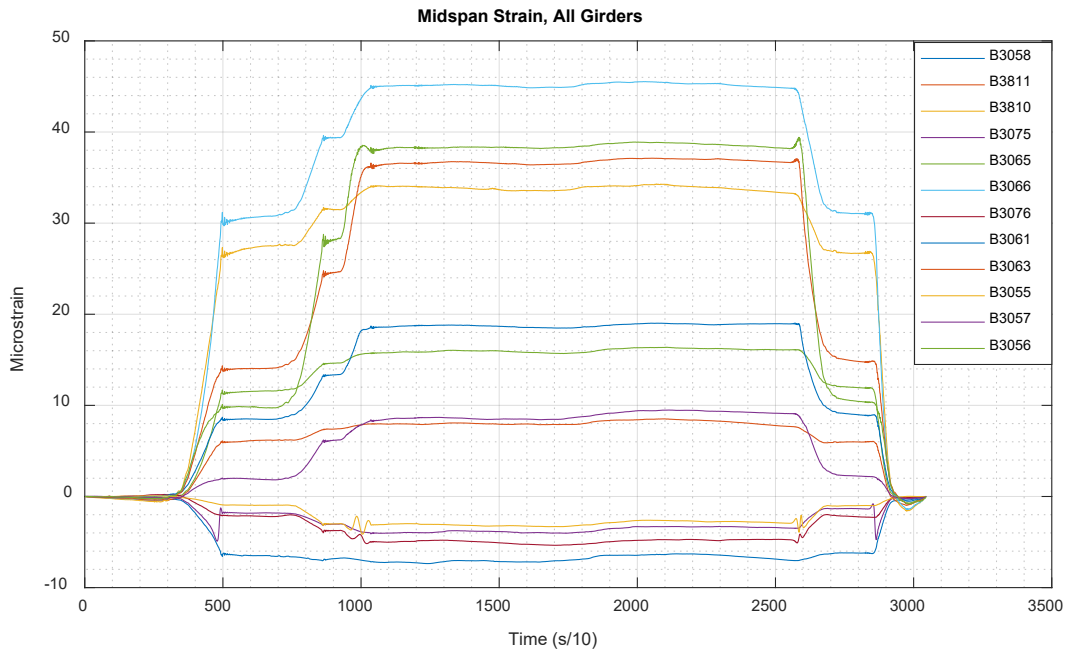

Figure 93: Bridge 2879 SBS_S_2_1 Strains - Ends

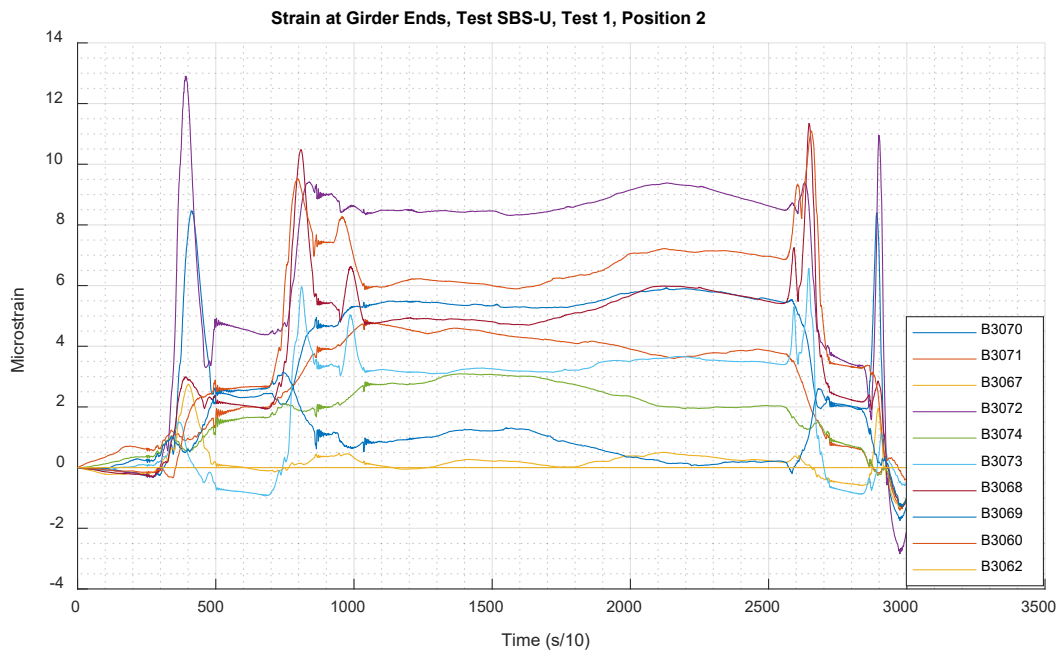Figure 94: Bridge 2879 SBS_U_2_1 Strains - Midspan
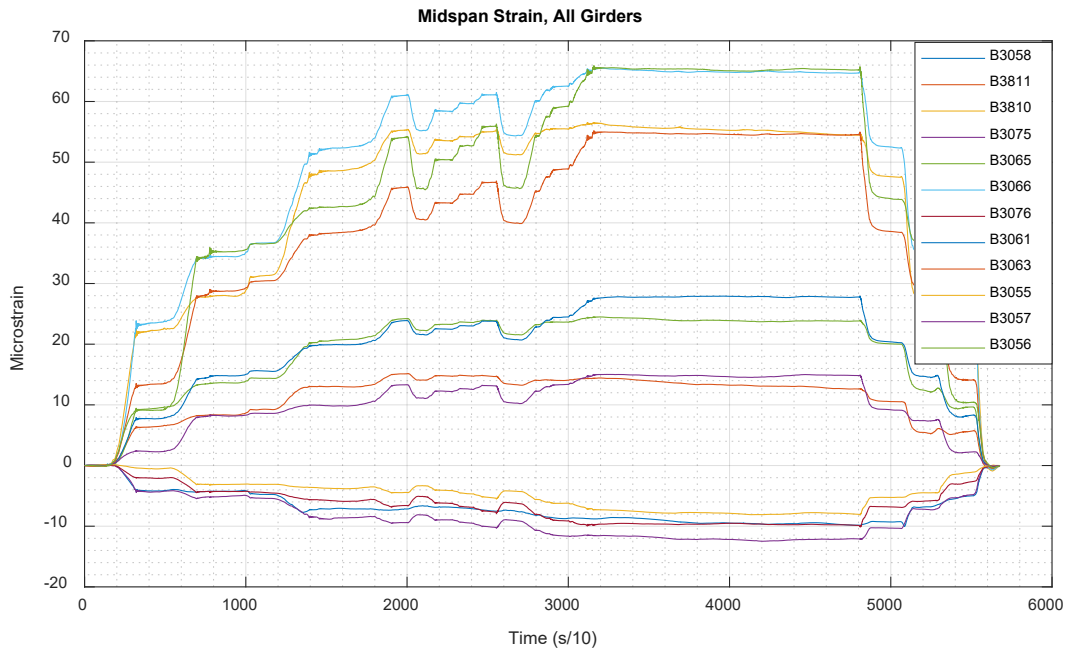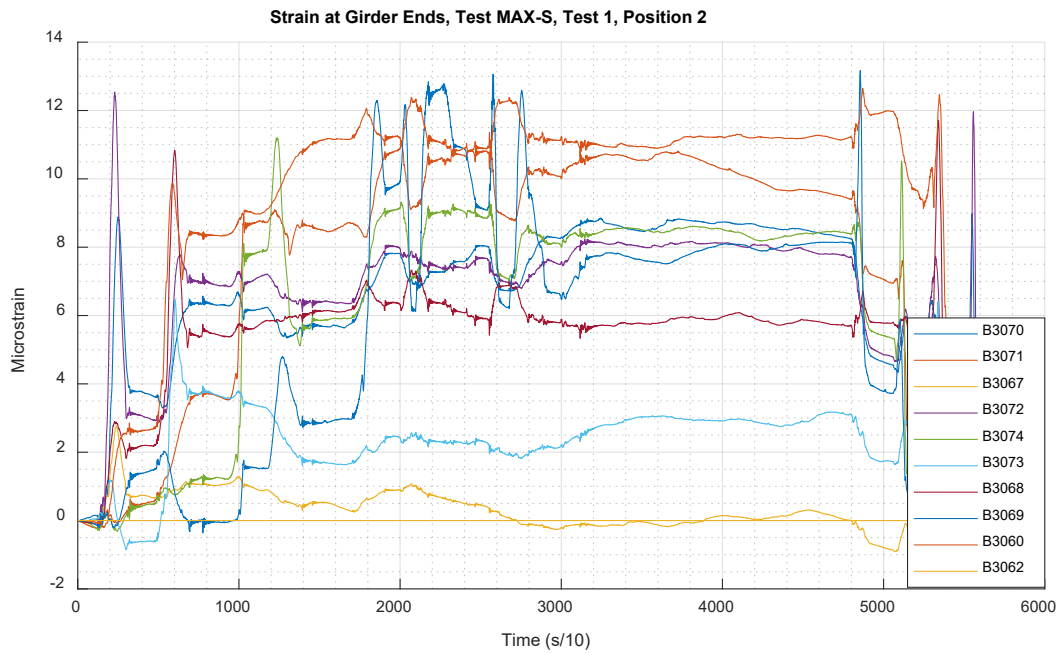

Figure 95: Bridge 2879 SBS_U_2_1 Strains – Ends

Figure 96: Bridge 2879 MAX_S_2_1 Strains - Midspan
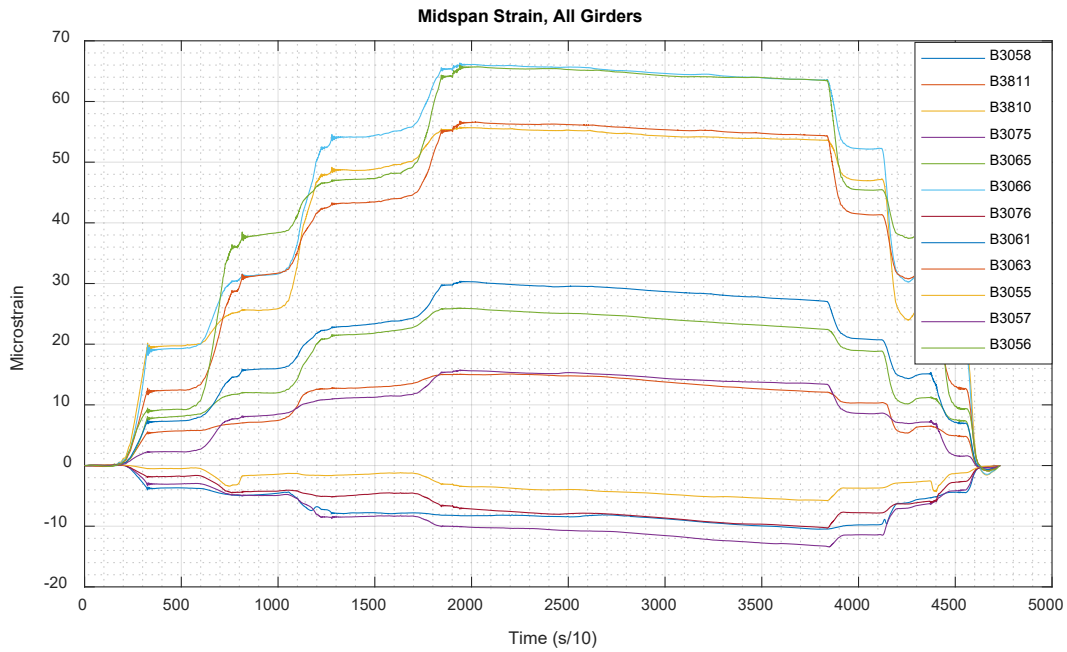

Figure 97: Bridge 2879 MAX_S_2_1 Strains - Ends

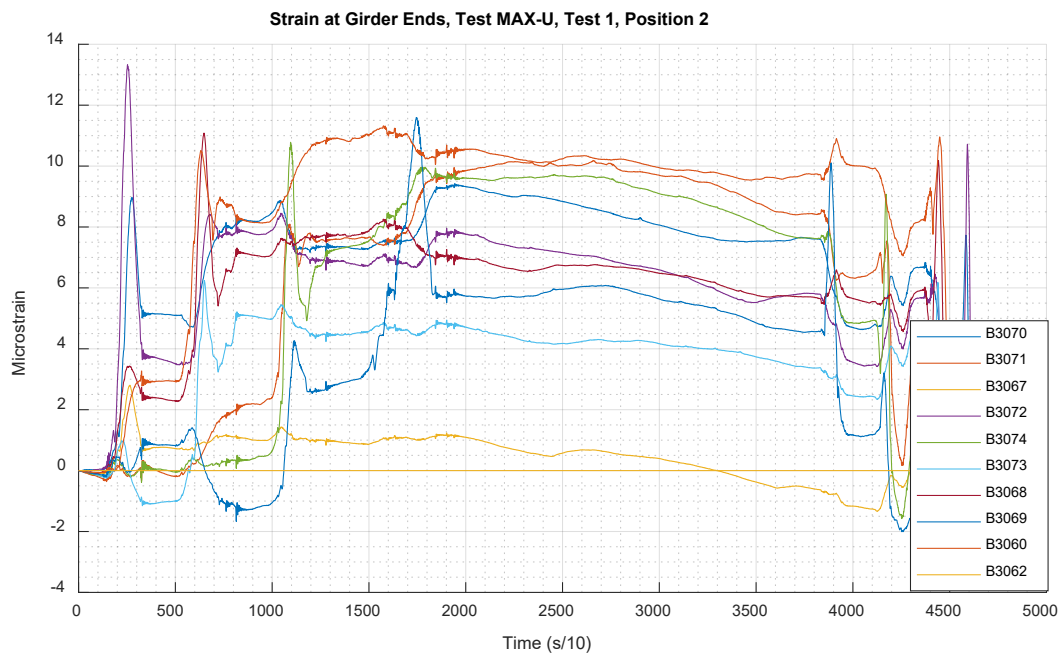Figure 98: Bridge 2879 MAX_U_2_1 Strains - Midspan

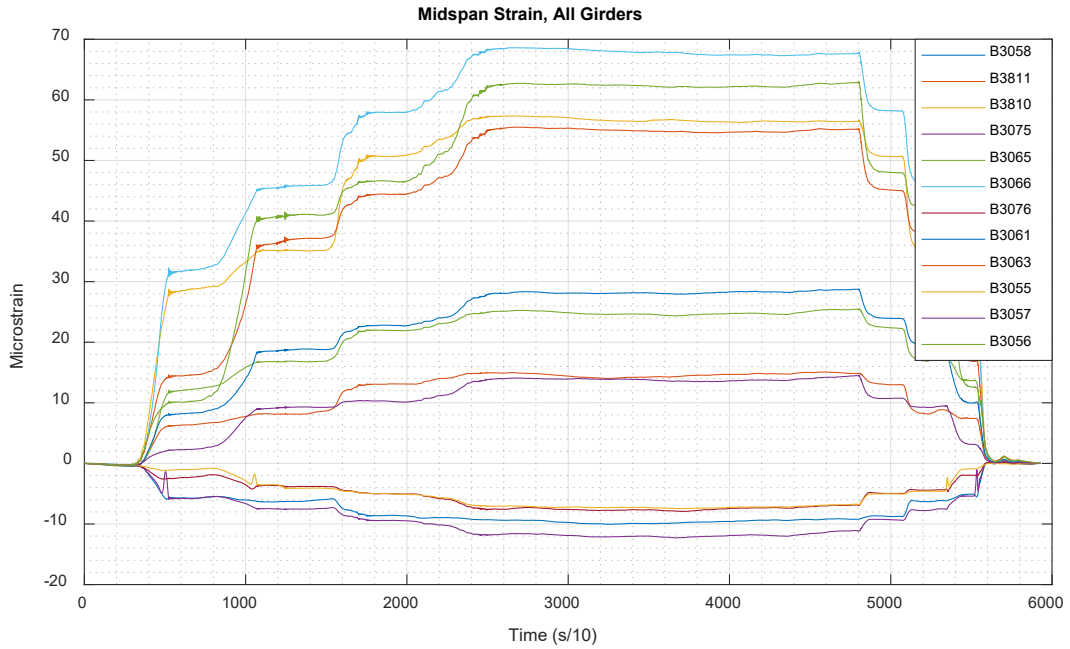Figure 99: Bridge 2879 MAX_U_2_1 Strains – Ends

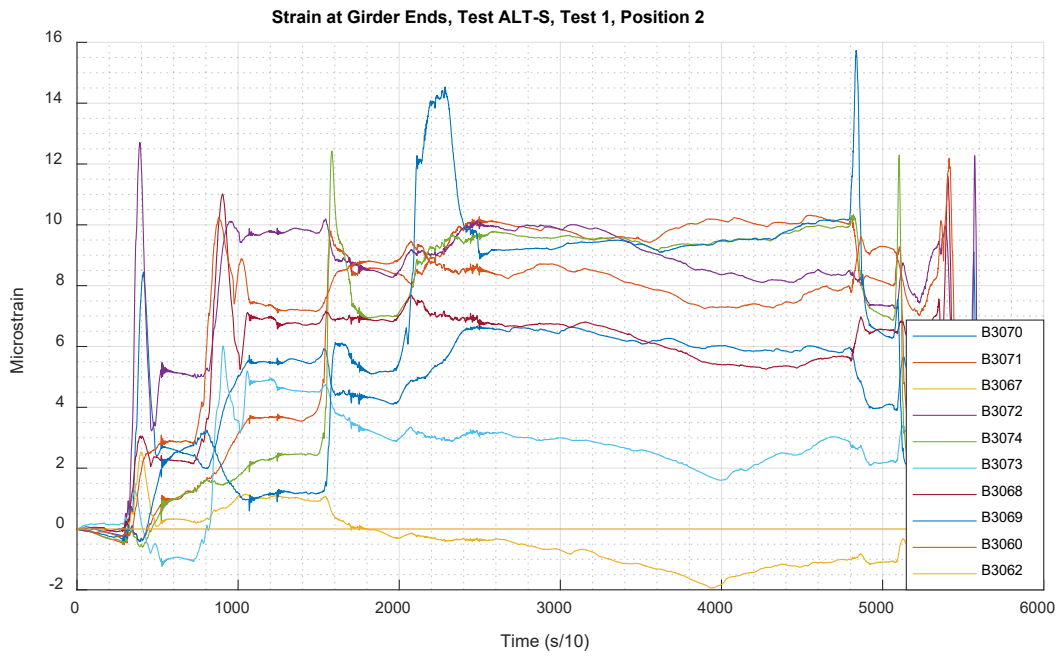Figure 100: Bridge 2879 ALT_S_2_1 Strains - Midspan
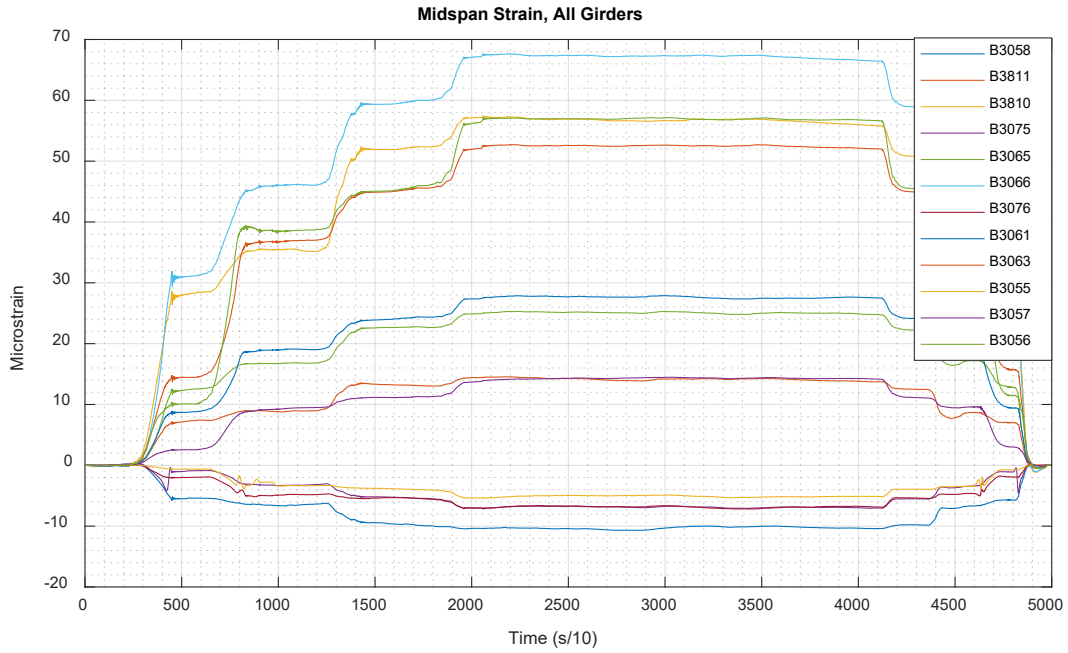

Figure 101: Bridge 2879 ALT_S_2_1 Strains – Ends

Figure 102: Bridge 2879 ALT_U_2_1 Strains - Midspan

Figure 103: Bridge 2879 ALT_U_2_1 Strains - Ends

A.5.5 Rating Factor Calculations
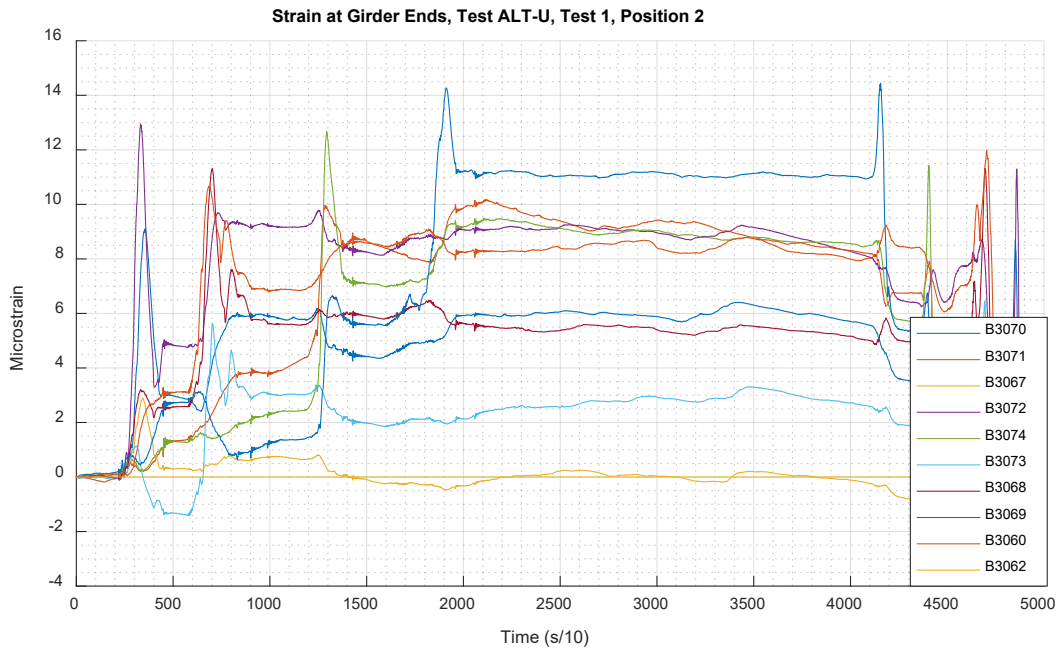
AASHTO Rating Calculations:

Bridge 2879 - Atkinson, Maine

Material Parameters:

Concrete Compressive Strength	$f'_c := 2.5 \; \textbf{ksi}$
Reinforcement Yield Strength	$F_y := 33 \; \textbf{ksi}$
Unit Weight: Reinforced Concrete	$\gamma_{RC} := 0.150 \; \dfrac{\textbf{kip}}{\textbf{ft}^3}$
Unit Weight: Wearing Surface	$\gamma_{ws} := 0.150 \; \dfrac{\textbf{kip}}{\textbf{ft}^3}$

Geometric Properties:

Span Length	$L := 50 \; \textbf{ft}$
Girder Spacing - Interior	$S := 90 \; \textbf{in}$
Girder Spacing - Exterior	$S_x := 54 \; \textbf{in}$
Number of Girders	$NG := 4$
Skew Angle	$skew := 30°$
Lane Width	$lanewidth := 10.5 \; \textbf{ft}$
Number of Lanes	$Nlane := 2$
Wearing Surface Thickness	$ws := 4 \; \textbf{in}$
Thickness of Pavement Overlay	$ws_2 := 0 \; \textbf{in}$
Girder Height - Interior	$h := 50 \; \textbf{in}$
Girder Height - Exterior	$h_x := 50 \; \textbf{in}$
Deck Thickness	$d_s := 8 \; \textbf{in}$
Web Width - Interior	$b_w := 22 \; \textbf{in}$
Web Width - Exterior	$b_{wx} := 17 \; \textbf{in}$
Curb Depth	$h_{curb} := 12 \; \textbf{in}$
Curb Width	$b_{curb} := 18 \; \textbf{in}$

$$y_{bar} := \begin{bmatrix} 3.333 \\ 3.875 \\ 5.518 \\ 3.875 \\ 3.333 \end{bmatrix} \textbf{in}$$

Height to Centroid of Reinforcement - Interior

$$y_{barx} := \begin{bmatrix} 3.583 \\ 4.125 \\ 5.75 \\ 4.125 \\ 3.583 \end{bmatrix} \textbf{in}$$

Height to Centroid of Reinforcement - Exterior

$$A_s := \begin{bmatrix} 7.5938 \\ 12.656 \\ 17.719 \\ 12.656 \\ 7.5938 \end{bmatrix} \textbf{in}^2$$

Area of Reinforcement - Interior

Area of Reinforcement - Exterior		$A_{sx} := \begin{bmatrix} 9.375 \\ 12.5 \\ 18.75 \\ 12.5 \\ 9.375 \end{bmatrix} in^2$

Distance from Centerline of Girder to Edge of Curb $\qquad\qquad d_e := -6.5 \ in$

Eccentricity of Centerline of Girders w.r.t. Centerline of Roadway $\qquad exc := 0 \ in$

<mark>Load and Analysis Parameters</mark>

Concentrated Load Due to Diaphragms on One Girder $\qquad\qquad P_{dint} := 2.833 \ kip$

Location of Intermediate Diaphragm
(Half, Third, Quarter) $\qquad\qquad loc_d := \text{"Third"}$

Distributed Load Due to Rail $\qquad\qquad\qquad\qquad\qquad w_{rail} := .219 \ \dfrac{kip}{ft}$

Structural Dead Load Factor $\qquad\qquad\qquad\qquad\qquad \gamma_{DC} := 1.25$

Wearing Surface Dead Load Factor $\qquad\qquad\qquad\qquad \gamma_{DW} := 1.25$

Live Load Factor $\qquad\qquad\qquad\qquad\qquad\qquad\qquad \gamma_{LL} := 1.35$

Live Load Impact Factor $\qquad\qquad\qquad\qquad\qquad\qquad IM := 0.33$

Flexural Resistance Factor $\qquad\qquad\qquad\qquad\qquad\qquad \phi := .9$

System Factor $\qquad\qquad\qquad\qquad\qquad\qquad\qquad\qquad \phi_s := 1.0$

Condition Factor $\qquad\qquad\qquad\qquad\qquad\qquad\qquad\qquad \phi_c := 1.0$

<mark>Initial Calculations</mark>

Web Height - Interior $\qquad\qquad\qquad\qquad\qquad\qquad d_g := h - d_s$

Web Height - Exterior $\qquad\qquad\qquad\qquad\qquad\qquad d_{gx} := h_x - d_s$

Include Wearing Surface in Section Height $\qquad\qquad h := h + \mathbf{if}\left(\gamma_{ws} = 0.15 \ \dfrac{kip}{ft^3}, ws, 0\right) = 54 \ in$

Depth to Centroid of Reinforcement - Interior $\qquad\qquad d := h - y_{bar}$

Depth to Centroid of Reinforcement - Exterior $\qquad\qquad d_x := h_x - y_{barx} + h_{curb}$

Moment Applied to Interior Girders from Diaphragm $\qquad M_d := \mathbf{if} \ loc_d = \text{"Half"} \qquad\qquad = 47.217 \ ft \cdot kip$

$$\left\| P_{dint} \cdot \dfrac{L}{4} \right.$$

$$\text{else if } loc_d = \text{"Third"}$$

$$\left\| P_{dint} \cdot \dfrac{L}{3} \right.$$

$$\text{else if } loc_d = \text{"Quarter"}$$

$$\left\| P_{dint} \cdot \dfrac{L}{4} + P_{dint} \cdot \dfrac{L}{4} \right.$$

Moment Applied to Exterior Girders from Diaphragm $\qquad M_{dx} := \dfrac{M_d}{2} = 23.608 \ ft \cdot kip$

Dictance Between Centroids of Deck and Web

$$e_g := \frac{d_g + d_s}{2} = 25 \ \textbf{in}$$

Area of Web

$$A := d_g \cdot b_w = 924 \ \textbf{in}^2$$

Moment of Inertia of Web

$$I := \frac{b_w \cdot d_g^3}{12} = \left(1.358 \cdot 10^5\right) \ \textbf{in}^4$$

Modular Ratio - Deck and Web

$$n := 1$$

Longitudinal Stiffness Parameter

$$K_g := n \cdot \left(I + A \cdot e_g^2\right) = \left(7.133 \cdot 10^5\right) \ \textbf{in}^4$$

Interior Moment Distribution Factor - 1 Lane

$$g_{m1} := 0.06 + \left(\frac{S}{14 \ \textbf{ft}}\right)^{0.4} \cdot \left(\frac{S}{L}\right)^{0.3} \cdot \left(\frac{K_g}{L \cdot d_s^3}\right)^{0.1} = 0.54$$

Interior Moment Distribution Factor - 2 Lane

$$g_{m2} := 0.075 + \left(\frac{S}{9.5 \ \textbf{ft}}\right)^{0.6} \cdot \left(\frac{S}{L}\right)^{0.2} \cdot \left(\frac{K_g}{L \cdot d_s^3}\right)^{0.1} = 0.721$$

Controling Interior Moment Distribution Factor

$$g_m := \max\left(g_{m1}, g_{m2}\right)$$

Roadway Width

$$W_r := lanewidth \cdot Nlane$$

Eccentricity of Design Lane From C.G. of Girders

$$e_1 := \frac{W_r}{2} - 5 \ \textbf{ft} + exc = 5.5 \ \textbf{ft}$$

Eccentricity of Exterior Girder From C.G. of Girders

$$X_{ext} := (NG - 1) \cdot \frac{S}{2} = 11.25 \ \textbf{ft}$$

Eccentricity of Each Girder

$$x_1 := X_{ext}$$
$$x_2 := X_{ext} - S$$
$$x_3 := X_{ext} - 2 \cdot S$$
$$x_4 := \textbf{if}\left(NG > 3, X_{ext} - 3 \cdot S, 0 \ \textbf{ft}\right)$$
$$x_5 := \textbf{if}\left(NG > 4, X_{ext} - 4 \cdot S, 0 \ \textbf{ft}\right)$$

Lever Rule Distribution Factor - One Lane

$$R_1 := \frac{1}{NG} + \frac{X_{ext} \cdot e_1}{x_1^2 + x_2^2 + x_3^2 + x_4^2 + x_5^2} = 0.47$$

$$g_{mR1} := \textbf{if}\left(P_{dint} > 0, 1.2 \cdot R_1, 0\right) = 0.564$$

Lever Rule Distribution Factor - Two Lanes

$$R_2 := \frac{2}{NG} + \frac{X_{ext} \cdot \left(e_1 - 5 \ \textbf{ft}\right)}{x_1^2 + x_2^2 + x_3^2 + x_4^2 + x_5^2} = 0.52$$

$$g_{mR2} := \textbf{if}\left(P_{dint} > 0, R_2, 0\right) = 0.52$$

Exterior Moment Distribution Factor

$$g_{mx1} := \frac{1.2 \cdot \left(S + d_e - 2 \ \textbf{ft}\right)}{2 \cdot S} = 0.397$$

$$ee := 0.77 + \frac{d_e}{9.1 \ \textbf{ft}} = 0.71$$

$$g_{mx2} := g_{m2} \cdot ee = 0.512$$

Skew Correction Factor	$g_{mx} := \max\left(g_{mx1}, g_{mx2}\right) = 0.512$
	$c_1 := 0.25 \cdot \left(\dfrac{K_g}{12 \cdot L \cdot d_s^{\ 3}}\right)^{0.25} \cdot \left(\dfrac{S}{L}\right)^{.5} = 0.064$
	$\theta := \mathbf{if}\left(skew \geq 30\,^\bullet, skew, 0\,^\bullet\right)$
	$C_\theta := 1 - c_1 \cdot \left(\tan\left(\theta\right)\right)^{1.5} = 0.972$
	$g_m := g_m \cdot C_\theta = 0.701$
	$g_{mx} := g_{mx} \cdot C_\theta = 0.498$

Interior DF

$g_m = 0.701$

Exterior DF

$g_{mx} = 0.498$

<mark>Loading</mark>

Interior Girder Dead Load	$w_{girder} := \gamma_{RC} \cdot b_w \cdot d_g = 0.963\ \dfrac{\textit{kip}}{\textit{ft}}$
Deck Dead Load	$w_{deck} := \gamma_{RC} \cdot S \cdot d_s = 0.75\ \dfrac{\textit{kip}}{\textit{ft}}$
Curb Dead Load	$w_{curb} := 2 \cdot \gamma_{RC} \cdot h_{curb} \cdot b_{curb} = 0.45\ \dfrac{\textit{kip}}{\textit{ft}}$
Dead Load from Nonstructural Components	$w_{ns} := \dfrac{w_{curb}}{NG} + w_{rail} = 0.332\ \dfrac{\textit{kip}}{\textit{ft}}$
Total Structural Dead Load on Interior Girders	$DC := w_{girder} + w_{deck} + w_{ns} = 2.044\ \dfrac{\textit{kip}}{\textit{ft}}$
Exterior Girder Dead Load	$w_{girderx} := \gamma_{RC} \cdot b_{wx} \cdot d_{gx} = 0.744\ \dfrac{\textit{kip}}{\textit{ft}}$
Exterior Deck Dead Load	$w_{deckx} := \gamma_{RC} \cdot S_x \cdot d_s = 0.45\ \dfrac{\textit{kip}}{\textit{ft}}$
Total Structural Dead Load on Exterior Girders	$DC_x := w_{girderx} + w_{deckx} + w_{ns} = 1.525\ \dfrac{\textit{kip}}{\textit{ft}}$
Wearing Surface Dead Load on Interior Girders	$DW := \gamma_{ws} \cdot \left(ws + ws_2\right) \cdot S = 0.375\ \dfrac{\textit{kip}}{\textit{ft}}$
Wearing Surface Dead Load on Exterior Girders	$DW_x := \gamma_{ws} \cdot \left(ws + ws_2\right) \cdot S_x = 0.225\ \dfrac{\textit{kip}}{\textit{ft}}$
Dead Load Moments	$M_{DC} := \dfrac{DC \cdot L^2}{8} + M_d \qquad M_{DCx} := \dfrac{DC_x \cdot L^2}{8} + M_{dx}$
	$M_{DW} := \dfrac{DW \cdot L^2}{8} \qquad\qquad M_{DWx} := \dfrac{DW_x \cdot L^2}{8}$

$$M_{DC} = 685.967 \ \boldsymbol{ft \cdot kip} \qquad M_{DCx} = 500.249 \ \boldsymbol{ft \cdot kip}$$

$$M_{DW} = 117.188 \ \boldsymbol{ft \cdot kip} \qquad M_{DWx} = 70.313 \ \boldsymbol{ft \cdot kip}$$

Live Load Moment - Truck Load

$$M_{Truck} := 32 \ \boldsymbol{kip} \cdot \left(\frac{L}{4}\right) + \frac{40 \ \boldsymbol{kip}}{2} \cdot \left(\frac{L}{2} - 14 \ \boldsymbol{ft}\right) = 620 \ \boldsymbol{ft \cdot kip}$$

Live Load Moment - Tandem

$$M_{Tandem} := 25 \ \boldsymbol{kip} \cdot \frac{L}{4} + \frac{25 \ \boldsymbol{kip}}{2} \cdot \left(\frac{L}{2} - 4 \ \boldsymbol{ft}\right) = 575 \ \boldsymbol{ft \cdot kip}$$

Live Load Moment - Lane

$$M_{Lane} := 0.64 \ \frac{\boldsymbol{kip}}{\boldsymbol{ft}} \cdot \frac{L^2}{8} = 200 \ \boldsymbol{ft \cdot kip}$$

Total HL-93 Live Load

$$M_{LL} := M_{Lane} + (1 + IM) \cdot \max\left(M_{Truck}, M_{Tandem}\right)$$

$$M_{LL} = \left(1.025 \cdot 10^3\right) \boldsymbol{ft \cdot kip}$$

Nominal Resistance

Depth Whitney Stress Block - Interior

$$a := A_s \cdot \frac{F_y}{0.85 \cdot f'_c \cdot S} = \begin{bmatrix} 1.31 \\ 2.184 \\ 3.057 \\ 2.184 \\ 1.31 \end{bmatrix} \boldsymbol{in}$$

Nominal Moment Resistance - Interior

$$M_n := \overrightarrow{F_y \cdot A_s \cdot \left(d - \frac{a}{2}\right)} = \begin{bmatrix} 1.044 \cdot 10^3 \\ 1.707 \cdot 10^3 \\ 2.288 \cdot 10^3 \\ 1.707 \cdot 10^3 \\ 1.044 \cdot 10^3 \end{bmatrix} \boldsymbol{ft \cdot kip}$$

Interior Nominal Moment Capacity

$$M_{capacity} := \max\langle M_n \rangle = \left(2.288 \cdot 10^3\right) \boldsymbol{ft \cdot kip}$$

Depth Whitney Stress Block - Exterior

$$a_x := A_{sx} \cdot \frac{F_y}{0.85 \cdot f'_c \cdot S_x} = \begin{bmatrix} 2.696 \\ 3.595 \\ 5.392 \\ 3.595 \\ 2.696 \end{bmatrix} \boldsymbol{in}$$

Nominal Moment Resistance - Exterior

$$M_{nx} := \overrightarrow{F_y \cdot A_{sx} \cdot \left(d_x - \frac{a_x}{2}\right)} = \begin{bmatrix} 1.471 \cdot 10^3 \\ 1.928 \cdot 10^3 \\ 2.761 \cdot 10^3 \\ 1.928 \cdot 10^3 \\ 1.471 \cdot 10^3 \end{bmatrix} \left(\boldsymbol{ft \cdot kip}\right)$$

Exterior Nominal Moment Capacity

$$M_{capacityx} := \max\langle M_{nx} \rangle = \left(2.761 \cdot 10^3\right) \boldsymbol{ft \cdot kip}$$

Interior Moment Rating Factor

$$RF_{Interior} := \frac{\phi \cdot \phi_s \cdot \phi_c \cdot M_{capacity} - \gamma_{DC} \cdot M_{DC} - \gamma_{DW} \cdot M_{DW}}{\gamma_{LL} \cdot M_{LL} \cdot g_m}$$

Exterior Moment Rating Factor

$$RF_{Exterior} := \frac{\phi \cdot \phi_s \cdot \phi_c \cdot M_{capacityx} - \gamma_{DC} \cdot M_{DCx} - \gamma_{DW} \cdot M_{DWx}}{\gamma_{LL} \cdot M_{LL} \cdot g_{mx}}$$

Interior   Exterior

$RF_{Interior} = 1.089$ $RF_{Exterior} = 2.574$

Concrete Compressive Strength - Larger is More Conservative $\qquad$ $f'_c := 5 \ \textbf{ksi}$

Concrte Elastic Modulus $\qquad$ $E_c := 1820 \ \textbf{ksi} \cdot \sqrt{\dfrac{f'_c}{\textbf{ksi}}} = \left\langle 4.07 \cdot 10^3 \right\rangle \ \textbf{ksi}$

==Interior Girders==

Maximum Recorded Strain $\qquad$ $\varepsilon_T := 62.49 \cdot 10^{-6}$

Maximum Applied Moment per Lane $\qquad$ $M_{Max} := 946.9 \ \textbf{ft} \cdot \textbf{kip}$

Uncracked Section Modulus $\qquad$ $S_{unc} := 21210 \ \textbf{in}^3$

Cracked Section Modulus $\qquad$ $S_{cr} := 8413 \ \textbf{in}^3$

Section Behavior $\qquad$ $Behavior := \text{"Uncracked"}$

Section Modulus Effective for Behavior $\qquad$ $S_e := \textbf{if} \left(Behavior = \text{"Uncracked"}, S_{unc}, S_{cr} \right)$

Calculated Strain $\qquad$ $\varepsilon_c := \dfrac{M_{Max} \cdot g_m}{S_e \cdot E_c} = 9.223 \cdot 10^{-5}$

Test Benefit Factor $\qquad$ $k_a := \dfrac{\varepsilon_c}{\varepsilon_T} - 1 = 0.476$

Ratio of Applied to HL-93 Moment $\qquad$ $r_M := \dfrac{M_{Max}}{M_{LL}} = 0.924$

Test Understanding Factor $\qquad$ $k_b := \textbf{if} \left(r_M > 0.7, 0.5, 0 \right) = 0.5$

Rating Improvement Factor $\qquad$ $k := 1 + k_a \cdot k_b = 1.238$

Improved Rating Factor $\qquad$ $RF_{Improved} := RF_{Interior} \cdot k = 1.348$

==Exterior Girders==

Maximum Recorded Strain $\qquad$ $\varepsilon_T := 77.32 \cdot 10^{-6}$

Maximum Applied Moment per Lane $\qquad$ $M_{Max} := 946.9 \ \textbf{ft} \cdot \textbf{kip}$

Uncracked Section Modulus $\qquad$ $S_{unc} := 15738 \ \textbf{in}^3$

Cracked Section Modulus $\qquad$ $S_{cr} := 4196 \ \textbf{in}^3$

Section Behavior $\qquad$ $Behavior := \text{"Uncracked"}$

Section Modulus Effective for Behavior $\qquad$ $S_e := \textbf{if} \left(Behavior = \text{"Uncracked"}, S_{unc}, S_{cr} \right)$

Calculated Strain $\qquad$ $\varepsilon_c := \dfrac{M_{Max} \cdot g_{mx}}{S_e \cdot E_c} = 8.831 \cdot 10^{-5}$

Test Benefit Factor

$$k_a := \frac{\varepsilon_c}{\varepsilon_T} - 1 = 0.142$$

Ratio of Applied to HL-93 Moment

$$r_M := \frac{M_{Max}}{M_{LL}} = 0.924$$

Test Understanding Factor

$$k_b := \mathbf{if}\left(r_M > 0.7, 0.5, 0\right) = 0.5$$

Rating Improvement Factor

$$k := 1 + k_a \cdot k_b = 1.071$$

Improved Rating Factor

$$RF_{ImprovedExt} := RF_{Exterior} \cdot k = 2.757$$

<mark>Improved Rating Factors</mark>

Interior

$$RF_{Improved} = 1.348$$

Exterior

$$RF_{ImprovedExt} = 2.757$$

Figure 104: Bridge 2879 Calculations

A.6 Columbia No. 3848

A.6.1 Experimental Configuration and Experimental Data Collected

Table 27: Bridge 3848 Experimental Configuration and Experimental Data Collected

File Contents	File Name	File Type
Sensors	Br3307 _Sensors.csv	CSV Format
Sensor Layout	Br3307_SensorLayout.mat	MATLAB Data File
Sensor Data	Br3848_ALT_S_2_1_Strain.mat	MATLAB Data File
	Br3848_ALT_U_2_1_Strain.mat	MATLAB Data File
	Br3848_MAX_S_1_1_Strain.mat	MATLAB Data File
	Br3848_MAX_S_2_1_Strain.mat	MATLAB Data File
	Br3848_MAX_S_3_1_Strain.mat	MATLAB Data File
	Br3848_MAX_U_2_1_Strain.mat	MATLAB Data File
	Br3848_SBS_S_2_1_Strain.mat	MATLAB Data File
	Br3848_SBS_U_2_1_Strain.mat	MATLAB Data File

A.6.2 Instrumentation
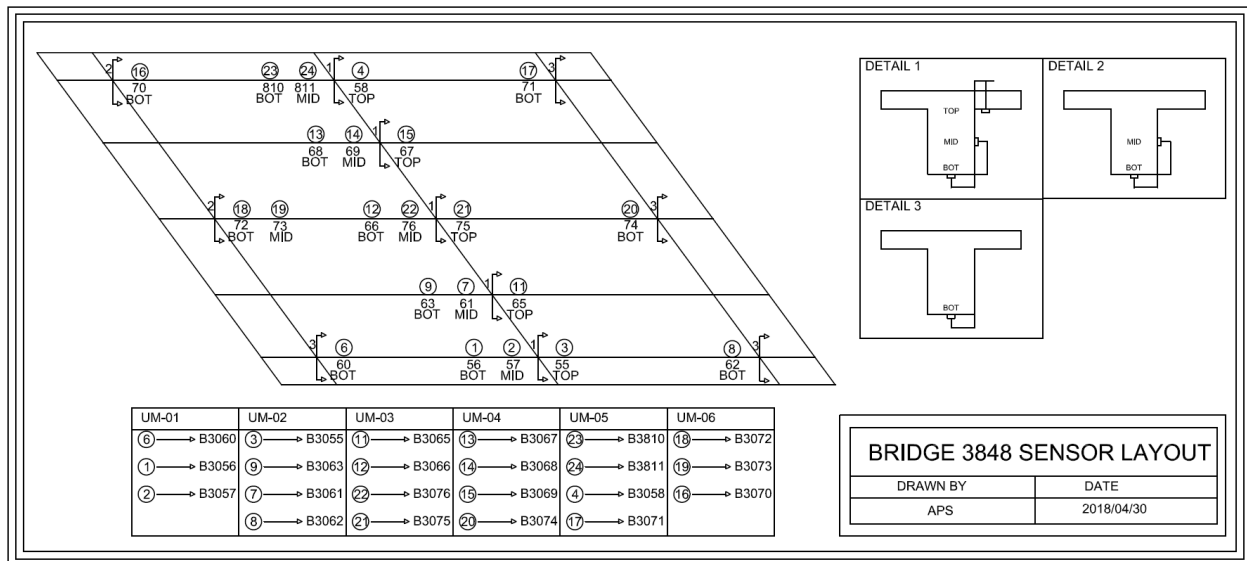
Figure 105: Bridge 3848 Sensor Layout

A.6.3 Loading
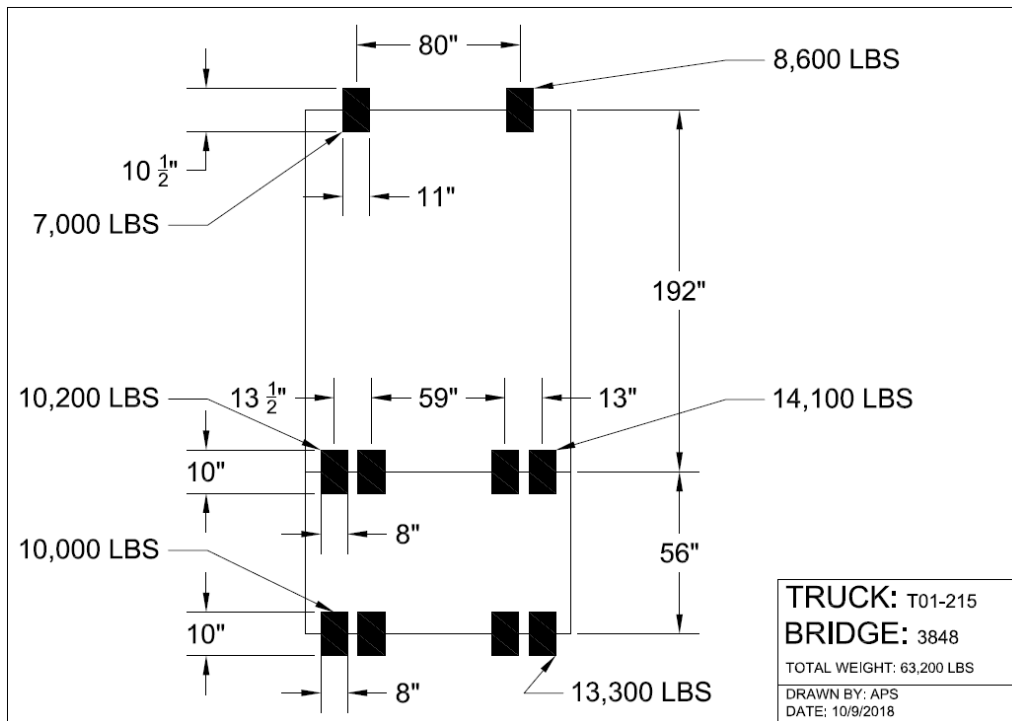
Figure 106: Bridge 3848 Truck T01-215 Loading
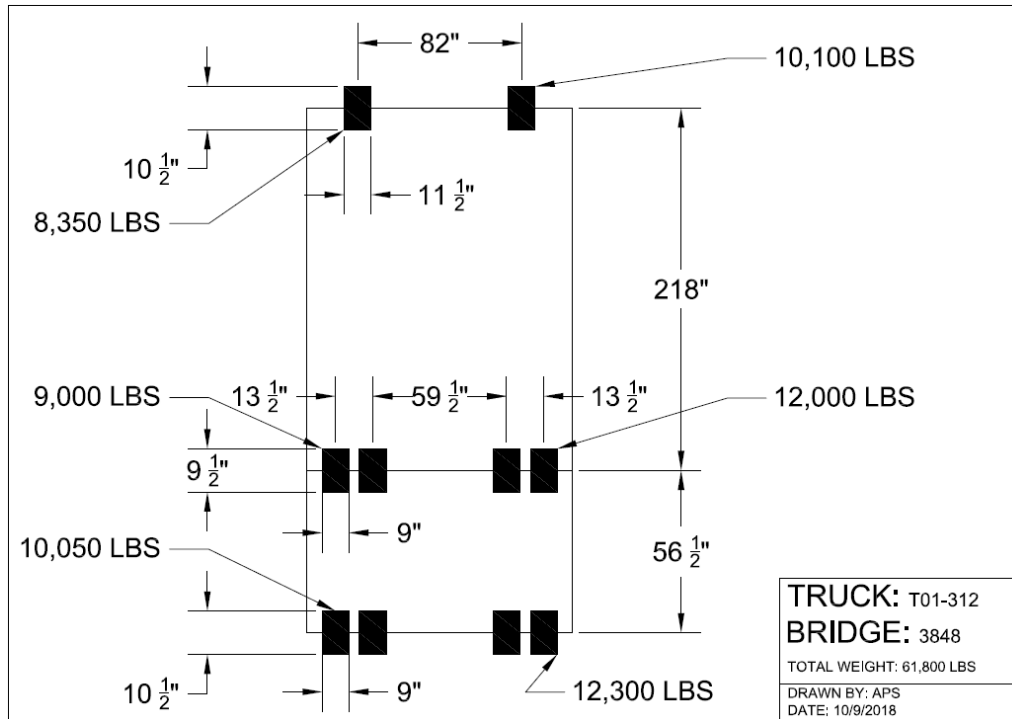
Figure 107: Bridge 3848 Truck T01-312 Loading
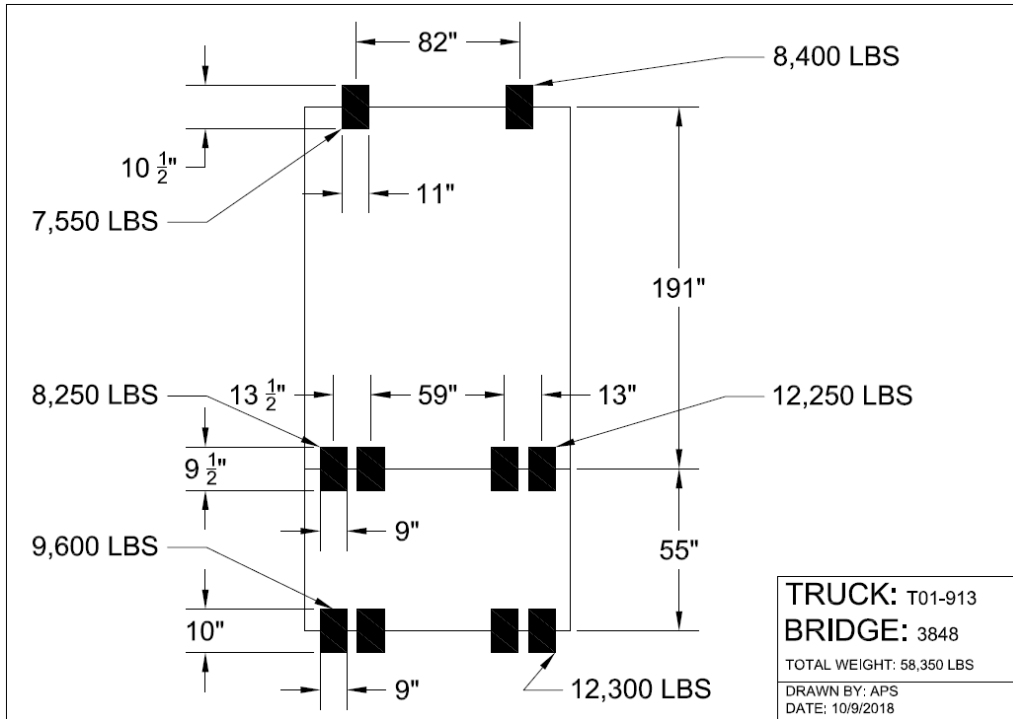
Figure 108: Bridge 3848 Truck T01-913 Loading
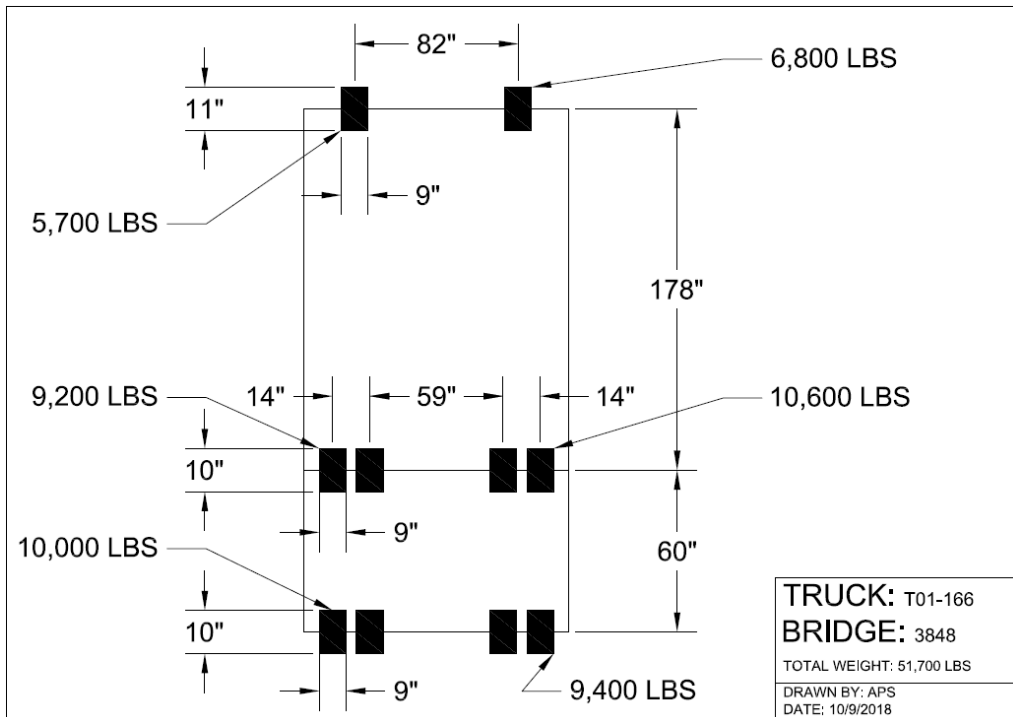
Figure 109: Bridge 3848 Truck T01-166 Loading
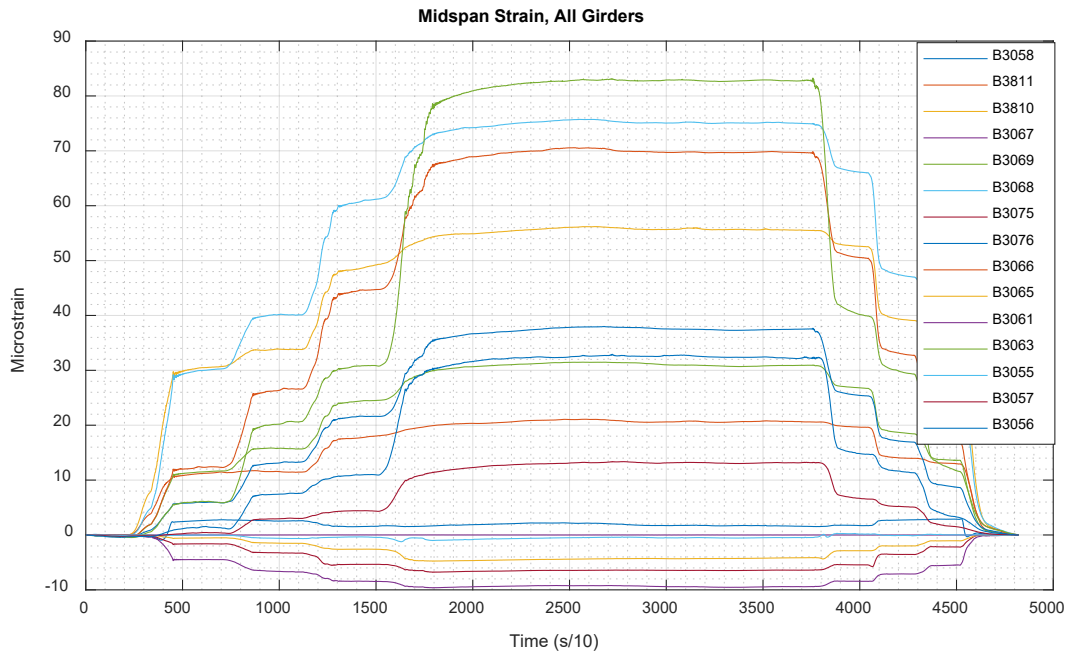
A.6.4 Representative Data Plots
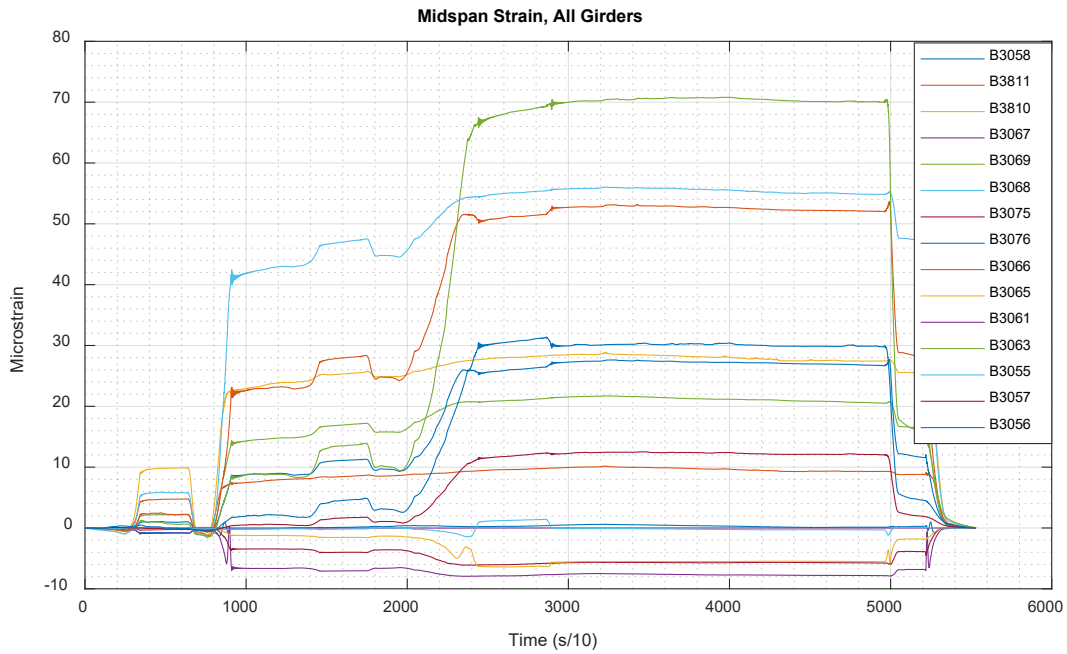
Figure 110: Bridge 3848 SBS_S_2_1 Strains - Midspan
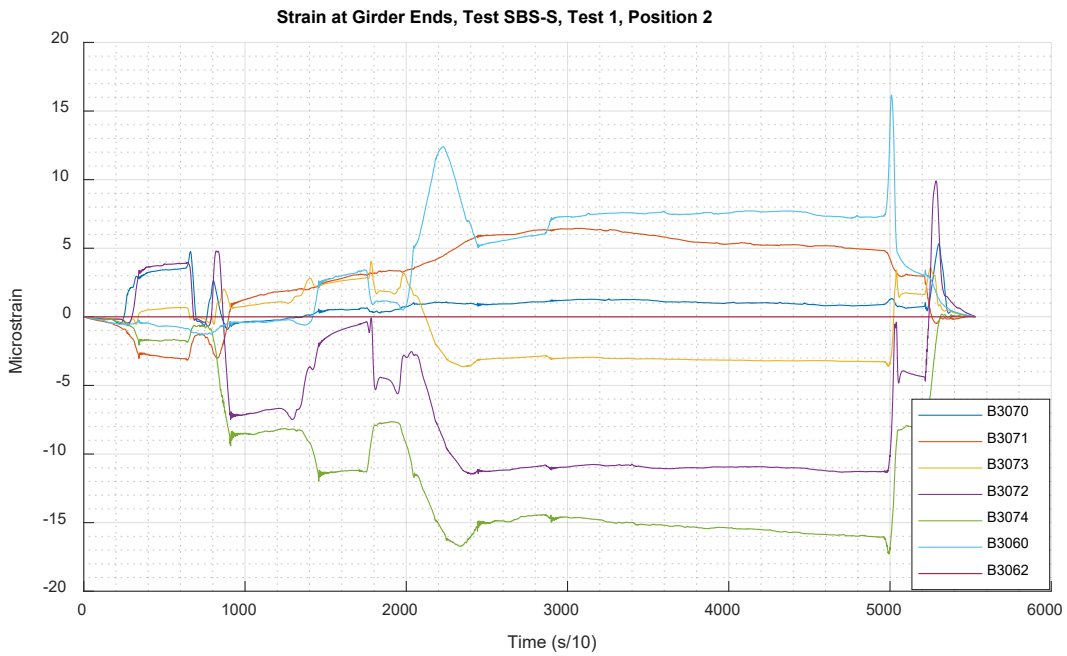
Figure 111: Bridge 3848 SBS_S_2_1 Strains – Ends
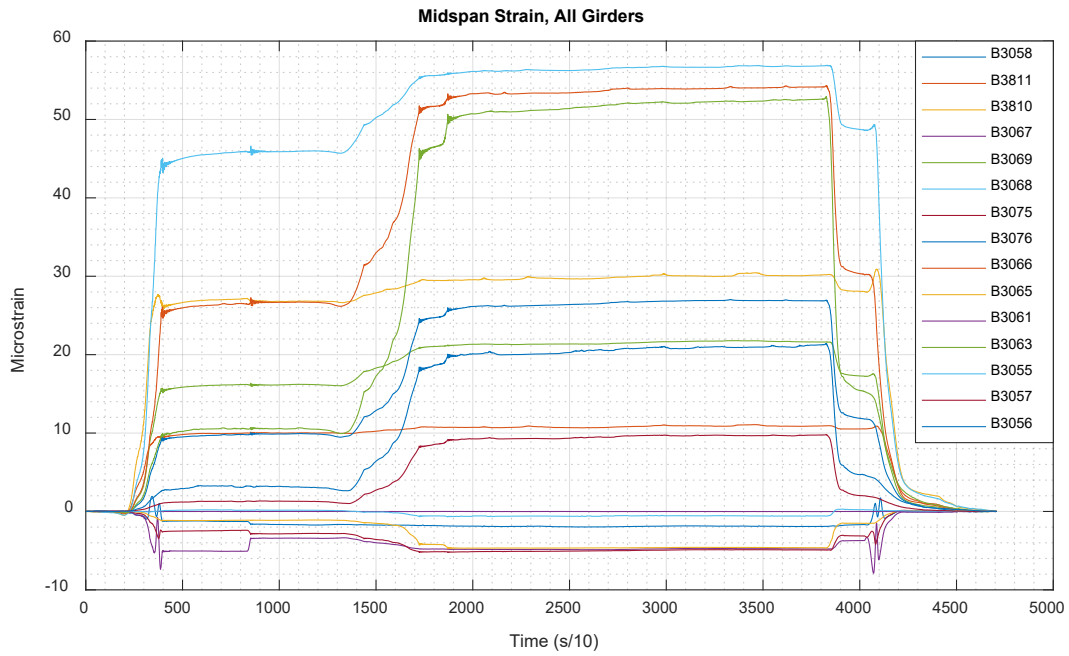
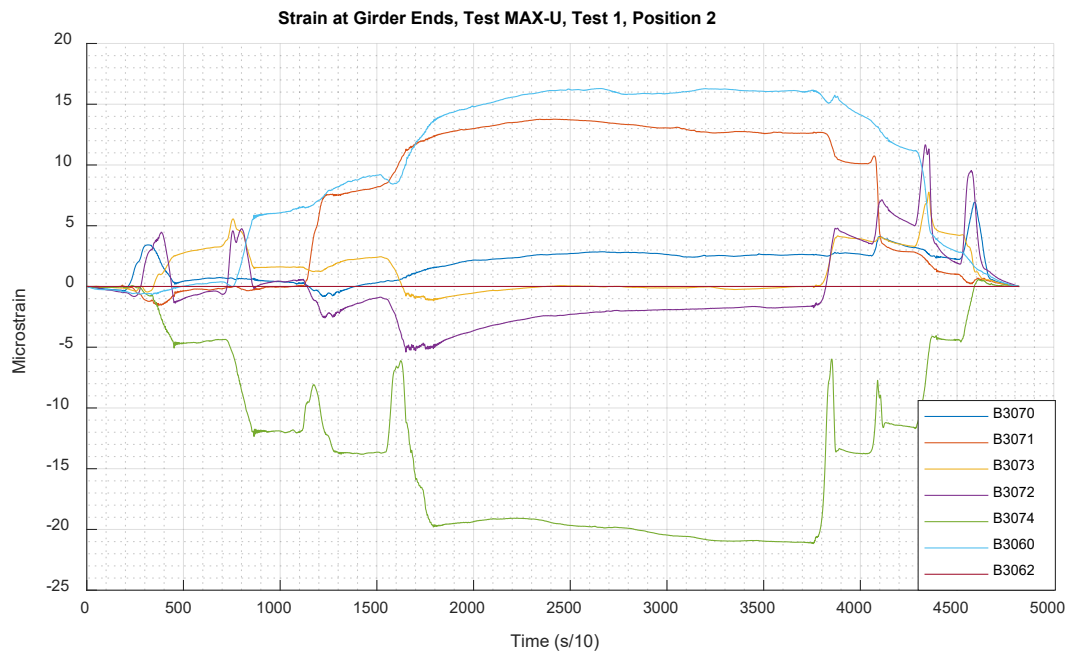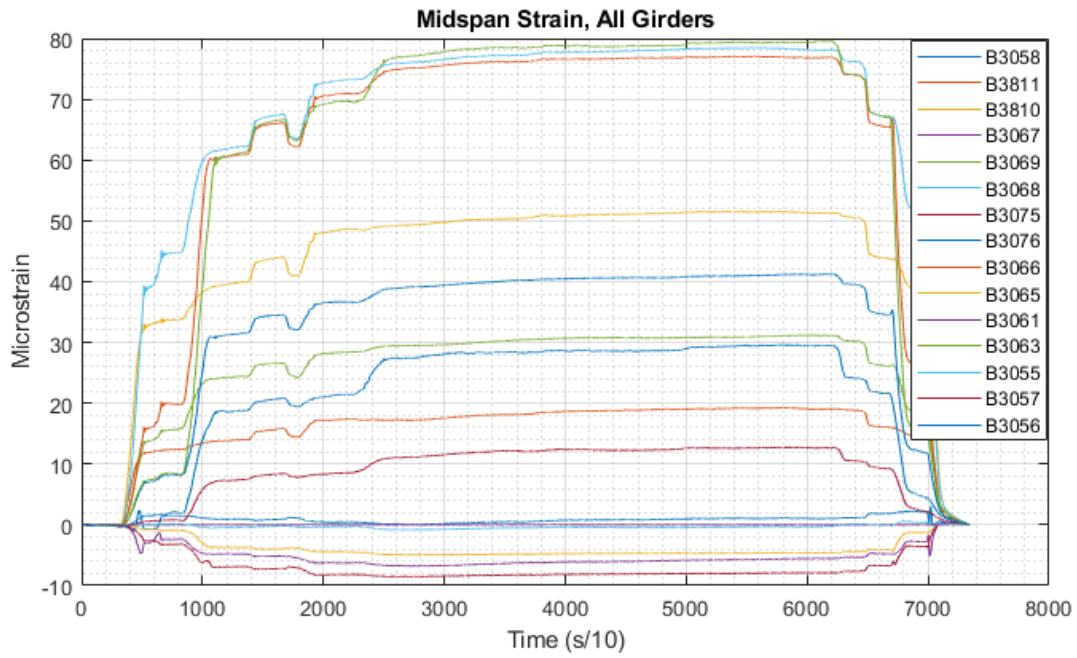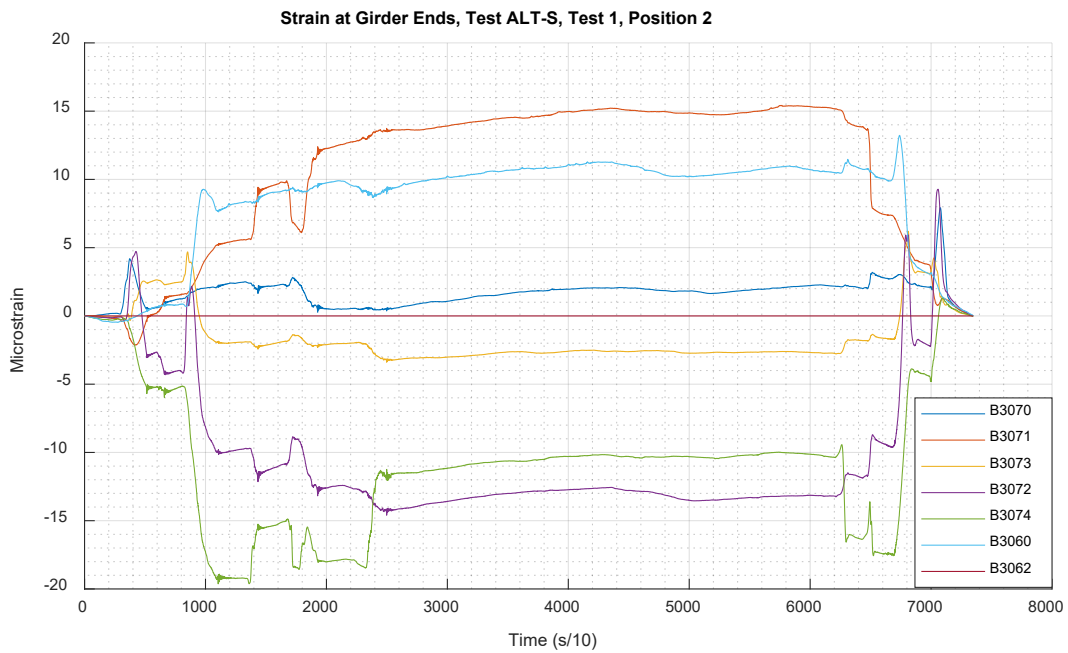Figure 112: Bridge 3848 SBS_U_2_1 Strains - Midspan
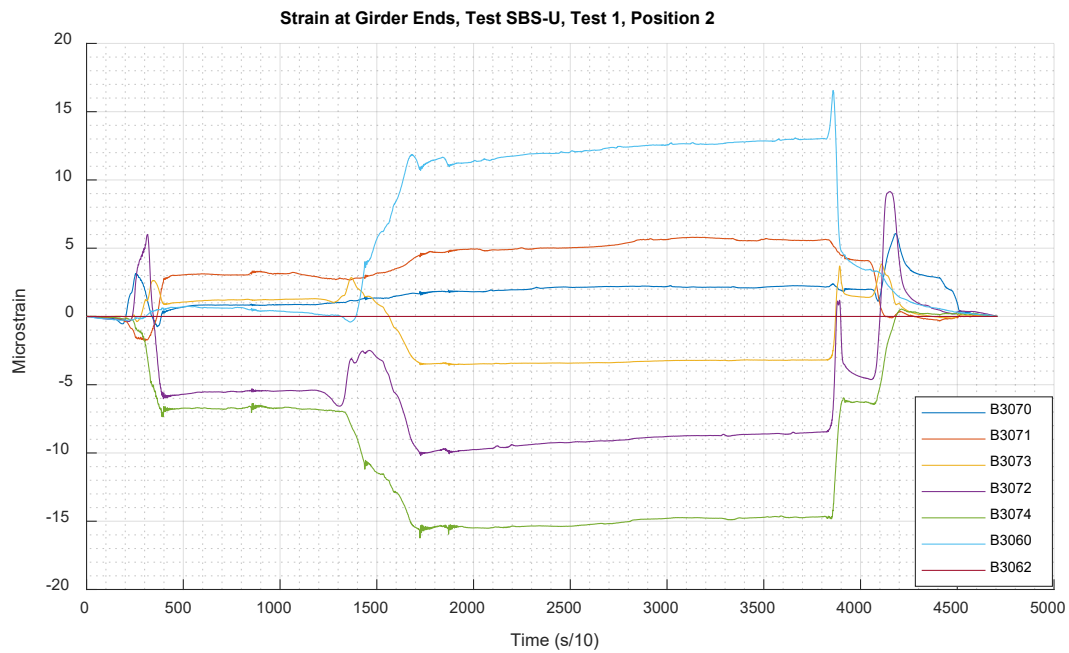
Figure 113: Bridge 3848 SBS_U_2_1 Strains - Ends
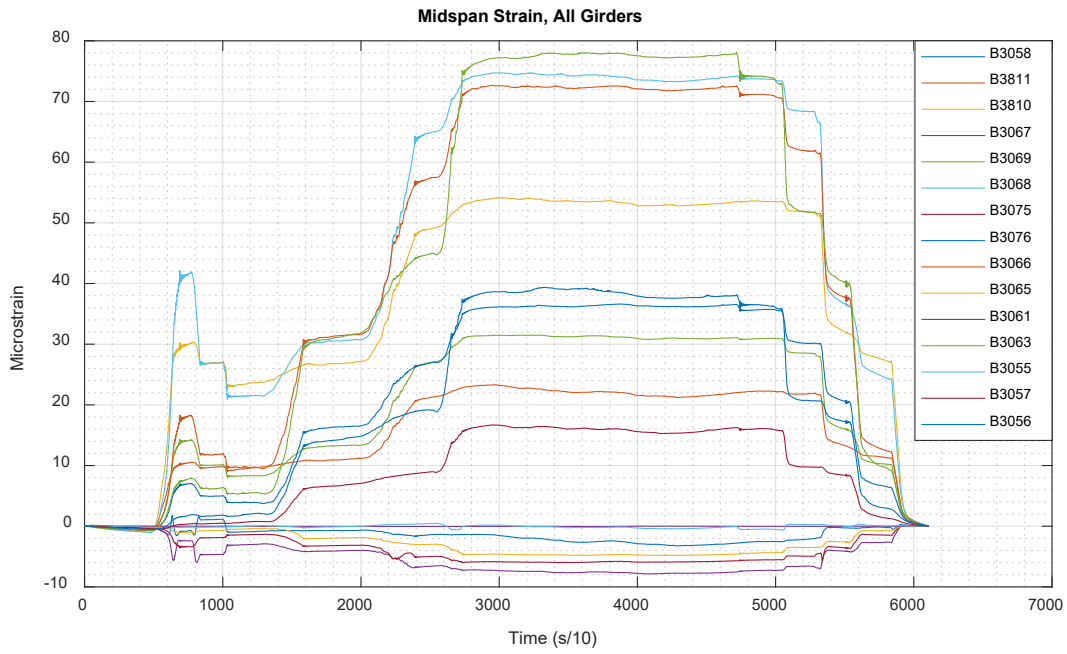
Figure 114: Bridge 3848 MAX_S_2_1 Strains - Midspan
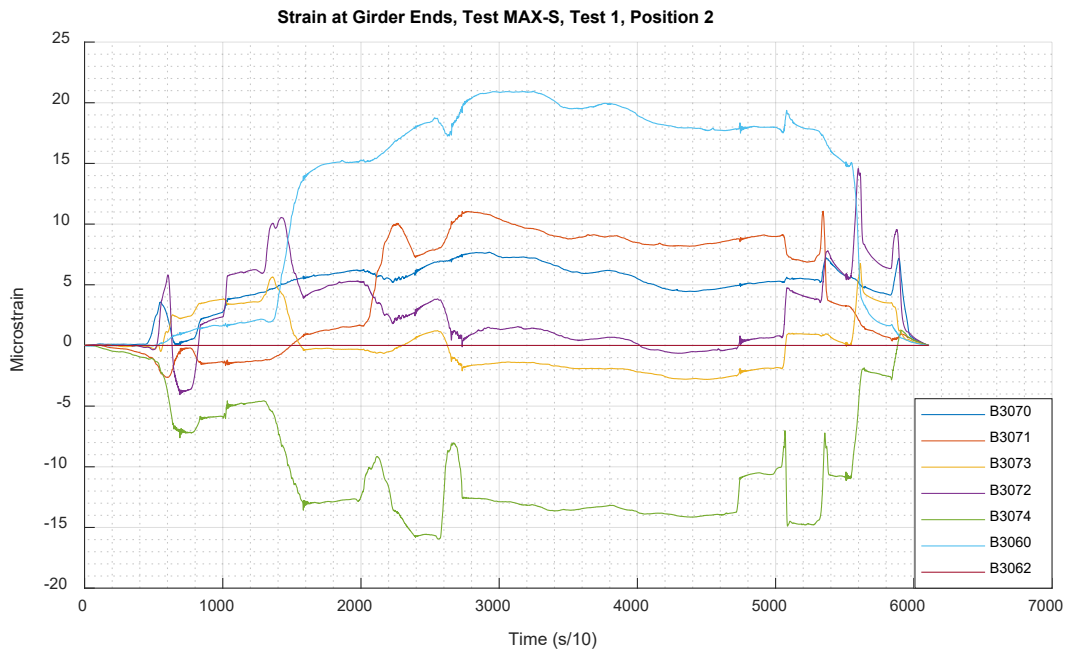
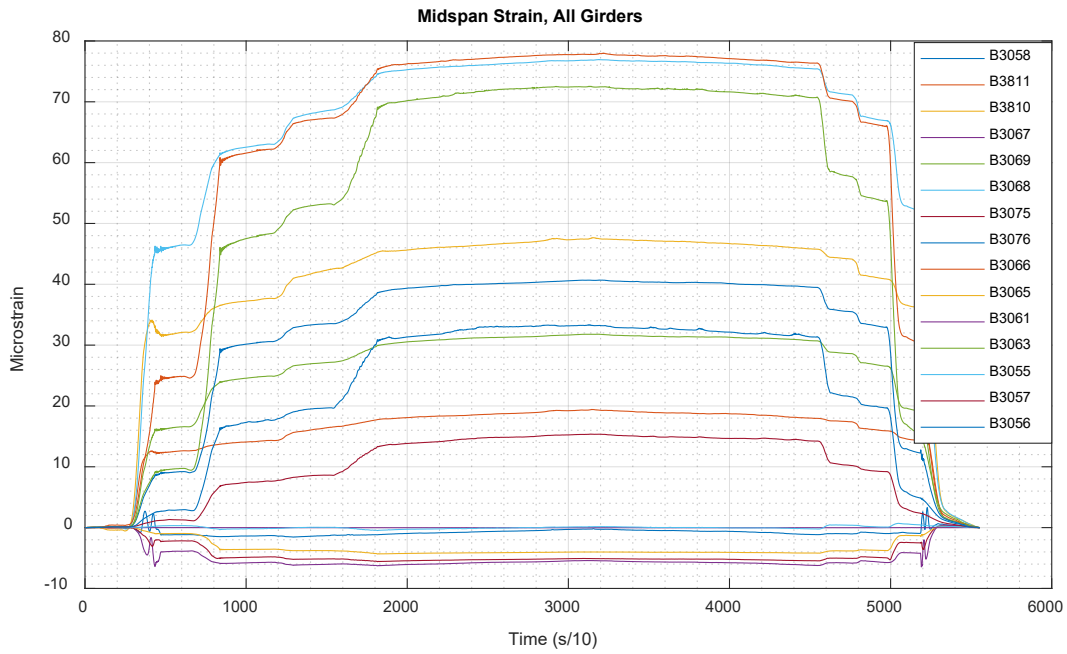Figure 115: Bridge 3848 MAX_S_2_1 Strains - Ends
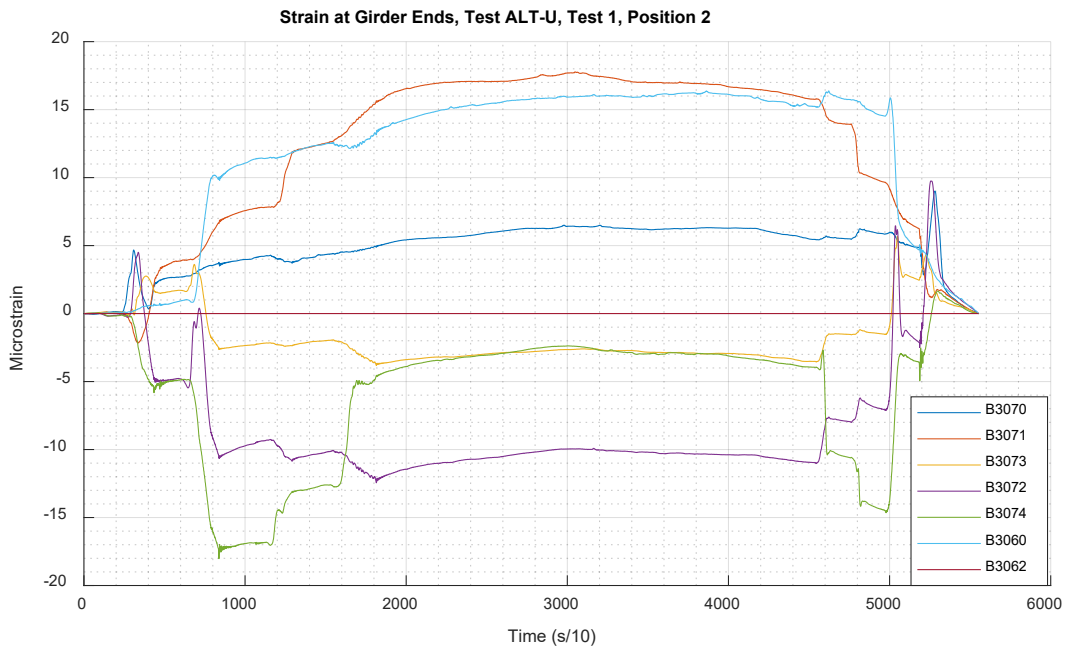
Figure 116: Bridge 3848 MAX_U_2_1 Strains - Midspan

Figure 117: Bridge 3848 MAX_U_2_1 Strains – Ends

Figure 118: Bridge 3848 ALT_S_2_1 Strains - Midspan

Figure 119: Bridge 3848 ALT_S_2_1 Strains - Ends

Figure 120: Bridge 3848 ALT_U_2_1 Strains - Midspan

Figure 121: Bridge 3848 ALT_U_2_1 Strains - Ends

A.6.5 Rating Factor Calculations

AASHTO Rating Calculations:

Bridge 3848 - Columbia, Maine

Material Parameters:

Concrete Compressive Strength	$f'_c := 2.5 \ \text{ksi}$
Reinforcement Yield Strength	$F_y := 33 \ \text{ksi}$
Unit Weight: Reinforced Concrete	$\gamma_{RC} := 0.150 \ \dfrac{\text{kip}}{\text{ft}^3}$
Unit Weight: Wearing Surface	$\gamma_{ws} := 0.150 \ \dfrac{\text{kip}}{\text{ft}^3}$

Geometric Properties:

Span Length	$L := 34 \ \text{ft}$
Girder Spacing - Interior	$S := 70.38 \ \text{in}$
Girder Spacing - Exterior	$S_x := 45.19 \ \text{in}$
Number of Girders	$NG := 5$
Skew Angle	$skew := 30 \ ^\circ$
Lane Width	$lanewidth := 11 \ \text{ft}$
Number of Lanes	$Nlane := 2$
Wearing Surface Thickness	$ws := 3 \ \text{in}$
Thickness of Pavement Overlay	$ws_2 := 1 \ \text{in}$
Girder Height - Interior	$h := 29.75 \ \text{in}$
Girder Height - Exterior	$h_x := 29.75 \ \text{in}$
Deck Thickness	$d_s := 5.75 \ \text{in}$
Web Width - Interior	$b_w := 19.5 \ \text{in}$
Web Width - Exterior	$b_{ux} := 16 \ \text{in}$
Curb Depth	$h_{curb} := 12 \ \text{in}$
Curb Width	$b_{curb} := 18 \ \text{in}$

Height to Centroid of Reinforcement - Interior

$$y_{bar} := \begin{bmatrix} 3.188 \\ 4.115 \\ 4.977 \\ 4.115 \\ 3.188 \end{bmatrix} \ \text{in}$$

Height to Centroid of Reinforcement - Exterior

$$y_{barx} := \begin{bmatrix} 3.188 \\ 4.888 \\ 5.313 \\ 4.888 \\ 3.188 \end{bmatrix} \ \text{in}$$

Area of Reinforcement - Interior

$$A_s := \begin{bmatrix} 5.0265 \\ 7.594 \\ 10.125 \\ 7.594 \\ 5.0625 \end{bmatrix} \ \text{in}^2$$

Area of Reinforcement - Exterior	$A_{sx} := \begin{bmatrix} 3.80 \\ 6.33 \\ 7.59 \\ 6.33 \\ 3.80 \end{bmatrix} \textbf{\textit{in}}^2$

Distance from Centerline of Girder to Edge of Curb $\qquad\qquad d_e := -7\ \textbf{\textit{in}}$

Eccentricity of Centerline of Girders w.r.t. Centerline of Roadway $\qquad exc := 0\ \textbf{\textit{in}}$

<mark>Load and Analysis Parameters</mark>

Concentrated Load Due to Diaphragms on One Girder $\qquad\qquad P_{dint} := 0\ \textbf{\textit{kip}}$

Location of Intermediate Diaphragm
(Half, Third, Quarter) $\qquad\qquad loc_d := \text{“Half”}$

Distributed Load Due to Rail $\qquad\qquad w_{rail} := 0.0121\ \dfrac{\textbf{\textit{kip}}}{\textbf{\textit{ft}}}$

Structural Dead Load Factor $\qquad\qquad \gamma_{DC} := 1.25$

Wearing Surface Dead Load Factor $\qquad\qquad \gamma_{DW} := 1.25$

Live Load Factor $\qquad\qquad \gamma_{LL} := 1.35$

Live Load Impact Factor $\qquad\qquad IM := 0.33$

Flexural Resistance Factor $\qquad\qquad \phi := .9$

System Factor $\qquad\qquad \phi_s := 1.0$

Condition Factor $\qquad\qquad \phi_c := 1.0$

<mark>Initial Calculations</mark>

Web Height - Interior $\qquad\qquad d_g := h - d_s$

Web Height - Exterior $\qquad\qquad d_{gx} := h_x - d_s$

Include Wearing Surface in Section Height $\qquad h := h + \textbf{if}\left(\gamma_{ws} = 0.15\ \dfrac{\textbf{\textit{kip}}}{\textbf{\textit{ft}}^3}, ws, 0\right) = 32.75\ \textbf{\textit{in}}$

Depth to Centroid of Reinforcement - Interior $\qquad d := h - y_{bar}$

Depth to Centroid of Reinforcement - Exterior $\qquad d_x := h_x - y_{barx} + h_{curb}$

Moment Applied to Interor Girders from Diaphragm $\qquad M_d := \text{if } loc_d = \text{“Half”} \qquad = 0\ \textbf{\textit{ft}}\cdot\textbf{\textit{kip}}$

$$\left\| P_{dint} \cdot \dfrac{L}{4} \right.$$

$$\text{else if } loc_d = \text{“Third”}$$

$$\left\| P_{dint} \cdot \dfrac{L}{3} \right.$$

$$\text{else if } loc_d = \text{“Quarter”}$$

$$\left\| P_{dint} \cdot \dfrac{L}{4} + P_{dint} \cdot \dfrac{L}{4} \right.$$

Moment Applied to Exterior Girders from Diaphragm $\qquad M_{dx} := \dfrac{M_d}{2} = 0\ \textbf{\textit{ft}}\cdot\textbf{\textit{kip}}$

Dictance Between Centroids of Deck and Web

$$e_g := \frac{d_g + d_s}{2} = 14.875 \ \mathbf{in}$$

Area of Web

$$A := d_g \cdot b_w = 468 \ \mathbf{in}^2$$

Moment of Inertia of Web

$$I := \frac{b_w \cdot d_g^{\ 3}}{12} = \left(2.246 \cdot 10^4\right) \ \mathbf{in}^4$$

Modular Ratio - Deck and Web

$$n := 1$$

Longitudinal Stiffness Parameter

$$K_g := n \cdot \left(I + A \cdot e_g^{\ 2}\right) = \left(1.26 \cdot 10^5\right) \ \mathbf{in}^4$$

Interior Moment Distribution Factor - 1 Lane

$$g_{m1} := 0.06 + \left(\frac{S}{14 \ \mathbf{ft}}\right)^{0.4} \cdot \left(\frac{S}{L}\right)^{0.3} \cdot \left(\frac{K_g}{L \cdot d_s^{\ 3}}\right)^{0.1} = 0.497$$

Interior Moment Distribution Factor - 2 Lane

$$g_{m2} := 0.075 + \left(\frac{S}{9.5 \ \mathbf{ft}}\right)^{0.6} \cdot \left(\frac{S}{L}\right)^{0.2} \cdot \left(\frac{K_g}{L \cdot d_s^{\ 3}}\right)^{0.1} = 0.628$$

Controling Interior Moment Distribution Factor

$$g_m := \max \left(g_{m1}, g_{m2}\right)$$

Roadway Width

$$W_r := lanewidth \cdot Nlane$$

Eccentricity of Design Lane From C.G. of Girders

$$e_1 := \frac{W_r}{2} - 5 \ \mathbf{ft} + exc = 6 \ \mathbf{ft}$$

Eccentricity of Exterior Girder From C.G. of Girders

$$X_{ext} := (NG - 1) \cdot \frac{S}{2} = 11.73 \ \mathbf{ft}$$

Eccentricity of Each Girder

$$x_1 := X_{ext}$$
$$x_2 := X_{ext} - S$$
$$x_3 := X_{ext} - 2 \cdot S$$
$$x_4 := \mathbf{if} \ (NG > 3, X_{ext} - 3 \cdot S, 0 \ \mathbf{ft})$$
$$x_5 := \mathbf{if} \ (NG > 4, X_{ext} - 4 \cdot S, 0 \ \mathbf{ft})$$

Lever Rule Distribution Factor - One Lane

$$R_1 := \frac{1}{NG} + \frac{X_{ext} \cdot e_1}{x_1^{\ 2} + x_2^{\ 2} + x_3^{\ 2} + x_4^{\ 2} + x_5^{\ 2}} = 0.405$$

$$g_{mR1} := \mathbf{if} \ (P_{dint} > 0, 1.2 \cdot R_1, 0) = 0$$

Lever Rule Distribution Factor - Two Lanes

$$R_2 := \frac{2}{NG} + \frac{X_{ext} \cdot (e_1 - 5 \ \mathbf{ft})}{x_1^{\ 2} + x_2^{\ 2} + x_3^{\ 2} + x_4^{\ 2} + x_5^{\ 2}} = 0.434$$

$$g_{mR2} := \mathbf{if} \ (P_{dint} > 0, R_2, 0) = 0$$

Exterior Moment Distribution Factor

$$g_{mx1} := \frac{1.2 \ (S + d_e - 2 \ \mathbf{ft})}{2 \cdot S} = 0.336$$

$$ee := 0.77 + \frac{d_e}{9.1 \ \mathbf{ft}} = 0.706$$

$$g_{mx2} := g_{m2} \cdot ee = 0.443$$

Skew Correction Factor

$$g_{mx} := \max\left(g_{mx1}, g_{mx2}\right) = 0.443$$

$$c_1 := 0.25 \cdot \left(\frac{K_g}{12 \cdot L \cdot d_s^3}\right)^{0.25} \cdot \left(\frac{S}{L}\right)^{.5} = 0.063$$

$$\theta := \mathbf{if}\left(skew \geq 30^\bullet, skew, 0^\bullet\right)$$

$$C_\theta := 1 - c_1 \cdot \left(\tan(\theta)\right)^{1.5} = 0.972$$

$$g_m := g_m \cdot C_\theta = 0.611$$

$$g_{mx} := g_{mx} \cdot C_\theta = 0.431$$

Interior DF   Exterior DF

$g_m = 0.611$ $g_{mx} = 0.431$

<mark>Loading</mark>

Interior Girder Dead Load

$$w_{girder} := \gamma_{RC} \cdot b_w \cdot d_g = 0.488 \; \frac{kip}{ft}$$

Deck Dead Load

$$w_{deck} := \gamma_{RC} \cdot S \cdot d_s = 0.422 \; \frac{kip}{ft}$$

Curb Dead Load

$$w_{curb} := 2 \cdot \gamma_{RC} \cdot h_{curb} \cdot b_{curb} = 0.45 \; \frac{kip}{ft}$$

Dead Load from Nonstructural Components

$$w_{ns} := \frac{w_{curb}}{NG} + w_{rail} = 0.102 \; \frac{kip}{ft}$$

Total Structural Dead Load on Interior Girders

$$DC := w_{girder} + w_{deck} + w_{ns} = 1.011 \; \frac{kip}{ft}$$

Exterior Girder Dead Load

$$w_{girderx} := \gamma_{RC} \cdot b_{wx} \cdot d_{gx} = 0.4 \; \frac{kip}{ft}$$

Exterior Deck Dead Load

$$w_{deckx} := \gamma_{RC} \cdot S_x \cdot d_s = 0.271 \; \frac{kip}{ft}$$

Total Structural Dead Load on Exterior Girders

$$DC_x := w_{girderx} + w_{deckx} + w_{ns} = 0.773 \; \frac{kip}{ft}$$

Wearing Surface Dead Load on Interior Girders

$$DW := \gamma_{ws} \cdot \left(ws + ws_2\right) \cdot S = 0.293 \; \frac{kip}{ft}$$

Wearing Surface Dead Load on Exterior Girders

$$DW_x := \gamma_{ws} \cdot \left(ws + ws_2\right) \cdot S_x = 0.188 \; \frac{kip}{ft}$$

Dead Load Moments

$$M_{DC} := \frac{DC \cdot L^2}{8} + M_d \qquad M_{DCx} := \frac{DC_x \cdot L^2}{8} + M_{dx}$$

$$M_{DW} := \frac{DW \cdot L^2}{8} \qquad M_{DWx} := \frac{DW_x \cdot L^2}{8}$$

$M_{DC} = 146.111 \ \boldsymbol{ft \cdot kip}$ $\qquad$ $M_{DCx} = 111.665 \ \boldsymbol{ft \cdot kip}$

$M_{DW} = 42.375 \ \boldsymbol{ft \cdot kip}$ $\qquad$ $M_{DWx} = 27.208 \ \boldsymbol{ft \cdot kip}$

Live Load Moment - Truck Load $\qquad$ $M_{Truck} := 32 \ \boldsymbol{kip} \cdot \left(\dfrac{L}{4}\right) + \dfrac{40 \ \boldsymbol{kip}}{2} \cdot \left(\dfrac{L}{2} - 14 \ \boldsymbol{ft}\right) = 332 \ \boldsymbol{ft \cdot kip}$

Live Load Moment - Tandem $\qquad$ $M_{Tandem} := 25 \ \boldsymbol{kip} \cdot \dfrac{L}{4} + \dfrac{25 \ \boldsymbol{kip}}{2} \cdot \left(\dfrac{L}{2} - 4 \ \boldsymbol{ft}\right) = 375 \ \boldsymbol{ft \cdot kip}$

Live Load Moment - Lane $\qquad$ $M_{Lane} := 0.64 \ \dfrac{\boldsymbol{kip}}{\boldsymbol{ft}} \cdot \dfrac{L^2}{8} = 92.48 \ \boldsymbol{ft \cdot kip}$

Total HL-93 Live Load $\qquad$ $M_{LL} := M_{Lane} + (1 + IM) \cdot \max\left(M_{Truck}, M_{Tandem}\right)$

$M_{LL} = 591.23 \ \boldsymbol{ft \cdot kip}$

Nominal Resistance

Depth Whitney Stress Block - Interior $\qquad$ $a := A_s \cdot \dfrac{F_y}{0.85 \cdot f'_c \cdot S} = \begin{bmatrix} 1.109 \\ 1.676 \\ 2.234 \\ 1.676 \\ 1.117 \end{bmatrix} \boldsymbol{in}$

Nominal Moment Resistance - Interior $\qquad$ $\overrightarrow{M_n := F_y \cdot A_s \cdot \left(d - \dfrac{a}{2}\right)} = \begin{bmatrix} 400.966 \\ 580.503 \\ 742.202 \\ 580.503 \\ 403.783 \end{bmatrix} \boldsymbol{ft \cdot kip}$

Interior Nominal Moment Capacity

$M_{capacity} := \max\langle M_n \rangle = 742.202 \ \boldsymbol{ft \cdot kip}$

Depth Whitney Stress Block - Exterior $\qquad$ $a_x := A_{sx} \cdot \dfrac{F_y}{0.85 \cdot f'_c \cdot S_x} = \begin{bmatrix} 1.306 \\ 2.175 \\ 2.608 \\ 2.175 \\ 1.306 \end{bmatrix} \boldsymbol{in}$

Nominal Moment Resistance - Exterior $\qquad$ $\overrightarrow{M_{nx} := F_y \cdot A_{sx} \cdot \left(d_x - \dfrac{a_x}{2}\right)} = \begin{bmatrix} 396.15 \\ 622.742 \\ 733.311 \\ 622.742 \\ 396.15 \end{bmatrix} (\boldsymbol{ft \cdot kip})$

Exterior Nominal Moment Capacity

$M_{capacityx} := \max\langle M_{nx} \rangle = 733.311 \ \boldsymbol{ft \cdot kip}$

Rating Factors

Interior Moment Rating Factor

$$RF_{Interior} := \frac{\phi \cdot \phi_s \cdot \phi_c \cdot M_{capacity} - \gamma_{DC} \cdot M_{DC} - \gamma_{DW} \cdot M_{DW}}{\gamma_{LL} \cdot M_{LL} \cdot g_m}$$

Exterior Moment Rating Factor

$$RF_{Exterior} := \frac{\phi \cdot \phi_s \cdot \phi_c \cdot M_{capacityx} - \gamma_{DC} \cdot M_{DCx} - \gamma_{DW} \cdot M_{DWx}}{\gamma_{LL} \cdot M_{LL} \cdot g_{mx}}$$

Interior   Exterior

$RF_{Interior} = 0.887$ $RF_{Exterior} = 1.414$

Concrete Compressive Strength - Larger is More Conservative

$$f'_c := 5 \; \mathbf{ksi}$$

Concrte Elastic Modulus

$$E_c := 1820 \; \mathbf{ksi} \cdot \sqrt{\frac{f'_c}{\mathbf{ksi}}} = \left(4.07 \cdot 10^3\right) \; \mathbf{ksi}$$

==Interior Girders==

Maximum Recorded Strain

$$\varepsilon_T := 89.35 \cdot 10^{-6}$$

Maximum Applied Moment per Lane

$$M_{Max} := 478.1 \; \mathbf{ft \cdot kip}$$

Uncracked Section Modulus

$$S_{unc} := 6065 \; \mathbf{in}^3$$

Cracked Section Modulus

$$S_{cr} := 1991 \; \mathbf{in}^3$$

Section Behavior

$$Behavior := \text{"Uncracked"}$$

Section Modulus Effective for Behavior

$$S_e := \mathbf{if} \left(Behavior = \text{"Uncracked"}, S_{unc}, S_{cr}\right)$$

Calculated Strain

$$\varepsilon_c := \frac{M_{Max} \cdot g_m}{S_e \cdot E_c} = 1.419 \cdot 10^{-4}$$

Test Benefit Factor

$$k_a := \frac{\varepsilon_c}{\varepsilon_T} - 1 = 0.589$$

Ratio of Applied to HL-93 Moment

$$r_M := \frac{M_{Max}}{M_{LL}} = 0.809$$

Test Understanding Factor

$$k_b := \mathbf{if} \left(r_M > 0.7, 0.5, 0\right) = 0.5$$

Rating Improvement Factor

$$k := 1 + k_a \cdot k_b = 1.294$$

Improved Rating Factor

$$RF_{Improved} := RF_{Interior} \cdot k = 1.148$$

==Exterior Girders==

Maximum Recorded Strain

$$\varepsilon_T := 47.36 \cdot 10^{-6}$$

Maximum Applied Moment per Lane

$$M_{Max} := 478.1 \; \mathbf{ft \cdot kip}$$

Uncracked Section Modulus

$$S_{unc} := 6086 \; \mathbf{in}^3$$

Cracked Section Modulus

$$S_{cr} := 1457 \; \mathbf{in}^3$$

Section Behavior

$$Behavior := \text{"Uncracked"}$$

Section Modulus Effective for Behavior

$$S_e := \mathbf{if} \left(Behavior = \text{"Uncracked"}, S_{unc}, S_{cr}\right)$$

Calculated Strain

$$\varepsilon_c := \frac{M_{Max} \cdot g_{mx}}{S_e \cdot E_c} = 9.986 \cdot 10^{-5}$$

Test Benefit Factor

$$k_a := \frac{\varepsilon_c}{\varepsilon_T} - 1 = 1.108$$

Ratio of Applied to HL-93 Moment

$$r_M := \frac{M_{Max}}{M_{LL}} = 0.809$$

Test Understanding Factor

$$k_b := \mathbf{if}\,(r_M > 0.7, 0.5, 0) = 0.5$$

Rating Improvement Factor

$$k := 1 + k_a \cdot k_b = 1.554$$

Improved Rating Factor

$$RF_{ImprovedExt} := RF_{Exterior} \cdot k = 2.197$$

Improved Rating Factors

Interior

$$RF_{Improved} = 1.148$$

Exterior

$$RF_{ImprovedExt} = 2.197$$

Figure 122: Bridge 3848 Calculations

A.7 Supplementary Figures

A.7.1 Live-Load Test Girder Lane Fraction Plots
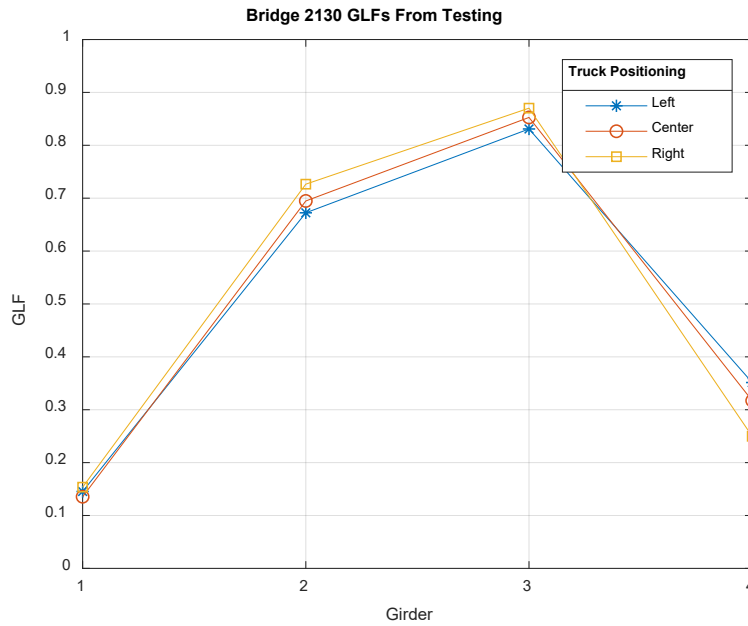
Figure 123: GLFs Calculated from Live-Load Testing – Bridge 2130 (Un-Skewed)
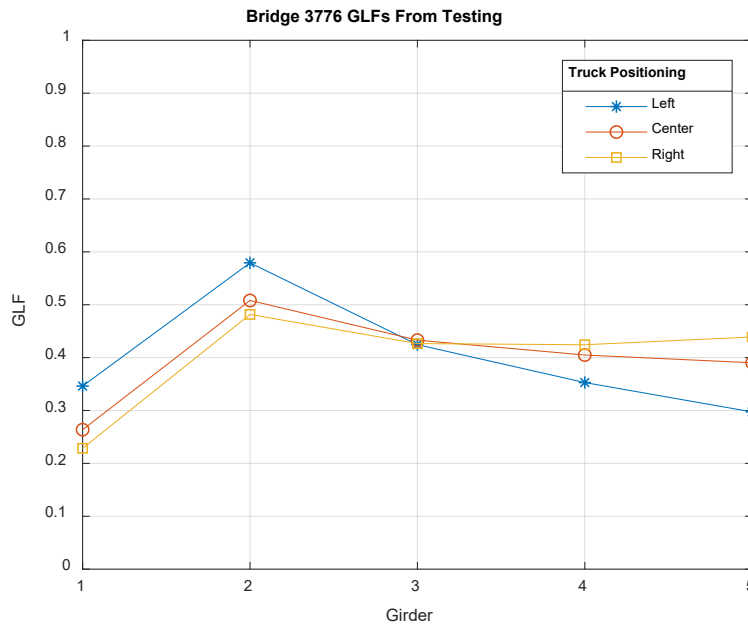
Figure 124: GLFs Calculated from Live-Load Testing – Bridge 3776 (Un-Skewed)
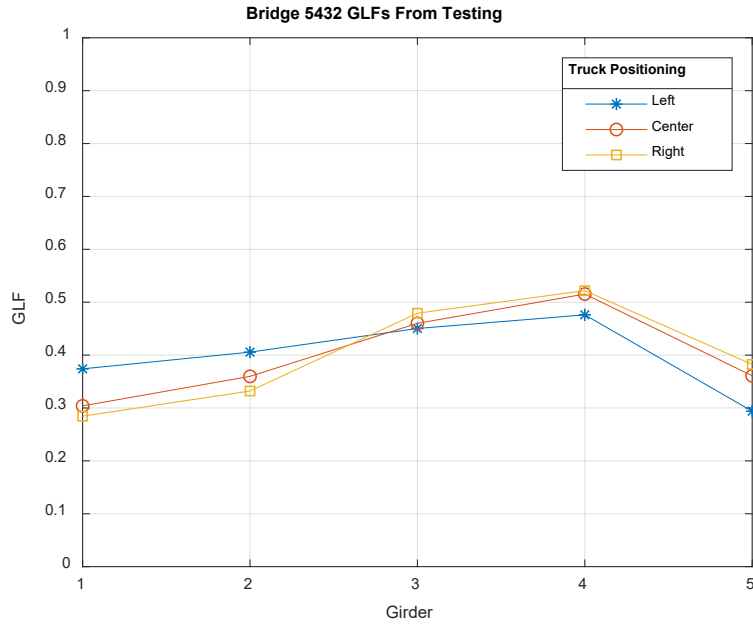
Figure 125: GLFs Calculated from Live-Load Testing – Bridge 5432 (Un-Skewed)
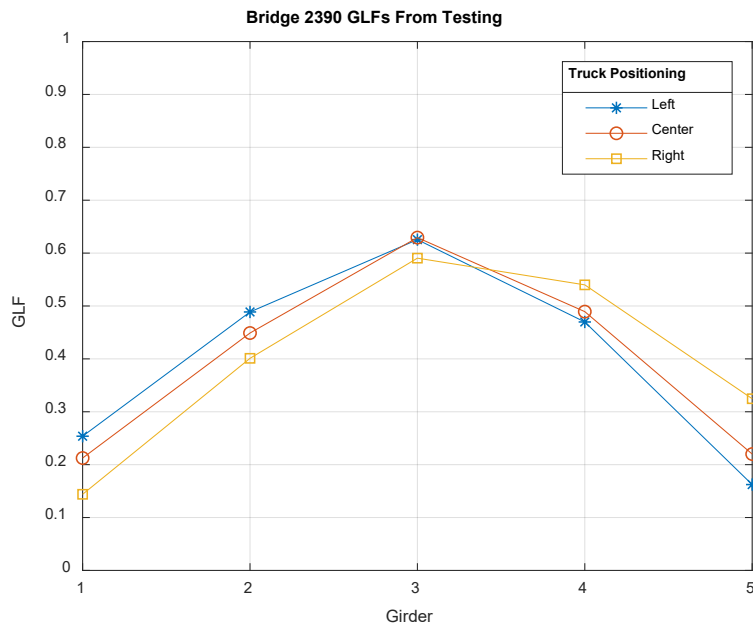
Figure 126: GLFs Calculated from Live-Load Testing – Bridge 2390 (Skewed)
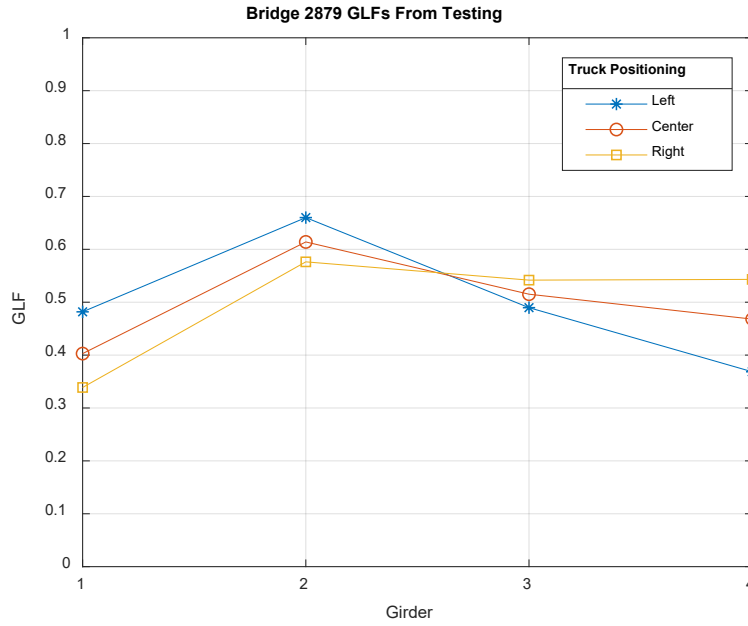
Figure 127: GLFs Calculated from Live-Load Testing – Bridge 2879 (Skewed)
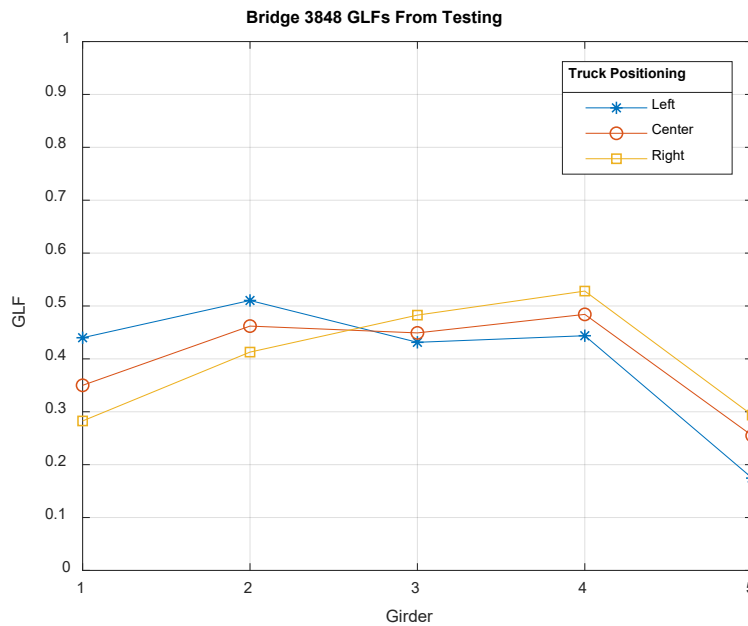
Figure 128: GLFs Calculated from Live-Load Testing – Bridge 3848 (Skewed)
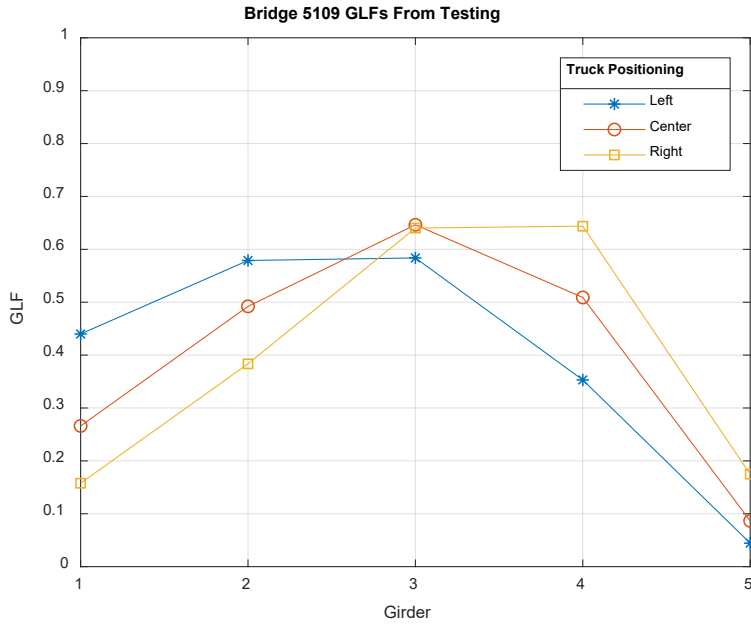
Figure 129: GLFs Calculated from Live-Load Testing – Bridge 5109 (Skewed)

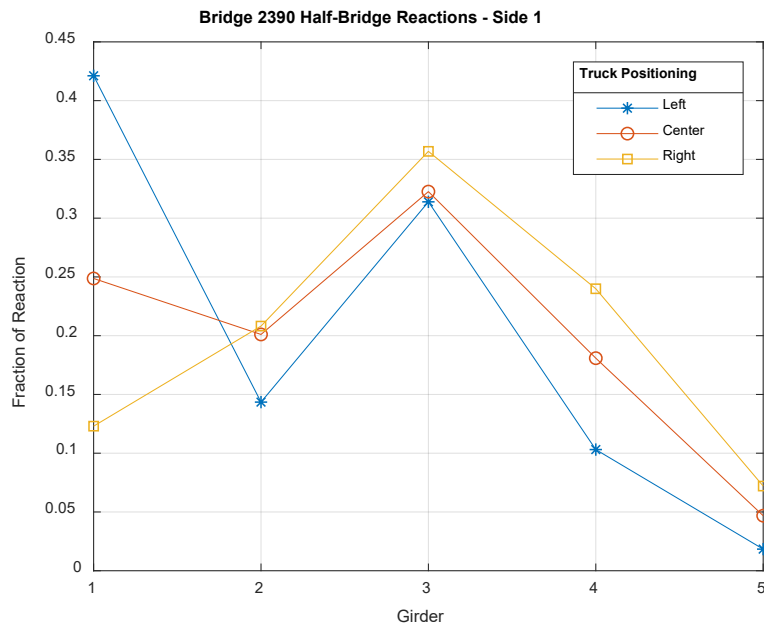## A.7.2 Fractions of Reaction Force from Linear Finite Element Analysis
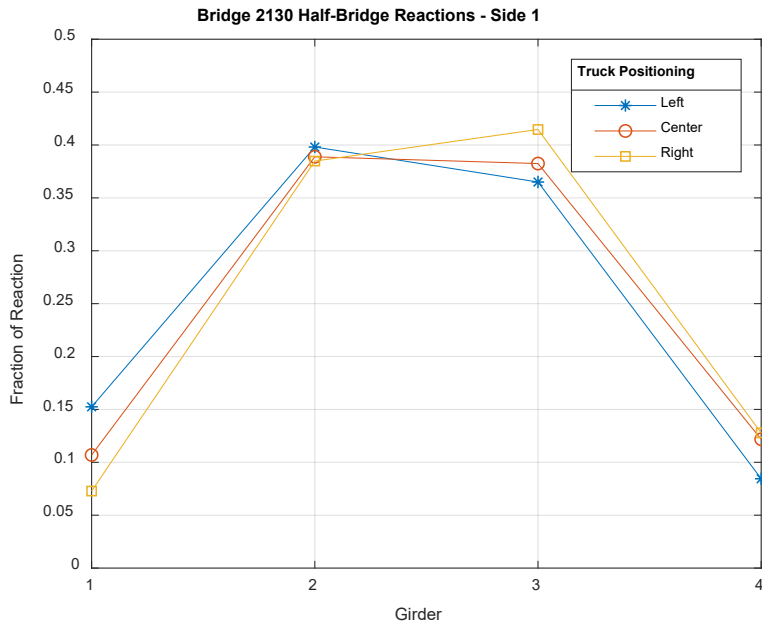
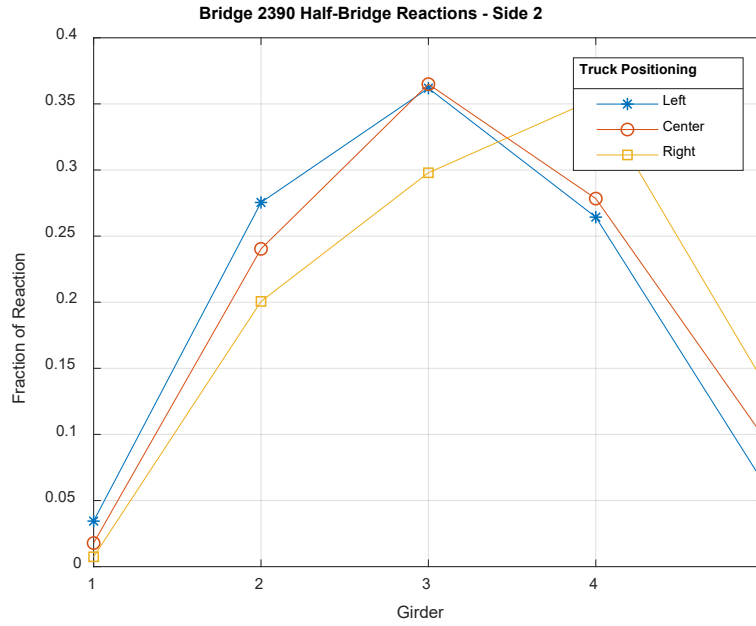Figure 130: Fractions of Reaction Force Attracted to Each Support at Side 1 – Bridge 2130 (Un-Skewed)
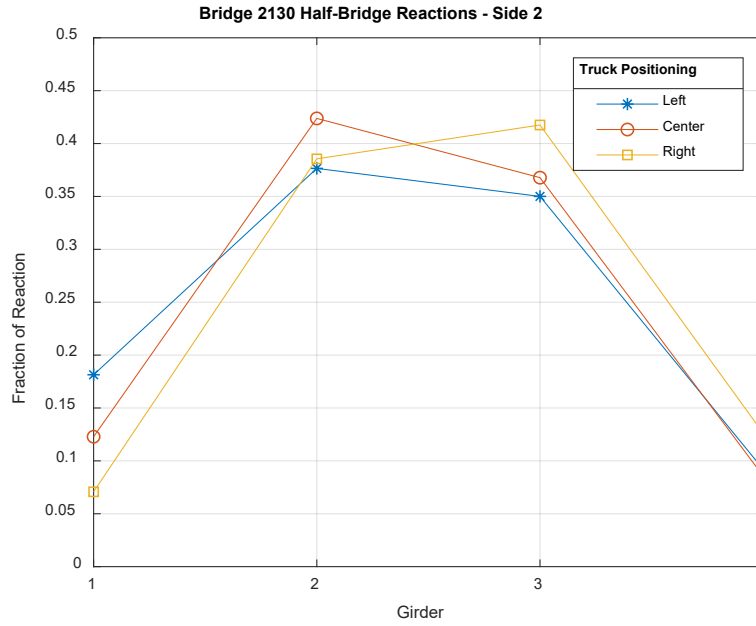
Figure 131: Fractions of Reaction Force Attracted to Each Support at Side 2 – Bridge 2130 (Un-Skewed)
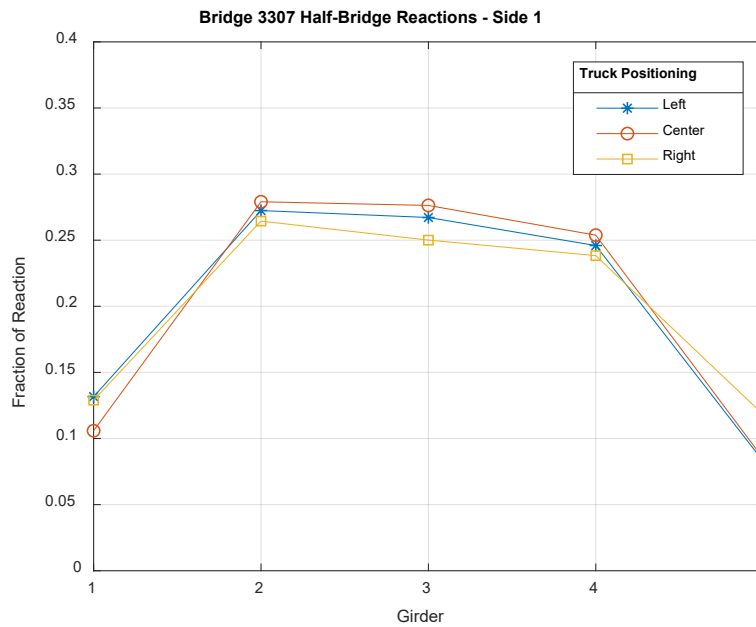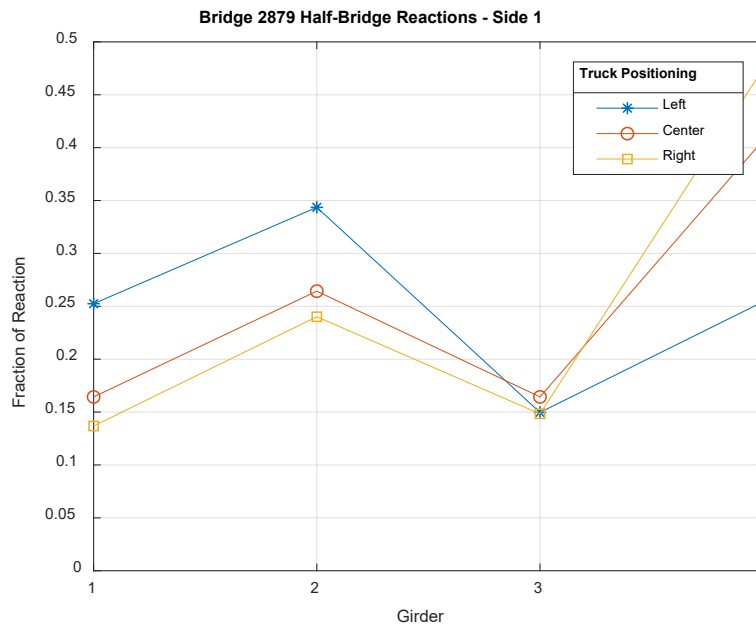

Figure 132: Fractions of Reaction Force Attracted to Each Support at Side 1 – Bridge 3307 (Un-Skewed)
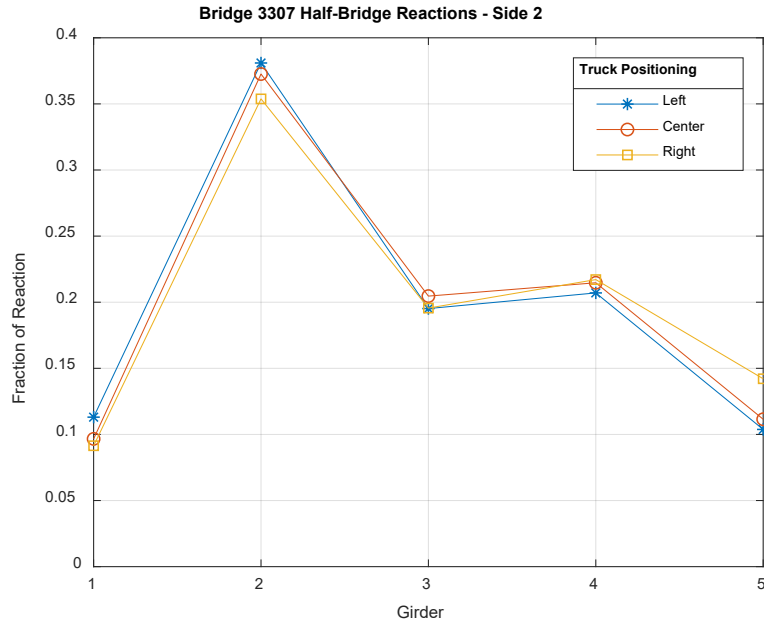
Figure 133: Fractions of Reaction Force Attracted to Each Support at Side 2 – Bridge 3307 (Un-Skewed)
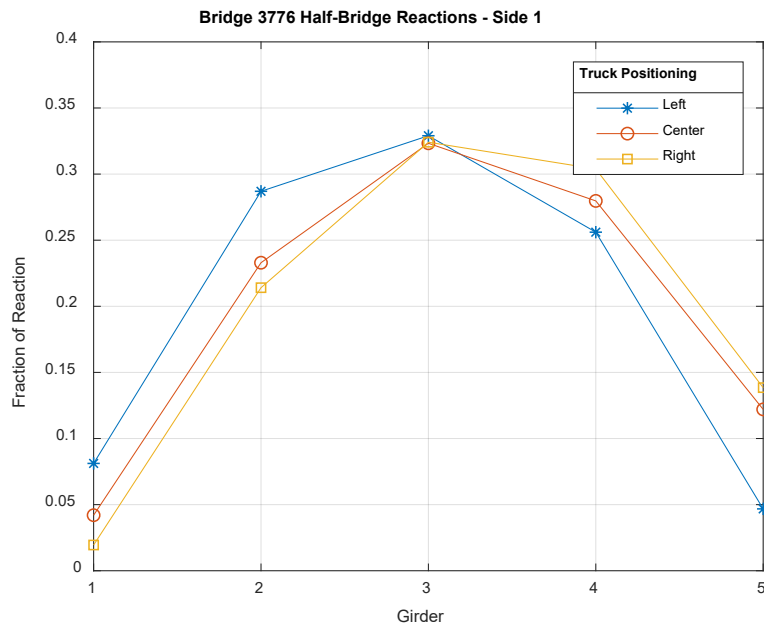
Figure 134: Fractions of Reaction Force Attracted to Each Support at Side 1 – Bridge 3776 (Un-Skewed)
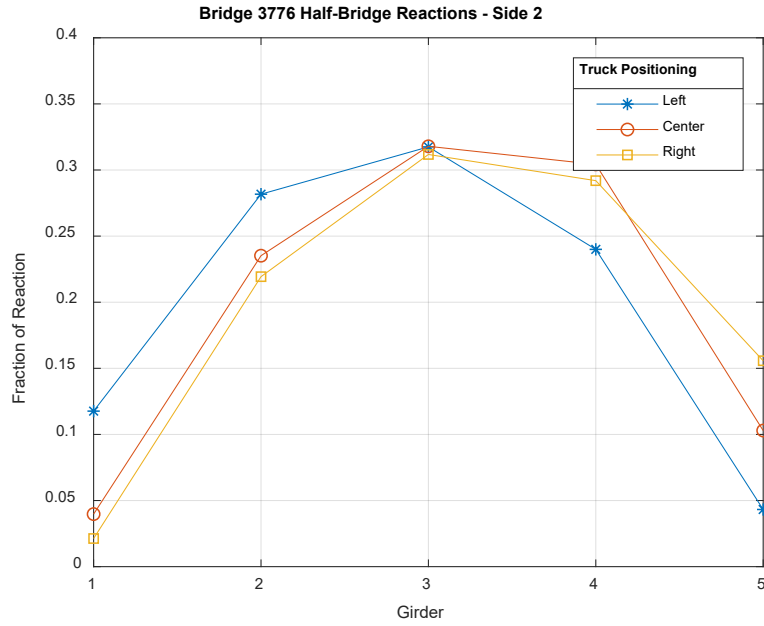
Figure 135: Fractions of Reaction Force Attracted to Each Support at Side 2 – Bridge 3776 (Un-Skewed)

Figure 136: Fractions of Reaction Force Attracted to Each Support at Side 1 – Bridge 2390 (Skewed)

Figure 137: Fractions of Reaction Force Attracted to Each Support at Side 2 – Bridge 2390
(Skewed)

Figure 138: Fractions of Reaction Force Attracted to Each Support at Side 1 – Bridge 2879
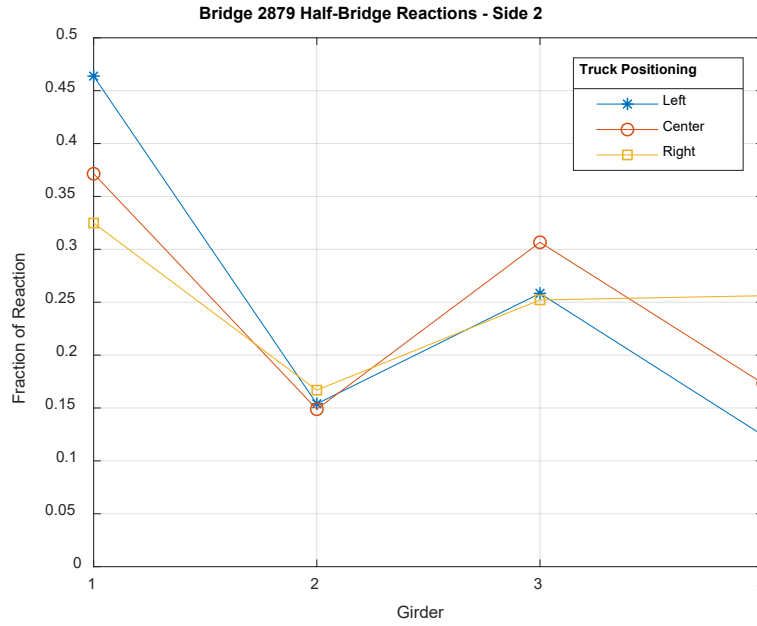(Skewed)

Figure 139: Fractions of Reaction Force Attracted to Each Support at Side 2 – Bridge 2879 (Skewed)
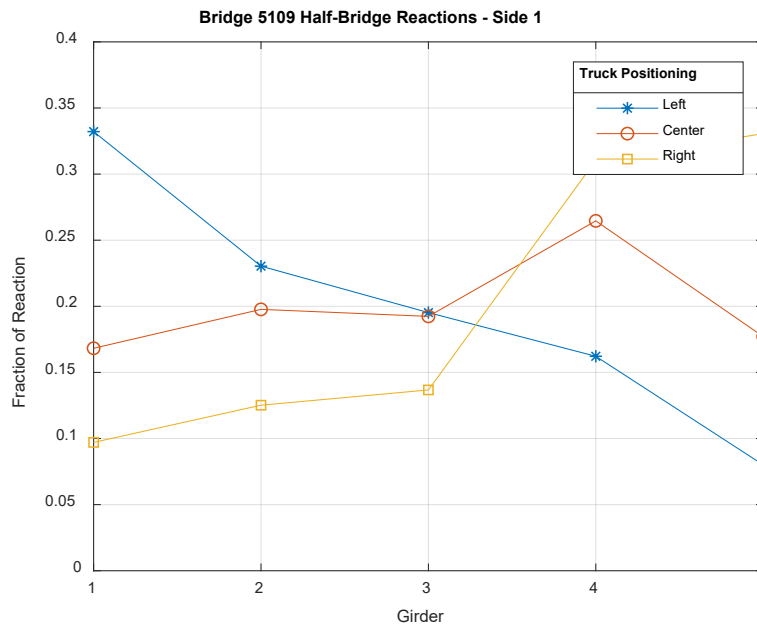

Figure 140: Fractions of Reaction Force Attracted to Each Support at Side 1 – Bridge 5109 (Skewed)
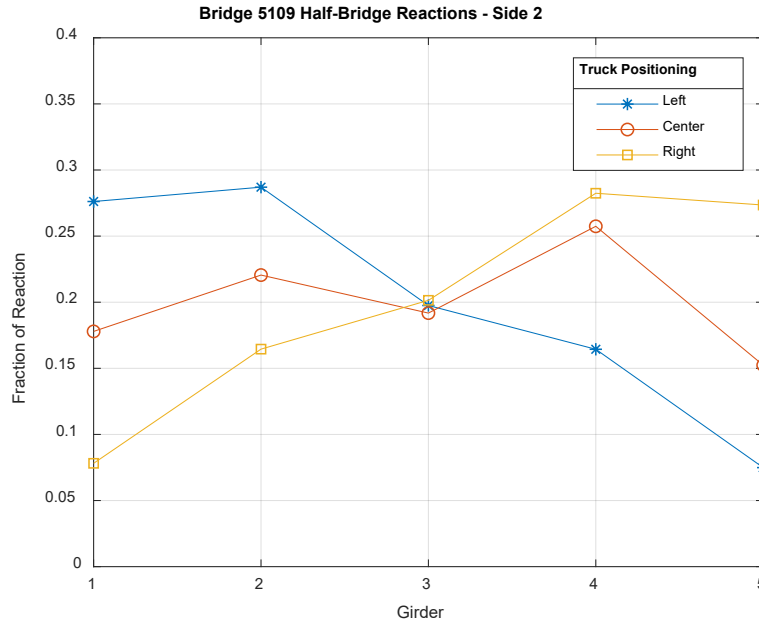
Figure 141: Fractions of Reaction Force Attracted to Each Support at Side 2 – Bridge 5109 (Skewed)
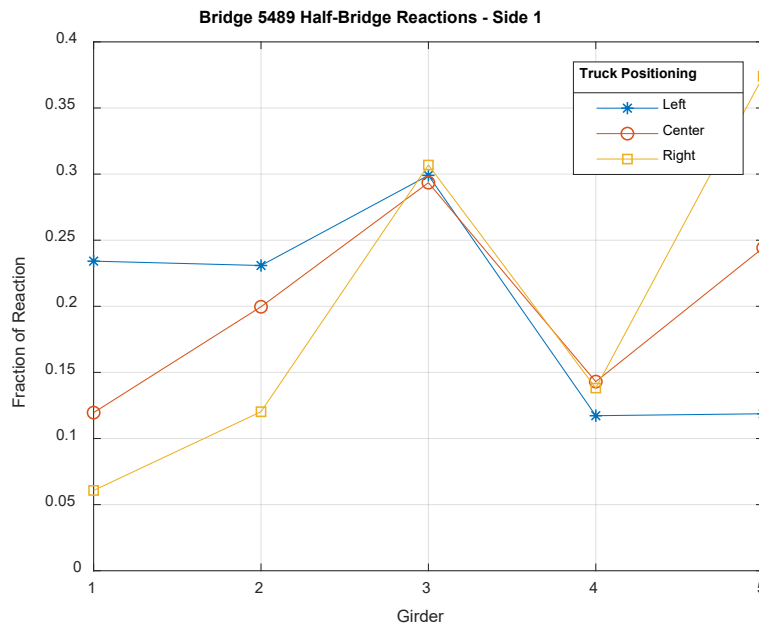

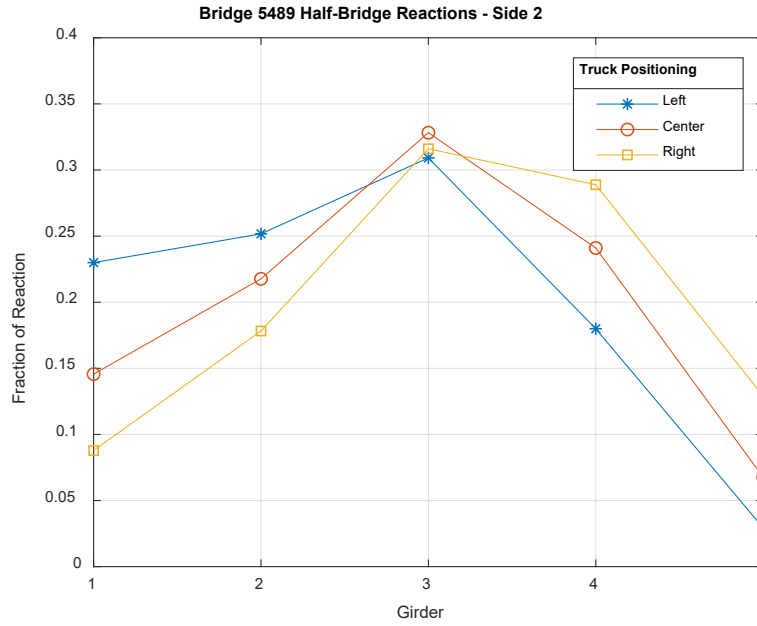Figure 142: Fractions of Reaction Force Attracted to Each Support at Side 1 – Bridge 5489 (Skewed)

Figure 143: Fractions of Reaction Force Attracted to Each Support at Side 2 – Bridge 5489 (Skewed)

A.7.3 Shear Rating MATLAB Code

Contents

- Inputs
- Analysis

```matlab
function RF = PFEA_shear(total_rxn,DL_rxn)
```

```matlab
% This fuction takes the maximum reaction forces recovered from a PFEA
% flexural rating analysis and calculates the shear rating based on AASHTO
% calculated shear capacities. The total reaction force and the reaction
% force due to dead load only are inputs (both in units of kip).

% All calculations based on AASHTO LRFD Bridge Design Guide (2012)

% Andrew Schanck
% 10/2/2019
```

Inputs

```matlab
% Shear reinforcement area (in^2)
Av = [.393 .393 .393 .393 .393];
% Steel yield stress (ksi)
fy = 33;
% T-beam web width (in)
bv = [20 20 20 20 20];
% T-beam height (in)
h = [35.75 35.75 35.75 35.75 35.75];
% Height of longitudinal steel centroid at girder end (in)
ys = [3.125 3.125 3.125 3.125 3.125];
% Depth of longitudinal steel (in)
de = h-ys;
% Steel elastic modulus (ksi)
Es = 29000;
% Area of longitudinal steel at girder end (in^2)
As = [5.0625 5.0625 5.0625 5.0625 5.0625];
% Concrete compressive strength (ksi)
fpc = 2.5;
% Stirrup spacing (in)
s = [12 12 12 12 12];
% Live load factor
load_factor = 1.35;
% Girder end moment resistance (in-kip)
Mn = [4987.7 5364.4 5364.4 5364.4 4987.7];
% Calculate live-load shear (kip)
rxn = total_rxn-DL_rxn;
% Make sure that the expected number of reactions is provided
if length(rxn) ~= length(Av)
    error('Must have as many ractions as girders.')
end
```

Analysis

```matlab
% Allocate a vector of rating factors
RF = zeros(size(rxn));
% For each girder
for ii = 1:length(rxn)
%     Calculate the effective shear depth (in)
    dv = max([0.9*de(ii),0.72*h(ii),Mn(ii)/(As(ii)*fy)]);
%     Calculate net longitudinal strain
    es = rxn(ii)/Es/As(ii);
%     Calculate beta factor for MCFT
    beta = 4.8/(1+750*es)*51/(39+dv);
%     Calculate theta factor for MCFT
    theta = 29+3500*es;
%     Calculate concrete shear resistance (kip)
    Vc = 0.0316*beta*sqrt(fpc)*bv(ii)*dv;
%     Calculate steel shear resistance (kip)
    Vs = Av(ii)*fy*dv*cotd(theta)/s(ii);
%     Calculate total shear resistance (kip)
    Vn = min([Vs+Vc,0.25*fpc*bv(ii)*dv]);
%     Calculate rating factor
    RF(ii) = (Vn-DL_rxn(ii))/(rxn(ii)*load_factor);
end
```

Published with MATLAB® R2017b

Figure 144: MATLAB PFEA Shear Rating Code